

MESON PROPERTIES IN AN EXTENDED
NONLOCAL NJL MODEL



THE UNIVERSITY
of MANCHESTER

A THESIS SUBMITTED TO THE UNIVERSITY OF MANCHESTER
FOR THE DEGREE OF DOCTOR OF PHILOSOPHY
IN THE FACULTY OF SCIENCE

By

Robert Plant

Department of Physics and Astronomy

March 1998

Contents

List of Figures	5
List of Tables	8
Abstract	9
Declaration	11
Copyright Notice	12
Acknowledgements	13
List of Abbreviations	14
1 Introduction	15
1.1 QCD	15
1.2 Overview	18
1.3 Chiral Symmetry	20
1.4 Constituent Quarks	21
1.5 The Pions	23
1.6 The Vector Mesons	24
2 Nonlocal Extended NJL Model	28
2.1 NJL Model	28
2.2 Variations on the Theme	30

2.3	The Nonlocal Model	31
2.4	Nonlocal Currents	35
2.5	Fierz Interactions and Currents	38
3	Quark and Meson Propagators	44
3.1	Quark Propagator	44
3.2	Meson Propagators	47
3.3	Loop Integrals	50
4	Ward Identities and Electromagnetism	55
4.1	Couplings to the Axial Current	55
4.2	GMOR Relation	58
4.3	Couplings to the Vector Current	61
4.4	Vector–Current Correlator	67
5	Numerical Results — Hadronic	71
5.1	Numerical Fits	71
5.2	Meson Spectrum	78
5.3	Hadronic Decays	80
6	Numerical Results — Electromagnetic	86
6.1	Meson Couplings to Currents	86
6.2	Pion Form Factor	88
6.3	$\pi^0 \rightarrow \gamma\gamma$ and Related Form Factor	101
6.4	Radiative Decays and a Related Form Factor	107
7	Next-to-Leading Order Treatment	113
7.1	NLO Corrections	113
7.2	Quark Propagator at NLO	115
7.3	Meson Propagators at NLO	119
7.4	Diagrams for Coupling to Currents at NLO	123

7.5	GMOR at NLO	128
8	Numerical Results — NLO	131
8.1	Model Parameters	131
8.2	Corrections to the Quark Propagator	132
8.3	Corrections to the Meson Properties	143
8.4	Physical Thresholds	146
8.5	Corrections to Pion Properties	146
8.6	Corrections to Sigma Properties	148
9	Conclusions	159
A	Pion Decay Constant at NLO	164
A.1	Cancellations	164
A.2	Chiral Expansion	175
B	Chiral Expansion of NLO Pion Amplitude	179
C	$\rho \rightarrow 4\pi$ in Effective Lagrangians	187
C.1	Effective Chiral Lagrangians	187
C.2	Hidden–Gauge Lagrangians	191
C.3	Massive Yang-Mills Lagrangians	193
C.4	CCWZ Lagrangians	197
C.5	$\rho \rightarrow 4\pi$, Motivation and Background	198
C.6	Decay Amplitude	200
	References	208

List of Figures

3.1	Schwinger–Dyson equation for the quark propagator in the ladder approximation.	45
3.2	Bethe–Salpeter equation for $\bar{q}q$ scattering in the ladder approximation.	48
3.3	Deformed integration contour in the p_4 plane.	51
3.4	The division of the integration region used in performing the naive part of the loop integrals.	52
4.1	Coupling of a particle to an external current.	56
4.2	The dressed γqq vertex.	63
4.3	Diagrams contributing to the vector–current correlator.	68
5.1	Meson propagators.	73
5.2	Propagators in the longitudinal channels.	74
5.3	The transverse–vector channel with $m_0(0)$ too large.	75
5.4	$1 \rightarrow 2$ meson decays.	81
6.1	Diagrams contributing to the spacelike pion form factor.	89
6.2	Absolute value of the pion form factor.	93
6.3	Contributions to the pion form factor below the ρ pole.	95
6.4	Effect of the model ρ meson on the pion form factor.	97
6.5	Contributions to the pion form factor above the ρ pole.	99
6.6	The pion form factor above the ρ pole, using parameter sets A and B.	100
6.7	Diagrams contributing to $\pi^0 \rightarrow \gamma\gamma$	101

6.8	The $\pi\gamma\gamma^*(q^2)$ transition form factor.	106
6.9	Effect of the model vector mesons on the $\pi\gamma\gamma^*(q^2)$ form factor.	107
6.10	The $\omega\pi\gamma^*(q^2)$ form factor.	109
6.11	Contributions to the $\omega\pi\gamma^*(q^2)$ form factor.	111
7.1	The LO and Fock diagrams in the Schwinger–Dyson equation.	115
7.2	A diagram in the Schwinger–Dyson equation at NLO.	116
7.3	Chain of two-quark loops.	116
7.4	The NLO part of the Schwinger–Dyson equation.	117
7.5	Diagrams contributing to the NLO quark self-energy.	119
7.6	The LO loop in the Bethe–Salpeter equation.	119
7.7	Diagrams appearing in the BSE at NLO as a consequence of the NLO quark self-energy.	120
7.8	Some diagrams in the Bethe–Salpeter equation at NLO.	121
7.9	Meson exchange diagrams in the BSE at NLO.	122
7.10	The three-point loops L and \bar{L}	122
7.11	The NLO diagrams (a) and (b) in the coupling of the pion to the axial current.	124
7.12	The NLO diagrams (c) to (j) in the coupling of the pion to the axial current.	125
7.13	The NLO diagrams (k) and (l) in the coupling of the pion to the axial current.	126
7.14	The NLO diagram (m) in the coupling of the pion to the axial current.	127
7.15	The NLO diagrams (n) and (o) in the coupling of the pion to the axial current.	127
8.1	LO meson propagators at spacelike momenta.	133
8.2	The function $a(p)$ in the inverse quark propagator at NLO.	135
8.3	The function $b(p)$ in the inverse quark propagator at NLO.	137

8.4	Contributions to the NLO part of $b(p)$	139
8.5	The function $b(p)$ in the inverse quark propagator of the extended model at NLO.	142
8.6	Contributions to the NLO part of $b(p)$ in the extended model.	152
8.7	The function $a(p)$ in the inverse quark propagator of the extended model at NLO.	153
8.8	Pion propagator for small energies at NLO.	154
8.9	Pion propagator for larger energies at NLO.	155
8.10	Contributions to the NLO part of the pion propagator.	156
8.11	Sigma propagator at NLO.	157
8.12	Contributions to the NLO part of the sigma propagator.	158
8.13	Imaginary part of the sigma propagator.	158
C.1	Diagrams contributing to $\rho\pi$ scattering.	196
C.2	Diagrams contributing to the $\rho^0 \rightarrow 4\pi$ decays.	201

List of Tables

5.1	Parameters of the nonlocal extended NJL model.	77
5.2	Pole positions in the quark propagator.	78
5.3	Meson masses and their couplings to quarks.	78
5.4	On-shell three-meson couplings.	82
6.1	Electromagnetic properties of mesons.	87
8.1	LO fit of the parameters of the nonlocal NJL model.	132
8.2	Calculations at LO with the nonlocal NJL model.	132
8.3	Properties of the quark propagator at NLO.	138
8.4	Properties of the quark propagator of the extended model at NLO. . .	141
8.5	Sigma meson masses at LO and NLO.	149
C.1	Decay widths for $\rho^0 \rightarrow 4\pi$	203

Abstract

UNIVERSITY OF MANCHESTER

ABSTRACT OF THESIS submitted by **Robert Plant** for the Degree of Doctor of Philosophy and entitled **Meson Properties in an Extended Nonlocal NJL Model**

Month and Year of Submission: March 1998

A nonlocal version of the NJL model is investigated. It is based on a separable quark–quark interaction, as suggested by the instanton liquid picture of the QCD vacuum. The interaction is extended to include terms that bind vector and axial-vector mesons. The nonlocality means that no further regulator is required. Moreover the model is able to confine the quarks by generating a quark propagator without poles at real energies. Features of the continuation of amplitudes from Euclidean space to Minkowski energies are discussed. These features lead to restrictions on the model parameters as well as on the range of applicability of the model. Conserved currents are constructed, and their consistency with various Ward identities is demonstrated. In particular, the Gell-Mann–Oakes–Renner relation is derived both in the ladder approximation and at meson loop level. The importance of maintaining chiral symmetry in the calculations is stressed throughout.

Calculations with the model are performed to all orders in momentum. Meson masses are determined, along with their strong and electromagnetic decay amplitudes.

Also calculated are the electromagnetic form factor of the pion and form factors associated with the processes $\gamma\gamma^* \rightarrow \pi^0$ and $\omega \rightarrow \pi^0\gamma^*$. The results are found to lead to a satisfactory phenomenology and demonstrate a possible dynamical origin for vector-meson dominance. In addition, the results produced at meson loop level validate the use of $1/N_c$ as an expansion parameter and indicate that a light and broad scalar state is inherent in models of the NJL type.

Declaration

No portion of the work referred to in this thesis has been submitted in support of an application for another degree or qualification of this or any other university or other institution of learning.

Copyright Notice

1. Copyright in the text of this thesis rests with the author. Copies (by any process) either in full, or of extracts, may be made only in accordance with instructions given by the author and lodged in the John Rylands University Library of Manchester. Details may be obtained from the Librarian. This page must form part of any such copies made. Further copies (by any process) of copies made in accordance with such instructions may not be made without the permission (in writing) of the author.
2. The ownership of any intellectual property rights which may be described in this thesis is vested in the University of Manchester, subject to any prior agreement to the contrary, and may not be made available for use by third parties without the written permission of the University, which will prescribe the terms and conditions of any such agreement.

Further information on the conditions under which disclosures and exploitation may take place is available from the Head of Department of Physics and Astronomy.

Acknowledgements

I should like to thank the staff and students of the Theory group for helping to make my time in the department a pleasant one. In particular, I am grateful to my fellow occupants of room 6-21 (Urban Weber, Anne Kienappel and Hiroko Short) for their friendship and good humour.

I have enjoyed many interesting discussions with my supervisor, Dr. Mike Birse. His relentless supply of helpful suggestions, encouragement and advice has often proved invaluable.

In the proof reading of this thesis, I have been assisted by both Hiroko Short and Mike Birse, who I thank for pointing out my tap-doles and various grammatical errors. Of course, any mistakes which remain are entirely my own fault.

List of Abbreviations

BSE	Bethe–Salpeter equation.
CCWZ	Callan, Coleman, Wess and Zumino.
ChPT	Chiral perturbation theory.
GMOR	Gell-Mann, Oakes and Renner.
KRSF	Kawarabayashi, Suzuki, Riazuddin and Fayyazuddin.
LO	Leading order in $1/N_c$.
NJL	Nambu and Jona–Lasinio.
NLO	Next-to-leading order in $1/N_c$.
PCAC	Partial conservation of the axial current.
QCD	Quantum chromodynamics.
SDE	Schwinger–Dyson equation.
VMD	Vector–meson dominance.

Chapter 1

Introduction

1.1 QCD

It is widely accepted that strong interactions are described by the theory of quantum chromodynamics [1] (QCD). This is an $SU(3)$ gauge theory of spin $\frac{1}{2}$ quarks which interact via the colour gauge field, the quanta of which are called gluons. The quarks themselves have one of six different flavours, which are identical with regard to the QCD Lagrangian, apart from their bare (current) masses. The non-Abelian nature of the gauge group means that there are also purely gluonic interactions, arising from the use of gauge-covariant field strengths. In perturbative calculations of the running coupling in the theory, these gluonic self interactions cause the gauge coupling strength to increase as the energy scale decreases. Hence the theory at low energies is intrinsically non-perturbative. At high energies the theory is weakly coupled, a property known as asymptotic freedom. Although the predictions of the theory have been successfully tested in this regime, where the perturbative technique is a valid one, a wide variety of alternative methods is required to probe the low-energy content of the theory.

There are several important features of strong-interaction physics which are thought to be consequences of the dynamics in the low-energy regime. These features should be reflected in any attempt to model the non-perturbative dynamics, if

only by means of their phenomenological implications. One such feature is that of dynamical chiral symmetry breaking. Apart from the current quark masses, the QCD Lagrangian is invariant under the global chiral transformations,

$$(1 - \gamma_5)\psi \rightarrow G_l(1 - \gamma_5)\psi, \quad (1 + \gamma_5)\psi \rightarrow G_r(1 + \gamma_5)\psi, \quad (1.1)$$

where $G_l \otimes G_r \in \text{SU}(N_f)_l \otimes \text{SU}(N_f)_r$. Since the current quark masses of the lightest two (or three) flavours are small one might hope for this to be a useful approximate symmetry at low energies, where the heavy-quark flavours are not relevant to the physics. However, the observed spectrum of excitations above the vacuum state does not exhibit chiral symmetry. The physical vacuum itself is therefore considered not to be invariant under chiral transformations, the axial part of the chiral group being a spontaneously broken symmetry. The required phase transition from the chiral vacuum to the physical vacuum, which realizes only the vector part of the group, is believed to be inherent in the non-perturbative sector of the theory. Associated with this transition is the appearance of a Goldstone boson. In practice, the small explicit chiral symmetry breaking, owing to the non-zero current quark masses, means that the Goldstone state is manifested only approximately in the guise of the light pseudoscalars.

Another important property of QCD is that of confinement, the requirement that only colour-singlet composite systems of quarks and gluons can be observed as asymptotic states. There being no proof that confinement must occur in QCD, the property is postulated on the basis that no coloured states have ever been detected. Qualitative arguments, based on the large N_c limit [2] or on the assumed failure of the cluster decomposition principle, indicate that confinement should be a non-perturbative effect, associated with strong, long-range forces between coloured objects. Some support for such ideas is provided by the phenomenological success of potential and string models of hadrons as well as by lattice gauge studies.

One possible approach towards a practical description of low-energy strong physics is the use of QCD sum rules [3], which aim to interpolate between the calculable

high-energy behaviour of the theory and low-energy phenomenology. Although this technique has a firm theoretical footing, there may be uncertainties introduced by the choice of formulation on the phenomenological side, while the results themselves can exhibit significant dependence on the mass scale at which the matching is performed. Another possibility is to attempt to simulate QCD on a lattice of space–time points [4]. In principle this approach could be a source of much information. However, it is very intensive numerically and accurate results are difficult to achieve, not least because of the uncontrolled approximations that are presently required in practice. Further, there is as yet an incomplete understanding of systematic errors, such as finite–size effects. Another method, which also explicitly encodes the full dynamical content of QCD, is to work in the formalism of the Schwinger–Dyson equations [5]. This formalism consists of an infinite tower of coupled integral equations linking the n -point functions of the theory to functions with fewer external lines. In order to make the system tractable it must be truncated, with some ansatz chosen to represent the physics neglected. The degree of approximation involved in that process is unquantified and, for an ansatz with any pretensions towards being realistic, the numerical situation can easily become prohibitive. The method does, however, have certain advantages over the lattice approach, such as the transparent connection between dynamical chiral symmetry breaking and the Goldstone character of the pion [6]. Yet another technique commonly applied is that of the effective chiral Lagrangian¹ where one works in terms of mesonic degrees of freedom and constructs Lagrangians consistent with chiral symmetry. Although such Lagrangians may contain many unknown coefficients, which must be determined by appeal to experiment, they are nevertheless at worst useful tools for elucidating the relationships between different physical processes.

Each of the methods outlined above is, at least in principle, capable of being fully consistent with QCD. An alternative line of attack, however, is to operate in a framework which relaxes that requirement from the outset. For instance, the starting

¹which is discussed further in Appendix C.

point could be to postulate some effective quark Lagrangian. In that style of approach one aims to construct a model which incorporates some important aspects of the low-energy QCD dynamics and yet with which actual calculations of observables are reasonably straightforward to perform. Considered from a purely phenomenological perspective, a model of that type should be capable of accounting for a wide range of experimental data, hopefully with a more limited set of free parameters than would be needed by a model formulated at the hadronic level. Moreover, one might hope that by exploring a variety of such models of interacting fermions it may be possible to gain some insight into the ways in which particular properties of the underlying dynamics influence the resulting observables. A simple and early example of the approach is the model of Nambu and Jona-Lasinio [7] (NJL) of which there will be a good deal more to say later.

1.2 Overview

The main body of this thesis will present work on the development of a model of interacting fermions. A simpler version of the model to be used was originally proposed by Bowler and Birse [8] as a tractable dynamical model which shares several features with low-energy QCD. Being based on a four-quark interaction vertex, it has some similarities with the model of NJL. However, since the interaction of Ref. [8] is taken to be nonlocal there are also some important differences. Amongst these are features which eliminate the traditional problems of the NJL model whilst nevertheless retaining much of the simplicity that is its chief merit. The nonlocal model was therefore suggested as one which offers an interesting improvement over the original NJL Lagrangian. This thesis investigates the proposed model in some detail, extending the treatment of Ref. [8] by including interaction terms that bind the vector and axial vector mesons as well as by developing a framework that enables electromagnetic quantities to be calculated.

The enlarged model to be described here is referred to as the nonlocal extended

NJL model, details of its definition and motivation being presented in Chp. 2. A part of that definition is the specification of transverse vector and axial currents, which are also discussed in that chapter. Calculations with the model will be performed to all orders in momentum but to a finite order in the $1/N_c$ expansion. Working initially at leading order (LO) in $1/N_c$, the resulting forms of the quark and meson propagators are presented in Chp. 3. In the following chapter, the means of coupling particles to external currents are explained and various Ward identities, such as the Gell-Mann–Oakes–Renner (GMOR) relation and that for the correlator of vector currents, are demonstrated to hold. Determination of the model parameters and the resulting meson spectrum are discussed in Chp. 5, along with the evaluations of purely hadronic meson decay modes. A variety of electromagnetic decays and form factors are calculated and discussed in Chp. 6. In addition, that chapter includes descriptions of how other identities are satisfied by the model calculations, specifically those for the pion charge and the anomalous π^0 decay amplitude. Since $1/N_c$ is not a particularly small expansion parameter, an obvious desire is to examine the corrections to the model at next-to-leading order (NLO). In Chp. 7, the theoretical basis for doing so is established, the extra contributions being given for the quark and meson propagators and for the pion decay constant. There are useful cancellations which can be found amongst the graphs contributing to the pion decay constant at NLO and these are detailed in Appendix A.1. It is important to ensure that the NLO treatment remains consistent with symmetry restrictions and to that end the GMOR relation is explicitly verified in Chp. 7, drawing on results derived in Appendices A and B. Numerical results from the NLO analysis are given in Chp. 8. There is some additional discussion and a summary of the findings in Chp. 9 where conclusions are also drawn.

Chiral Symmetry Constraints

In the work on the nonlocal extended NJL model, a considerable amount of attention will be devoted to showing that the model calculations satisfy various identities which

follow from chiral symmetry. Since the interactions in the model are constructed to be chirally symmetric, such identities will provide useful checks on the calculations, helping to verify that all of the relevant contributions to a process have been correctly identified and evaluated. This is important to establish because a failure at any stage to incorporate chiral symmetry correctly could greatly distort the results for observables. The point is highlighted in Appendix C with a calculation of the rare decay $\rho \rightarrow 4\pi$. Although this decay mode of the ρ meson is yet to be observed, some authors [9, 10] have recently expressed hopes that it might be possible to detect it in forthcoming experiments. Following some general comments about the construction of chiral effective Lagrangians, the appendix describes computations of the decay using a variety of such phenomenological Lagrangians. The decay widths deduced from all of these chirally-symmetric approaches are an order of magnitude smaller than those which have been estimated in models that did not respect all of the symmetry constraints [9, 10, 11]. The process therefore gives a dramatic illustration of the need to make sure that such constraints are enforced.

Brief consideration will also be given in Appendix C to the possible implications that a measurement of the $\rho \rightarrow 4\pi$ partial width could have for the effective Lagrangians used. In particular, comments will address the issue of whether the decay might be able to test any of the phenomenological notions associated with the vector mesons. Such notions will be amongst those probed within the context of the nonlocal extended NJL model. In the remainder of this introductory chapter, it therefore seems appropriate to draw the reader's attention to some of those phenomenological ideas which will be of particular relevance to the work.

1.3 Chiral Symmetry

The concept of chiral symmetry is a very powerful one, underpinning almost all of the phenomenology which has been developed in low-energy strong physics. In order for it to be so useful a principle it is necessary that the current quark masses be

small. The symmetry is then almost satisfied by the QCD Lagrangian. The current masses should be small in comparison with, say, the proton mass, which one might reasonably consider to be a typical energy scale of the strong interaction. In the most recent update from the Particle Data Group [12], the following values were quoted for the current quark masses²:

$$m_u = 2 \text{ to } 8 \text{ MeV}, \quad m_d = 5 \text{ to } 15 \text{ MeV}, \quad m_s = 100 \text{ to } 300 \text{ MeV}, \quad (1.2)$$

with the other three quark flavours being heavier still. The up and down flavours of quark can therefore be regarded as light in the above sense. Going further, if the strange quark were also incorporated then a three-flavoured chiral symmetry might prove a useful tool. However, since the strange quark's bare mass is significantly larger, there are many practical applications where one would need to include appropriate symmetry-violating effects to obtain satisfactory results. While the study of strangeness is an important subject in its own right, the attention of this thesis will be focused on the lightest two flavours.

1.4 Constituent Quarks

Of the strongly-interacting states that have been so far observed there are two main classes: mesons, the quantum numbers of which may be accounted for in terms of those of an underlying $\bar{q}q$ pair; and (anti-) baryons, similarly described with a $(\bar{q}\bar{q}\bar{q})$ qqq structure. For completeness, it should also be pointed out that there is some tentative evidence for other possible structures in observed bound states, such as the purely gluonic, $\bar{q}q$ molecules or hybrid $\bar{q}qg$ states. The concerns here are with the mesons, being the simplest bound systems in which to attempt to model the internal dynamical structure.

²In general, the values of the quark masses are dependent upon the renormalization scheme adopted and the scale at which they are evaluated. The estimates quoted refer to a mass-independent subtraction scheme, at a scale of $\mathcal{O}(1\text{GeV})$.

The quarks referred to in the above categorizations of hadronic spectroscopy are not to be identified with those elementary fields with masses of a few MeV (Eq. 1.2) found in the QCD Lagrangian. Although sharing the same discrete quantum numbers as those fields, the quarks that appear in simple spectroscopic descriptions are objects with masses of a few hundred MeV. Effective masses of that order are required in straightforward spectroscopic treatments of hadronic properties, such as their masses and magnetic moments. It is postulated that the acquisition of such an effective mass occurs as a consequence of the non-perturbative interactions of the bare quarks with the non-trivial vacuum structure. The generation of masses for particles through spontaneous symmetry breaking is a familiar phenomenon from the Higgs mechanism of the electroweak model [13] and is well illustrated by the inclusion of fermions in the linear sigma model [14]. More particularly, the simplest available order parameter for dynamical symmetry breaking in QCD is provided by the matrix element $\langle 0|\bar{\psi}\psi|0\rangle_0$, defined³ by⁴

$$\langle 0|\bar{\psi}\psi|0\rangle_0 = -i\text{Tr} \int \frac{d^4p}{(2\pi)^4} S_0(p), \quad (1.3)$$

where $S_0(p)$ is the full two-point function dressed by the interactions of the theory and evaluated at zero current quark mass. As throughout the text, the chiral limit of a quantity is here denoted by the subscript zero. Now, the most general form of the dressed quark propagator is

$$S^{-1}(p) = (1 + a(p^2))\not{p} - b(p^2). \quad (1.4)$$

For there to be a non-zero condensate in the physical vacuum, clearly it must be that $b(p^2) \neq 0$ to give a non-vanishing Dirac trace in Eq. 1.3. The existence of a scalar term in Eq. 1.4 can be interpreted as an effective mass for the constituent quark, the generation of which is therefore inextricably entwined with the spontaneous

³Strictly speaking, to give a complete definition, one should specify a particular renormalization scheme and the scale at which the scalar condensate is to be evaluated. Nevertheless the expression given is sufficient for the present purpose of supplying a suitable order parameter.

⁴Here ‘Tr’ is used to denote a trace over flavour, colour and Dirac indices; the symbol ‘tr’ will later be used to indicate a trace over Dirac indices only.

breakdown of chiral symmetry. While it is obvious that this mass must run (since asymptotic freedom demands that $b(p^2 \rightarrow -\infty) \rightarrow 0$), in many studies it is assumed to be approximately constant over the low-energy range (up to ~ 1 GeV). Such an assumption is not in conflict with many phenomenological consequences, but can be a source of difficulties when imposed upon a dynamical model, such as that of NJL.

1.5 The Pions

Chp. 1.1 mentioned the important role played by the light pseudoscalar mesons which, in the chiral limit, are the massless Goldstone modes associated with dynamical chiral symmetry breaking. A simple early model which embodies chiral symmetry is the celebrated linear sigma model of Gell-Mann and Lévy [14]. As well as pseudoscalar fields for the pions, the model contains a scalar field which acquires a vacuum expectation value ($-f_\pi$) and is thereby responsible for the spontaneous symmetry breakdown. The ground state is degenerate with respect to pionic excitations that lie on the chiral circle⁵, $\sigma^2 + \underline{\pi}^2 = f_\pi^2$. An axial symmetry transformation acts to move the system between these degenerate states. Its effect can be parameterized by the matrix element of the axial current, $J_5^{a\mu} = \frac{1}{2}\bar{\psi}\tau^a\gamma^\mu\gamma_5\psi$, between the vacuum and a single pion,

$$\langle 0 | J_5^{a\mu}(x) | \pi^b(q) \rangle = \delta^{ab} i f_\pi q^\mu e^{-iqx}. \quad (1.5)$$

The above matrix element controls the weak decay of the charged pion, $\pi^\pm \rightarrow l^\pm \nu_l$ ($l = \mu, e$) [15] from which a numerical value for the pion decay constant, f_π , can be determined. The quantity is a crucial element in any chiral model since it is the physical value which sets a scale for the dynamical symmetry breaking process. Taking the divergence of Eq. 1.5 gives

$$\langle 0 | \partial_\mu J_5^{a\mu}(x) | \pi^b(q) \rangle = \delta^{ab} f_\pi m_\pi^2 e^{-iqx}, \quad (1.6)$$

relating the pion mass to the explicit breaking of axial symmetry. The relationship was further developed by Gell-Mann, Oakes and Renner [16] (GMOR) who derived

⁵note that the convention is followed where an underscore denotes an isotriplet.

the result

$$f_\pi^2 m_\pi^2 = -\overline{m}_c \langle 0 | \overline{\psi} \psi | 0 \rangle_0 + \mathcal{O}(m_c^2), \quad (1.7)$$

where \overline{m}_c is the average of the up and down current quark masses. A further assumption is required to obtain Eq. 1.7, namely the partial conservation of the axial current (PCAC). Although the current quark masses explicitly break the axial part of the chiral group, its current is regarded as conserved in the first instance, the effects of the actual symmetry breaking often being small corrections which can reasonably be treated perturbatively. Eq. 1.6 implies that a suitably-normalized $\partial_\mu J_5^{a\mu}$ could be used as the field describing an on-shell pion. Making the PCAC assumption then means that an extrapolation of this operator from the pion mass shell to $q^2 = 0$ should be a smooth one and hence that low-energy matrix elements of the axial current divergence are dominated by the pion. Application of this notion can be very powerful. Its plausibility may be justified a posteriori from the successes of its many consequences. When combined with current algebra (the commutation relations of the vector and axial currents), there are a wide variety of soft pion theorems which can be deduced [17].

Interpretation of the scalar (sigma) meson in the linear sigma model is far more controversial. The particle is excited by forces which act to restore a Wigner–Weyl realization of chiral symmetry, its mass parameterizing the resistance of the vacuum to such forces. However, since there does not exist an unambiguous physical state to identify with the field, it remains the subject of debate. Such issues are discussed more fully in Chps. 5 and 8.

1.6 The Vector Mesons

Although soft pion theorems provide much useful information about processes at the lowest energies there are important dynamical effects, not solely determined by symmetry considerations, which become relevant as energies increase. In the discussion of such effects, the existence of more massive particles becomes significant. The lightest

of these are the vector mesons. As is discussed in Appendix C.1, the exchange of such resonant particles is the dominant contribution to pion dynamics beyond the lowest energies. The vector mesons are also among the main ingredients in meson exchange models of nuclear forces [18]. Although pion exchange accounts for the major part of the long-range inter-nuclear force, inclusion of the ω meson can help to explain the short distance repulsion between nucleons. Furthermore, the particle is considered to be responsible for part of the spin-orbit interaction. The ρ meson proves to be a lesser, but still significant inclusion⁶, being relevant at comparable length scales of ~ 1 fm. The possibility of $\rho - \omega$ mixing [19] is an interesting and much-debated aspect of inter-nuclear forces, providing a mechanism [20] for observed charge-symmetry violations [21]. In addition, this mixing has been suggested as a potential source for CP violation in B-meson decays [22].

The vector mesons are also highly conspicuous in discussions of the electromagnetic couplings of hadrons. Indeed, the very existence of the ω meson⁷ was first proposed in 1957 [23] in order to interpret nucleon form factors⁸. The ρ resonance was suggested on similar grounds shortly afterwards [28]. Since these particles have the same discrete quantum numbers as the photon they can participate as intermediates in electromagnetic interactions. This point soon led to the phenomenological concept of vector meson dominance (VMD) [26], the idea that such intermediate states might actually make the dominant contributions to electromagnetic matrix elements. The concept is perhaps most dramatically suggested by the pion form factor, which is strongly peaked at the ρ meson mass [29]. Moreover, the variation with momentum of this form factor, over a fairly wide range of q^2 , can be well described using simply a canonical ρ meson propagator. Experimental support for VMD can also be

⁶there are also contributions from combined $\pi\rho$ exchange which can have important consequences [18].

⁷although named as ρ^0 by the author of the initial paper.

⁸A tentative suggestion for a new, heavy meson to account for the phenomenological NN spin-orbit force can also be traced back to that year [24]. However, it was not until three years later that this was thought to be a vector state [25, 26] and treated seriously [27] in that context.

inferred from various other mesonic form factors [30], from electromagnetic meson decays [31] and from photoproduction processes in nuclear physics [32]. The underlying reasons for these successes are unclear. It is therefore of interest to examine whether there might be any support for the concept within a dynamical framework such as that of the nonlocal extended NJL model. VMD can be expressed more concretely as the assumption of an identity between the electromagnetic current and the canonical interpolating fields of the vector mesons [33],

$$J_{\text{EM}}^\mu(x) = -eg_{\rho\gamma}\rho^{0\mu}(x) - eg_{\omega\gamma}\omega^\mu(x) + \dots \quad (1.8)$$

where the dots refer to more massive vector resonances. The constants $g_{V\gamma}$ parameterizing the coupling strengths between the photon and the vector mesons are to be considered as being defined by the above field–current identity, Eq. 1.8. They can be determined experimentally from the decays $V \rightarrow e^+e^-$. An essential point to note, without which Eq. 1.8 would be invalid, is that a spin-1 field coupled to a conserved current of necessity has no divergence itself, by virtue of its Proca equation⁹.

Another phenomenological concept, closely related to VMD, is that of a universal coupling of the vector mesons [17, 34]. Electromagnetic gauge invariance requires that the photon be universally coupled to all other elementary fields. The couplings to composite states are complicated by associated form factors, but for a real photon these simply reduce to the known charge of the state. Suppose now that one is prepared to accept an extreme form of VMD where the field–current identity is saturated by the lightest vector resonances. Since photon–hadron couplings then take place exclusively via intermediate ρ and ω mesons, it follows that the couplings of these particles to strong states should themselves be universal. The statement will only be true on the photon mass shell and strictly therefore universal coupling can only apply to the interactions of the interpolating vector fields defined by Eq. 1.8 at the off-shell point $q^2 = 0$. Away from that point, universality can only persist by means of apparently improbable coincidences relating the strong and electromagnetic form factors of

⁹the Euler–Lagrange equation for that field.

various targets. With that basis, an extrapolation of the principle over a fairly large interval of q^2 , from zero to the on-shell vector meson mass, is highly dubious; it is certainly far more implausible than the PCAC extrapolation from zero to m_π^2 . Surprisingly, however, such a bold step turns out rather well from the phenomenological perspective: relations between the resulting predictions for $\rho \rightarrow e^+e^-$, $\rho \rightarrow \pi^+\pi^-$ and the phenomenological ρNN coupling used in nuclear models [35] are reasonably well satisfied. As with VMD, the reasons for the success of universality are not known, presumably lying in some approximate property yet to be unearthed from the dynamics. Alternatively, there might of course just be some coincidence amongst the particular vector-meson couplings whose values can be determined. This interesting question is an issue which will receive some attention in the remainder of the thesis. Appendix C includes comment on whether detection of the $\rho^0 \rightarrow \pi^+\pi^-2\pi^0$ decay could in practice probe the strength of the $\rho\rho\rho$ vertex, which would then strengthen or weaken the experimental support for universality. Also, Chp. 6 includes discussion on whether universality might arise from within the nonlocal extended NJL model.

Chapter 2

Nonlocal Extended NJL Model

2.1 NJL Model

The Nambu–Jona-Lasinio (NJL) model [7, 36, 37] was described in the introduction (Chp. 1) as a dynamical model which is very much simpler than QCD but which shares several qualitative features with it. Most notably, the NJL model supports a dynamically–broken chiral symmetry, with the pions as approximate Goldstone bosons. Since such features have long been known in low-energy strong physics, the model has been widely used as a starting point for the description of light mesonic states as fermion–antifermion composites, predating QCD and retaining its popularity to date. Viewed as a low-energy approximation to some underlying, strongly–coupled fermionic theory, variations of the model have also been studied in the context of the top-quark–condensate picture of a composite Higgs boson [38].

The original NJL model is based on fermionic fields interacting through a local, chirally–invariant, four-point vertex¹. The local nature of the interaction produces a great simplification of the corresponding Schwinger–Dyson and Bethe–Salpeter equations. The main defects of the model, however, are direct consequences of this locality.

¹The precise form of the action is discussed in Chp. 2.3.

Specifically, they are that the loop integrals diverge (and so must somehow be regulated) and that the model is non-confining.

The absence of confinement in the NJL model occurs because the dynamically-generated constituent quark mass is momentum independent. This fact imposes a severe restriction on the range of applicability of the model, since a $\bar{q}q$ continuum opens up at energies of twice the constituent mass. Only the pions lie unambiguously below this threshold. The model also includes the chiral partner of the pion, which is located on the threshold (indeed, just above it if one works beyond the chiral limit) and may, if desired, include other mesonic states. Without confinement, however, and with an otherwise reasonable constituent quark mass of ~ 300 MeV, the ρ meson and other such states would lie above the $\bar{q}q$ threshold and so could decay into free $\bar{q}q$ states.

Since the NJL model is non-renormalizable, in practice it is necessary to apply some form of ultra-violet regularization with a cut-off parameter that remains finite. The details of the scheme adopted must be regarded as a part of the specification of the model. A variety of schemes have been used in the literature, such as hard three- and four-momentum cut-offs, proper time and Pauli-Villars regulators. Although the model does contain regularization-independent information [39, 40] and results with the various regularization schemes have been found to be qualitatively similar [41], the choice of any particular scheme lacks a sound physical motivation. A feature of many of the schemes is that as well as the form of the cut-off, a definite momentum routing must be specified for loop diagrams with two-or-more quark lines [42]. In practice a symmetric routing is often implicitly taken in order to maintain Ward identities. Another aspect of concern is that the regularization scheme must be specified yet further if one wishes to calculate beyond leading order in the $1/N_c$ expansion, a new cut-off being required for meson loops [43, 44, 45].

The need for a finite regulator in the model is somewhat problematical in the anomalous sector. If low-energy theorems for anomalous processes (such as that for

$\pi^0 \rightarrow \gamma\gamma$) are to hold then a complete set of quark states is required. This can be achieved by leaving the anomalous diagrams ad hoc unregulated [46] or else by including additional terms in the Lagrangian in order to recover the anomalous Ward identities [40]. Related problems occur in the presence of interactions of a vector character [46, 47, 48, 49] if one attempts to apply the regularization prescription to both the anomalous and non-anomalous sectors.

2.2 Variations on the Theme

Many attempts have been made to generalize the original NJL model [50] with the aim of eliminating some of the unwanted features discussed in Chp 2.1 but retaining its successful phenomenological aspects [36, 37]. One promising approach, which provides some motivation for the model which is studied here, is suggested by the instanton-liquid studies pioneered by Dyakonov and Petrov [51]. In that picture, the QCD vacuum is viewed in terms of a liquid of instantons (and anti-instantons), the gluonic configurations which connect topologically-distinct states within the vacuum. The instantons induce an effective quark vertex of the 't Hooft structure [52, 53], which is nonlocal but has a separable form. The separable nature of this interaction retains as far as possible the simplifying features of a local model, with the nonlocality providing a natural cut-off on all loop integrals. A similar class of model assumes a separable dependence on the relative momentum of the $\bar{q}q$ pair and has been studied in Refs.[54, 55, 56, 57].

Other models with simple interactions have been suggested based on various other types of gluonic field configurations postulated within the QCD vacuum. For example, Efimov and coworkers [58, 59] start with a constant (anti-) self-dual background gluon field in Euclidean space and base their four-quark vertex on one-gluon exchange within such a background. Yet another recent model [60] used a four-quark vertex mediated by a random colour matrix, as an attempt to simulate a strongly-fluctuating background gluon field (see also[61]).

It should also be mentioned that there are explicit studies of the QCD Schwinger–Dyson equations based on one-gluon exchange forces between the quarks, often using effective gluon propagators [62, 63] (also see the review [5] and other references therein).

The work here develops and further explores a model proposed by Bowler and Birse [8]. It is based on a nonlocal, separable, four-quark vertex and is therefore similar to the instanton–liquid model of Ref. [51]. The differences from the instanton model are that more general choices of the interaction form factor and the possible couplings are admitted. The particular choice of form factor which is adopted in the numerical computations can lead to quark confinement, in the sense of a quark propagator without poles at real energies. It also ensures the convergence of all quark loop integrals, unlike that chosen in the separable model of Ref. [64]. Only the pions and their scalar partner were studied in Ref. [8]. In the spirit of the extended NJL model [37, 39, 40, 46, 65, 66, 67, 68, 69], other mesonic degrees of freedom, such as the vector mesons, can be incorporated. Including these particles enables the role of the confinement mechanism to be probed, since they have masses of around twice a typical constituent quark mass.

2.3 The Nonlocal Model

Formally at least, one can imagine integrating out gluonic degrees of freedom to leave an effective action for QCD expressed in terms of quark fields only. As in the usual NJL model, such an action is truncated to include only the simplest interactions possible, keeping the two-body forces between quarks, as described by four-quark vertices. Indeed, at leading order in $1/N_c$, all six-quark and higher interactions could be absorbed into effective couplings for the four-quark terms, by replacing extra $\bar{\psi}\Gamma\psi$ factors with their vacuum expectation values. This is just the procedure followed in the three-flavour extended NJL model [68, 69] with a six-quark, $U(1)_A$ -breaking

't Hooft determinant² [52]. If there is flavour asymmetry then the process induces effective four-quark couplings that depend on the flavour channel. However, there is no need to consider such effects in any detail since the present work specializes to two flavours with isospin symmetry. The action may be written as

$$S = \int d^4x \bar{\psi}(x)(i\cancel{\partial} - m_c)\psi(x) + \sum_i \int \prod_n d^4x_n H_i(x_1, x_2, x_3, x_4) \\ \times \bar{\psi}(x_1)\Gamma_i^\alpha\psi(x_3)\bar{\psi}(x_2)\Gamma_{i\alpha}\psi(x_4). \quad (2.1)$$

The object Γ_i^α in Eq. 2.1 denotes Dirac, colour and isospin matrices. That the matrix combinations between the quarks at x_1 and x_3 are the same as those between x_2 and x_4 is a consequence of parity and the Lorentz, flavour and colour invariance of the action. Imposing $SU(2)_l \otimes SU(2)_r \otimes U(1)_V$ symmetry restricts certain of the possible Dirac and isospin structures to appear in the combinations

$$H_1(1 \otimes 1 + i\gamma_5\tau^a \otimes i\gamma_5\tau^a), \quad H_2(\gamma^\mu\tau^a \otimes \gamma_\mu\tau^a + \gamma^\mu\gamma_5\tau^a \otimes \gamma_\mu\gamma_5\tau^a), \\ H_5(\tau^a \otimes \tau^a + i\gamma_5 \otimes i\gamma_5), \quad H_6(\sigma_{\mu\nu} \otimes \sigma^{\mu\nu} - \sigma_{\mu\nu}\tau^a \otimes \sigma^{\mu\nu}\tau^a), \quad (2.2)$$

whilst the strengths of the following interactions are unconstrained by symmetry considerations:

$$H_3(\gamma^\mu \otimes \gamma_\mu), \quad H_4(\gamma^\mu\gamma_5 \otimes \gamma_\mu\gamma_5). \quad (2.3)$$

A wide variety of the models mentioned in Chp. 2.2 can be expressed in the above form, differing according to the ansatz taken for $\{H_i(x_1, x_2, x_3, x_4)\}$. The original NJL model, for instance, has $H_1 \sim \int d^4x \prod_n \delta(x - x_n)$ and a constant coupling strength, whereas one-gluon exchange models use $H_i \sim \delta(x_1 - x_3)\delta(x_2 - x_4)D(x_1 - x_2)$. The present approach is motivated in part by the instanton-liquid model [51]. Within the zero-mode approximation to that picture, there is a $2N_f$ -point quark interaction, which is of separable form. Recent lattice calculations offer some support for such notions [71], suggesting that instantons do indeed dominate the vacuum gluon structures and showing also the importance of the zero modes to the quark propagator. In

²In fact, this six-quark interaction had been proposed several years earlier [70], albeit on a purely phenomenological basis.

momentum space, a separable interaction is one of the form

$$H_i(p_1, p_2, p_3, p_4) = \frac{1}{2}(2\pi)^4 G_i f(p_1) f(p_2) f(p_3) f(p_4) \delta(p_1 + p_2 - p_3 - p_4). \quad (2.4)$$

In the model of Ref. [51] the function $f(p)$ has a particular form and for two flavours of quark the relation $G_1 = -G_5$ follows from the structure of the 't Hooft determinant. Also present in that model is an interaction of tensor character but it is $1/N_c$ suppressed.

The model studied here is similar to that of Dyakonov and Petrov [51], in that it is based on an interaction with the separable form (Eq. 2.4). However, a more phenomenological attitude is taken towards the form factor $f(p)$ and the allowed couplings (Eqs. 2.2 and 2.3). Only interactions in the colour-singlet channels are considered. A unit matrix in colour space is therefore assumed to be implicitly included whenever a matrix combination Γ_i^α is written. The G_1 coupling (in the ladder approximation) produces the pions and their isoscalar scalar partner, σ . Couplings in the spin-1 channels, G_2 , G_3 and G_4 , are responsible for the ρ , a_1 , ω and f_1 mesons. Including the G_5 coupling also allows the model to describe an isovector scalar and an isoscalar pseudoscalar meson. The lowest-lying meson with quantum numbers corresponding to the former is $a_0(980)$, whilst the latter is a non-strange state with the quantum numbers of the η and η' , to be referred to as η^* .

The analysis does not include the possible tensor interactions, described by the coupling G_6 . As can be seen from the following identity these can contribute in the (axial) vector channels:

$$(\bar{\psi} \sigma_{\mu\nu} \psi)^2 = \frac{2T^\nu}{q^2} (\bar{\psi} \sigma^{\mu\alpha} q_\alpha \psi \cdot \bar{\psi} \sigma_{\nu\beta} q^\beta \psi + \bar{\psi} \sigma^{\mu\alpha} \gamma_5 q_\alpha \psi \cdot \bar{\psi} \sigma_{\nu\beta} \gamma_5 q^\beta \psi), \quad (2.5)$$

q being an arbitrary four-vector and $T^{\mu\nu}$ the transverse projector,

$$T^{\mu\nu} = g^{\mu\nu} - \frac{q^\mu q^\nu}{q^2}. \quad (2.6)$$

Such couplings were discussed in Ref. [68]. They give rise to anomalous magnetic-moment couplings of the vector mesons to constituent quarks³. In the absence of any

³The piece of axial character in Eq. 2.5 would constitute an independent channel since

strong phenomenological need for such an effect these terms can be safely omitted.

For the sake of simplicity, all of the possible independent interactions are assumed to contain the same form factor, differing only through the constant coupling strengths, $\{G_i\}$. In the analytic work, no assumptions are required about the detailed behaviour⁴ of the form factor. Of course, a specific choice must be made to obtain numerical results. As in Ref. [8], the form factor is taken to be Gaussian in Euclidean space⁵,

$$f(p_E) = \exp(-p_E^2/\Lambda^2). \quad (2.7)$$

This choice was shown to be able to give quark confinement. In fact, the possibility of taking a different Λ for each of the independent couplings has also been examined⁶. Doing so does not lead to any very significant effects. This is because the main qualitative features are dominated by the form of the quark self-energy which, in the ladder approximation, depends only on the G_1 interaction.

To give a complete specification of the model, there are two additional choices which have to be made. One of them concerns an ambiguity in the transverse vector and axial currents of the model. This is a general feature of any theory with a nonlocal action. Its resolution is described in the next section. The other decision concerns the analytic continuation of amplitudes from Euclidean to Minkowski space. Numerical evaluations are performed in Euclidean space because the form factor (Eq. 2.7) is defined for Euclidean momenta. Since the quark propagator of the model contains poles at complex energies, it follows that the usual Wick rotation of the integration contour [72] is not an appropriate continuation above a certain value of the energy of an external line. Any theory of this type therefore requires an alternative continuation prescription above that energy. The method which is followed, along with further

its potential mixing with the transverse axial state vanishes in the flavour symmetric case.
⁴It is necessary only that the form factor vanishes at large Euclidean momentum so that surface terms may be discarded when integrations by parts are performed.

⁵The Euclidean conventions used are that $p^0 = ip_{4E}$ and $\underline{p} = -\underline{p}_E$, so that $pk = -(pk)_E$ and $\int d^4p = i \int d^4p_E$.

⁶Note that there are then some straightforward modifications which one must make to various of the analytic expressions to be presented.

discussion of these issues, is presented in Chp. 3.3.

2.4 Nonlocal Currents

The usual, local expressions for the vector and axial currents do not satisfy the correct continuity equations when one uses the equations of motion derived from the action of Eqs. 2.1 to 2.4. The continuity equations for these local currents contain terms which arise as a direct consequence of the nonlocality of the action. For example,

$$\begin{aligned} \frac{1}{2}\partial_\mu(\bar{\psi}(x)\gamma^\mu\psi(x)) &= -i\sum_i\int\prod_n d^4x_n H_i(x_1, x_2, x_3, x_4) \\ &\times \bar{\psi}(x_1)\Gamma_i^\alpha\psi(x_3)\bar{\psi}(x_2)\Gamma_{i\alpha}\psi(x_4) (\delta(x-x_3) - \delta(x-x_1)). \end{aligned} \quad (2.8)$$

In order to obtain symmetry currents with the same divergences as the corresponding local currents in QCD, and hence to maintain the corresponding Ward identities, one has to introduce additional, nonlocal terms into the currents. A Noether-like method of construction for these nonlocal terms was developed⁷ in Ref. [8]. The procedure consists of substituting for the differences of delta functions in equations like 2.8 according to the identity

$$\delta(x-x_1) - \delta(x-x_2) = \int_0^1 d\lambda \frac{dz^\mu}{d\lambda} \partial_\mu \delta(x-z), \quad (2.9)$$

$z(\lambda)$ being some arbitrary path from x_1 to x_2 . The right-hand side of Eq. 2.8 can then be expressed as a divergence and a suitable conserved current defined.

The divergence requirement for a current determines its longitudinal component which is, therefore, a path-independent object. In Ref.[8] the choice of path was irrelevant since the authors were interested only in the longitudinal component of the axial current, so as to determine the pion decay constant. The transverse part of a current, however, is sensitive to the particular path chosen for $z(\lambda)$. Indeed, ambiguity in the transverse current is a feature of any method used to construct a (partially) conserved current corresponding to a nonlocal action. If one wishes

⁷Some alternative, but more cumbersome, methods are also mentioned in that reference.

to consider electromagnetic processes, as in Chp. 6, then it is necessary to assume some form for the transverse current. This assumption is an additional part of the specification of the model. In subsequent calculations, the straight line ansatz [8],

$$z(\lambda) = (1 - \lambda)x_1 + \lambda x_2, \quad (2.10)$$

is used, since it respects both Lorentz and translational invariance. In practice, several of the electromagnetic observables evaluated in Chp. 6 turn out to be dominated by the local piece of the vector current and so should not be very sensitive to the choice of path.

The nonlocal terms in the currents, induced by the nonlocal nature of the action, are given by the momentum–space expressions presented below. (Note that where momentum derivatives with respect to $p_i \pm p_j$ occur, then the combination $p_i \mp p_j$ is understood to be held fixed.) In the isoscalar vector current, the nonlocal pieces are all of the structure

$$J_{(I)}^\mu = \frac{1}{(2\pi)^{12}} \sum_i G_i \int \prod_n d^4 p_n \bar{\psi}(p_1) \Gamma_i^\alpha \psi(p_3) \bar{\psi}(p_2) \Omega_{i\alpha} \psi(p_4) \\ \times \delta(p_1 + p_2 + q - p_3 - p_4) \int_0^1 d\lambda f(p_2) f(p_4) \frac{\partial}{\partial (p_1 + p_3)_\mu} f(p_1 + \lambda q) f(p_3 - q + \lambda q), \quad (2.11)$$

which is referred to as type I. The sum over $G_i(\Gamma_i^\alpha \otimes \Omega_{i\alpha})$ in Eq. 2.11 runs over the same combinations of couplings and Dirac and isospin matrices as those found in the action (Eqs. 2.2 and 2.3).

The isovector vector current also has nonlocal contributions of the type-I structure. In this case the isospin and Dirac matrices appear in the combinations⁸

$$G_1(\tau^a \otimes 1 + i\gamma_5 \otimes i\gamma_5 \tau^a), \quad G_2(\gamma^\nu \otimes \gamma_\nu \tau^a + \gamma^\nu \gamma_5 \otimes \gamma_\nu \gamma_5 \tau^a), \\ G_3(\gamma^\nu \tau^a \otimes \gamma_\nu), \quad G_4(\gamma^\nu \gamma_5 \tau^a \otimes \gamma_\nu \gamma_5), \\ G_5(1 \otimes \tau^a + i\gamma_5 \tau^a \otimes i\gamma_5), \quad G_6(\sigma_{\nu\alpha} \tau^a \otimes \sigma^{\nu\alpha} - \sigma_{\nu\alpha} \otimes \sigma^{\nu\alpha} \tau^a). \quad (2.12)$$

⁸Although the G_6 interaction will not appear in the calculations, the corresponding terms in the nonlocal currents are nonetheless stated. Note that a tensor interaction must be considered in a description of vector states at NLO in $1/N_c$, a vertex of that character being generated from the Fierz rearrangement of the other couplings (see Chp. 2.5).

Another type of nonlocal structure also arises in this current,

$$\begin{aligned}
J_{(II)}^\mu &= \frac{i\epsilon^{abc}}{2(2\pi)^{12}} \sum_i G_i \int \prod_n d^4 p_n \bar{\psi}(p_1) \Gamma_i^\alpha \tau^b \psi(p_3) \bar{\psi}(p_2) \Omega_{i\alpha} \tau^c \psi(p_4) \\
&\quad \times \int_0^1 d\lambda \left[f(p_1) f(p_2) \frac{\partial}{\partial(p_3 - p_4)_\mu} f(p_3 - q + \lambda q) f(p_4 - \lambda q) \right. \\
&\quad \left. - f(p_3) f(p_4) \frac{\partial}{\partial(p_1 - p_2)_\mu} f(p_1 + q - \lambda q) f(p_2 + \lambda q) \right] \delta(p_1 + p_2 + q - p_3 - p_4). \quad (2.13)
\end{aligned}$$

The above type-II structure contributes in those interaction channels corresponding to isovector states. The Dirac matrices appear in the combinations

$$\begin{aligned}
G_1(i\gamma_5 \otimes i\gamma_5), & \quad G_2(\gamma^\nu \otimes \gamma_\nu + \gamma^\nu \gamma_5 \otimes \gamma_\nu \gamma_5), \\
G_5(1 \otimes 1), & \quad -G_6(\sigma_{\nu\alpha} \otimes \sigma^{\nu\alpha}). \quad (2.14)
\end{aligned}$$

Turning now to the isovector axial current, the type-I terms are again present.

They involve the matrix combinations

$$\begin{aligned}
G_1\epsilon^{abc}(\tau^c \otimes i\gamma_5 \tau^b), & \quad G_2(\gamma^\nu \gamma_5 \otimes \gamma_\nu \tau^a + \gamma^\nu \otimes \gamma_\nu \gamma_5 \tau^a), \\
G_3(\gamma^\nu \gamma_5 \tau^a \otimes \gamma_\nu), & \quad G_4(\gamma^\nu \tau^a \otimes \gamma_\nu \gamma_5), \\
G_5\epsilon^{abc}(i\gamma_5 \tau^b \otimes \tau^c). & \quad iG_6\epsilon^{abc}(\sigma_{\nu\alpha} \gamma_5 \tau^c \otimes \sigma^{\nu\alpha} \tau^b). \quad (2.15)
\end{aligned}$$

There are no type-II pieces in this current, but a third kind of nonlocal structure does occur,

$$\begin{aligned}
J_{(III)}^\mu &= \frac{i}{(2\pi)^{12}} \sum_i G_i \int \prod_n d^4 p_n \bar{\psi}(p_1) \Gamma_i^\alpha \psi(p_3) \bar{\psi}(p_2) \Omega_{i\alpha} \psi(p_4) \\
&\quad \times \int_0^1 d\lambda \left[f(p_2) f(p_3) \frac{\partial}{\partial(p_1 + p_4)_\mu} f(p_1 + q - \lambda q) f(p_4 - \lambda q) \right. \\
&\quad \left. - f(p_1) f(p_4) \frac{\partial}{\partial(p_2 + p_3)_\mu} f(p_2 + \lambda q) f(p_3 - q + \lambda q) \right] \delta(p_1 + p_2 + q - p_3 - p_4). \quad (2.16)
\end{aligned}$$

The relevant terms in this case are

$$\begin{aligned}
G_1(i\gamma_5 \tau^a \otimes 1), & \quad G_2\epsilon^{abc}(\gamma^\nu \gamma_5 \tau^c \otimes \gamma_\nu \tau^b), \\
G_5(i\gamma_5 \otimes \tau^a), & \quad iG_6(\sigma^{\nu\alpha} \gamma_5 \tau^a \otimes \sigma_{\nu\alpha}). \quad (2.17)
\end{aligned}$$

It is straightforward to see that a dependence on the path variable, λ , does not appear in the longitudinal components of the currents. Since Lorentz invariance demands that the interaction form factor depends only on the square of its argument, one has, in the case of type-I contributions,

$$q_\mu \frac{\partial}{\partial(p_1 + p_3)_\mu} f(p_1 + \lambda q) f(p_3 - q + \lambda q) = \frac{1}{2} \frac{d}{d\lambda} f(p_1 + \lambda q) f(p_3 - q + \lambda q). \quad (2.18)$$

The λ integral in $q_\mu J_{(I)}^\mu$ is therefore trivial, and produces a difference in form factors. Similar results can be seen to hold for the longitudinal components of the other nonlocal structures (Eqs. 2.13 and 2.16).

Useful checks on the above expressions for the currents are provided by various Ward identities which follow from (partial) current conservation. Several of these identities are demonstrated explicitly in Chps. 4 and 6. In the case of the axial current, an extension of the arguments in Ref. [8] can be used to show that the Gell-Mann–Oakes–Renner (GMOR) relation [16] holds (Chp. 4.2). For the vector currents, checks are made that the two–point correlator of vector currents is purely transverse (Chp. 4.4), that the γqq Ward identity is satisfied (Chp. 4.3), that the pion charge is unity (Chp. 6.2), and that the low-energy theorem for the anomalous decay $\pi^0 \rightarrow \gamma\gamma$ is satisfied (Chp. 6.3).

2.5 Fierzed Interactions and Currents

When the action of Eq. 2.1 is used at leading order in the $1/N_c$ expansion the anti-quark located at x_1 is always associated with the quark at x_3 whilst the position x_2 is similarly linked to x_4 . Working with a four-quark vertex beyond LO, however, there are contributions to be included where this will no longer be the case. These are known as the Fock or “exchange” terms and may be isolated by first performing a Fierz transformation on the action. Such contributions are then easily extracted by using the Fierzed action in just the same way that one uses the original action at LO.

The Fierzed action of this model consists of the following terms:

$$\begin{aligned}
& \frac{1}{4N_c}(G_1 - 2G_3 + 2G_4 - G_5 + 12G_6) (1 \otimes 1 + i\gamma_5\tau^a \otimes i\gamma_5\tau^a), \\
& \frac{1}{4N_c}(-2G_2 + G_3 + G_4) (\gamma_\mu\tau^a \otimes \gamma^\mu\tau^a + \gamma_\mu\gamma_5\tau^a \otimes \gamma^\mu\gamma_5\tau^a), \\
& \frac{1}{4N_c}(-2G_1 + 6G_2 + G_3 + G_4 - 2G_5) (\gamma_\mu \otimes \gamma^\mu), \\
& \frac{1}{4N_c}(2G_1 + 6G_2 + G_3 + G_4 + 2G_5) (\gamma_\mu\gamma_5 \otimes \gamma^\mu\gamma_5), \\
& \frac{1}{4N_c}(-G_1 - 2G_3 + 2G_4 + G_5 - 12G_6) (\tau^a \otimes \tau^a + i\gamma_5 \otimes i\gamma_5), \\
& \frac{1}{8N_c}(G_1 - G_5 - 4G_6) (\sigma_{\mu\nu} \otimes \sigma^{\mu\nu} - \sigma_{\mu\nu}\tau^a \otimes \sigma^{\mu\nu}\tau^a). \tag{2.19}
\end{aligned}$$

The nonlocal terms in the vector and axial–vector currents of the model also involve four quark fields and so will also be subject to such effects at NLO. These Fock pieces in the currents will introduce further ambiguity through the definition of their transverse parts. One way of isolating a suitable set of terms would be simply to construct nonlocal current terms from the Fierzed action of Eq. 2.19 with exactly the same method as was described in Chp. 2.4 for deducing the nonlocal LO currents from the standard action (Eqs. 2.1 to 2.4). This method of determining the Fock terms of a current will be called the Fierzed–action method. It leads to nonlocal current structures of the same forms as those presented previously (Eqs. 2.11, 2.13 and 2.16), with the appropriate matrix insertions obtained by replacing the coupling constants in the original sets of insertions by the corresponding combinations in the Fierzed action. So, for example, the presence of the type-I term $G_1\epsilon^{abc}(\tau^c \otimes i\gamma_5\tau^b)$ in the axial current constructed from the original action implies that there is a type-I Fock term of $(4N_c)^{-1}(G_1 - 2G_3 + 2G_4 - G_5 + 12G_6)\epsilon^{abc}(\tau^c \otimes i\gamma_5\tau^b)$.

An alternative and equally obvious approach towards finding the Fock terms of the model’s currents would be just to make a Fierz transformation of the LO currents already derived. This procedure is referred to as the Fierzed–current method. Through its application one encounters new types of nonlocal structure. The Fierz transformation swaps the roles of the $\psi(p_3)$ and $\psi(p_4)$ fields. If the momenta are then

relabelled so that $p_3 \leftrightarrow p_4$, the resulting nonlocal terms will have different types of form-factor structure. It becomes convenient to define new nonlocal structure types, IV and V, as:

$$\begin{aligned}
J_{(IV)}^\mu &= \frac{1}{(2\pi)^{12}} \sum_i G_i \int \prod_n d^4 p_n \bar{\psi}(p_1) \Gamma_i^\alpha \psi(p_3) \bar{\psi}(p_2) \Omega_{i\alpha} \psi(p_4) \\
&\times \int_0^1 d\lambda \left[f(p_2) f(p_3) \frac{\partial}{\partial(p_1 + p_4)_\mu} f(p_1 + q - \lambda q) f(p_4 - \lambda q) \right. \\
&\left. + f(p_1) f(p_4) \frac{\partial}{\partial(p_2 + p_3)_\mu} f(p_2 + \lambda q) f(p_3 - q + \lambda q) \right] \delta(p_1 + p_2 + q - p_3 - p_4), \quad (2.20)
\end{aligned}$$

$$\begin{aligned}
J_{(V)}^\mu &= \frac{1}{(2\pi)^{12}} \sum_i G_i \int \prod_n d^4 p_n \bar{\psi}(p_1) \Gamma_i^\alpha \tau^a \psi(p_3) \bar{\psi}(p_2) \Omega_{i\alpha} \psi(p_4) \\
&\times \int_0^1 d\lambda \left[f(p_1) f(p_2) \frac{\partial}{\partial(p_3 - p_4)_\mu} f(p_3 - q + \lambda q) f(p_4 - \lambda q) \right. \\
&\left. + f(p_3) f(p_4) \frac{\partial}{\partial(p_1 - p_2)_\mu} f(p_1 + q - \lambda q) f(p_2 + \lambda q) \right] \delta(p_1 + p_2 + q - p_3 - p_4). \quad (2.21)
\end{aligned}$$

The matrix combinations in the type I to V currents which constitute the Fock terms within the Fierz–current method are given below.

For the Fock terms of the isoscalar vector current only the type-IV structure is relevant. Apart from an overall symmetry factor of a half, the insertions appearing in this case are just the same as those in Eq. 2.19, the Fierz–action. This result highlights the difference between the Fierz–action and Fierz–current methods of construction, which lies in the identity of the fields which one connects via the $z(\lambda)$ path (Eq. 2.9). In the Fierz–action method, one first swops the roles of the $\psi(p_3)$ and $\psi(p_4)$ fields and then connects the $\psi(p_1)$ to the $\psi(p_4)$ field, ending up with the type-I structure after relabelling. In the Fierz–current method, however, the order of operations is reversed, a path being established to link the $\psi(p_1)$ and $\psi(p_3)$ fields followed by the rearrangement which swops the roles played by $\psi(p_3)$ and $\psi(p_4)$. There can be no a priori physical reason to prefer one of these schemes over the other, since they are equally natural ways of arriving at suitable exchange currents. For purely practical reasons, however, the Fierz–action method may prove the more useful when one wishes to perform NLO calculations involving transverse currents. This is

simply because the nonlocal structure types I to III are retained, IV and V not being required. One can therefore often write down an appropriate NLO diagram very easily, merely by changing the overall coefficient in the expression for a corresponding LO diagram.

Calculation of the nonlocal Fock terms in the currents by the two methods described above does at least provide a useful check on the algebra of the Fierz transformations. The longitudinal components, of course, are dictated by continuity requirements and so should be identical in the two cases. For the isoscalar vector current such an equivalence is straightforward to verify, by noting the identity

$$q_\mu J_{(IV)}^\mu(\Gamma_i^\alpha \otimes \Omega_{i\alpha}) = q_\mu J_{(I)}^\mu(\Gamma_i^\alpha \otimes \Omega_{i\alpha}) + q_\mu J_{(I)}^\mu(\Omega_{i\alpha} \otimes \Gamma_i^\alpha). \quad (2.22)$$

The calculations of the Fock terms in the isovector currents can be similarly checked, with the aid of the following identities:

$$q_\mu j_{(II)}^\mu = -2q_\mu J_{(III)}^\mu, \quad (2.23)$$

$$q_\mu j_{(V)}^\mu(\Gamma_i^\alpha \otimes \Omega_{i\alpha}) = q_\mu J_{(I)}^\mu(\Gamma_i^\alpha \otimes \Omega_{i\alpha}) - q_\mu J_{(I)}^\mu(\Omega_{i\alpha} \otimes \Gamma_i^\alpha),$$

where $j_{(V)}^\mu$ is defined to be the nonlocal structure of type-V (Eq. 2.21) but omitting the τ^a matrix and $j_{(II)}^\mu$ is to be understood as the type-II structure (Eq. 2.13) without the matrices τ^b and τ^c and the overall factor of ϵ^{abc} .

It remains to state the Fock terms of the isovector currents within the Fierzed-current approach. In the isovector vector current, there are the following type-III terms:

$$\begin{aligned} & \frac{1}{8N_c}(G_1 + 2G_3 - 2G_4 - G_5 + 12G_6) \epsilon^{abc}(\tau^b \otimes \tau^c), \\ & \frac{1}{8N_c}(-G_1 + 2G_3 - 2G_4 + G_5 - 12G_6) \epsilon^{abc}(i\gamma_5\tau^b \otimes i\gamma_5\tau^c), \\ & \frac{1}{8N_c}(2G_2 - G_3 - G_4) \epsilon^{abc}(\gamma_\nu\tau^b \otimes \gamma^\nu\tau^c + \gamma_\nu\gamma_5\tau^b \otimes \gamma^\nu\gamma_5\tau^c), \\ & \frac{1}{16N_c}(G_1 - G_5 - 4G_6) \epsilon^{abc}(\sigma_{\nu\alpha}\tau^b \otimes \sigma^{\nu\alpha}\tau^c), \end{aligned} \quad (2.24)$$

together with the type-IV terms

$$\begin{aligned}
& \frac{1}{2N_c}(-G_3 + G_4) (\tau^a \otimes 1 + i\gamma_5 \tau^a \otimes i\gamma_5), \\
& \frac{1}{4N_c}(-G_1 + 2G_2 + G_3 + G_4 - G_5) (\gamma_\nu \tau^a \otimes \gamma^\nu), \\
& \frac{1}{4N_c}(G_1 + 2G_2 + G_3 + G_4 + G_5) (\gamma_\nu \gamma_5 \tau^a \otimes \gamma^\nu \gamma_5),
\end{aligned} \tag{2.25}$$

and the type-V insertions

$$\begin{aligned}
& \frac{1}{4N_c}(G_1 - G_5 + 12G_6) (1 \otimes 1 - i\gamma_5 \otimes i\gamma_5), \\
& \frac{1}{4N_c}(-G_1 + 4G_2 - G_5) (\gamma_\nu \otimes \gamma^\nu), \\
& \frac{1}{4N_c}(G_1 + 4G_2 + G_5) (\gamma_\nu \gamma_5 \otimes \gamma^\nu \gamma_5), \\
& \frac{1}{8N_c}(G_1 - G_5 - 4G_6) (\sigma_{\nu\alpha} \otimes \sigma^{\nu\alpha}).
\end{aligned} \tag{2.26}$$

The Fock terms of the isovector axial current include insertions into the type-I structure,

$$\begin{aligned}
& \frac{1}{4N_c}(G_1 - G_5 + 12G_6) \epsilon^{abc} (\tau^c \otimes i\gamma_5 \tau^b + i\gamma_5 \tau^c \otimes \tau^b), \\
& \frac{1}{4N_c}(G_1 - 4G_2 + G_5) (\gamma_\nu \otimes \gamma^\nu \gamma_5 \tau^a - \gamma_\nu \gamma_5 \tau^a \otimes \gamma^\nu), \\
& \frac{1}{4N_c}(G_1 + 4G_2 + G_5) (\gamma_\nu \tau^a \otimes \gamma^\nu \gamma_5 - \gamma_\nu \gamma_5 \otimes \gamma^\nu), \\
& \frac{i}{8N_c}(-G_1 + G_5 + 4G_6) \epsilon^{abc} (\sigma_{\nu\alpha} \gamma_5 \tau^b \otimes \sigma^{\nu\alpha} \tau^c),
\end{aligned} \tag{2.27}$$

along with pieces of type-III structure,

$$\begin{aligned}
& \frac{1}{4N_c}(G_1 - 2G_3 + 2G_4 - G_5 + 12G_6) (i\gamma_5 \tau^a \otimes 1), \\
& \frac{1}{4N_c}(G_1 + 2G_3 - 2G_4 - G_5 + 12G_6) (\tau^a \otimes i\gamma_5), \\
& \frac{1}{4N_c}(2G_2 - G_3 - G_4) \epsilon^{abc} (\gamma_\nu \gamma_5 \tau^b \otimes \gamma^\nu \tau^c), \\
& \frac{i}{8N_c}(G_1 - G_5 - 4G_6) (\sigma_{\nu\alpha} \gamma_5 \tau^a \otimes \sigma^{\nu\alpha}),
\end{aligned} \tag{2.28}$$

and the following type-IV terms:

$$\begin{aligned}
& \frac{1}{2N_c} (-G_3 + G_4) \epsilon^{abc} (i\gamma_5 \tau^b \otimes \tau^c), \\
& \frac{1}{4N_c} (G_1 + G_2 + G_3 + G_4 + G_5) (\gamma_\nu \tau^a \otimes \gamma^\nu \gamma_5), \\
& \frac{1}{4N_c} (-G_1 + G_2 + G_3 + G_4 - G_5) (\gamma_\nu \otimes \gamma^\nu \gamma_5 \tau^a).
\end{aligned} \tag{2.29}$$

Chapter 3

Quark and Meson Propagators

3.1 Quark Propagator

An essential ingredient of the calculations with the extended nonlocal NJL model is the dressed quark propagator. It is constructed by means of the corresponding Schwinger–Dyson equation (SDE). Initially at least, this equation is treated in the ladder approximation, truncating the one-quark irreducible kernel with just the tree-level interaction. This is equivalent to working at leading order (LO) in a $1/N_c$ expansion. In order to define such an expansion for a model based on four-quark interaction vertices, the coupling constants must be designated as quantities of some particular order in N_c . In the $1/N_c$ expansion of QCD [2, 73], the large N_c limit is defined by allowing the number of colours to tend to infinity but with the product $g^2 N_c$ being held constant. Setting $\{G_i\}$ to be of order N_c^{-1} is therefore consistent with the interpretation that the four-quark interaction is generated through one gluon exchange. There is, however, no need to appeal to that prejudice. Sufficient justification for adopting this choice for the order of $\{G_i\}$ is that it is necessary in order to produce the same large N_c scaling of observables (such as the meson masses and couplings) as in QCD.

Fig. 3.1 gives an illustration of the diagrams that are summed in the ladder approximation. In terms of a momentum-dependent quark “mass” $m(p)$ defined from

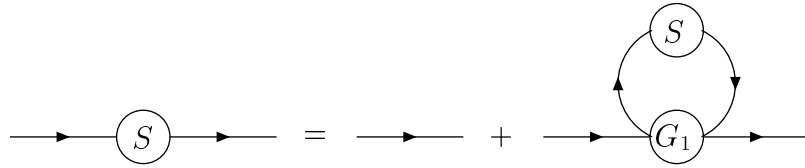


Figure 3.1: The Schwinger–Dyson equation for the quark propagator in the ladder approximation.

the dressed quark propagator by

$$S^{-1}(p) = \not{p} - m(p), \quad (3.1)$$

the LO SDE can be written as

$$m(p) = m_c + iG_1 f^2(p) \text{Tr} \int \frac{d^4 k}{(2\pi)^4} \frac{\not{k} + m(k)}{k^2 - m^2(k)} f^2(k). \quad (3.2)$$

The dressing at this order occurs only through the interaction in the isoscalar scalar channel, as described by the coupling G_1 . The integral in Eq. 3.2 is very similar to that appearing in the quark condensate (defined in Eq. 1.3), differing only through the presence of the interaction form factors, $f^2(k)$. In the original NJL model there are no such form factors and so the condensate and SDE integrals are identical. With both the local and nonlocal models, however, it is clear that the dynamical generation of a quark mass is intimately connected to the appearance of a non-zero condensate¹. In the numerical treatment of the model, loop integrals like that in Eq. 3.2 are evaluated in Euclidean space, since the form factor has been defined for Euclidean momenta. Physical results are then obtained by analytically continuing back to Minkowski space.

Notice that the separable nature of the interaction produces a great simplification since the dependence on the external momentum p factorizes out of the loop integral.

¹It is possible *in principle* with a nonlocal model to have a dynamical quark mass without producing a non-zero condensate. For this to occur in a separable model $f^2(k)$ would have to change sign at some point, a situation that is hardly physically plausible.

The solution to the LO SDE can therefore be written in the form

$$m(p) = m_c + (m(0) - m_c)f^2(p). \quad (3.3)$$

Hence to obtain the full LO quark propagator it is necessary to determine only the constant $m(0)$. This can be done straightforwardly using iterative methods. In practice it is convenient to use Eq. 3.2 to determine the parameter G_1 for a given value of $m_0(0)$, the zero-momentum quark mass in the chiral limit. This requires a single integral to be evaluated. With the choice of a Gaussian form factor, the Gauss–Laguerre technique (taking p_E^2 as the non-trivial integration variable) is eminently suitable for performing such integrals, which converge with only a moderate number of abscissae. If a non-zero current quark mass is introduced, it is a simple matter to iterate from $m_0(0)$ to find the solution for $m(0)$.

The denominator of the quark propagator, $p^2 - m^2(p^2)$, does not have a zero at positive (Minkowski) p^2 if $m(0)$ is sufficiently large². This property provides a sufficient, although not strictly a necessary [5, 74], condition for confinement. Although there are still poles in the quark propagator, they are shifted into the complex p^2 plane. Such behaviour is by no means uncommon in models of quark confinement based on the solution of a Schwinger–Dyson equation [5, 63, 75, 76] in the ladder approximation. Because of the simplifications due to the separable interaction, the present model provides a convenient setting in which to investigate some of the practical implications of this mechanism for confinement. As pointed out by Lee and Wick [77] (see also Ref. [78]), particles which have a complex mass of this type should not be admitted as asymptotic states if one is to have a unitary S-matrix. When amplitudes have been defined in Euclidean space, the prescription for analytically continuing them back to Minkowski space must respect this requirement, as described in more detail in Chp. 3.3.

²The absence of a pole at a spacelike momentum, which would indicate tachyonic behaviour, is guaranteed if the running quark mass is always positive (i.e., if the interaction form factor is real).

3.2 Meson Propagators

The meson masses and vertex functions are found using the Bethe–Salpeter equation (BSE). This can be considered in its homogeneous or inhomogeneous form. As is usual in studies of NJL-like models, it is dealt with here in the framework of the latter, which provides a normalization for the on-shell vertex function. In order to maintain Ward identities [79] one must use a truncation scheme which is consistent with that applied to the SDE (Chp. 3.1). In the case of the BSE, the ladder approximation entails keeping just the tree-level couplings from the action in the two-quark irreducible scattering kernel. The separable nature of the interaction allows the $\bar{q}q$ scattering matrix, T , to be written in the form

$$T(p_1, p_2, p_3, p_4) = \prod_n f(p_n) \delta(p_1 + p_2 - p_3 - p_4) \hat{T}(q), \quad (3.4)$$

where the total momentum of the $\bar{q}q$ pair is denoted by $q = p_1 - p_3 = p_4 - p_2$. The LO BSE, shown schematically in Fig. 3.2, may be conveniently expressed in terms of \hat{T} as

$$\hat{T}(q) = G + GJ(q)\hat{T}(q), \quad (3.5)$$

where G is simply a matrix of the coupling constants from the action (Eqs. 2.1 to 2.4) and $J(q)$ is composed of the loop integrals

$$J_{ij}(q) = i\text{Tr} \int \frac{d^4p}{(2\pi)^4} f^2(p_+) f^2(p_-) \Gamma_i S(p_-) \Gamma_j S(p_+). \quad (3.6)$$

In the above equation the notation $p_{\pm} = p \pm \frac{1}{2}q$ has been introduced. The quark propagators to be used in Eq. 3.6 are the dressed propagators obtained by solving the ladder SDE.

The mesonic bound states are located at the poles of \hat{T} . These can be determined from the equation

$$\det(1 - GJ(q)) = 0. \quad (3.7)$$

Symmetry restrictions on the possible form of the interactions mean that the matrix G is diagonal with respect to flavour and Lorentz structures. The full scattering

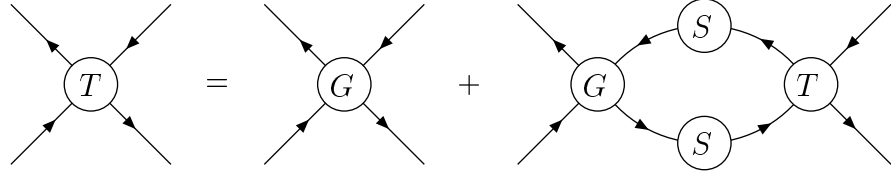


Figure 3.2: The Bethe–Salpeter equation for $\bar{q}q$ scattering in the ladder approximation.

matrix, however, is only block–diagonal, since there may be certain non-zero off-diagonal elements of J . In particular there is a non-vanishing loop integral which leads to mixing between the pseudoscalar and longitudinal axial channels. This πa_1 (and $\eta^* f_1$) mixing is an example of the partial Higgs mechanism that is discussed in Appendix C.3 in relation to effective Lagrangians of π, ρ and a_1 mesons. It produces an axial as well as a pseudoscalar component in the vertex function of the pion (and η^*). In the flavour symmetric case there is no analogous mixing between the scalar and vector channels. This can be seen from the fact that the integrand in the corresponding element of J (Eq. 3.6) is odd under $p \rightarrow -p$. The absence of such a potential mixing means that the longitudinal vector channel is quite independent of the scalar one. It is therefore important to check numerically that a pole does not develop in the former channel, since that would be unphysical.

For later ease of reference, the various non-zero elements of J are labelled as follows for the Dirac matrices inserted:

$$\begin{aligned}
 J_{SS} &: 1 \otimes 1, & J_{VV}^T &: T_{\mu\nu}(\gamma^\mu \otimes \gamma^\nu), & J_{VV}^L &: q^{-2}(-i\not{q} \otimes i\not{q}), \\
 J_{PP} &: i\gamma_5 \otimes i\gamma_5, & J_{AP} &: m_\pi^{-1}(-i\not{q}\gamma_5 \otimes i\gamma_5), & J_{PA} &: m_\pi^{-1}(i\gamma_5 \otimes i\not{q}\gamma_5), \\
 J_{AA}^T &: T_{\mu\nu}(\gamma^\mu\gamma_5 \otimes \gamma^\nu\gamma_5), & J_{AA}^L &: m_\pi^{-2}(-i\not{q}\gamma_5 \otimes i\not{q}\gamma_5), & &
 \end{aligned} \tag{3.8}$$

where $T_{\mu\nu}$ is the transverse projector defined in Eq. 2.6. Working in the above basis the mixing elements are equal, $J_{AP} = J_{PA}$.

To describe the coupling of an on-shell meson to constituent quarks one represents

the relevant channel of \hat{T} , near to the corresponding pole position, as

$$\frac{\bar{V}(q) \otimes V(q)}{m^2 - q^2}, \quad (3.9)$$

where $V(q)$ and $\bar{V}(q)$ are referred to as the vertex functions for the meson in the initial and final states respectively. In the above expression any polarization indices have been suppressed. The homogeneous BSE is written in terms of such vertex functions and is only satisfied at an on-shell point. Off mass shell any decomposition into vertex and propagator which one might make in a channel of \hat{T} becomes purely a matter of convenience — the off-shell vertex function and meson propagator are not themselves well defined, only the combination occurring in \hat{T} being meaningful. From the homogeneous BSE the relationship between the vertex functions of the initial and final states can be found³, $\bar{V} = \gamma^0 V^\dagger \gamma^0$. For the particles of interest, these functions are:

$$\begin{aligned} V_\pi(q) &= (g_{\pi qq} - m_\pi^{-1} \tilde{g}_{\pi qq} \not{q}) i \gamma_5 \tau^a, & V_\sigma(q) &= g_{\sigma qq}, \\ V_{\rho s}(q) &= g_{\rho qq} \not{q}_s \tau^a, & V_{a_1 s}(q) &= g_{a_1 qq} \not{q}_s \gamma_5 \tau^a, & V_{\omega s}(q) &= g_{\omega qq} \not{q}_s, \\ V_{\eta^*}(q) &= (g_{\eta^* qq} - m_{\eta^*}^{-1} \tilde{g}_{\eta^* qq} \not{q}) i \gamma_5, & V_{a_0}(q) &= g_{a_0 qq} \tau^a. \end{aligned} \quad (3.10)$$

For all particles except the pseudoscalars there is no mixing, and so each has a single coupling constant $g_{i qq}$ to describe its on-shell coupling to quarks. These couplings are related to the corresponding loop integrals (Eq. 3.6) by

$$\frac{1}{g_{i qq}^2} = (-1)^S \left. \frac{dJ_{ii}}{dq^2} \right|_{q^2=m^2}, \quad (3.11)$$

where S is the spin of the meson. The couplings of the pion to quarks, $g_{\pi qq}$ and $\tilde{g}_{\pi qq}$, are given by

$$g_{\pi qq}^2 = -G_1 \frac{(1 - G_2 J_{AA}^L(m^2))}{D'_\pi(m^2)}, \quad g_{\pi qq} \tilde{g}_{\pi qq} = \frac{G_1 G_2 J_{PA}(m^2)}{D'_\pi(m^2)}, \quad (3.12)$$

³See, for example, Ref. [55] where the authors work initially with a general interaction kernel for fermion–anti-fermion scattering.

where the prime indicates a derivative with respect to q^2 and the pseudoscalar–axial determinant $D_\pi(q^2)$ is defined to be

$$D_\pi(q^2) = (1 - G_1 J_{PP}(q^2))(1 - G_2 J_{AA}^L(q^2)) - G_1 G_2 J_{AP}^2(q^2). \quad (3.13)$$

Similar expressions hold for the couplings of the η^* , with G_5 and G_4 playing the roles of G_1 and G_2 respectively.

3.3 Loop Integrals

When expressed in Euclidean space, the loop integrals appearing in the ladder BSE (Eq. 3.6) take the form

$$J_{ij}(q^2) = -N_c N_f \int \frac{d^4 p}{(2\pi)^4} \frac{f^2(p_+) f^2(p_-) t_{ij}(p^2, q^2, p \cdot q)}{(p_+^2 + m_+^2)(p_-^2 + m_-^2)}, \quad (3.14)$$

where t_{ij} is the appropriate Dirac trace and all momenta are to be understood as Euclidean. The symbols m_\pm are introduced here as a shorthand for the quark mass evaluated at p_\pm . Consider such an integral evaluated at some timelike momentum, $q = (\underline{0}, iq_0)$. Operating with a confining parameter set, each quark propagator considered as a function of energy has four poles at complex energies corresponding to a pair of complex–conjugate poles in p^2 . As q_0 is increased these poles in $S(p_\pm)$ are translated parallel to the imaginary p_4 axis. For any given value of $|\underline{p}|$, there is a value of q_0 for which poles of the p_- and p_+ quark propagators meet on the real p_4 axis, pinching the contour of integration. For larger values of q_0 the poles cross this axis and may contribute an imaginary part to the propagator in the meson channel, depending on the prescription used to continue the integral beyond the pinch point. Such a configuration of the poles is shown in Fig. 3.3.

The usual prescription for an analytic continuation of amplitudes from Euclidean to Minkowski space is based on a Wick rotation of the integration contour [72]. This procedure would indeed give rise to an imaginary part of the meson propagator, corresponding physically to the opening of a threshold for the decay of a meson into other states. As was explained in Chp. 3.1 that situation is inappropriate here.

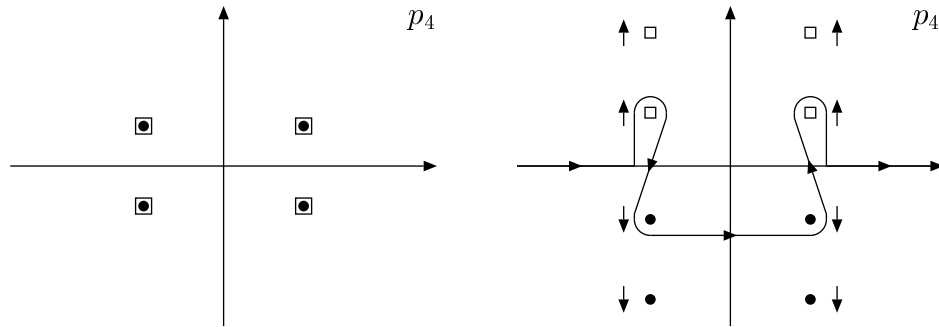


Figure 3.3: The pole structure of J loop integrals in the p_4 plane. On the left-hand side of the figure, the pole positions at $q_0 = 0$ are indicated. The open boxes denote the poles of the p_- propagator and the filled circles those of the p_+ propagator. The right-hand side of the figure shows the deformed integration contour, beyond the pinch point. The arrows here indicate the directions in which the poles move as q_0 increases.

A legitimate continuation, suitable for energies where the integration contour becomes pinched, was originally suggested by Cutkosky *et al* [78]. It amounts to the deformation of the integration contour displayed in Fig. 3.3. Whilst the prescription ensures that the resulting meson propagator does not develop an unphysical imaginary part above the pseudo-threshold energy where the contour becomes pinched by the complex poles, it does mean that the propagator cannot be analytically continued past that point. Since the method is not unique, the choice of continuation prescription must be regarded as an additional assumption that forms part of the specification of any model with a quark propagator of this type. The suggestion of Cutkosky *et al.* is adopted in the present calculations having been shown in Ref. [78] to be consistent with the requirements of unitarity and macrocausality.

As discussed by both Cutkosky *et al.* [78] and Lee and Wick [77], microcausality violations can occur in models with a Euclidean metric and states of complex mass. However, in order for such violations to be measurable, Lee and Wick [77] have estimated that one would need to create a wave packet of width $\ll \gamma^{-1}$, where the complex mass is $M + \frac{1}{2}i\gamma$. In any event, microcausality in this model is intrinsically broken by the use of an action with nonlocal interactions.

In the numerical evaluations of quark loop integrals, one can take a contour in p_4

that runs along the real axis. For energies $|q_0|$ above the pseudo-threshold, following the prescription of Cutkosky *et al.* means that one must also include contributions from the residues of the poles that have crossed the axis. For a given external energy these contributions are required at zero three-momentum up to a maximum value at the pinch point. At larger three-momenta the integration contour in the p_4 plane is just the real axis. Both the naive integral over Euclidean four-momentum in Eq. 3.14 and the residue contributions diverge at the pinch point, although these divergences cancel to leave a finite result [78]. This cancellation occurs at the level of the integrated result rather than at all values of three-momentum flowing round the loop. In numerical work one therefore needs to regulate the two contributions when evaluating them separately. An accurate knowledge of the locations of the poles in the quark propagator (and hence of the pinch point) is clearly a prerequisite of any regulating method. It can be efficiently acquired by applying the simplex technique [80] to minimize the modulus of $p_E^2 + m_0^2(p_E)$.

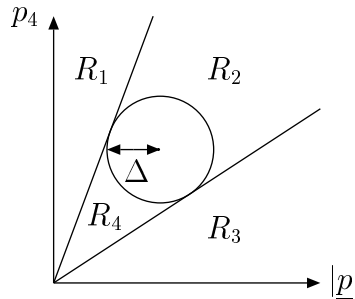


Figure 3.4: In evaluating the naive integral over Euclidean momenta the integration region is divided as in the figure, the pinch point being at the centre of the circle. The situation for negative values of p_4 is obtained by a reflection in the $|p|$ axis.

The method of regularization actually used involves dividing the region of integration as shown in Fig. 3.4. A function with the same divergence as the naive integral is subtracted from it when p lies within a radius Δ of the pinch point. The remainder is then integrated over the circular region according to the robust method of Sag and Szekeres [81]. A similar function is used to cancel the divergent part of the residue

contribution when $|\underline{p}|$ is less than Δ from its pinch value and is chosen to cancel exactly with the piece that has been cut out of the naive integral. Both the regulated and unregulated parts of the $|\underline{p}|$ integral over the residue contributions are evaluated with the NAG routine D01AJF. This routine uses an adaptive strategy, concentrating its efforts over any regions where the integrand behaves poorly. Since the regulated integrands are necessarily the difference of two large numbers the decision to use robust methods is one dictated by safety considerations.

The other integrations required in the evaluation of J are of the naive integrand over the regions labelled $R_1 \dots R_4$ in Fig. 3.4. The semi-infinite range of integration in $R_1 \dots R_3$ together with the particular form factor chosen (Eq. 2.7) strongly suggests that these regions be dealt with in terms of p_E^2 and an angular variable, integration over the former being performed using the Gauss–Laguerre technique. The angular parts of these integrals are treated adaptively, which proves to be useful in R_2 owing to the shape of that region near to the angular limits. Integration over R_4 is done with the NAG routine D01FDF which transforms the region onto a circle and then uses the Sag and Szekeres method.

Each of the numerical integrations that are summed to give the value of $J(q)$ depends on the regularizing parameter Δ . An important check on the regularization used (and on the accuracy of the integration routines themselves) is that the overall results obtained should be independent of Δ . This does indeed prove to be the case for a wide range of values, although the results become somewhat less accurate when Δ is small ($\lesssim 20$ MeV). At small Δ the contributions from $R_1 \dots R_3$ are dominant. However, these are difficult to evaluate accurately if they include some of the area close to the pinch point, in which the integrand may be badly behaved. A good description of the offending area requires many local integrand evaluations, a procedure which is not well-suited to the Gauss–Laguerre routines. In practice, the accuracy of evaluating $J(q)$ is found to be best with $\Delta \sim 150$ MeV.

It should be noted that the quark propagator of the nonlocal model has in fact

many complex-conjugate pairs of poles. Such an analytic structure is also found in the pion propagator of the NJL model within the proper time regularization scheme [82]. In the present model these additional poles occur with both confining and non-confining parameter sets and are found at large momenta. Since their positions depend on the detailed behaviour of the form factor for large momenta, they are regarded here as being unphysical artifacts of the model. With the parameter sets selected for the calculations that are detailed in Chps. 5 and 6, the next set of poles would result in another pseudo-threshold at energies of ~ 2 GeV. The model is not intended to be credible at such momenta. Indeed, in Chp. 5.1 a more stringent upper limit is imposed on the range of applicability of the model. Hence, the extra poles do not pose a practical problem.

Chapter 4

Ward Identities and Electromagnetism

4.1 Couplings to the Axial Current

The electromagnetic or weak decay constant of a meson is given by the matrix element between the vacuum and that meson of the appropriate current. In a nonlocal model of the type considered here, there are contributions to such matrix elements arising from both the usual local current and the nonlocal pieces discussed in Chp. 2.4. Both of these must be included in order to maintain related Ward identities, which follow from current conservation. The contributions from the nonlocal part of the current are generated by closing one of the $\bar{\psi}\Gamma\psi$ structures in on itself and using the other to forge the link to the meson. The corresponding diagrams are shown in Fig. 4.1.

Consider for example the pion decay constant, defined through Eq. 1.5. The loop integral arising from the local part of the axial current is very similar to J_{AP} , except that only two (rather than four) form factors are present. One must also include a nonlocal contribution generated by the $G_1(i\gamma_5\tau^a \otimes 1)$ term with type-III structure (Eq. 2.16) in the axial current. As was described by Bowler and Birse [8], this diagram can be written as a sum of terms, each of which factorizes into two loop integrals. One

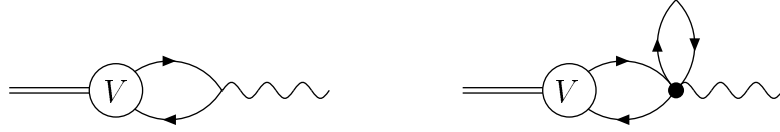


Figure 4.1: Coupling of a particle to an external current. V denotes the particle's vertex function (Eq. 3.9).

of these is somewhat similar to that in the scalar quark condensate, whilst the other has a pseudoscalar insertion and a pion vertex function. It is convenient to refer to the loop integrals involved as being one-quark or two-quark, according to the number of quark propagators they contain. The contribution of this diagram to f_π is

$$\begin{aligned} & \frac{iG_1}{2m_\pi^2} \int \frac{d^4k}{(2\pi)^4} \frac{\text{Tr}[\mathbf{k} + m(k^2)]}{k^2 - m^2(k^2)} \int \frac{d^4p}{(2\pi)^4} \frac{\text{Tr}V_\pi(q)(\not{p}_- + m_-)\gamma_5\tau^a(\not{p}_+ + m_+)}{(p_+^2 - m_+^2)(p_-^2 - m_-^2)} \\ & \times f(p_+)f(p_-) \left[f^2(k) \left(f^2(p_+) + f^2(p_-) \right) - f(p_+)f(p_-)f(k) \left(f(k+q) + f(k-q) \right) \right]. \quad (4.1) \end{aligned}$$

In the extended version of the model there is another nonlocal contribution, which is induced by the term $G_2(\gamma^\nu \otimes \gamma_\nu \gamma_5 \tau^a)$ with type-I structure (Eq. 2.11) in the axial current. In this case, the one-quark loop has a vector insertion. Although the vacuum expectation value of $\bar{\psi}\gamma^\nu\psi$ vanishes by Lorentz invariance, a non-zero integral is produced by a combination of form factors which is anti-symmetric in the loop momentum. The contribution of the diagram to f_π is

$$\begin{aligned} & \frac{-iG_2}{2m_\pi^2} \int \frac{d^4k}{(2\pi)^4} \frac{\text{Tr}\gamma^\nu[\mathbf{k} + m(k^2)]}{k^2 - m^2(k^2)} f(k) \left(f(k+q) - f(k-q) \right) \\ & \times \int \frac{d^4p}{(2\pi)^4} \frac{\text{Tr}V_\pi(q)(\not{p}_- + m_-)\gamma_\nu\gamma_5\tau^a(\not{p}_+ + m_+)}{(p_+^2 - m_+^2)(p_-^2 - m_-^2)} f^2(p_+)f^2(p_-). \quad (4.2) \end{aligned}$$

These pieces of f_π arising from the nonlocal current are significant numerically and are needed in order to satisfy the Gell-Mann–Oakes–Renner relation, as demonstrated in the next section.

In the numerical evaluation of integrals like those in Eqs. 4.1 and 4.2, there are two non-trivial integration variables. When the external energy lies below the pseudo-threshold (see Chp. 3.3), the Gauss–Laguerre technique enables such integrals to be performed quickly and accurately. The integration variables used in such routines are p_4^2 and \underline{p}^2 , with p_4 having been defined to be in the direction of q .

A determination of the coupling strength of the a_1 particle to the transverse axial current requires the calculation of diagrams very similar to those concerning f_π . The contributing terms from the nonlocal current are also those relevant to the a_1 case. There is, however, an important difference from the analogous nonlocal diagrams for f_π in that the integral over the path variable λ for the transverse current is non-trivial. In general therefore, a numerical integration over λ is also required. In practice though, with a Gaussian form factor (Eq. 2.7), such integrals can be performed analytically, being expressed in terms of error functions. In the type-I nonlocal structure (Eq. 2.11), λ appears only in the form factors associated with one of the loops. Hence, a diagram induced by a term of this structure is the product of two separate loop integrals. This is not so for contributions induced by type-II (Eq. 2.13) or type-III (Eq. 2.16) terms in the current, where the integrals for the one- and two-quark loops do not factorize.

For those diagrams generated by a type-I term, the numerical situation is that of a product of two two-dimensional integrals, the integrand of one containing the analytically-derived combination of error functions. If the external energy is below pseudo-threshold then these integrals are performed by Gauss–Laguerre methods as above. Otherwise they must be computed with residue contributions included, as discussed in Chp. 3.3. The diagrams generated by type-II or type-III terms in the nonlocal transverse current have a coupled-integral structure. Using the analytical result for the λ integration then necessitates a four-dimensional numerical integral. It therefore becomes more efficient to treat the λ integral numerically. At each value of λ , the integrand is a product of two two-dimensional integrals each of which can be dealt with in the usual fashion. The λ integration is itself straightforward since the

integrands that have been considered vary only very slowly in this variable.

4.2 GMOR Relation

The GMOR relation (Eq. 1.7) was shown to hold at LO in Ref. [8], where a version of the model was used which had only the G_1 coupling. In this section the proof is extended to allow for the other possible couplings in the action (Eqs. 2.2 and 2.3), again at LO. When the model is considered at NLO (Chp. 7), the corrections introduced are also shown to be consistent with the GMOR relation. As a trailer for some of the arguments and cancellations invoked in that case, the much simpler LO proof with only the G_1 coupling is revisited below. The method differs from that of Ref. [8], being based on the identity

$$\not{q}\gamma_5 = S^{-1}(p_+)\gamma_5 + \gamma_5 S^{-1}(p_-) + (m_+ + m_-)\gamma_5. \quad (4.3)$$

Taking the diagram for the coupling of the pion to the local axial current and contracting it with q_μ gives an expression for its contribution to $f_\pi m_\pi^2$. The local current gives rise to a factor of $\not{q}\gamma_5$ which can be replaced by the right-hand side of Eq. 4.3 to give

$$if_\pi m_\pi^2 = \frac{g_{\pi qq}}{2} N_c N_f \left[\int \frac{d^4 p}{(2\pi)^4} f(p_+) f(p_-) (m_+ + m_-) \text{tr} \gamma_5 S(p_-) \gamma_5 S(p_+) \right. \\ \left. + \int \frac{d^4 p}{(2\pi)^4} f(p) (f(p+q) + f(p-q)) \text{tr} S(p) \right], \quad (4.4)$$

where, in the absence of mixing, $g_{\pi qq}$ is determined from Eq. 3.11. In the nonlocal contribution to the decay constant (Eq. 4.1), the ladder SDE (Eq. 3.2) simplifies the piece which has a factor of $f^2(k)$ since it allows one to replace G_1 times the k loop by $-i(m(0) - m_c)$. A cancellation can then be seen to operate between this piece and the first of the integrals in Eq. 4.4, leaving only $2m_c$ from the factor of $(m_+ + m_-)$ that appears in Eq. 4.4. It is just this process of cancellation between a local-current diagram and part of a nonlocal contribution which is so useful in the analysis of the

more complex diagrams at NLO. Recalling the definition of J_{PP} (Eqs. 3.6 and 3.8) in order to simplify the remaining part of Eq. 4.1, one has

$$if_{\pi}m_{\pi}^2 = m_c g_{\pi qq} N_c N_f \int \frac{d^4 p}{(2\pi)^4} f(p_+) f(p_-) \text{tr} \gamma_5 S(p_-) \gamma_5 S(p_+) \\ + \frac{g_{\pi qq}}{2} N_c N_f (1 - G_1 J_{PP}(q)) \int \frac{d^4 p}{(2\pi)^4} f(p) (f(p+q) + f(p-q)) \text{tr} S(p). \quad (4.5)$$

To deduce the GMOR relation now requires only the chiral expansion of $J_{PP}(q)$. It is straightforward to verify the result¹ of Bowler and Birse that

$$1 - G_1 J_{PP}(q) = -G_1 m_c \frac{\langle \bar{\psi} \psi \rangle_0}{m_0(0)^2} - G_1 \frac{q^2}{Z_{\pi 0}} + \mathcal{O}(q^4, m_c^2), \quad (4.6)$$

where Z_{π} is defined as $g_{\pi qq}^2(G_2 = 0)$. An explicit expression for Z_{π} in the chiral limit was originally presented in Ref. [8] and is:

$$Z_{\pi 0}^{-1} = \frac{2N_c N_f}{m_0(0)^2} \int \frac{d^4 p_E}{(2\pi)^4} \frac{m_0(p_E)^2 - m'_0(p_E) m_0(p_E) p_E^2 + (m'_0(p_E))^2 p_E^4}{[p_E^2 + m_0(p_E)^2]^2}, \quad (4.7)$$

a prime denoting differentiation with respect to the square of the momentum argument. Substituting the expansion of Eq. 4.6 into Eq. 4.5 and evaluating the integrals in the chiral limit one arrives at

$$f_{\pi 0} = \frac{m_0(0)}{g_{\pi qq 0}}, \quad (4.8)$$

which is the equivalent of the Goldberger–Treiman relation [83] in the model. Using this relation in Eq. 4.6, which is set equal to zero at the pion pole, produces the GMOR relation.

The pion mass and decay constant are altered by mixing with the longitudinal axial–vector component of the G_2 interaction (see Chp. 3.2). The above proof is now developed to incorporate those effects, the other couplings in the extended model having no impact at LO.

To calculate the pion mass at leading order in the current quark mass, the pion determinant (Eq. 3.13) must be expanded up to first order in m_c and q^2 . Expanding the J_{AP} and J_{AA}^L integrals appropriately gives

$$J_{PA} = \sqrt{q^2} \left(I_6 - \frac{1}{2} \tilde{I}_6 \right) + \dots,$$

¹Note that the ladder SDE is called upon to obtain the expression quoted.

$$J_{AA}^L = \frac{-1}{2G_1} + \frac{3I_8}{2} + \dots, \quad (4.9)$$

where the dots refer to irrelevant higher-order terms and the following integrals have been defined:

$$\begin{aligned} I_n &= 4N_c N_f \int \frac{d^4 p_E}{(2\pi)^4} \frac{f^4(p_E) m_0^{\left(\frac{n}{2}-2\right)}(p_E)}{[p_E^2 + m_0^2(p_E)]^2}, \\ \tilde{I}_6 &= 4N_c N_f \int \frac{d^4 p_E}{(2\pi)^4} \frac{f^4(p_E) p_E^2 m_0'(p_E)}{[p_E^2 + m_0^2(p_E)]^2}. \end{aligned} \quad (4.10)$$

By substituting the chiral expansions of Eqs. 4.6 and 4.9 into the pion determinant one finds that

$$m_\pi^2 = -\frac{m_c X}{m_0(0)^2} \langle \bar{\psi} \psi \rangle_0, \quad (4.11)$$

where X is

$$X = \left(1 + \frac{G_2}{2G_1} - \frac{3G_2 I_8}{2}\right) \left[G_2 \left(I_6 - \frac{1}{2} \tilde{I}_6 \right)^2 + \frac{1}{Z_{\pi 0}} \left(1 + \frac{G_2}{2G_1} - \frac{3G_2 I_8}{2}\right) \right]^{-1}. \quad (4.12)$$

The GMOR relation will therefore be satisfied by the extended model under the condition

$$f_{\pi 0}^2 = \frac{m_0(0)^2}{X}. \quad (4.13)$$

Now, if one uses the expansions of the J integrals in the definitions of $g_{\pi qq}$ and $\tilde{g}_{\pi qq}$ (Eq. 3.12) then, at leading order in the chiral expansion, these couplings to quarks are found to be

$$g_{\pi qq 0}^2 = X, \quad \frac{\tilde{g}_{\pi qq}}{g_{\pi qq 0}} = \frac{G_2 m_\pi \left(I_6 - \frac{1}{2} \tilde{I}_6 \right)}{\left(1 + \frac{G_2}{2G_1} - \frac{3G_2 I_8}{2}\right)} + \dots \quad (4.14)$$

Notice that since $g_{\pi qq 0}^2 = X$, the condition of Eq. 4.13 is simply the modified Goldberger-Treiman relation in the extended model.

The calculation of f_π in the extended model can profitably be decomposed into two parts. The first consists simply of the same contributions as when $G_2 = 0$, although allowing for the change in the $g_{\pi qq}$ coupling. In the remaining part a factor of $\tilde{g}_{\pi qq}$ is extracted, so that

$$f_\pi = \frac{g_{\pi qq}}{\sqrt{Z_\pi}} f_\pi|_{G_2=0} + \tilde{g}_{\pi qq} l. \quad (4.15)$$

Using Eq. 4.8 for f_{π_0} at $G_2 = 0$ together with Eqs. 4.12, 4.14 and 4.15, the Goldberger–Treiman condition may be rewritten as

$$l = \frac{m_0(0)}{Z_{\pi_0}} \frac{g_{\pi qq_0}}{\tilde{g}_{\pi qq}} \left(\frac{Z_{\pi_0}}{X} - 1 \right) + \dots \quad (4.16)$$

$$= \frac{m_0(0)}{m_\pi} \left(I_6 - \frac{1}{2} \tilde{I}_6 \right) + \dots \quad (4.17)$$

Finally, it is necessary to make an explicit calculation of l , at leading order in the chiral expansion, from those additional contributions to f_π which are generated by non-zero G_2 . Considering the diagrams already present without the G_2 interaction, such contributions come from the extra covariant in the pion vertex function. From the coupling of the pion to the local axial current one obtains

$$l_{\text{loc}} = \frac{1}{m_\pi} \left[\frac{\langle \bar{\psi} \psi \rangle_0}{4m_0(0)} + \frac{3}{4} I_6 m_0(0) \right]. \quad (4.18)$$

There is also a similar contribution originating from the two-loop diagram where the one-quark loop has a scalar insertion (Eq. 4.1). However, this contribution turns out to be sub-leading in the chiral expansion. The remainder of l comes from the entirety of the nonlocal diagram given in Eq. 4.2. With the assistance of Eq. 4.14 the first term in its chiral expansion is found to be

$$l_{\text{non-loc}} = \frac{-1}{m_\pi} \left[\frac{\langle \bar{\psi} \psi \rangle_0}{4m_0(0)} - \frac{1}{4} I_6 m_0(0) + \frac{1}{2} \tilde{I}_6 m_0(0) \right]. \quad (4.19)$$

Adding together Eqs. 4.18 and 4.19 does indeed produce the expression on the right-hand side of the condition of Eq. 4.17, thereby establishing the proof.

4.3 Couplings to the Vector Current

The couplings controlling the electromagnetic decays of the vector mesons can be calculated in a similar manner to the pion decay constant, discussed in Chp. 4.1 above. Again the nonlocal contributions are numerically important and are essential if related Ward identities are to be satisfied. An example of such an identity is presented in Chp. 4.4 below, where the correlator of two vector currents is shown to be purely

transverse. There is, however, an alternative approach towards calculating the couplings to the vector mesons. One can instead work with a general formulation of the dressed γqq vertex in the model. That vertex is described in some detail in this section since it is a necessary ingredient in the calculation of many other electromagnetic observables.

Since the coupling of dressed quarks to the photon is unknown² one is obliged to take some ansatz for it in order to calculate electromagnetic processes. A popular scheme in the literature [85, 86, 87], sometimes called the impulse approximation, involves a dressed γqq vertex only, neglecting irreducible couplings of the photon to more than two quarks. The γqq vertex itself is chosen to be of the Ball-Chiu [88] form, the chief virtue of which is that it is a simple solution of the Ward–Takahashi identity

$$q^\mu \Gamma_\mu(p, q) = S_F^{-1}(p_+) - S_F^{-1}(p_-), \quad (4.20)$$

where q is the photon momentum flowing away from the vertex, Γ_μ , and p is the momentum flowing through the vertex. (The isospin structure has been suppressed here.) For a quark propagator without wavefunction renormalization the Ball-Chiu vertex is

$$\Gamma^\mu = \gamma^\mu + \frac{p^\mu}{(p \cdot q)}(m_- - m_+). \quad (4.21)$$

With the nonlocal NJL model studied here, use of the impulse approximation does not provide an appropriate prescription for the calculation of electromagnetic observables. For example, as is discussed in Chp. 6.2, it would not produce the correctly-normalized value of the pion charge. In this model, the electromagnetic couplings are completely specified once a particular ansatz has been chosen for the nonlocal part of the vector current. The uncertainty inherent in the construction of the transverse part of the current is discussed in Chp. 2.4. Despite this, gross features of the nonlocal current would remain unchanged with different path ansatze.

The various pieces of the full γqq vertex within the treatment of the extended

²Although some numerical work on a BSE for the γqq vertex has been attempted by Frank [84].

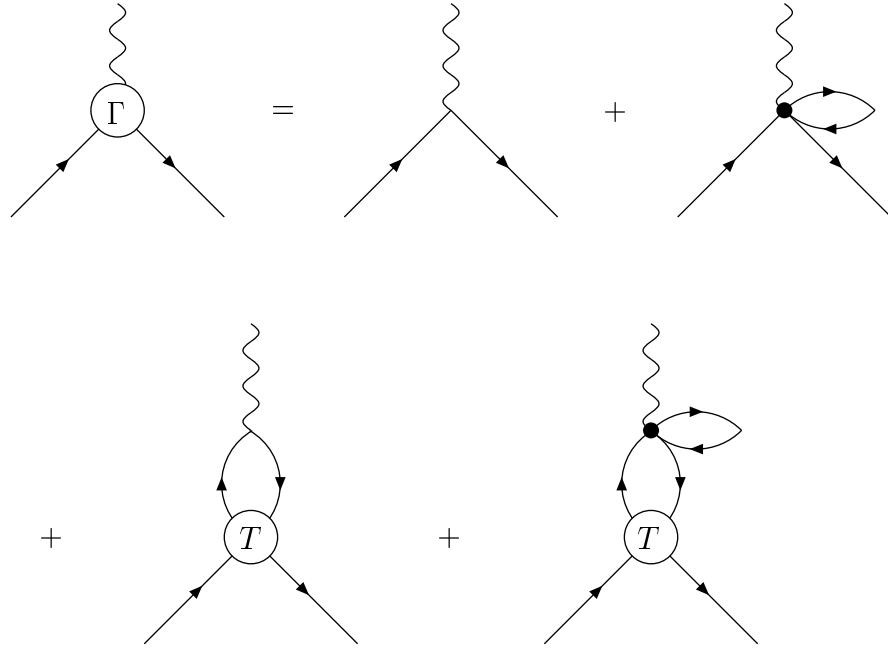


Figure 4.2: The dressed γqq vertex. T denotes the $\bar{q}q$ scattering matrix in either the transverse or longitudinal vector channel.

nonlocal NJL model are shown diagrammatically in Fig. 4.2. From the local current, there is simply a contribution to Γ_μ of the usual form, γ_μ . The nonlocal current induces contributions where there is a closed one-quark loop, similar to those appearing in the pion decay constant and described in Chp. 4.1. In the electromagnetic case, the diagram where the closed loop has a scalar insertion can be simplified by using the ladder SDE (Eq. 3.2) to express it as

$$-(m(0) - m_c) \int_0^1 d\lambda \frac{\partial}{\partial p^\mu} f^2(p + (\lambda - \frac{1}{2})q). \quad (4.22)$$

Together with the local contribution, this would constitute the full vertex in a version of the model without vector mesons. Since the Ward–Takahashi identity of Eq. 4.20 imposes an important constraint on the form of the vertex it should be verified in the present approach. To do so, one uses the following identity, which is a special case of

Eq. 2.18:

$$q^\mu \frac{\partial}{\partial p^\mu} f^2\left(p + \left(\lambda - \frac{1}{2}\right)q\right) = \frac{d}{d\lambda} f^2\left(p + \left(\lambda - \frac{1}{2}\right)q\right). \quad (4.23)$$

The λ integral involved in $q^\mu \Gamma_\mu$ is then seen to be trivial, and hence the Ward identity is indeed satisfied by the sum of γ^μ and Eq. 4.22.

In the extended model, with vector-meson degrees of freedom, there is another contribution to Γ_μ that involves a one-quark loop. This has a vector insertion and is given by

$$-i\gamma_\nu f(p_-)f(p_+)G_2N_cN_f \int \frac{d^4k}{(2\pi)^4} \frac{4k^\nu}{k^2 - m^2(k^2)} \int_0^1 d\lambda \frac{\partial}{\partial k^\mu} f(k-q+\lambda q)f(k+\lambda q). \quad (4.24)$$

In addition, there are pieces which contain the propagator of an intermediate $\bar{q}q$ state in the vector channels. As is illustrated in the final two graphs of Fig. 4.2, the propagation of such intermediates is described by the T matrix of the ladder BSE (Eq. 3.5), which may be coupled to the vector current via local or nonlocal loops. The contribution to Γ_μ from the longitudinal channel is

$$\begin{aligned} & i\frac{\not{q}}{q^2} f(p_-)f(p_+) \frac{G_2N_cN_f}{1 - G_2J_{VV}^L(q)} \int \frac{d^4k}{(2\pi)^4} \frac{f(k_-)f(k_+)}{(k_-^2 - m_-^2)(k_+^2 - m_+^2)} \\ & \quad \times \text{tr}\tilde{\Gamma}_\mu(k, q)(\not{k}_- + m_-)\not{q}(\not{k}_+ + m_+), \end{aligned} \quad (4.25)$$

while the transverse channel gives

$$\begin{aligned} & i\left(\gamma^\nu - \frac{q^\nu \not{q}}{q^2}\right) f(p_-)f(p_+) \frac{G_2N_cN_f}{1 - G_2J_{VV}^T(q)} \int \frac{d^4k}{(2\pi)^4} \frac{f(k_-)f(k_+)}{(k_-^2 - m_-^2)(k_+^2 - m_+^2)} \\ & \quad \times \text{tr}\tilde{\Gamma}_\mu(k, q)(\not{k}_- + m_-)\gamma_\nu(\not{k}_+ + m_+), \end{aligned} \quad (4.26)$$

where $\tilde{\Gamma}_\mu(k, q)$ is the two-quark-irreducible γqq vertex consisting of the sum of γ_μ and Eqs. 4.22 and 4.24. In these expressions, m_\pm denotes the quark mass evaluated at k_\pm .

To check that the additional contributions in the extended version of the model (Eqs. 4.24 to 4.26) remain consistent with the Ward identity for the vertex, note first that the quark propagator is unchanged. Hence, the sum of the local piece and Eq. 4.22 still saturates the identity. In the contribution of the expression 4.24 to $q^\mu \Gamma_\mu$, Eq. 2.18

enables the integration over the path variable to be performed. This part of $q^\mu \Gamma_\mu$ is then

$$-i \frac{\not{q}}{q^2} f(p_-) f(p_+) G_2 N_c N_f \int \frac{d^4 k}{(2\pi)^4} \frac{4q \cdot k}{k^2 - m^2(k^2)} f(k) (f(k+q) - f(k-q)). \quad (4.27)$$

The purely transverse piece in Eq. 4.26, which involves a propagating ρ meson, is obviously irrelevant in the Ward identity. Thus cancellation must occur between Eq. 4.27 and the piece coming from Eq. 4.25. To demonstrate this explicitly, one needs the result for $q^\mu \tilde{\Gamma}_\mu$. This is given by the sum of Eq. 4.27 and the expression on the right-hand side of Eq. 4.20. Using this fact, the contribution to $q^\mu \Gamma_\mu$ from the longitudinal $\bar{q}q$ intermediate states (Eq. 4.25) can be expressed as

$$i \frac{\not{q}}{q^2} f(p_+) f(p_-) \left[\int \frac{d^4 k}{(2\pi)^4} \frac{\text{tr}(\not{q} + m_- - m_+) (\not{k}_- + m_-) \not{q} (\not{k}_+ + m_+)}{(k_+^2 - m_+^2)(k_-^2 - m_-^2)} f(k_+) f(k_-) \right. \\ \left. - G_2 J_{VV}^L(q) \int \frac{d^4 k}{(2\pi)^4} \frac{4q \cdot k}{k^2 - m^2(k^2)} f(k) (f(k+q) - f(k-q)) \right] \frac{G_2 N_c N_f}{1 - G_2 J_{VV}^L(q)}. \quad (4.28)$$

The Dirac trace in the first line of the above expression may be written as

$$4(q \cdot k_-)(k_+^2 - m_+^2) - 4(q \cdot k_+)(k_-^2 - m_-^2). \quad (4.29)$$

Hence, in each of the resulting terms of Eq. 4.29, one of the factors $k_\pm^2 - m_\pm^2$ can be cancelled with the denominator of the integral. Shifting the integration variable from k to k_\pm as appropriate, then the first integral inside the square brackets of Eq. 4.28 may be cast into the same form as the second, demonstrating the required cancellation.

Note that the above discussion of vector-meson contributions to the dressed γqq vertex has referred to the presence of the G_2 coupling in the isovector interaction channel. The results in the isoscalar channel are completely analogous, with the replacement of G_2 by G_3 .

For the purpose of practical calculations, it is convenient to collect together the various contributions to the vertex into the following form:

$$\begin{aligned}\Gamma_\mu(p, q) &= \gamma_\mu Q + \left(\gamma_\mu - \frac{q_\mu \not{q}}{q^2} \right) f(p_-) f(p_+) B(q^2) \\ &\quad - 2Q \int_0^1 d\lambda (p + (\lambda - \frac{1}{2})q)_\mu m'(p + (\lambda - \frac{1}{2})q),\end{aligned}\quad (4.30)$$

where the prime denotes a derivative with respect to the square of the momentum argument and the flavour structure is reinstated by using the charge matrix $Q = \frac{1}{2}(\tau^3 + \frac{1}{3})$. The function $B(q^2)$ accounts for the presence of vector mesons in the model and is given by

$$B(q^2) = \frac{1}{2} \left(\tau^3 B_2(q^2) + \frac{1}{3} B_3(q^2) \right), \quad (4.31)$$

where the functions $B_i(q^2)$ are:

$$\begin{aligned}B_i(q^2) &= \left\{ \frac{1}{1 - G_i J_{VV}^T(q^2)} \right\} \left\{ A_i(q^2) + iG_i N_c N_f \int \frac{d^4 k}{(2\pi)^4} \frac{f(k_-) f(k_+)}{(k_-^2 - m_-^2)(k_+^2 - m_+^2)} \right. \\ &\quad \times \left[\left(4m_- m_+ - 4k^2 + q^2 + \frac{8}{3} \left(k^2 - \frac{(q \cdot k)^2}{q^2} \right) \right) \right. \\ &\quad \left. \left. - \frac{8}{3} (m_+ + m_-) \left(k^2 - \frac{(q \cdot k)^2}{q^2} \right) \int_0^1 d\lambda m'(k + (\lambda - \frac{1}{2})q) \right] \right\},\end{aligned}\quad (4.32)$$

and the $A_i(q^2)$ in the above equation originate from the one-quark loop with a vector insertion and are given by

$$\begin{aligned}A_i(q^2) &= -\frac{8i}{3} G_i N_c N_f \int \frac{d^4 k}{(2\pi)^4} \frac{k^2 - (q \cdot k)^2 / q^2}{k^2 - m^2(k^2)} \\ &\quad \times \int_0^1 d\lambda \left(f'(k + \lambda q) f(k - q + \lambda q) + f(k + \lambda q) f'(k - q + \lambda q) \right).\end{aligned}\quad (4.33)$$

Writing $A_i(q^2)$ and $B_i(q^2)$ in Euclidean space and then performing an integration by parts in Eq. 4.33, one finds that $B_i(0) = 0$. This is simply a consequence of the differential form of the vertex Ward identity, Eq. 4.20,

$$\Gamma_\mu(p, 0) = Q \frac{\partial}{\partial p^\mu} S_F^{-1}(p). \quad (4.34)$$

Hence, in processes where the photon is on-shell, the $\gamma q q$ vertex is unchanged by the existence of vector-meson degrees of freedom in the model.

Returning to the issue of coupling an on-shell vector meson to the vector current, the amplitude can be calculated from a quark loop linking the meson vertex function to that part of the γqq vertex which does not include the contribution from the propagating transverse vector channel (Eq. 4.26). Attempting to include that piece of the vertex would cause the amplitude to diverge. Diagrammatically, it would merely amount to the addition of another bubble onto the vector–meson chain (see Fig. 7.3). Since the expression 4.26 is purely transverse, the Ward identity for the vertex still holds.

4.4 Vector–Current Correlator

This section presents a proof that the model satisfies a Ward identity requiring the correlator of a vector current with an arbitrary current, J , to be purely transverse. The diagrams to be considered are analogous to those discussed in Chps. 4.2 and 4.3 regarding the coupling of a meson to the vector or axial current. The proof constitutes a further useful test of the general procedure for the couplings of currents, as well as providing a check on the result for the nonlocal vector current constructed in Chp. 2.4. Suppressing any Dirac or isospin indices that might be associated with J , the correlator is defined as:

$$\Pi_\mu^a(q) = i \int d^4x e^{iqx} \langle 0 | T \{ V_\mu^a(x) J(0) \} | 0 \rangle, \quad (4.35)$$

with vector–current conservation implying the Ward identity

$$q^\mu \Pi_\mu^a = 0. \quad (4.36)$$

In the analysis that follows, use of the isovector vector current is assumed when writing the expressions, and so J must also be of isovector character to obtain a non-zero correlator. In the isoscalar case, one proceeds in exactly the same way but with all τ matrices set to unity and with the coupling constant G_2 replaced by G_3 .

The diagrams relevant to the correlator are shown in Fig. 4.3. The first diagram appearing in that figure shows a two-quark loop which couples J to the local part of

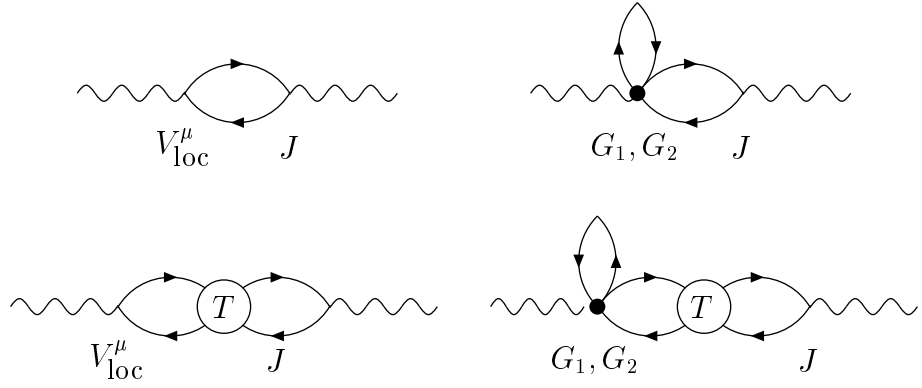


Figure 4.3: Diagrams contributing to the vector–current correlator.

the vector current. It makes the following contribution to $q^\mu \Pi_\mu^a(q)$:

$$\frac{i}{2} \int \frac{d^4 p}{(2\pi)^4} \frac{\text{Tr} \not{q} \tau^a (\not{p}_- + m_-) \Gamma_J (\not{p}_+ + m_+)}{(p_-^2 - m_-^2)(p_+^2 - m_+^2)}. \quad (4.37)$$

In writing the above expression, Γ_J has been used to represent the matrix insertion into the loop due to the J current. Note that it has components in the flavour, colour and Dirac spaces.

The second diagram in Fig. 4.3 shows the direct coupling of J to nonlocal terms in the vector current. A diagram of this form is generated by the $G_1(\tau^a \otimes 1)$ type-I term (Eq. 2.12) in the current and contributes the following to $q^\mu \Pi_\mu^a(q)$:

$$\begin{aligned} \frac{G_1}{2} \int \frac{d^4 k}{(2\pi)^4} \frac{\text{Tr} (\not{k} + m(k^2))}{k^2 - m^2(k^2)} f^2(k) \int \frac{d^4 p}{(2\pi)^4} \frac{\text{Tr} \tau^a (\not{p}_- + m_-) \Gamma_J (\not{p}_+ + m_+)}{(p_-^2 - m_-^2)(p_+^2 - m_+^2)} \\ \times (f^2(p_+) - f^2(p_-)). \end{aligned} \quad (4.38)$$

The expressions given in Eqs. 4.37 and 4.38 are the only LO contributions in a version of the model which has just the G_1 coupling. They should therefore cancel with each other, since the Ward identity of Eq. 4.36 must hold in that version. The Dirac trace in Eq. 4.37 may be simplified with the help of the identity

$$\not{q} = (\not{p}_+ - m_+) - (\not{p}_- - m_-) + (m_+ - m_-). \quad (4.39)$$

Each of the first two terms on the right–hand side of Eq. 4.39 enables one to cancel a factor of a quark propagator in the corresponding integrals. On translating the

integration variables, the resulting contributions from these two terms can be seen to cancel with each other. Furthermore, since the k integral of Eq. 4.38 is known from the ladder SDE (Eq. 3.2), the sum of Eqs. 4.37 and 4.38 becomes

$$\begin{aligned} & \frac{i}{2} \int \frac{d^4 p}{(2\pi)^4} \frac{\text{Tr} \tau^a (\not{p}_- + m_-) \Gamma_J (\not{p}_+ + m_+)}{(p_-^2 - m_-^2)(p_+^2 - m_+^2)} (m_+ - m_-) \\ & - \frac{i}{2} (m(0) - m_c) \int \frac{d^4 p}{(2\pi)^4} \frac{\text{Tr} \tau^a (\not{p}_- + m_-) \Gamma_J (\not{p}_+ + m_+)}{(p_-^2 - m_-^2)(p_+^2 - m_+^2)} (f^2(p_+) - f^2(p_-)) \end{aligned} \quad (4.40)$$

which is zero, as required.

If an interaction in the vector channel, G_2 , is included in the model then there are additional diagrams involved in the correlator. One such diagram is similar to that of Eq. 4.38 but with a vector rather than a scalar insertion into the one-quark loop. It is generated by the $G_2(\gamma^\nu \otimes \gamma_\nu \tau^a)$ type-I term in the vector current. The other additional diagrams (see Fig. 4.3) involve intermediate vector states, described by the T matrix of the ladder BSE. When the intermediate $\bar{q}q$ state is connected to the local part of the vector current it produces a contribution to $q^\mu \Pi_\mu^a(q)$ of

$$\begin{aligned} & \frac{-1}{2q^2} \frac{G_2}{1 - G_2 J_{VV}^L(q)} \int \frac{d^4 p}{(2\pi)^4} \frac{\text{Tr} \not{q} \tau^a (\not{p}_- + m_-) \not{q} \tau^b (\not{p}_+ + m_+)}{(p_-^2 - m_-^2)(p_+^2 - m_+^2)} f(p_+) f(p_-) \\ & \times \int \frac{d^4 k}{(2\pi)^4} \frac{\text{Tr} \not{q} \tau^b (\not{k}_- + m(k_-)) \Gamma_J (\not{k}_+ + m(k_+))}{(k_-^2 - m^2(k_-))(k_+^2 - m^2(k_+))} f(k_+) f(k_-). \end{aligned} \quad (4.41)$$

The integral over p in the above expression may be rewritten by substituting from Eq. 4.39 for the \not{q} insertion coming from the contraction of q^μ and the local current (i.e., the insertion associated with the isospin matrix τ^a). One then obtains

$$\begin{aligned} & \frac{-1}{2q^2} \frac{G_2}{1 - G_2 J_{VV}^L(q)} \int \frac{d^4 k}{(2\pi)^4} \frac{\text{Tr} \not{q} \tau^b (\not{k}_- + m(k_-)) \Gamma_J (\not{k}_+ + m(k_+))}{(k_-^2 - m^2(k_-))(k_+^2 - m^2(k_+))} f(k_+) f(k_-) \\ & \times \left\{ \int \frac{d^4 p}{(2\pi)^4} \frac{\text{Tr} \tau^a (\not{p}_- + m_-) \not{q} \tau^b (\not{p}_+ + m_+)}{(p_-^2 - m_-^2)(p_+^2 - m_+^2)} f(p_+) f(p_-) (m_+ - m_-) \right. \\ & \left. + \int \frac{d^4 p}{(2\pi)^4} \frac{\text{Tr} \tau^a \not{q} \tau^b (\not{p} + m(p^2))}{p^2 - m^2(p^2)} f(p) (f(p+q) - f(p-q)) \right\}. \end{aligned} \quad (4.42)$$

Consider now the diagram which is generated by the nonlocal $G_1(\tau^a \otimes 1)$ type-I term and has an intermediate longitudinal vector state. This diagram cancels the contribution coming from the first of the p integrals in the expression 4.42. The origin of

that piece was the term $m_+ - m_-$ in the \not{q} identity used in writing Eq. 4.42. Hence, this process of cancellation between a nonlocal diagram with a scalar insertion and an analogous local-current diagram is identical to the one described above which operates between Eqs. 4.37 and 4.38.

Taking stock, there remains a piece from Eq. 4.42 as well as the two diagrams induced by the nonlocal type-I structure $G_2(\gamma^\nu \otimes \gamma_\nu \tau^a)$. These diagrams contribute the following to $q^\mu \Pi_\mu^a(q)$:

$$\begin{aligned} & \frac{G_2}{2q^2} \int \frac{d^4 p}{(2\pi)^4} \frac{\text{Tr} \not{q}(\not{p} + m(p^2))}{p^2 - m^2(p^2)} f(p) (f(p+q) - f(p-q)) \\ & \times \int \frac{d^4 k}{(2\pi)^4} \frac{\text{Tr} \not{q} \tau^a (\not{k}_- + m(k_-)) \Gamma_J (\not{k}_+ + m(k_+))}{(k_-^2 - m^2(k_-))(k_+^2 - m^2(k_+))} f(k_-) f(k_+) \end{aligned} \quad (4.43)$$

and:

$$\begin{aligned} & \frac{iG_2}{2(q^2)^2} \frac{G_2}{1 - G_2 J_{VV}^L(q)} \int \frac{d^4 p}{(2\pi)^4} \frac{\text{Tr} \not{q}(\not{p} + m(p^2))}{p^2 - m^2(p^2)} f(p) (f(p+q) - f(p-q)) \\ & \times \int \frac{d^4 \ell}{(2\pi)^4} \frac{\text{Tr} \not{q} \tau^a (\not{\ell}_- + m(\ell_-)) \not{q} \tau^b (\not{\ell}_+ + m(\ell_+))}{(\ell_-^2 - m^2(\ell_-))(\ell_+^2 - m^2(\ell_+))} f^2(\ell_-) f^2(\ell_+) \\ & \times \int \frac{d^4 k}{(2\pi)^4} \frac{\text{Tr} \not{q} \tau^b (\not{k}_- + m(k_-)) \Gamma_J (\not{k}_+ + m(k_+))}{(k_-^2 - m^2(k_-))(k_+^2 - m^2(k_+))} f(k_-) f(k_+). \end{aligned} \quad (4.44)$$

Using the fact that the ℓ integral in Eq. 4.44 is by definition (Eqs. 3.6 and 3.8) just

$$-i\delta^{ab} q^2 J_{VV}^L(q), \quad (4.45)$$

the sum of Eqs. 4.43 and 4.44 can be seen to cancel with the remaining piece of Eq. 4.42, thereby completing the proof.

Chapter 5

Numerical Results — Hadronic

5.1 Numerical Fits

The nonlocal extended NJL model, as defined in Chp. 2, has seven parameters which must be fixed from experimental information. They are: the current quark mass (m_c), the range of the form factor (Λ) and five interaction coupling constants. Considering first the couplings G_1 and G_2 only, the quantities chosen for fitting the model parameters are $m_\pi = 140$ MeV, $f_\pi = 93$ MeV and $m_\rho = 770$ MeV. At LO, these quantities do not depend on the remaining three couplings. This leaves one parameter undetermined which may be used to characterize each of several parameter sets investigated. This parameter is taken to be $m_0(0)$, the zero-momentum quark mass obtained in the chiral limit of the ladder SDE (Eq. 3.2).

The above approach to fixing the parameters is convenient in that it can be performed with a reasonably straightforward fitting procedure. One begins by selecting the desired value for the chiral quark mass and guessing the values of Λ and m_c . From the chiral limit of the ladder SDE, the G_1 coupling is immediately deduced. The current quark mass can then be introduced into the SDE which is solved by iteration to obtain $m(0)$. G_2 is calculated as the inverse of $J_{VV}^T(m_\rho^2)$ (see Eq. 3.7) whereupon all of the relevant model parameters are established in order for f_π and m_π to be found. Λ

and m_c are then adjusted and the process repeated until the correct pion observables are produced.

Once a fit parameter set has been determined from the above prescription then the remaining three couplings may be fixed independently to reproduce the mass of the corresponding meson: G_3 is set by requiring $m_\omega = 783$ MeV; G_4 by $m_{f_1} = 1282$ MeV; and G_5 by $m_{a_0} = 982$ MeV. The meson masses are given by Eq. 3.7, whilst f_π is set by the coupling of the pion to the axial current (Eq. 1.5) and is calculated as described in Chp. 4.1. The contributions to f_π from the nonlocal part of the current are significant: the scalar and vector loop pieces described in that chapter accounting respectively for $\sim 35\%$ and $\sim -10\%$ of the total value.

In terms of $m_0(0)$, the possible fits have a restricted range. Having a coupling strong enough to realize confinement requires that $m_0(0) \gtrsim 270$ MeV. Below that value, the model should only be used up to an energy corresponding to the appearance of the $\bar{q}q$ continuum at twice the value of the (purely real) quark pole. In fact only a very limited range of non-confining sets are possible because the empirical masses of the vector mesons are located in this continuum for $m_0(0) \lesssim 250$ MeV.

An upper limit on the acceptable values for $m_0(0)$ is imposed by the behaviour of the meson propagators above the pseudo-threshold energy (Chp. 3.3). The dramatic changes in behaviour which can occur beyond this point may be seen in Figs. 5.1 and 5.2, where the denominators of the propagators in various scattering channels are plotted for a fit parameter set with $m_0(0) = 300$ MeV (set C of Table 5.1).

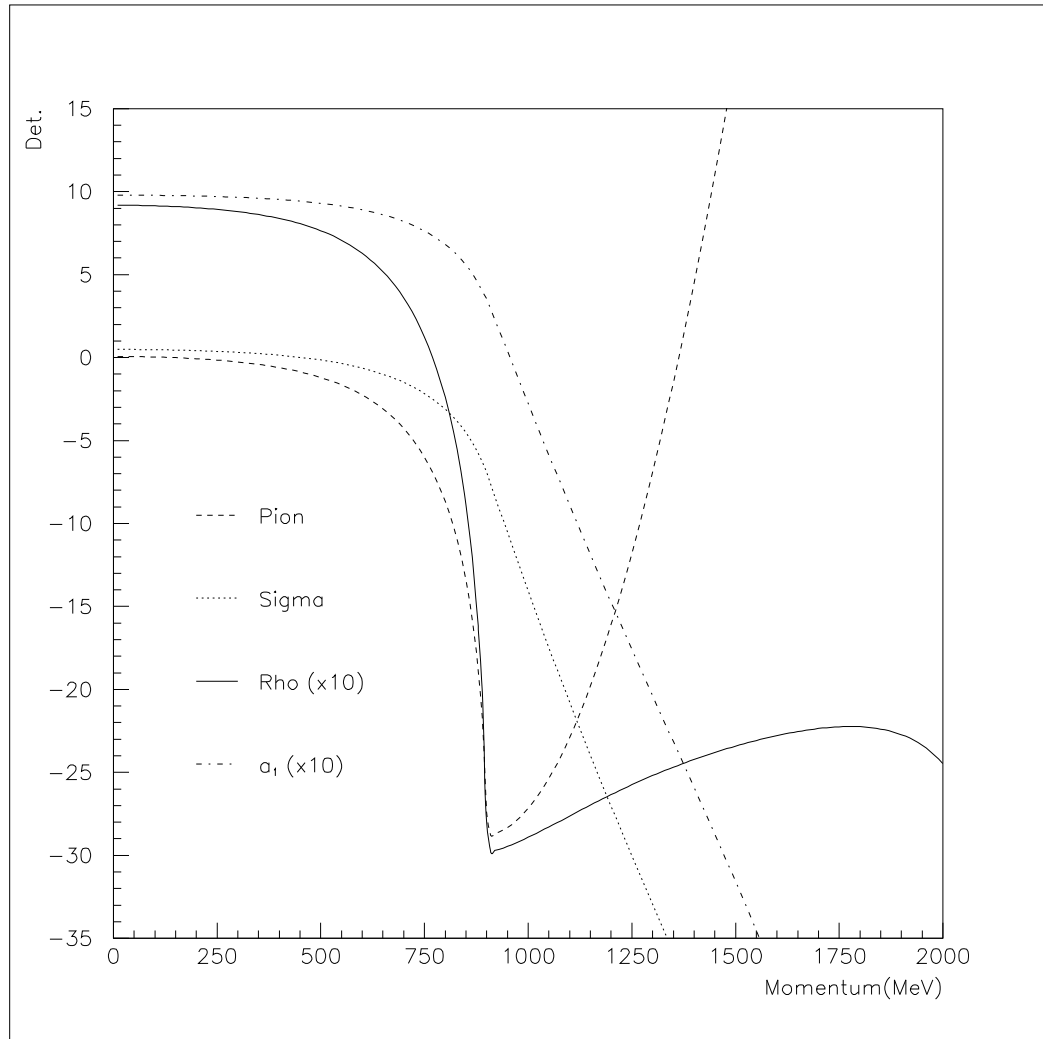


Figure 5.1: The figure shows the denominator of the propagator in the sigma channel, $1 - G_1 J_{SS}$, along with the pion determinant defined in Eq. 3.13, as functions of timelike meson momentum. Also displayed are the denominators of the ρ and a_1 propagators, $1 - G_2 J_{VV,AA}^T$, scaled by a factor of 10.

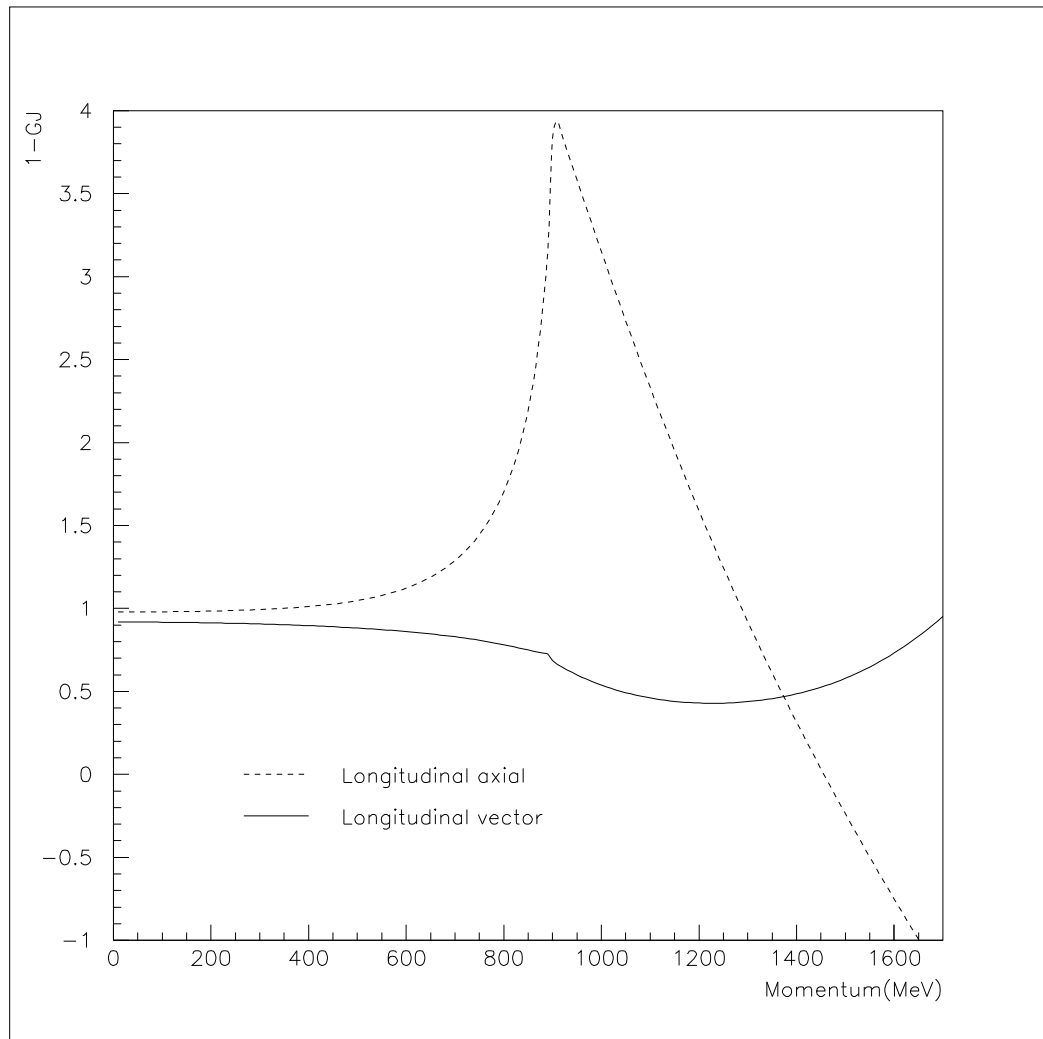


Figure 5.2: The figure shows the denominators of the propagators in the longitudinal channels, $1 - G_2 J_{VV,AA}^L$, as functions of timelike meson momentum.

With the parameters used to draw Figs. 5.1 and 5.2, the pseudo–threshold occurs at an energy of 895 MeV. At larger values of $m_0(0)$ this energy decreases. As suggested by the behaviour in Fig. 5.1, for large enough $m_0(0)$ two additional poles appear in the transverse–vector channel above the ρ pole. Such a situation is shown in Fig. 5.3. The first of these extra poles has a residue of the wrong sign to describe a physical particle. Although one might be willing to consider parameter sets with the extra poles, provided that they lie well above the energies of interest, in practice this is possible only for values of $m_0(0)$ within a very narrow range¹, ~ 320 to 330 MeV.

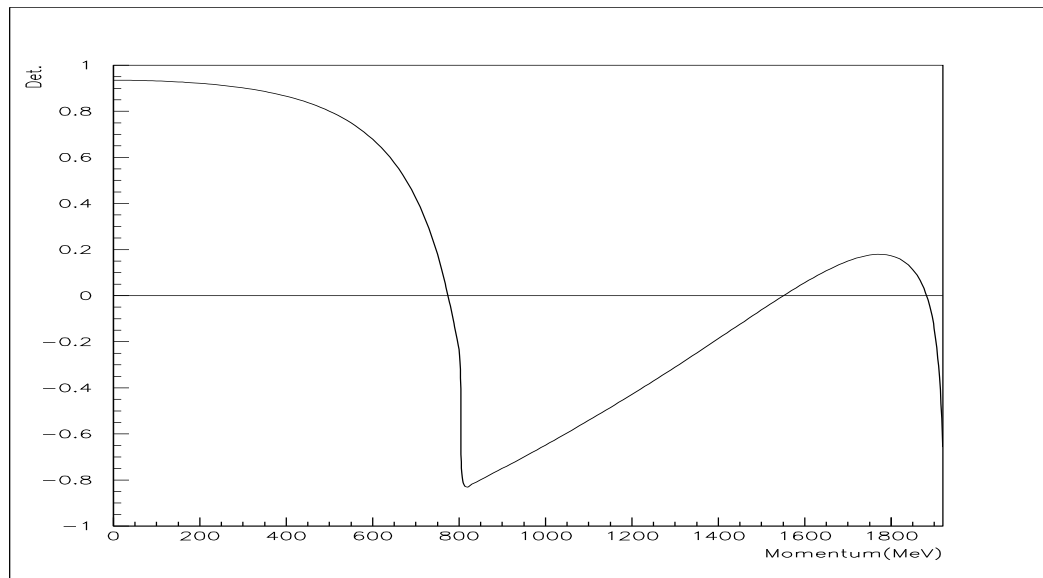


Figure 5.3: The figure shows the denominator of the transverse–vector propagator, $1 - G_2 J_{VV}^T$, as a function of timelike meson momentum, for a set of parameters where $m_0(0)$ is unacceptably large.

A pronounced change in behaviour beyond the pseudo–threshold is also observed in the longitudinal–vector channel (Fig. 5.2) and seems to be important in ensuring that no poles are present in this channel. An unphysical pole does occur, however, in the pion propagator (Fig. 5.1). This unwanted pole is located between 1.3 and 1.45 GeV, depending on the parameter set used. As is implied by Fig. 5.2, its origin is the

¹Above this range, the minimum in Fig. 5.3 occurs at a positive value and so the vector meson becomes an unfeasibly heavy state.

behaviour of the longitudinal axial scattering channel (which changes sign near to the unphysical pole). Since this channel appears in the pion determinant (Eq. 3.13) due to πa_1 mixing, the extra pole would not be present in a minimal version of the model, with the G_1 interaction only. One should only attempt to use the extended model at energies below the position of the unphysical pole. Note that although there is a similar pole in the η^* propagator, it lies at a higher energy than in the pion case.

In this and in subsequent chapters, numerical results are presented for parameter sets which lie near each edge of the acceptable range for $m_0(0)$. From evaluations with some other parameter sets, the variation of results over the full range has been found to be generally monotonic; where it is not, the dependence on $m_0(0)$ is fairly weak. Specifically, results are quoted for $m_0(0) = 280$ MeV (henceforth referred to as set A) and 320 MeV (set B)². Details of these parameter sets are given in Table 5.1. For completeness, the parameter set at $m_0(0) = 300$ MeV is also defined in that table (set C). This is a set in the middle part of the range, using which many of the figures have been drawn.

Values of the zero-momentum quark masses calculated with these parameters at non-zero m_c are also quoted in Table 5.1. They indicate that the effect of non-zero m_c in the ladder SDE is a significant one, a current mass of ~ 10 MeV causing the zero-momentum dynamical quark mass to increase by ~ 50 MeV. It is thus worth examining the related issue of deviations of f_π and m_π from the values which would be obtained at leading order in the chiral expansion. Evaluating the pion quark coupling with m_c set to zero and then using the Goldberger–Treiman relation of Eq. 4.8 gives the values for $f_{\pi 0}$ in Table 5.1. The shifts in f_π induced by the current quark mass are therefore seen to be appreciable, as might be anticipated from the shifts in the dynamical mass. In contrast, the GMOR relation stands up quite well, the entries m_π (GMOR) in Table 5.1 giving the pion masses at leading order in m_c . Such observations suggest

²Note that set B, having $m_0(0)$ close to the maximum admissible value, contains unphysical poles in the transverse vector channels of the type discussed earlier. The first of these occurs at an energy of 1575 MeV in the isoscalar channel and so lies above the unphysical pole in the pion channel.

Parameter	Set A	Set B	Set C
$m_0(0)(\text{MeV})$	280	320	300
$m(0)(\text{MeV})$	326	370	347
$m_c(\text{MeV})$	8.4	11.0	9.6
$\Lambda(\text{MeV})$	995	846	918
$G_1(\text{GeV}^{-2})$	37.1	57.6	46.1
$G_2(\text{GeV}^{-2})$	-5.70	-6.53	-6.57
$G_3(\text{GeV}^{-2})$	-5.20	-5.86	-5.99
$G_4(\text{GeV}^{-2})$	-0.80	-4.14	-2.24
$G_5(\text{GeV}^{-2})$	2.57	4.76	3.34
$f_{\pi 0}(\text{MeV})$	84.6	85.1	85.0
$m_\pi(\text{GMOR})(\text{MeV})$	143.6	143.2	143.3

Table 5.1: Values of the model parameters, fitted as discussed in the text. Also shown are the pion decay constant in the chiral limit, the pion mass predicted by GMOR and the dynamical quark mass.

that the restoring forces against deviations from the chiral circle are rather weak in this model. Associated with such a softness of the vacuum, one would expect to find a light sigma meson. This does indeed prove to be the case, as is discussed shortly.

In the chiral limit, the model quark condensate is $-(206\text{MeV})^3$ and $-(189\text{MeV})^3$ for sets A and B respectively. With non-zero current quark mass, the condensate integral is quadratically divergent. If it is regulated by subtracting the perturbative condensate, slightly higher values of $-(212\text{MeV})^3$ and $-(193\text{MeV})^3$ are obtained. These are similar in size to values for the condensate estimated from QCD sum rules [3]. However, one should bear in mind that the condensate in QCD is a quantity which depends upon the renormalization scale and so one ought to be careful about comparing it directly with the value obtained in a model of this type.

Table 5.2 lists the positions of the first few sets of poles in the quark propagator. Since it is only the first group of poles which is considered to have physical relevance, the model should only be used up to a maximum energy of twice the real part of the second set of poles. This limit is at 2.3 GeV and 1.9 GeV for the parameter sets A and B respectively, and so is sufficiently far above the upper limit imposed by the unphysical pole in the pion channel not to be of practical concern.

Set A	Set B
$\pm 496 \pm 130i$	$\pm 404 \pm 257i$
$\pm 1168 \pm 790i$	$\pm 962 \pm 702i$
$\pm 1488 \pm 1155i$	$\pm 1242 \pm 1005i$
$\pm 1742 \pm 1436i$	$\pm 1463 \pm 1240i$

Table 5.2: Positions of the lowest four sets of poles in the quark propagator. The values given are of $\sqrt{p^2}$ in MeV.

5.2 Meson Spectrum

In Table 5.3, the calculated meson masses are given, along with their on-shell couplings to quarks, as defined in Eqs. 3.11 to 3.13. As described in Chp. 5.1, in some instances the empirical masses have been used to fix model parameters.

Particle	Set A			Set B		
	Mass	g_{iqq}	\tilde{g}_{iqq}	Mass	g_{iqq}	\tilde{g}_{iqq}
π	Fit	3.44	0.0739	Fit	3.91	0.0715
σ	443.2	3.51	–	465.8	4.06	–
ρ	Fit	1.12	–	Fit	1.11	–
a_1	946.8	1.13	–	1061.5	2.27	–
ω	Fit	1.07	–	Fit	1.05	–
f_1	Fit	0.89	–	Fit	2.51	–
a_0	Fit	0.75	–	Fit	1.71	–
η^*	874.9	0.83	0.190	899.4	2.36	1.448

Table 5.3: The calculated meson masses (in MeV) and the couplings of the mesons to quarks.

The scalar isoscalar state is rather light. For comparison, the mass of the corresponding particle in the NJL model [36, 37, 66, 67] is $m_\sigma^2 = m_\pi^2 + 4m^2$, where m is the mass of the constituent quark. Interestingly, the σ mass in the nonlocal model varies only slowly with the dynamical quark mass.

There are a number of analyses of low-energy $\pi\pi$ scattering which have attempted empirical determinations of the mass of the scalar isoscalar meson. However, the issue has remained a contentious one owing to the very strong coupling between this state

and the two-pion channel. While some analyses find masses of $\mathcal{O}(1 \text{ GeV})$ [89], others indicate a much lighter state [90]. The sigma masses of this model, like those in the NJL model, are compatible with the latter. Phenomenologically, however, it is perhaps a more important point that the coupling of the model scalar meson to two pions is qualitatively strong (in Chp. 5.3 it is shown to be comparable to that for a particle of equivalent mass in the linear sigma model). It is therefore eminently plausible that the $1/N_c$ corrections (which include two-pion intermediate states) to the scalar isoscalar channel could prove very significant. The results that have been obtained from a full NLO treatment of the nonlocal model are presented in Chp. 8.

The calculated a_1 mass in the nonlocal model is somewhat smaller than the observed 1230 MeV [12]. In the case of parameter set A, it lies a little below the pseudo-threshold, but for most of the range of admissible $m_0(0)$ it is above that energy. The ρ - a_1 mass splitting is found to increase with increasing dynamical quark mass, although not so rapidly as suggested by the NJL [66, 67] expression $m_{a_1}^2 = m_\rho^2 + 6m^2$, obtained from the derivative expansion of the bosonized model. As a consequence of the upper bound on the constituent mass, which follows from the effect of the pseudo-threshold on the transverse-vector channel, it is not possible to reproduce simultaneously the empirical values of both the ρ and a_1 masses in the ladder approximation. Since the a_1 meson is a very broad resonance this is not altogether surprising, NLO diagrams (such as one with a $\rho\pi$ loop) being potentially important for an accurate description of the channel.

Since there are important flavour-mixing effects in the isoscalar pseudoscalar sector, a realistic calculation for these mesons would require a three-flavoured version of the model. The η^* mass in the two-flavour model should not therefore be directly compared with experiment. It is nevertheless somewhat reassuring to note that this mass lies between the physical η and η' masses of 547 and 958 MeV respectively. Another possibly important feature in the description of the state is the effect of axial-pseudoscalar mixing with the longitudinal f_1 channel. Indeed, in a Bethe-Salpeter

study of a three-flavour model [91], the $\not{q}\gamma_5$ term in the vertex function of the η was found to make significant contributions to both its mass (~ 70 MeV) and decay constant (~ 30 MeV). A similar effect has also been observed in the NJL model [68]. In the present model, if the f_1 particle is omitted by setting G_4 to zero, then the η^* mass with parameter set A is reduced by around 20 MeV, whereas with set B it falls by over 110 MeV. These rather different behaviours are another consequence of the dramatic changes in the meson propagators which can occur at the pseudo-threshold. When $G_4 = 0$, the η^* mass lies below the pseudo-threshold energy for the full range of admissible parameter sets. For non-zero G_4 , the mixing acts to increase the η^* mass and for parameter sets with $m_0(0) \gtrsim 310$ MeV the mass is pushed above the pseudo-threshold, where the effect can be greatly enhanced. In addition, the gradient of the determinant D_{η^*} (cf. Eq. 3.13 and Fig. 5.1) changes significantly above the pseudo-threshold with the result that for these parameter sets the coupling of the η^* to quarks is considerably stronger.

5.3 Hadronic Decays

At leading order in $1/N_c$, the three-meson vertices are calculated from a quark loop with insertions of three vertex functions. In this section results are presented for those inter-meson couplings which correspond to physical decay amplitudes. In such cases all of the mesons are on-shell, where the vertex functions (and hence the mesonic couplings) are unambiguous.

For an initial state of momentum q decaying to particles with momenta q_1 and q_2 , the quark propagators in the triangular loop are evaluated at $p \pm \frac{1}{2}q$ and $p + \frac{1}{2}(q_2 - q_1)$. If the initial state has a mass which is greater than twice the real part of the quark pole, then its decay modes will be sensitive to pseudo-threshold effects. By analogy with the loop integral in the BSE for that particle, residue contributions must be taken into account in the three-point diagrams (see the discussion of Chp. 3.3). It is also possible that further residue contributions would be required were a final-state

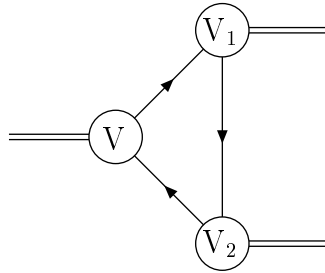


Figure 5.4: $1 \rightarrow 2$ meson decays. There is also a similar diagram where $V_1 \leftrightarrow V_2$.

particle to lie above the pseudo-threshold energy. However, such a situation is not encountered in practice for any of the amplitudes considered.

The meson couplings that have been evaluated are defined by the following matrix elements:

$$\begin{aligned}
 \langle \pi^a(q_1)\pi^b(q_2)|\sigma(q) \rangle &= -g_{\sigma\pi\pi}\delta^{ab}, \\
 \langle \pi^b(q_1)\pi^c(q_2)|\rho^a(q) \rangle &= ig_{\rho\pi\pi}\epsilon^{abc}(q_2 \cdot \epsilon - q_1 \cdot \epsilon), \\
 \langle \sigma(q_1)\pi^b(q_2)|a_1^a(q) \rangle &= \frac{1}{2}ig_{a_1\sigma\pi}\delta^{ab}(q_1 \cdot \epsilon - q_2 \cdot \epsilon), \\
 \langle \rho^b(q_1)\pi^c(q_2)|a_1^a(q) \rangle &= \epsilon^{abc}(g_{a_1\rho\pi}(\epsilon_\rho^* \cdot \epsilon_{a_1}) - h_{a_1\rho\pi}(q_2 \cdot \epsilon_\rho^*)(q_2 \cdot \epsilon_{a_1})). \quad (5.1)
 \end{aligned}$$

The numerical values calculated for the above couplings are given in Table 5.4, along with the corresponding decay widths. Working in the rest frame of the initial state particle, the integrations have been performed in terms of the variables p_4 (in the direction of q), $|\underline{p}|$ and ψ (the angle between \underline{p} and \underline{q}_1). If the angular integration is done first then the result can be treated analogously to an element of $J(q)$ (as described in Chps. 3.3 and 4.1). The variation of the integrands with ψ tends to be dominated by a factor of $\sin \psi$ coming from the Jacobian. It has therefore been advantageous to choose this as a weighting function in the NAG routine D01ANF which evaluates the ψ integral by approximating the other factors with a Chebyshev series over adaptive intervals.

Coupling	Set A		Set B	
	Value	Width(MeV)	Value	Width(MeV)
$g_{\sigma\pi\pi}$ (MeV)	1438	108.0	1625	135.1
$g_{\rho\pi\pi}$	5.52	126.0	5.26	114.0
$g_{a_1\sigma\pi}$	10.65	74.0	11.77	116.4
$g_{a_1\rho\pi}$ (MeV)	2174	44.0	4604	376.2
$h_{a_1\rho\pi}$ (GeV ⁻¹)	18.19	–	10.87	–
R	–0.048	–	–0.087	–

Table 5.4: The on-shell three-meson couplings, as defined in Eq. 5.1. Also presented in the table are the corresponding partial widths. R is the ratio of the d - to s -wave amplitudes in $a_1 \rightarrow \rho\pi$ and is specified in Eq. 5.2.

If the sigma meson of the model is to be interpreted analogously to the scalar particle of the linear sigma model then its coupling to two pions should be strong. Whilst the values in Table 5.4 do not indicate a particularly broad state, the width is appreciably reduced by the small available phase space. A useful comparison, however, is provided by the prediction for the two-pion coupling $g_{\sigma\pi\pi}$ from the linear sigma model [14]. In that model, the coupling is $g_{\sigma\pi\pi} = (m_\sigma^2 - m_\pi^2)/f_\pi$ which, for the sigma masses of parameter sets A and B, gives $g_{\sigma\pi\pi} = 1901$ MeV and 2122 MeV respectively. These values are $\sim 30\%$ larger than those quoted in Table 5.4, indicating that the coupling to pions of the scalar meson in the nonlocal NJL model is qualitatively similar to that of the linear-sigma-model particle. As mentioned previously, this strong coupling highlights the importance of going beyond LO in $1/N_c$ in the description of the scalar channel.

The calculated ρ meson decay width compares reasonably well with the empirical value of 151 MeV. In contrast, the equivalent LO calculation in an extended NJL model, using the physical ρ mass, significantly underestimates the decay rate [92, 93]. Even with the improved description of the nonlocal model, it is not possible to choose model parameters that reproduce both the empirical mass and decay width of the ρ in the LO approximation. Note, however, that if the model parameters for a given $m_0(0)$ are refitted to the empirical value of $g_{\rho\pi\pi}$ rather than to the ρ mass, then the

results for observables are not qualitatively different from those of the original fit. For instance, this procedure would increase the ρ mass itself by ~ 20 to 60 MeV.

The coupling $g_{a_1\sigma\pi}$ is not a direct observable, although the process it describes would be involved in the physical decay of $a_1 \rightarrow 3\pi$. The partial widths for $a_1 \rightarrow \sigma\pi$ found in this model are similar to those estimated from the extended NJL model³ [94] and from Weinberg's mended realization of chiral symmetry⁴ [95]. In contrast, the Particle Data Group [12] quotes an experimental upper bound on the final state $\pi(\pi\pi)_S$ of $\sim 0.7\%$ of the total a_1 width of ~ 400 MeV. The strong couplings obtained here suggest that the model may not be consistent with this experimental result. However, the situation is far from clear. The two-stage process $a_1 \rightarrow \sigma\pi \rightarrow 3\pi$ would have to be integrated over various momenta of the intermediate scalar resonance, where the $a_1\sigma\pi$ and $\sigma\pi\pi$ couplings may be reduced from their on-shell values. A hint that this may indeed be so is provided by the $\sigma\pi\pi$ loop integral, which vanishes⁵ when the total energy is around 800 MeV (see also Chp. 8.6). Furthermore, there is an amplitude for the $\pi(\pi\pi)_S$ final state originating from a direct, four-point $a_1 \rightarrow 3\pi$ diagram which has not been calculated. Although this contribution has been estimated to be small from the first term in the derivative expansion of the extended NJL model [67], higher order terms in the expansion are liable to be important for processes involving the a_1 . Hence, it remains plausible that the direct contribution might conspire to cancel some of the amplitude due to the intermediate scalar state. As is discussed in Ref. [96] however, such a cancellation is not required by any underlying principle such as chiral symmetry.

The dominant decay mode of the a_1 is to $\rho\pi$. Although the parameter set B

³The authors of the cited reference quoted $\Gamma(a_1 \rightarrow \sigma\pi) \approx 60$ MeV.

⁴On the basis of which it is predicted that $\Gamma(a_1 \rightarrow \sigma\pi) = 2^{-\frac{3}{2}}\Gamma(\rho \rightarrow \pi\pi) \approx 53$ MeV.

⁵As noted previously, the couplings $a_1\sigma\pi$ and $\sigma\pi\pi$ for an off-shell sigma meson are not well defined. Each could be multiplied by an arbitrary function so long as the product of the two couplings and the sigma propagator is preserved. However, although the magnitude of an off-shell coupling is undetermined, any zeros in the corresponding loop integral must indicate that the coupling has genuinely vanished. The statement in the main text is therefore independent of the extrapolation scheme used.

does produce a credible, broad width, with set A the state seems to be very narrow. Since the final state has a combined mass of 910 MeV, the allowed phase space for the decay is drastically reduced at the model a_1 masses as compared to the empirical mass. Using parameter set A, the a_1 mass is only 946.8 MeV and so the small decay width of 44 MeV may simply be a consequence of the phase-space suppression.

In order to examine whether the $a_1\rho\pi$ coupling is reasonably well described by the extended nonlocal NJL model, it is here compared with the description of the same process using a phenomenological mesonic Lagrangian. The CCWZ formalism (see Appendix C.4) offers a particularly convenient basis for the comparison since the a_1 mass in that framework can be set to any desired value without violating the constraints of chiral symmetry. A suitable Lagrangian is one obtained by converting the simplest Lagrangian of the massive Yang-Mills scheme (Appendix C.3) into its CCWZ equivalent and then adjusting the a_1 mass⁶. The relevant interaction vertices are included in the Lagrangian of Eq. C.11, with the Yang-Mills couplings being given in Eq. C.13. They yield the predictions $g_{a_1\rho\pi} = f_\pi^{-1}(g_4(q_{a_1} \cdot q_\pi) + g_3(q_\rho \cdot q_\pi))$ and $h_{a_1\rho\pi} = f_\pi^{-1}(g_4 - g_3)$. Taking $f_\pi = 93$ MeV, $m_\rho = 770$ MeV and $Z^2 = 1/2$ to be the parameters specifying the original massive Yang-Mills Lagrangian, together with the empirical a_1 mass, gives a broad state of width 490 MeV. Using the a_1 masses found in the model with parameter sets A and B, the effective Lagrangian gives very much smaller widths, 23 and 132 MeV respectively. This suggests that the small widths calculated in the nonlocal model are largely due to the the small a_1 mass rather than any underestimate of the coupling strength.

The amplitude for the decay $a_1 \rightarrow \rho\pi$ is a mixture of s - and d -wave components. In terms of the decay parameters defined in Eq. 5.1, the ratio of the d - to s -wave

⁶The same conclusions are reached if one starts from the simplest Lagrangian for π , ρ and a_1 mesons in the hidden-symmetry formalism [97]. The $a_1\rho\pi$ interaction terms in the CCWZ representation of both models are generated from the gauge-covariant kinetic terms in the original representations. These contain AAV structures, which become interactions of the appropriate form after the shift in the axial field induced by diagonalization (Appendix C.3). With the minimal Lagrangians of both schemes one therefore has $g_3 = g_4$ due to the structure of the original kinetic terms, with g_3 being set by the mixing parameter.

amplitudes is

$$R = -\sqrt{2} \frac{(E_\rho - m_\rho)g_{a_1\rho\pi} + |\mathbf{q}_\rho|^2 m_{a_1} h_{a_1\rho\pi}}{(E_\rho + 2m_\rho)g_{a_1\rho\pi} + |\mathbf{q}_\rho|^2 m_{a_1} h_{a_1\rho\pi}}, \quad (5.2)$$

where E_ρ and \mathbf{q}_ρ are the energy and three-momentum of the ρ , in the a_1 rest frame. This quantity has been determined by the ARGUS collaboration [98] from τ -decay data to be -0.11 ± 0.02 . The effective Lagrangian approach discussed above requires higher-order couplings in order to obtain a non-zero $h_{a_1\rho\pi}$ and so this ratio provides a test of such higher-order effects. From the values of R given in Table 5.4, the ratio for the parameter set A is seen to be rather low whereas the value for set B is consistent with the observed one. Overall, it is set B that provides the better description of both the a_1 mass and its hadronic decays.

Chapter 6

Numerical Results — Electromagnetic

Additional tests of models in which mesons are constructed as $\bar{q}q$ composites are provided by electromagnetic decays and form factors that probe the internal meson structure. In order to calculate such processes it is necessary to specify the photon–quark coupling, which requires additional assumptions to be made about the form of the nonlocal current. This was discussed in Chp. 2.4. The resultant coupling in the nonlocal extended NJL model and the means of calculating the electromagnetic decays of the vector mesons were described in Chp. 4.3.

6.1 Meson Couplings to Currents

The photon–vector-meson couplings are defined by

$$\begin{aligned}\langle 0|J^{\mu a}|\rho_s^b\rangle &= -g_{\rho\gamma}\delta^{ab}\epsilon_s^\mu, \\ \langle 0|J^\mu|\omega_s\rangle &= -g_{\omega\gamma}\epsilon_s^\mu.\end{aligned}\tag{6.1}$$

Their empirical values, deduced from $\rho \rightarrow e^+e^-$ and $\omega \rightarrow e^+e^-$ [12], are $g_{\rho\gamma} = 0.1177$ GeV² and $g_{\omega\gamma} = 0.0359$ GeV². The calculated values for these couplings, given in Table 6.1, are in reasonable agreement with the experimental ones. Similarly to the

case of the pion decay constant (Chp. 5.1), the nonlocal diagrams with scalar and vector one-quark loops are numerically significant, producing respectively $\sim 8\%$ and $\sim -30\%$ of the coupling.

	Set A	Set B		Set A	Set B
Quantity	Value	Value	Quantity	Value	Value
$g_{\rho\gamma}(\text{GeV}^2)$	0.0889	0.0773	g_ρ	6.67	7.67
$g_{\omega\gamma}(\text{GeV}^2)$	0.0308	0.0265	g_ω	19.92	23.12
$\langle r_\pi^2 \rangle (\text{fm}^2)$	0.346	0.344	–	–	–
$g_{\pi\gamma\gamma}$	0.505	0.501	–	–	–
$g_{\omega\pi\gamma}(\text{GeV}^{-1})$	–2.29	–2.25	$\Gamma(\omega \rightarrow \pi\gamma)$ (keV)	692	669
$g_{\rho\pi\gamma}(\text{GeV}^{-1})$	–0.755	–0.707	$\Gamma(\rho \rightarrow \pi\gamma)$ (keV)	71.6	62.7
$g_{a_1\pi\gamma}(\text{MeV})$	140.2	201.5	$\Gamma(a_1 \rightarrow \pi\gamma)$ (keV)	24.7	45.7

Table 6.1: Electromagnetic properties of mesons. The various couplings appearing in the table are defined in Eqs. 6.1, 6.2, 6.13, 6.23 and 6.27. Also given are the corresponding radiative decay widths of the spin-1 mesons and the mean-square charge radius of the pion.

Values for the dimensionless quantities g_v , as given by

$$g_v = \frac{m_v^2}{g_{v\gamma}}, \quad (6.2)$$

can also be seen in Table 6.1. Universal coupling of the ρ (see Chp. 1.6) would predict that $g_\rho = g_{\rho\pi\pi}$. If one compares the results for g_ρ with those for $g_{\rho\pi\pi}$ in Table 5.4 it is clear that the universality relation is violated in the model, although notably less so with parameter set A, where both of these couplings are closer to the empirical ones. The deviations from universality reflect the fact that the vector current of the model is able to couple through many possible states. Since the ρ meson is just one such state there is no a priori reason to expect universality to hold.

Another interesting comparison one can make with regard to the $\rho\gamma$ coupling concerns the analogous coupling of the a_1 meson to the transverse axial current. A coupling strength g_{a_1} is defined similarly to $g_{v\gamma}$,

$$\langle 0 | J_5^{\mu a} | a_{1s}^b \rangle = -g_{a_1} \delta^{ab} \epsilon_s^\mu. \quad (6.3)$$

Evaluating this coupling as described in Chp. 4.1 one obtains values for g_{a_1} of 0.072 GeV² and 0.138 GeV² with parameter sets A and B respectively. The coupling strength from the local–current contribution is here reduced by about a third due to the inclusion of the nonlocal diagram with a vector one-quark loop. Another nonlocal diagram is also present but its effect is relatively minor. No direct experimental measurement of g_{a_1} exists against which to test these results, but the quantity does appear in Weinberg’s sum rules [99]. If one assumes complete vector and axial–vector meson dominance¹ in Weinberg’s first and second sum rules, then the following relations are obtained:

$$\frac{g_{\rho\gamma}^2}{m_\rho^2} - \frac{g_{a_1}^2}{m_{a_1}^2} = f_\pi^2, \quad (6.4)$$

$$g_{\rho\gamma} = g_{a_1}. \quad (6.5)$$

The results of the model for parameter set A are consistent with these vector–dominance versions of the sum rules, at the $\sim 15\%$ level. In contrast, the results with set B clearly fail to satisfy the relations.

6.2 Pion Form Factor

A further test of the extent to which vector–meson dominance holds in the nonlocal NJL model is provided by the pion form factor. This function receives contributions from the two kinds of diagram shown in Fig. 6.1.

The diagram on the left–hand side of the figure is based on a triangular loop, and is often the only one considered in calculations of the form factor. For a timelike momentum q carried by the external current, the situation is similar to that discussed in Chp. 5.3 for the triangle diagrams in hadronic decays, with pseudo–threshold effects coming into play at energies beyond twice the real part of the quark pole. The same

¹i.e., that the isovector vector and axial–vector spectral functions are given entirely by delta functions at the ρ and a_1 masses respectively. The assumption neglects the non-zero widths of these particles as well as the existence of heavier resonances.

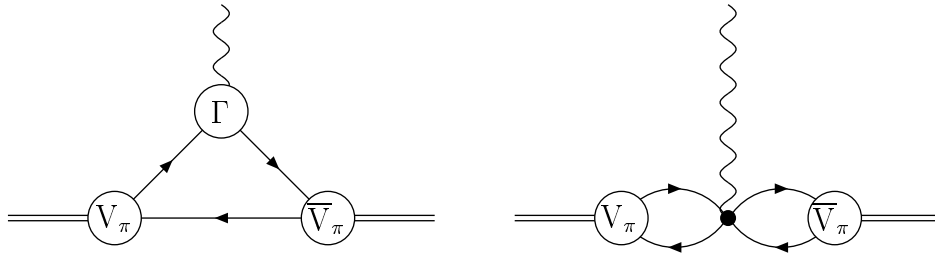


Figure 6.1: The spacelike pion form factor. There is another, similar triangle diagram where the photon couples to the anti-quark.

numerical methods are used as in that case. For spacelike momenta the triangular diagrams can be evaluated in a similar manner, working in the Breit frame.

The other kind of diagram in Fig. 6.1 links the vector current to the initial- and final-state pions by means of two-quark loops. It will be referred to as a two-body diagram and is generated by the terms $G_1(i\gamma_5 \otimes i\gamma_5)$ and $G_2(\gamma^\nu \gamma_5 \otimes \gamma_\nu \gamma_5)$ with type-II structure (Eq. 2.13) in the nonlocal isovector current. The contribution from these diagrams can be written as a sum over terms, each of which is a product of two loop integrals that are somewhat similar to those in J_{PP} , J_{AP} or J_{AA}^L . The path variable in a type-II nonlocal current is associated with both of the $\bar{\psi}\Gamma\psi$ pairs and hence the two loops are connected to each other through the integral over the path. Numerically, such two-body diagrams are best evaluated in a way² similar to the type-III nonlocal diagram which is involved in coupling the a_1 to the axial current (see Chp. 4.1). Since the quark propagators occurring in the two-quark loops have arguments of $p \pm \frac{1}{2}q_\pi$, pseudo-threshold effects are not relevant here.

Note that the two kinds of diagram in Fig. 6.1 are separately gauge invariant. For the triangular diagrams, gauge invariance follows directly from the charge conjugation properties of the dressed quark propagator and the vertices (see Ref. [100] for example). With two-body diagrams of the form occurring in this model, it is also a simple matter

²Specifically, a numerical integration over the path variable is performed, and has as its integrand the product of two three-dimensional integrals. These latter integrals are evaluated with the same numerical methods as for the triangular diagrams.

to check that they can have no component which is proportional to the momentum of the current. If such a diagram is contracted with the current's momentum, Eq. 2.18 can then be used to perform the resulting path integral, whereupon the expression vanishes.

A need for two-body diagrams to be included has also been noted in the context of models where the four-quark interaction is dependent only on the relative momentum of the $\bar{q}q$ pair [55, 56]. In such a model the analogue of the two-body diagram can be reduced to a single two-quark loop integral, where one of the the πqq vertex functions is modified by the presence of the photon. Such diagrams make no contribution to the pion charge, unlike the two-body diagrams required in the present model. Indeed, the fact that the pion's charge should be unity, $F_\pi(0) = 1$, supplies an important check on the model calculations, both analytical and numerical. Calculation of the charge from the full expressions for the contributing diagrams would be quite complicated, but it is rather more practicable to demonstrate the result analytically if one works in the chiral limit.

Consider initially a simplified version of the model where G_1 is the only coupling included. When a bare γ_μ insertion is used at the γqq vertex of the triangular loops it yields the following contribution to $F_\pi(0)$:

$$2N_c N_f g_{\pi qq}^2 \int \frac{d^4 p_E}{(2\pi)^4} \frac{f^4(p_E) - \frac{1}{2} p_E^2 f^2(p_E) f^{2'}(p_E)}{[p_E^2 + m_0(p_E)^2]^2}, \quad (6.6)$$

the prime denoting differentiation with respect to p_E^2 . The only other piece of the γqq vertex in this version of the model is an insertion of scalar character (given in Eq. 4.22). The resulting contribution, however, turns out to be of $\mathcal{O}(m_\pi)$ and so the condition can only be satisfied through the introduction of a contribution that comes from the two-body diagram. This is:

$$-2N_c N_f g_{\pi qq}^2 \int \frac{d^4 p_E}{(2\pi)^4} \frac{f^2(p_E) f^{2'}(p_E) - \frac{1}{4} p_E^2 (f^{2'}(p_E))^2 + p_E^2 f^3(p_E) f''(p_E)}{p_E^2 + m_0(p_E)^2}. \quad (6.7)$$

In deriving the expression above one exploits the fact that the path variable, λ , always appears in conjunction with q and hence at $q = 0$ it vanishes from the integrand. The

two-body diagram is then a product of two separated loop integrals, one of which is simply $J_{PP}(m_\pi^2)$. This factor is not found in Eq. 6.7, however, since it has been eliminated (along with the factor of G_1 in the nonlocal current) by invoking the pion BSE, $G_1 J_{PP}(m_\pi^2) = 1$.

Integration by parts can be used to remove the second derivative of an interaction form factor from Eq. 6.7. Adding the contributions of Eqs. 6.6 and 6.7 then gives

$$2N_c N_f g_{\pi qq}^2 \int \frac{d^4 p_E}{(2\pi)^4} \frac{f^4(p_E) - p_E^2 f^2(p_E) f'^2(p_E) + p_E^4 f^2(p_E) (f'(p_E))^2}{[p_E^2 + m_0(p_E)^2]^2}. \quad (6.8)$$

This integral should be compared to the one in Eq. 4.7 for $Z_{\pi 0}^{-1}$. Recalling that equation, and the definition of Z_π , the expression 6.8 is seen to reduce to unity, as required.

Proceeding now to the case of the extended model, the contributions discussed above are no longer sufficient to produce the correct normalization of the pion charge. This is because there are changes to $g_{\pi qq}^2$ which cause it to deviate from $Z_{\pi 0}$. A modification is also made to the dressed γqq vertex, specifically the introduction of the piece of Eq. 4.30 that is proportional to $B(q^2)$. Since $B(0) = 0$ however, this effect does not have any implications for the charge of the pion. The new contributions arising from the triangular diagrams therefore originate solely in the additional $\not{q}\gamma_5$ term of the pion vertex functions. At leading order in the chiral expansion, and using the bare γqq vertex, this extra term yields a contribution of

$$4N_c N_f \frac{g_{\pi qq} \tilde{g}_{\pi qq}}{m_\pi} \int \frac{d^4 p_E}{(2\pi)^4} \frac{f^4(p_E) m_0(p_E)}{[p_E^2 + m_0(p_E)^2]^2}, \quad (6.9)$$

whilst the corresponding result from the dressed scalar piece of the γqq vertex is

$$-2N_c N_f \frac{g_{\pi qq} \tilde{g}_{\pi qq}}{m_\pi} \int \frac{d^4 p_E}{(2\pi)^4} \frac{p_E^2 f^4(p_E) m_0'(p_E)}{[p_E^2 + m_0(p_E)^2]^2}. \quad (6.10)$$

The two-body diagrams are also altered due to non-zero G_2 because of the extra invariant at the pion vertices. Furthermore, there is a new diagram of this kind which arises from the type-II term $G_2(\gamma^\nu \gamma_5 \otimes \gamma_\nu \gamma_5)$ in the nonlocal vector current. At $q = 0$ both of the two-body diagrams simplify to a sum over terms which are products of

two independent loop integrals. In each term, one of these integrals is just $J_{PP}(m_\pi^2)$, $J_{AP}(m_\pi^2)$ or $J_{AA}^L(m_\pi^2)$. Since J_{AP} is $\mathcal{O}(m_\pi)$ in the chiral expansion (Eq. 4.9), terms containing it can be discarded. Although J_{AA}^L is of zeroth order in the pion mass, it always appears in these diagrams accompanied by at least one factor of $\tilde{g}_{\pi qq}$, which is itself of $\mathcal{O}(m_\pi)$ (see Eq. 4.14). Only the terms that are proportional to J_{PP} survive in the chiral limit. This means that the new diagram involving the G_2 term from the nonlocal current does not in fact contribute to the pion charge at this level. In the remaining contributions, consider now the loop which multiplies J_{PP} . Where this loop deals with the $\not{q}\gamma_5$ structure of a pion vertex there is an associated factor of $\tilde{g}_{\pi qq}$ that reduces the contribution to one of $\mathcal{O}(m_\pi)$. Hence, non-zero G_2 does not affect the two-body contribution in the chiral limit.

Recalling the notation defined in Eq. 4.10, the sum of contributions to $F_\pi(0)$ in the chiral limit of the extended model can be written as

$$\frac{g_{\pi qq}^2}{Z_{\pi 0}} + \frac{g_{\pi qq} \tilde{g}_{\pi qq}}{m_\pi} \left(I_6 - \frac{1}{2} \tilde{I}_6 \right), \quad (6.11)$$

the first term coming from Eq. 6.8 and the second from Eqs. 6.9 and 6.10. Using now Eqs. 4.12 and 4.14 for the πqq couplings in the chiral limit, the above expression is easily shown to be unity, completing the proof.

Numerically one can test that the pion charge is unity to all orders in the chiral expansion. This has indeed been verified, the result holding to the accuracy of the integration routines used.

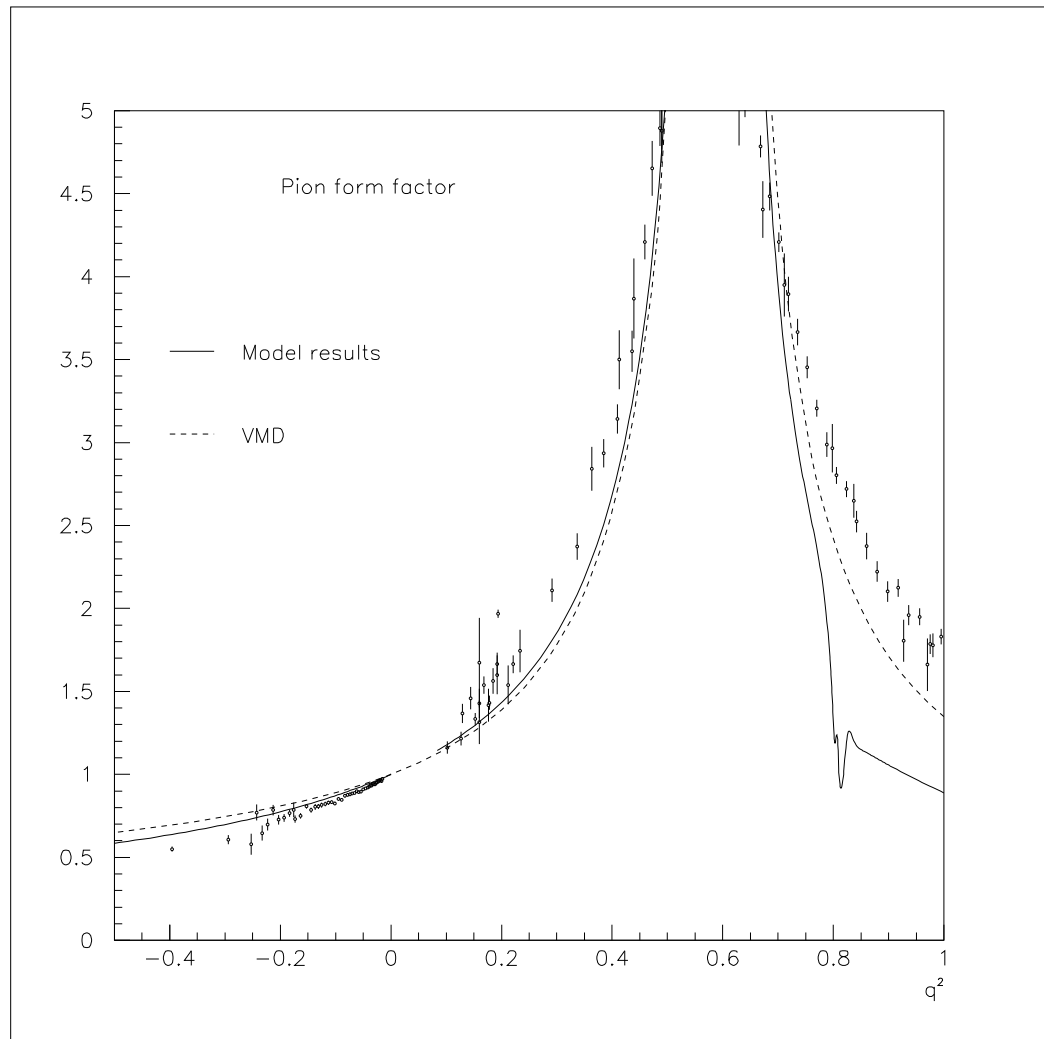


Figure 6.2: The absolute value of the pion form factor, $|F_\pi(q^2)|$, is plotted against q^2 in GeV^2 . The solid line is the model result; the dashed line is the VMD approximation to it. The data points are from Refs. [29, 101, 102].

The absolute value of the form factor over a range of values of q^2 can be seen in Fig. 6.2, for a fit parameter set with $m_0(0) = 300$ MeV (detailed in Chp. 5.1). Also shown on the figure are experimental data points, taken from Refs. [101, 102] for the region of spacelike q^2 and from Ref. [29] for timelike q^2 . In the LO approximation, the model form factor has a pole at the ρ meson mass. Below the pole, very little variation with $m_0(0)$ is found in the results when other parameter sets are used. In this region the model curve is seen to be in fairly good agreement with the data, although its rise is a little shallower. This is confirmed by the calculated values of the mean-square pion radius, which are given in Table 6.1. They are somewhat smaller than the experimental result [101] of 0.439 ± 0.008 (fm)².

The dashed curve in Fig. 6.2, labelled VMD, is plotted to test whether or not the model result for the form factor is consistent with VMD. Under the assumption of ρ dominance of the photon-pion coupling, the form factor is

$$F_\pi(q^2) = 1 - \frac{g_{\rho\pi\pi}}{g_\rho} \frac{q^2}{q^2 - m_\rho^2}. \quad (6.12)$$

The ratio of $g_{\rho\pi\pi}$ to g_ρ is underestimated by the model³, and hence when one uses the model couplings in Eq. 6.12, the resulting VMD form factor rises somewhat more slowly than the data. Nonetheless this VMD approximation to the model curve is not a bad one, particularly at low q^2 .

³The values of these couplings are given in Tables 5.4 and 6.1. For the fit parameter set with $m_0(0) = 300$ MeV, as used in drawing Fig. 6.2, they are $g_{\rho\pi\pi} = 5.26$ and $g_\rho = 6.89$.

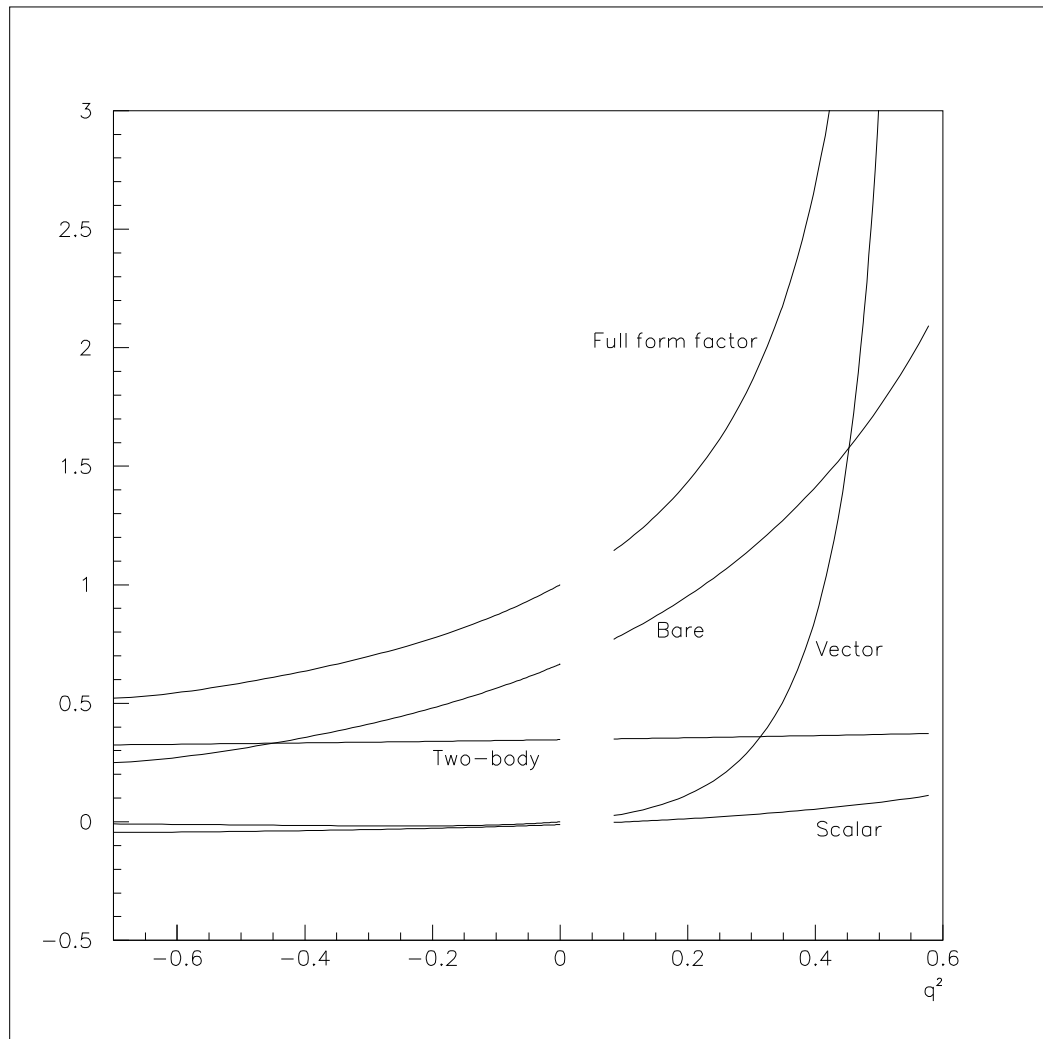


Figure 6.3: Various contributions to the pion form factor, below the ρ pole. The different contributions are plotted against q^2 in GeV^2 and are defined in the text.

Fig. 6.3 illustrates the individual contributions to the form factor, below the ρ pole. The curve labelled as “bare” is the contribution coming from the triangle diagram with the local γqq coupling (the γ_μ part of the vertex, as illustrated by the first diagram in the representation of the dressed γqq vertex in Fig. 4.2). The curve labelled “scalar” comes from the triangle diagram with a nonlocal coupling (as in the second diagram of Fig. 4.2), the one-quark loop having a scalar insertion (this part of the vertex is given by Eq. 4.22). This “scalar” contribution is negligible over the range of q^2 considered. All other contributions from the triangle diagrams are combined into the curve labelled “vector” and correspond to the part of Eq. 4.30 that is proportional to $B(q^2)$. Since the transverse ρ meson propagator is contained in the function $B_2(q^2)$ (Eq. 4.32), this curve makes the dominant contribution close to the ρ pole. At spacelike momenta, however, it is found to supply only a very small contribution, being even smaller than the “scalar” piece. This is hardly surprising since one would expect that a version of the model without the ρ meson (and hence without any “vector” curve) should be able to give a reasonable account of the spacelike form factor. The point is verified by Fig. 6.4 in which the model calculation with the extended model is compared to that produced when the model has only the G_1 interaction. These model form factors are clearly very similar in the spacelike region but it is also obvious that the incorporation of the ρ meson is necessary for a satisfactory description of the timelike region.

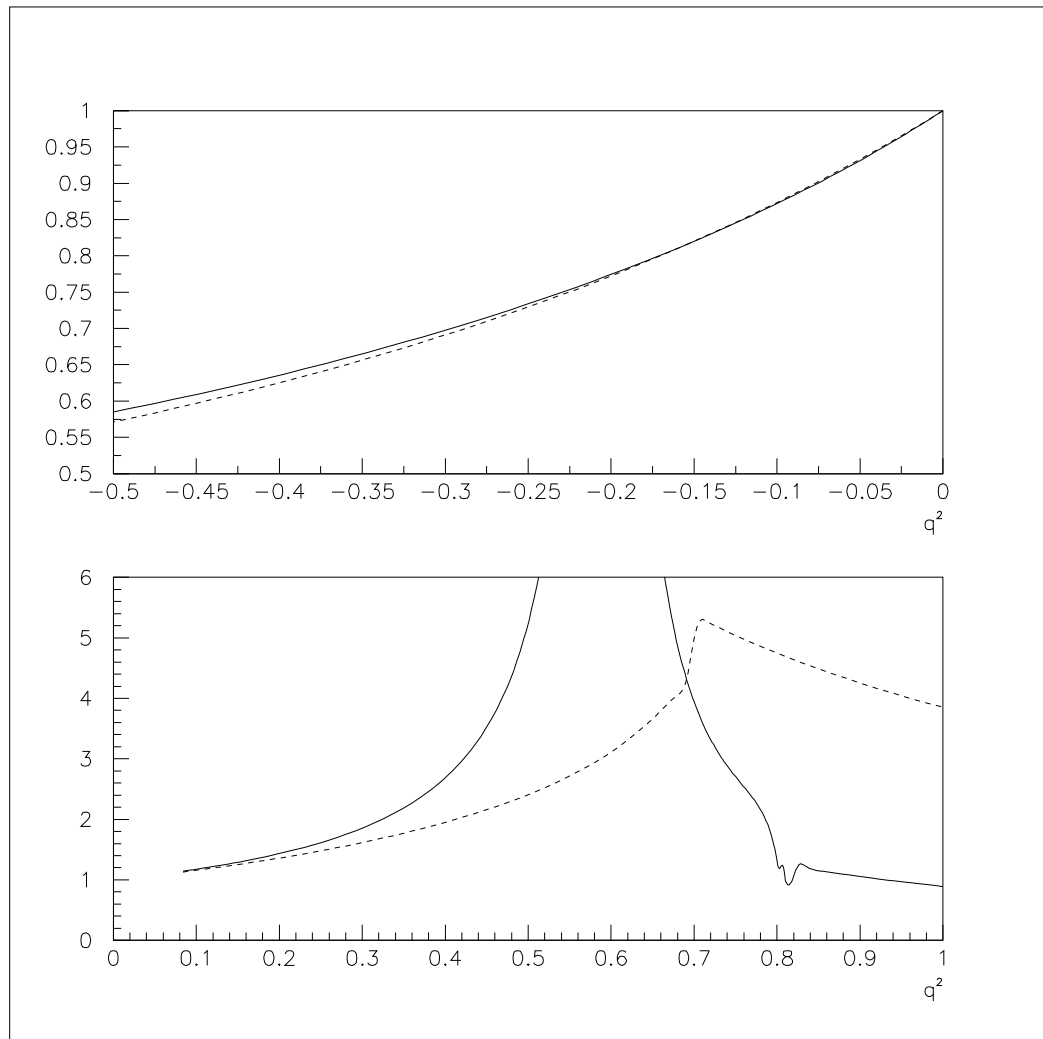


Figure 6.4: The absolute value of the pion form factor, $|F_\pi(q^2)|$, is plotted against q^2 in GeV^2 . The solid line gives the result calculated from the extended model, just as in Fig. 6.2. The dashed line gives the form factor calculated from the version of the model which has the G_1 coupling only. Both curves use a fit parameter set with $m_0(0) = 300$ MeV as specified in Chps. 5.1 and 8.1.

The contribution from the two-body diagrams can be seen in Fig. 6.3 and proves to be relatively small in the vicinity of the ρ mass. However it varies only very slowly with momentum, and so quite rapidly becomes important as the spacelike momentum increases. This is as expected since, for large momentum transfer to the pion, the pion vertex functions cut down the triangle-diagram contributions. Even at $q^2 = 0$ though, the two-body diagrams are significant. They are responsible for around a third of the pion charge, clearly demonstrating the importance of including their contribution.

It is interesting to note that, away from the pole, much of the variation with momentum is controlled by the “bare” contribution to the form factor, which accounts for $\sim 77\%$ of the mean-square charge radius, $\langle r_\pi^2 \rangle$. Although this curve has no ρ pole, when added to the “vector” contribution, the sum is quite close to that of the VMD approximation to the model. This implies that a cancellation operates between the “bare” contribution and states above the ρ in the “vector” piece, leaving the ρ pole as the dominant overall feature. In contrast, although a similar mean-square radius has been obtained with an extended NJL model [103], most of that value was ascribed to a diagram involving an intermediate ρ meson, the bare photon vertex accounting for just 32%.

Above the ρ pole, the measured form factor is not well described by the model curve. A possible explanation is suggested by Fig. 6.5, which breaks the form factor down into its various contributions for $q^2 > m_\rho^2$.

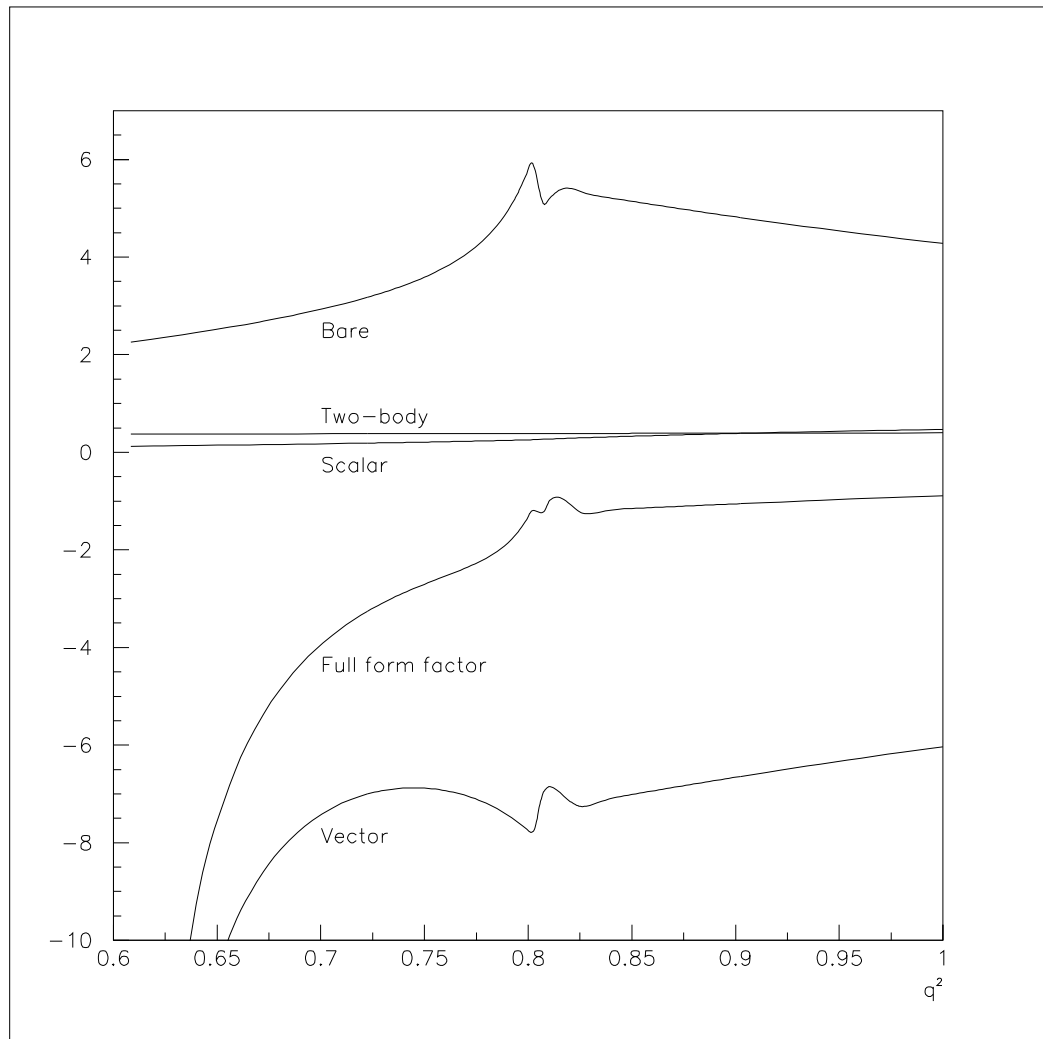


Figure 6.5: Various contributions to the timelike pion form factor, above the ρ pole. The different contributions are plotted against q^2 in GeV^2 and are defined in the text.

One observes in Fig. 6.5 that there is a substantial cancellation at work between the “bare” and “vector” contributions, while the “scalar” and “two-body” pieces are negligible over this region. The net result is therefore liable to be very sensitive to fine details of the model in this regime. In common with the results for the J loop integrals (presented in Chp. 5.1), the “bare” and “vector” contributions to the pion form factor are seen in Fig. 6.5 to undergo qualitative changes of behaviour at the pseudo–threshold energy. This acts to disrupt the cancellation between them near to that point. A consequence is the prominence of the rather strange structure seen just above the pseudo–threshold in Fig. 6.2. This cancellation between large amplitudes suggests that the results of the model should not be regarded as reliable in the region. The statement is borne out by the strong dependence of the model results above the ρ pole on the parameter set chosen, which is readily apparent if one compares the plots in Figs. 6.2 and 6.6.

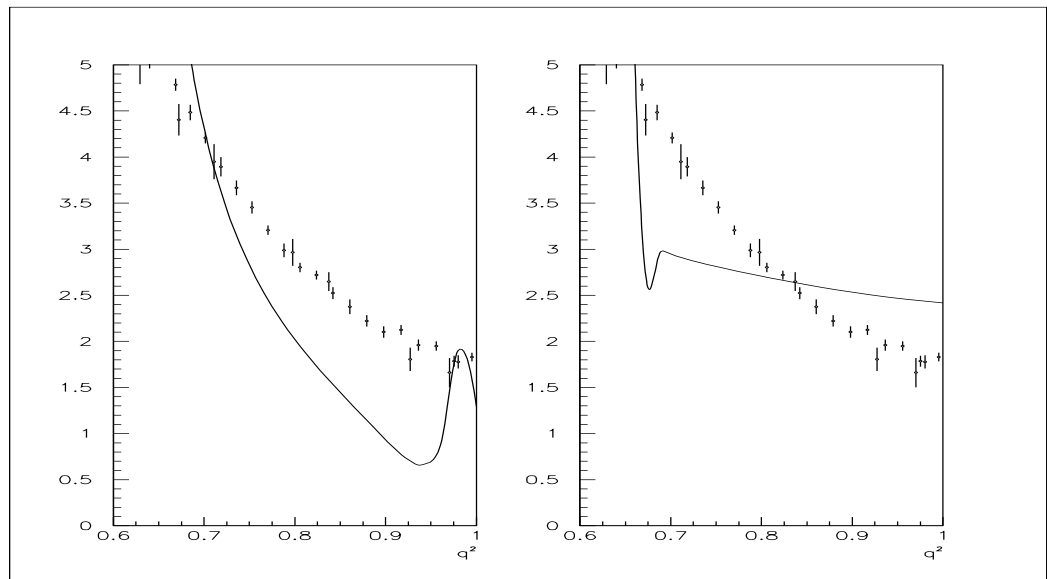


Figure 6.6: The modulus of the pion form factor, $|F_\pi(q^2)|$, above the ρ pole is plotted against q^2 in GeV^2 , along with data points from Refs. [29, 101, 102]. The results of the model with parameter sets A and B are shown on the left– and right–hand sides of the figure respectively.

6.3 $\pi^0 \rightarrow \gamma\gamma$ and Related Form Factor

Use of the conserved current constructed in Chp. 2.4 implicitly ensures that electromagnetic Ward identities are satisfied by the model. Several examples of these were discussed in Chps. 4.3, 4.4 and 6.2. Another important one is the amplitude for the decay $\pi^0 \rightarrow \gamma\gamma$, which is an example of an anomalous process. Such processes involve the complete set of quark states and so present a problem for the usual NJL model [40, 46, 47, 48, 49], where the use of a regulator means that high-energy quark states are discarded. In the nonlocal model studied here, the low-energy theorem for $\pi^0 \rightarrow \gamma\gamma$ may be shown to be automatically satisfied, provided that one includes both of the diagrams displayed in Fig. 6.7. As well as the traditional triangle diagram [13, 79, 104], there is a two-body diagram that has a dressed γqq vertex (Eq. 4.30) for one of the photons and a $\gamma qqqq$ vertex for the other.

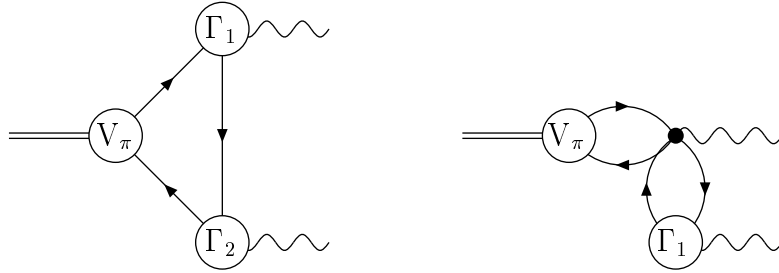


Figure 6.7: Diagrams contributing to $\pi^0 \rightarrow \gamma\gamma$. There are also similar diagrams with $\Gamma_1 \leftrightarrow \Gamma_2$.

The anomalous nature of the axial part of the chiral symmetry group implies that $g_{\pi\gamma\gamma} = \frac{1}{2}$ in the chiral limit [104], this coupling being defined through the amplitude

$$\langle \gamma(q_1)\gamma(q_2)|\pi^0 \rangle = \frac{-2\alpha_{\text{EM}}}{\pi f_\pi} g_{\pi\gamma\gamma} \epsilon_{\alpha\beta\mu\nu} q_1^\alpha q_2^\beta \epsilon_1^{*\mu} \epsilon_2^{*\nu}. \quad (6.13)$$

Working in the chiral limit, consider first the simpler case where vector meson degrees of freedom are not present in the model, setting $G_2 = G_3 = 0$. The triangle diagrams where both of the photons are coupled through the local current (bare γ_μ insertions

at the γqq vertices) contribute an amplitude of

$$4i\epsilon_{\alpha\beta\mu\nu}q_1^\alpha q_2^\beta \epsilon_1^{*\mu} \epsilon_2^{*\nu} e^2 g_{\pi qq0} \int \frac{d^4p}{(2\pi)^4} \frac{f^2(p)}{[p^2 - m_0^2(p^2)]^3} \left(-2m_0(p^2) + 4m_0'(p^2) \frac{(p \cdot q)^2}{q^2} + 4m_0'(p^2) \frac{[p \cdot (q_1 - q_2)]^2}{(q_1 - q_2)^2} \right), \quad (6.14)$$

where the prime denotes a derivative with respect to p^2 . The photons in the triangular-loop diagrams can also be coupled via the nonlocal current, having an insertion of scalar character (this γqq insertion is given in Eq. 4.22). The contribution from diagrams where one of the photons is coupled in this way is

$$4i\epsilon_{\alpha\beta\mu\nu}q_1^\alpha q_2^\beta \epsilon_1^{*\mu} \epsilon_2^{*\nu} e^2 g_{\pi qq0} \int \frac{d^4p}{(2\pi)^4} \frac{f^2(p)4m_0'(p^2)}{[p^2 - m_0^2(p^2)]^3} \left(p^2 - \frac{(p \cdot q)^2}{q^2} - \frac{[p \cdot (q_1 - q_2)]^2}{(q_1 - q_2)^2} \right). \quad (6.15)$$

Diagrams with a nonlocal coupling at both photon vertices do not make any contribution to the amplitude because the resulting Dirac trace vanishes. Converting the sum of Eqs. 6.14 and 6.15 into Euclidean space, and changing variable to

$$t = \frac{m_0^2(p_E^2)}{p_E^2}, \quad (6.16)$$

leads to a total amplitude of

$$-2\epsilon_{\alpha\beta\mu\nu}q_1^\alpha q_2^\beta \epsilon_1^{*\mu} \epsilon_2^{*\nu} \frac{\alpha_{\text{EM}}}{\pi} \frac{g_{\pi qq0}}{m_0(0)} \int_0^\infty \frac{dt}{(1+t)^3}. \quad (6.17)$$

The low-energy theorem now follows by invoking the analogue of the Goldberger–Treiman relation in the model. This is just Eq. 4.8, derived both in Ref. [8] and in Chp. 4.2 by considering f_π in the chiral limit.

In the extended model with vector mesons, the pion–quark coupling is affected by the pseudoscalar–axial mixing induced by the G_2 coupling (see Eqs. 3.10, 3.12 and 3.13). However, the form of f_π is also modified (as described in Chp. 4.1) in just such a way that the Goldberger–Treiman relation remains valid (Chp. 4.2). In addition, note that since the photons in this process are on-shell the relevant dressed γqq vertices are composed solely of the same bare and nonlocal (Eq. 4.22) pieces as in the version of

the model without vector mesons (this issue is discussed in Chp. 4.3). The sum of the contributions 6.14 and 6.15 therefore yields $g_{\pi\gamma\gamma} = \frac{1}{2}$, just as in the simpler version of the model.

The analysis outlined above is in agreement with the work of Ref. [79] where it was shown that, for a quark propagator without wavefunction renormalization, the anomaly is saturated by taking only the leading part of the pion Bethe–Salpeter amplitude, together with dressed γqq structures subject to the Ward identity for that vertex. The statement is non-trivial because terms in the pion amplitude that are linear in momentum can contribute to the decay amplitude, even in the chiral limit. For instance, the $\not{q}\gamma_5$ term which appears in $V_\pi(q)$ for the extended version of this model gives rise to additional triangle–diagram contributions. From such diagrams with two local photon vertices, one finds

$$4i\epsilon_{\alpha\beta\mu\nu}q_1^\alpha q_2^\beta \epsilon_1^{*\mu} \epsilon_2^{*\nu} e^2 \frac{\tilde{g}_{\pi qq}}{m_\pi} \int \frac{d^4 p}{(2\pi)^4} \frac{f^2(p)}{[p^2 - m_0^2(p^2)]^3} \left(-2p^2 - 2m_0^2(p^2) + 4\frac{(p \cdot q)^2}{q^2} + 4\frac{[p \cdot (q_1 - q_2)]^2}{(q_1 - q_2)^2} \right). \quad (6.18)$$

Since $\tilde{g}_{\pi qq}$ is of $\mathcal{O}(m_\pi)$ in the chiral expansion (Eq. 4.14), the above contribution is of $\mathcal{O}(1)$. Similar diagrams with one local and one nonlocal photon vertex give

$$4i\epsilon_{\alpha\beta\mu\nu}q_1^\alpha q_2^\beta \epsilon_1^{*\mu} \epsilon_2^{*\nu} e^2 \frac{\tilde{g}_{\pi qq}}{m_\pi} \int \frac{d^4 p}{(2\pi)^4} \frac{f^2(p)8m_0(p^2)m_0'(p^2)}{[p^2 - m_0^2(p^2)]^3} \left(p^2 - \frac{(p \cdot q)^2}{q^2} - \frac{[p \cdot (q_1 - q_2)]^2}{(q_1 - q_2)^2} \right). \quad (6.19)$$

The diagrams with two nonlocal vertices again have a vanishing Dirac trace.

Since the sum of Eqs. 6.18 and 6.19 is non-zero, there must be some other contribution that cancels them in the full amplitude for the anomalous process. The relevant piece arises from the two-body diagram that is displayed on the right–hand side of Fig. 6.7. Terms in the nonlocal vector current of the form⁴ $G_2(\gamma^\nu \gamma_5 \otimes \gamma_\nu \gamma_5)$ with a type-I (Eq. 2.11) structure are responsible for the $\gamma qqqq$ vertex. This diagram factorizes into two separate loop integrals, the loop between the two photons producing the

⁴For the sake of simplicity, isospin factors have been suppressed here.

anomalous $\epsilon_{\alpha\beta\mu\nu}$ factor. The other loop is nothing more than a linear combination of the familiar integrals $J_{AP}(m_\pi^2)$ and $J_{AA}^L(m_\pi^2)$. This combination can be simplified by recalling the definitions of the pion–quark coupling constants in Eq. 3.12. The contribution from this diagram in the chiral limit is given by

$$4i\epsilon_{\alpha\beta\mu\nu}q_1^\alpha q_2^\beta \epsilon_1^{*\mu} \epsilon_2^{*\nu} e^2 \frac{\tilde{g}_{\pi qq}}{m_\pi} \int \frac{d^4p}{(2\pi)^4} \frac{4f(p)f'(p)}{[p^2 - m_0^2(p^2)]^2} \left(p^2 - \frac{(p \cdot q)^2}{q^2} - \frac{[p \cdot (q_1 - q_2)]^2}{(q_1 - q_2)^2} \right). \quad (6.20)$$

Converting to Euclidean space and integrating by parts, the above expression can be shown to cancel exactly with the sum of Eqs. 6.18 and 6.19, demonstrating that the low-energy theorem for $\pi^0 \rightarrow \gamma\gamma$ holds in the extended model.

In practice, the existence of non-zero current quark masses means that the physical amplitude differs slightly from its value in the chiral limit. In an explicit calculation of the full model amplitude, the two-body diagrams are treated by first performing the path integration analytically. One can then apply the usual methods (see Chp. 5.3) for dealing with a single three–dimensional loop integral. The numerical results calculated with the nonlocal NJL model for $g_{\pi\gamma\gamma}$ are given in Table 6.1. The deviations from $\frac{1}{2}$ are small and are consistent with those in the experimental value [12], $g_{\pi\gamma\gamma} = 0.503 \pm 0.018$.

The related process where one of the photons is off-shell, $\gamma\gamma^* \rightarrow \pi^0$, enables one to probe the structure of the neutral pion. A corresponding form factor can be defined as

$$F_{\pi\gamma}(q^2) = \frac{\langle \gamma^*(q^2)\gamma|\pi^0 \rangle}{\langle \gamma(q^2=0)\gamma|\pi^0 \rangle}. \quad (6.21)$$

It is straightforward to develop the model calculations above in order to evaluate this form factor. The same numerical methods for dealing with the two-body diagrams can be applied both off- and on-shell. The triangular diagrams are again evaluated analogously to those in the hadronic decay amplitudes of Chp. 5.3, but working here in a frame chosen such that the spacelike momentum of the off-shell photon has no component in the fourth Euclidean direction.

Early experimental measurements of the transition form factor were attempted at small timelike momenta [12, 105] but were subject to large uncertainties. Until recently the best results were those obtained by the CELLO collaboration [105] in the spacelike region, which extends from $-m_\pi^2$. Their experiment investigated $e^+e^- \rightarrow e^+e^-\pi^0$ events where one of the fermions is scattered through a very small angle (i.e., is lost down the beam pipe), thereby indicating that the intermediate photon it emitted was almost real. Five data points for the form factor were quoted and are marked by open circles in Fig. 6.8. Also displayed on that figure is the new data reported by the CLEO collaboration [106] who revisited the experiment at improved precision. Their data is marked with filled boxes on the figure which also shows the results of the model calculation at the fit parameter set with $m_0(0) = 300$ MeV.

The model results are not sensitive to the choice of parameter set and are dominated by the contribution from the triangle diagram with local photon couplings. They are in good agreement with the new experimental data and are comparable to the results obtained in other Bethe–Salpeter approaches [86, 87].

The dashed curve in Fig. 6.8 is the VMD prediction for the form factor, given by

$$F_{\pi\gamma}(q^2) = 1 - \frac{2\pi^2 f_\pi}{g_{\pi\gamma\gamma}} \sum_{V=\rho,\omega} \frac{g_{V\pi\gamma}}{g_V} \frac{q^2}{q^2 - m_V^2}, \quad (6.22)$$

and using the values of the couplings calculated in the model⁵. (The couplings $g_{V\pi\gamma}$, describing the decays $V \rightarrow \pi\gamma$, are discussed in the following section.) In this case, the VMD approximation to the model result is rather poorer than it was for the pion form factor (Fig. 6.2). VMD is not inconsistent with the model at low momenta in this process, but the difference between them becomes appreciable as the spacelike momentum increases.

⁵which are $g_{\pi\gamma\gamma} = 0.504$, $g_\rho = 6.89$, $g_{\rho\pi\gamma} = -0.712$ GeV⁻¹, $g_\omega = 20.62$ and $g_{\omega\pi\gamma} = -2.14$ GeV⁻¹ for the fit parameter set with $m_0(0) = 300$ MeV that is used in drawing Fig. 6.8.

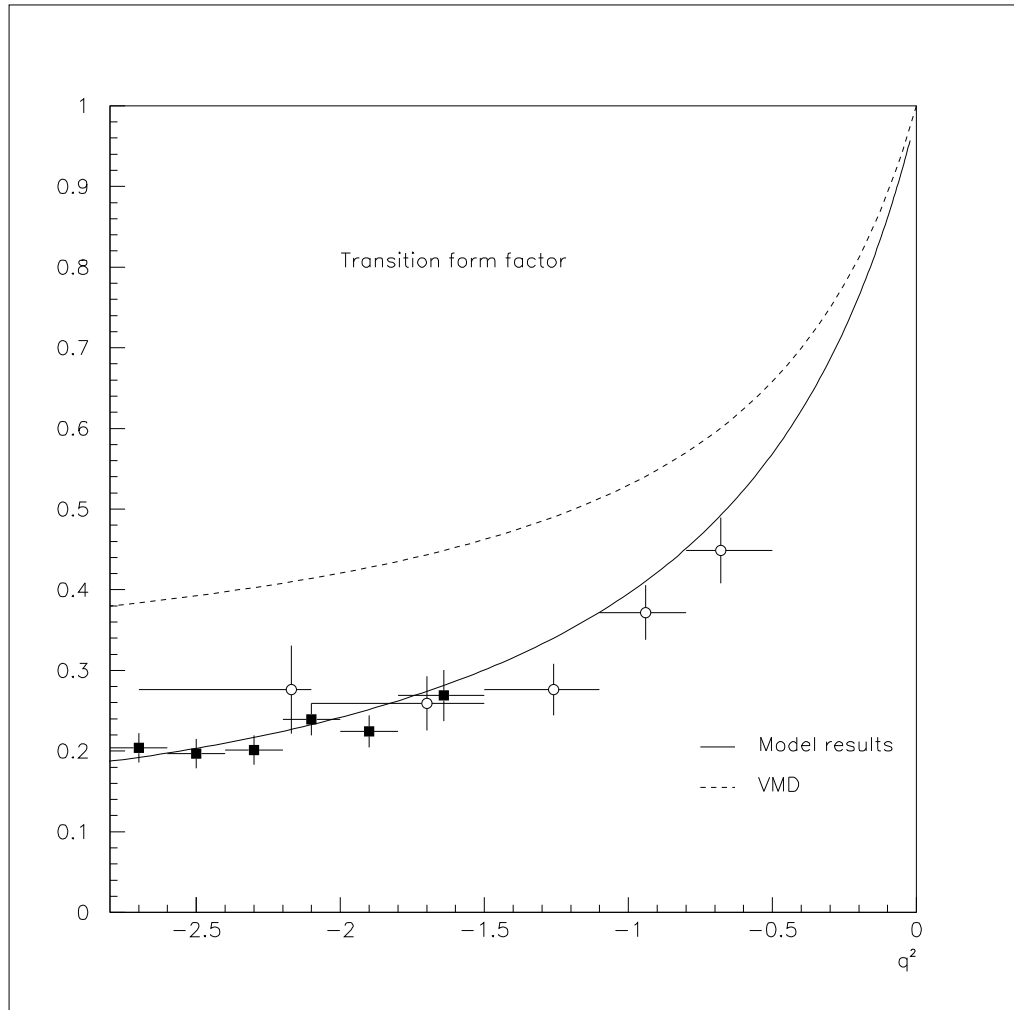


Figure 6.8: The $\pi\gamma\gamma^*(q^2)$ transition form factor, defined in Eq. 6.21, is plotted against q^2 in GeV^2 . The solid line is the model result; the dashed line is the VMD approximation to it. The data points are from Refs. [105] (open circles) and [106] (filled boxes). In both of the experiments the data was measured in Q^2 bins, the extents of which are plotted here as the horizontal error bars. The vertical errors in $F_{\pi\gamma}$ are statistical only.

For the on-shell amplitude in the chiral limit the chiral anomaly ensures that the effects of including vector mesons in the model cancel out. In fact, such cancellations seem to persist to a large extent in the off-shell amplitude and at non-zero current quark mass. Evidence for this claim is supplied by Fig. 6.9, where the transition form factor is shown in a simpler version of the model which includes only the pions and the sigma meson. As in the case of the pion form factor at spacelike momenta, there is little difference between the extended and simple versions of the model, with both giving a good description of the data.

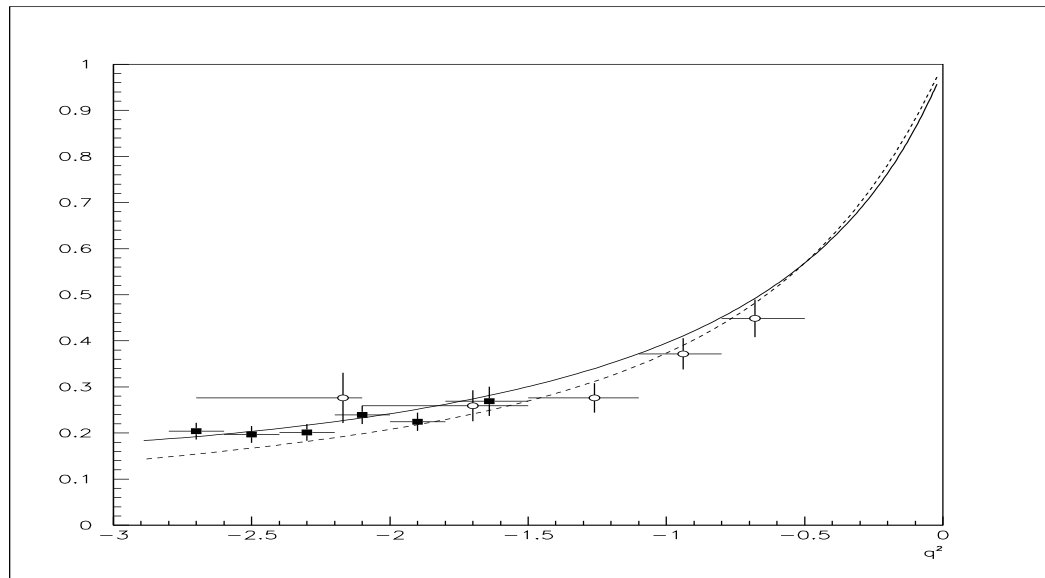


Figure 6.9: The $\pi\gamma\gamma^*(q^2)$ transition form factor is plotted against q^2 in GeV^2 . The solid line gives the result calculated with the extended version of the model, just as in Fig. 6.8. The dashed line gives the result calculated from the version of the model which has the G_1 coupling only. Both curves use a fit parameter set with $m_0(0) = 300$ MeV as specified in Chps. 5.1 and 8.1.

6.4 Radiative Decays and a Related Form Factor

This section discusses the model results for the decays of spin-1 mesons into $\pi\gamma$ final states. Schematically, the calculations involve triangle and two-body diagrams, analogous to those of Fig. 6.7.

Just as in the anomalous pion decay, the piece of the nonlocal current that gives rise to the two-body diagrams for $V \rightarrow \pi\gamma$ is the type-I (Eq. 2.11) term with Dirac structure $G_2(\gamma^\nu\gamma_5 \otimes \gamma_\nu\gamma_5)$. These two-body diagrams may similarly be reduced to a single two-quark loop integral, the other loop being a known combination of pionic J integrals. The resulting contributions do not prove to be numerically important in these decays, producing less than 1% of the total amplitudes.

Results for these couplings, as defined by

$$\begin{aligned}\langle\gamma(q_1)\pi^0(q_2)|\omega\rangle &= ieg_{\omega\pi\gamma}\epsilon_{\alpha\beta\mu\nu}q_1^\alpha q_2^\beta\epsilon_\gamma^{*\mu}\epsilon_\omega^\nu, \\ \langle\gamma(q_1)\pi^b(q_2)|\rho^a\rangle &= i\delta^{ab}eg_{\rho\pi\gamma}\epsilon_{\alpha\beta\mu\nu}q_1^\alpha q_2^\beta\epsilon_\gamma^{*\mu}\epsilon_\rho^\nu,\end{aligned}\quad (6.23)$$

are given in Table 6.1, along with the corresponding decay widths. Since isospin symmetry has been assumed there is no ϵ^{ab3} component to the $\rho\pi\gamma$ matrix element. The decay widths obtained for the charged and neutral ρ mesons are therefore equal. These model results agree well with the experimental values [12]:

$$\begin{aligned}\Gamma(\omega \rightarrow \pi\gamma) &= 717 \pm 43\text{keV}, \\ \Gamma(\rho^0 \rightarrow \pi^0\gamma) &= 121 \pm 31\text{keV}, \\ \Gamma(\rho^\pm \rightarrow \pi^\pm\gamma) &= 68 \pm 8\text{keV},\end{aligned}\quad (6.24)$$

the difference between the measured charged and neutral ρ decays not being considered statistically significant in view of the large error bars [107].

Extending the $\omega\pi\gamma$ amplitude to off-shell photon momenta, the model description can be compared to the form factor as measured in Ref. [108]. The reaction $\pi^-p \rightarrow n\omega \rightarrow n\pi^0\mu^+\mu^-$ was studied to investigate the form factor in the range from $4m_\mu^2$ to $(m_\omega - m_\pi)^2$. Working with a definition of

$$F_{\omega\pi}(q^2) = \frac{\langle\gamma^*(q^2)\pi|\omega\rangle}{\langle\gamma(q^2=0)\pi|\omega\rangle},\quad (6.25)$$

the model results and the experimental data are shown in Fig. 6.10. In common with the other electromagnetic form factors presented in this chapter, the fit parameter set where $m_0(0) = 300$ MeV has been used in plotting the model results, which have been found not to be sensitive to the set chosen.

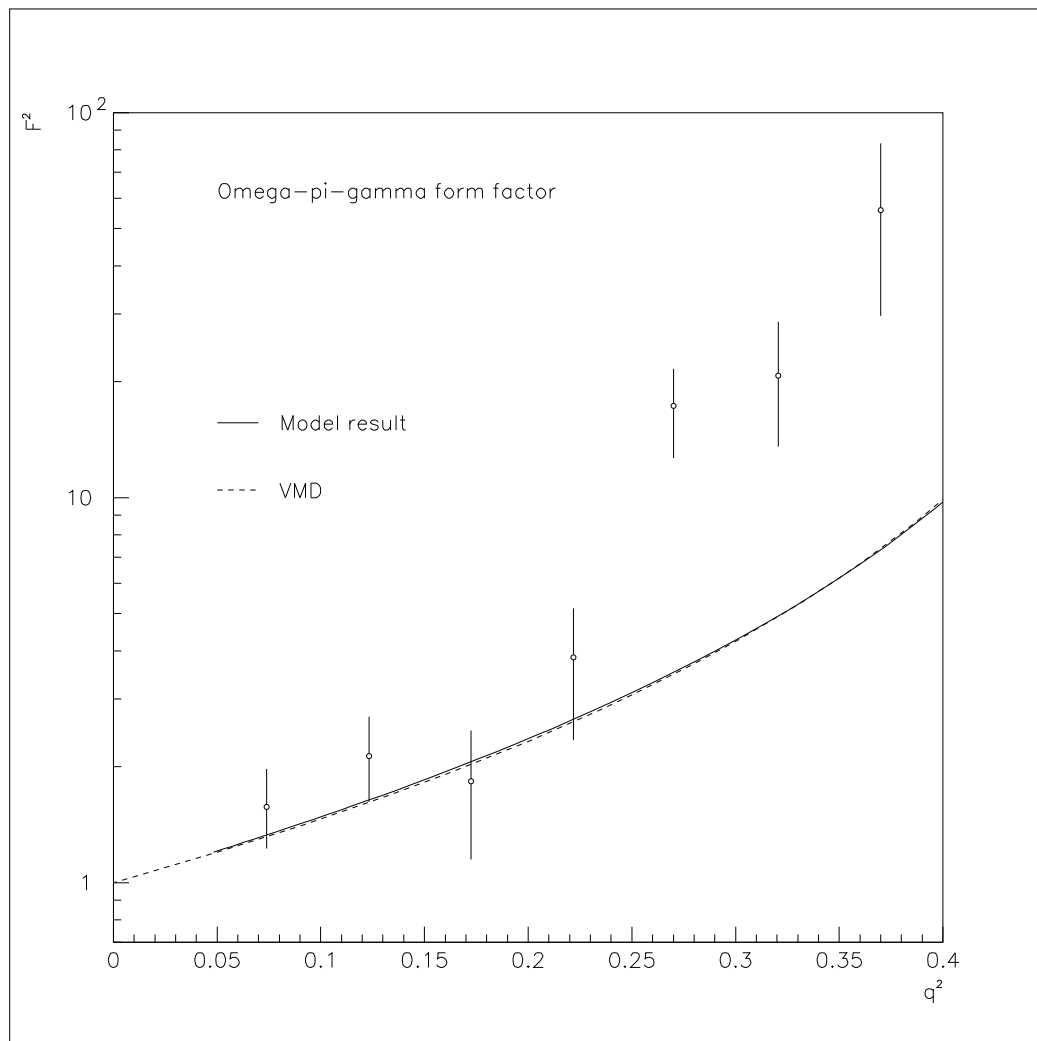


Figure 6.10: The $\omega\pi\gamma^*(q^2)$ form factor is defined by Eq. 6.25. Its square is plotted on a logarithmic scale against q^2 in GeV^2 . The solid line is the model result; the dashed line is the VMD approximation to it. Data points are taken from Ref. [108].

In Fig. 6.10 the model is seen to be in agreement with the data points at low q^2 but there is a discrepancy at higher energies. The same observations are true of other theoretical calculations [109]. It may be that there is some effect on this form factor from the tail of the ρ' resonance [30]. Another potentially important missing ingredient in the present calculation is $\omega\phi$ mixing, since a calculation of this form factor within an SU(3) effective Lagrangian approach [110] has found a significant dependence on the mixing strength. Improved data would be needed to draw any firmer conclusions and there are indeed hopes that the experimental situation will be clarified by forthcoming experiments at VEPP-2M or DAΦNE [107].

For this form factor, comparison with the VMD prediction,

$$F_{\omega\pi}(q^2) = 1 - \frac{g_{\omega\rho\pi}}{g_{\omega\pi\gamma}g_\rho} \frac{q^2}{q^2 - m_\rho^2}, \quad (6.26)$$

is not completely straightforward, since the coupling $g_{\omega\rho\pi}$ cannot be calculated on-shell. Nonetheless, a reasonable estimate of it can be made by extrapolating to the soft-pion limit⁶ (zero pion four-momentum). For a variety of fit parameter sets over the admissible range, the results for $g_{\omega\rho\pi}$ determined in this way are within 20% of the prediction of universal coupling, $g_{\omega\rho\pi} = g_{\omega\pi\gamma}g_\rho$. The curve corresponding to Eq. 6.26 with the estimated $\omega\rho\pi$ coupling⁷ is that which is labelled as VMD in Fig. 6.10. It provides a very good approximation to the results of the full calculation in the model.

⁶In that limit, the pseudoscalar-axial mixing element, J_{PA} , vanishes. Hence, the vertex function for the soft pion is taken to be $g_{\pi qq} i\gamma_5 \tau^a$.

⁷For the parameter set used in plotting the figure it is estimated to be 15.2 GeV^{-1} . The other couplings needed are quoted in footnote 4.

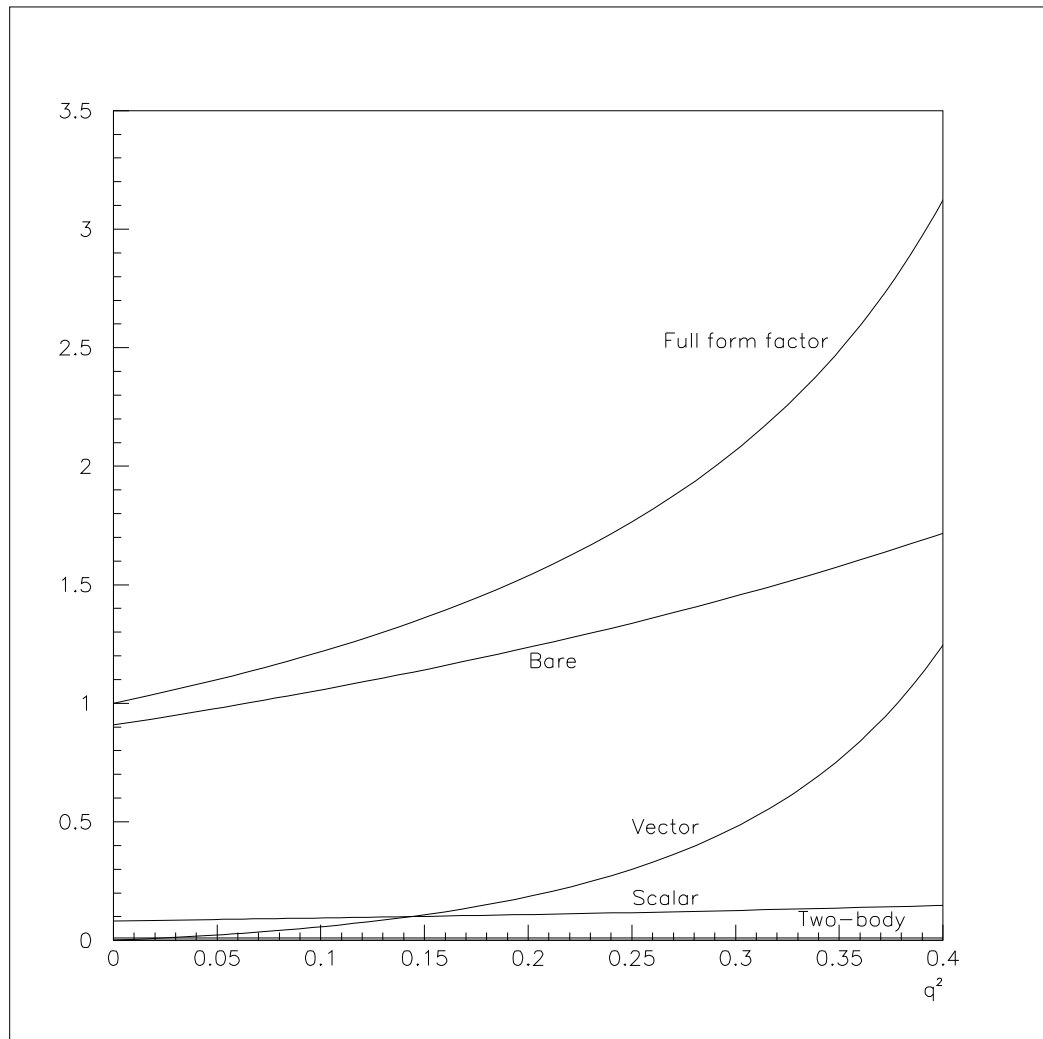


Figure 6.11: Various contributions to the $\omega\pi\gamma^*(q^2)$ form factor are plotted against q^2 in GeV^2 . The contributions are defined in the text (see Chp. 6.2).

Decomposing the form factor as in Chp. 6.2, the individual contributions are shown in Fig. 6.11. The two-body diagrams are negligible over the region considered. The contribution coming from the “scalar” part of the dressed γqq vertex (Eq. 4.22) is larger but is still a minor effect. As in the case of the pion form factor (Chp. 6.2), the model result turns out to be dominated by the bare, local photon vertex and the “vector” part of the γqq vertex. The latter contribution includes the model ρ meson propagator and so it becomes increasingly important as the timelike momentum increases towards the ρ pole. It appears that a cancellation is acting between the local contribution and that from states other than the ρ meson in the “vector” contribution so as to produce a result which is close to that of VMD with universality.

In the amplitude for the decay $a_1^\pm \rightarrow \pi^\pm \gamma$, the contribution due to two-body diagrams is generated by the terms in the nonlocal current $G_1(i\gamma_5 \otimes i\gamma_5)$ and $G_2(\gamma^\nu \gamma_5 \otimes \gamma_\nu \gamma_5)$ which have a type-II structure (Eq. 2.13). These are the very terms that gave rise to the two-body diagrams in the pion form factor (Chp. 6.2). The same numerical methods are used in computing the analogous $a_1 \pi \gamma$ diagrams. Since the a_1 mass lies above the pseudo-threshold energy for parameter set B, the evaluation of both the triangle and the two-body diagrams requires residue contributions in that case.

Gauge invariance imposes the following structure on the decay amplitude:

$$\langle \gamma(q_1) \pi^b(q_2) | a_1^a \rangle = i\epsilon^{ab3} e g_{a_1 \pi \gamma} \left[\epsilon_{a_1} \cdot \epsilon_\gamma^* + \frac{2(q_2 \cdot \epsilon_{a_1})(q_2 \cdot \epsilon_\gamma^*)}{(m_{a_1}^2 - m_\pi^2)} \right]. \quad (6.27)$$

In the isosymmetric case, there is no δ^{ab} component to the amplitude, which is consistent with the fact that the radiative decay of the neutral a_1 meson has not been detected [12]. The values calculated for $g_{a_1 \pi \gamma}$, and the corresponding decay widths, can be seen in Table 6.1. With parameter set A the scalar part of the nonlocal photon coupling and the two-body diagrams make relatively small contributions to the total amplitude. Working with set B, these contributions are substantial but largely cancel with each other. The final results for all choices of parameters are much smaller than the experimental measurement [111] of 640 ± 246 keV.

Chapter 7

Next-to-Leading Order Treatment

7.1 NLO Corrections

From even the most cursory survey of the literature it is apparent that the NJL model has long been popular in low-energy strong physics. However, almost all calculations with the model, and its various offspring (Chp. 2.2), have been restricted to leading order (LO) in the $1/N_c$ expansion. To a large extent, this is because the calculations at next-to-leading order (NLO) are much more complicated, both analytically and numerically. Part of the original motivation for the NJL model, and one of the reasons for its continued popularity, is its very simplicity at LO. One might therefore take the view that a large increase in complexity is not justified for a model that was never intended to produce highly accurate numerical results. An additional point of difficulty is that the model must be specified further at NLO since one has to regularize both quark and meson loops.

On the other hand, since $1/N_c$ is such a modest expansion parameter, it does seem important to try to estimate the size of some NLO effects. Even if were of interest for no other reason, this is a necessary aspect of the validation of the perturbative approach. For some quantities it may be that the expansion coefficients conspire to make the NLO term similar in size to the LO one. This possibility has to be eliminated

if a LO calculation is to be viewed as a reasonable approximation to the full model result.

The most appealing point about a NLO analysis, however, is that the LO treatment of a four-quark model neglects *physical* processes that are known to be qualitatively important (see Chps. 5.2, 5.3 and 6.2). For instance, several of the particles described by such models (σ , ρ , a_1) are broad states, yet the model meson propagators at LO are purely real. At NLO the particle widths are incorporated in a completely natural way, by including diagrams with purely mesonic intermediates in the BSE. Such diagrams might well prove important in model descriptions of, say, the sigma meson.

In this and the following chapter, work is presented which aims to go some way towards an improved understanding of four-quark models at NLO. Some aspects of the original NJL model at NLO have been investigated by various authors. Several such works, however, have been concerned only with subsets of the full NLO corrections [93, 112, 113]. As stressed in Refs. [43, 44], this is a somewhat unsatisfactory approach since failure to include all of the relevant diagrams can cause Ward identities and chiral symmetry constraints to be violated. To this author's knowledge, consistent NLO treatments are only available in Refs. [43, 44, 45], using respectively an effective action method, an appropriate selection of Feynman diagrams and a bosonized approximation. In the remainder of this chapter, the Feynman diagrams required at NLO in the nonlocal NJL model are presented. This model is a particularly convenient one in which to examine NLO effects. Since it does not need regularization, one avoids ambiguities that occur in the original NJL model. In addition, the Gaussian form factor (Eq. 2.7) of the nonlocal model allows complicated NLO diagrams to be evaluated efficiently with Gaussian numerical techniques. Note that some preliminary work on quark properties at NLO in the nonlocal model can be found in Ref. [114].

7.2 Quark Propagator at NLO

At NLO the quark self-energy is supplemented by two new kinds of diagram, specifically a tadpole and a meson cloud contribution. A starting point for deducing both of these contributions is the Fock diagram, which arises from the Fierzed form of the action (discussed in Chp. 2.5).

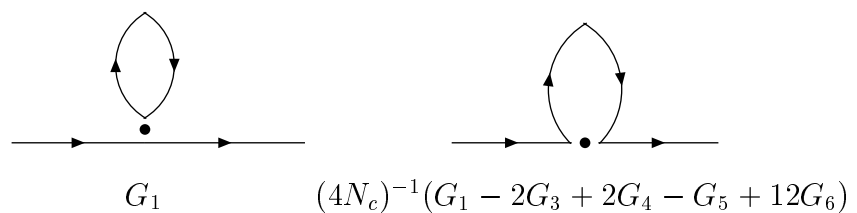


Figure 7.1: The LO and Fock diagrams in the Schwinger–Dyson equation are shown on the left– and right–hand sides of the figure respectively. Note that they have been distinguished by separating slightly the quark lines associated with each of the $\bar{\psi}\psi$ factors in the interaction.

The interaction terms of the Fierzed action (Eq. 2.19) describe the consequences of exchanging the quark fields in the model action of Eqs. 2.1 to 2.4. They lead to diagrams which are very similar to those at LO but are suppressed by one power of N_c due to a restriction on the sum over colour. Fig. 7.1 illustrates the point with a comparison of the LO and Fock diagrams in the Schwinger–Dyson equation. In the LO diagram, the one-quark loop is obtained by closing in on itself one of the $\bar{\psi}\psi$ factors from the G_1 interaction. Any colour of quark can flow around the resulting loop. The Fock diagram though is constructed by breaking the one-quark loop of the LO diagram and attaching the ends to the legs of the propagating quark. The same colour index must then be maintained throughout the diagram.

The Fock diagram in Fig. 7.1 can be used as a seed for other NLO contributions to the SDE. An example is shown in Fig. 7.2. It is generated by inserting a two-quark loop into the Fock diagram. Such a loop is simply a J integral from the LO BSE

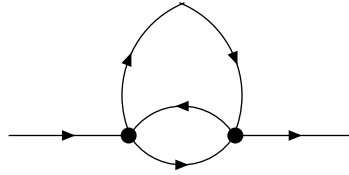


Figure 7.2: A diagram in the Schwinger–Dyson equation at NLO.

(Chp. 3.2). In comparison with the Fock diagram, the diagram in Fig. 7.2 has an additional factor of an interaction coupling constant, which is of $\mathcal{O}(N_c^{-1})$. However, this is compensated for by a factor of N_c from the colour trace over the two-quark loop and so Fig. 7.2 constitutes another NLO contribution. One can insert more two-quark loops in a similar fashion, thereby generating many more NLO diagrams. Combining all such diagrams amounts to a sum over chains of the two-quark loops (illustrated by Fig. 7.3).

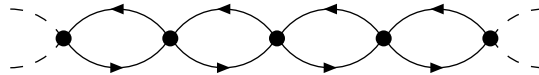


Figure 7.3: A chain of two-quark loops. Sums of such chains are used in the construction of the T matrix at LO.

Recalling Chp. 3.2, the sum of chains can be seen to produce the $\bar{q}q$ scattering matrix at LO. In fact, at NLO, the full SDE can be expressed in terms of the ladder diagram of Fig. 3.1 and the extra diagram shown in Fig. 7.4. The SDE becomes:

$$\begin{aligned}
 S_F^{-1}(p) &= \not{p} - m_c - iG_1 f^2(p) \text{Tr} \int \frac{d^4 k}{(2\pi)^4} S_F(k) f^2(k) \\
 &+ i f^2(p) \sum_i \int \frac{d^4 k}{(2\pi)^4} \hat{T}(\bar{\Gamma}_i \otimes \Omega_i; k) \bar{\Gamma}_i S_F(p-k) \Omega_i f^2(p-k), \quad (7.1)
 \end{aligned}$$

where the notation $\hat{T}(\bar{\Gamma} \otimes \Omega; q)$ has been introduced to denote that channel of the scattering matrix $\hat{T}(q)$ which describes the propagation from a $\bar{q}q$ state with matrix structure Ω to the state with structure $\bar{\Gamma}$. It is to be understood as the LO scattering matrix of Eq. 3.5, which is clearly of $\mathcal{O}(N_c^{-1})$. The summation over the index i indicates that all of the Dirac and isospin structures in the scattering matrix are to be included.

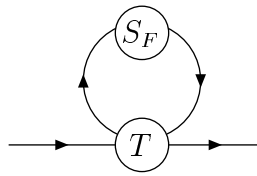


Figure 7.4: The NLO part of the Schwinger–Dyson equation.

Note that the Fock diagram on the right-hand side of Fig. 7.1 is implicit in the second of the integrals appearing in Eq. 7.1. As the seed for the scattering matrix, it can be isolated simply by taking the first term from the right-hand side of Eq. 3.5.

Equation 7.1 illustrates that in general the quark SDE and meson BSE form part of a system of coupled integral equations. A perturbative expansion in $1/N_c$ therefore provides a great simplification by allowing the solutions to be built up separately one order at a time. Although the SDE as written above contains all of the required terms at LO and NLO, it also includes some unwanted higher order terms. In order to restrict it to the terms of interest the full quark propagator is written in the form

$$S_F^{-1}(p) = S^{-1}(p) + \Sigma_N(p) + \dots$$

$$S_F(p) = S(p) - S(p)\Sigma_N(p)S(p) + \dots, \quad (7.2)$$

where Σ is the quark self-energy and a convention is followed whereby a symbol with the subscript N represents the NLO contribution to that quantity. The same symbol without this subscript is to be understood as referring to the quantity evaluated at

LO. In Eq. 7.2, therefore, the dots indicate irrelevant terms beyond NLO. Substituting the decomposition into Eq. 7.1 and equating terms at each order of $1/N_c$, one of course recovers the familiar ladder SDE (Eq. 3.2) at LO. The NLO terms meanwhile consist of a contribution involving the scattering matrix along with a piece coming from a NLO self-energy insertion into the ladder self-energy diagram,

$$\begin{aligned} \Sigma_N(p) &= iG_1 f^2(p) \text{Tr} \int \frac{d^4 k}{(2\pi)^4} S(k) \Sigma_N(k) S(k) f^2(k) \\ &+ i f^2(p) \sum_i \int \frac{d^4 k}{(2\pi)^4} \hat{T}(\bar{\Gamma}_i \otimes \Omega_i; k) \bar{\Gamma}_i S(p-k) \Omega_i f^2(p-k). \end{aligned} \quad (7.3)$$

One can substitute for $\Sigma_N(k)$ in Eq. 7.3 using the full expression on the right-hand side of that equation. This immediately leads to an explicit expression for the NLO self-energy:

$$\Sigma_N(p) = c f^2(p) + i f^2(p) \sum_i \int \frac{d^4 k}{(2\pi)^4} \hat{T}(\bar{\Gamma}_i \otimes \Omega_i; k) \bar{\Gamma}_i S(p-k) \Omega_i f^2(p-k), \quad (7.4)$$

where

$$\begin{aligned} c &= \frac{-G_1}{1 - G_1 J_{SS}(0)} \sum_i \text{Tr} \int \frac{d^4 k}{(2\pi)^4} \int \frac{d^4 \ell}{(2\pi)^4} \hat{T}(\bar{\Gamma}_i \otimes \Omega_i; k - \ell) \\ &\quad \times S(k) \bar{\Gamma}_i S(\ell) \Omega_i S(k) f^4(k) f^2(\ell). \end{aligned} \quad (7.5)$$

The two pieces of Eq. 7.4 are the tadpole and meson cloud contributions advertised at the start of this section. In diagrammatic language, they are shown in Fig. 7.5. The diagram on the left-hand side of the figure is responsible for the contribution $c f^2(p)$. It is generated by the exchange of a zero-momentum σ meson between the quark and a virtual meson. Since c is a momentum-independent constant this contribution is of the same form as the LO running quark “mass”, $m(0) - m_c$ (see Eqs. 3.1 and 3.3). The other diagram in Fig. 7.5 illustrates the emission and subsequent reabsorption of a virtual meson. Its evaluation requires an explicit integration to be performed at each value of the quark momentum and produces a wavefunction renormalization \not{p} component as well as a scalar term.

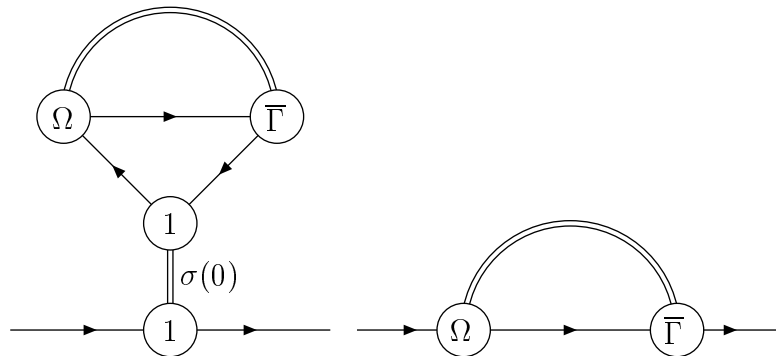


Figure 7.5: Diagrams contributing to the NLO quark self-energy. A double line is used to denote the propagation of a $\bar{q}q$ state, as described by the LO scattering matrix. The $\bar{q}q$ system has initial and final state matrix structures that are specified in the open circles at the ends of the double line.

7.3 Meson Propagators at NLO

At LO, the mesonic bound states are constructed from the ladder Bethe–Salpeter equation, as described in Chp. 3.2. The natural basis for discussion of the NLO version of this equation deals with corrections to the basic two-quark loop, J_{ij} . On incorporating the NLO contributions into an expanded definition of J , the scattering matrix will retain the form of Eqs. 3.4 and 3.5. Such NLO corrections are of three distinct kinds. They arise from a NLO quark self-energy insertion, from t-channel one-meson exchange between the quarks and from the combination of two three-meson vertices.

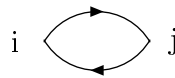


Figure 7.6: The LO loop in the Bethe–Salpeter equation.

The graphical notation of Fig. 7.6 is used in this section. The figure represents the two-quark loop that appears in the LO BSE. Each cross denotes the relevant matrix insertion (Γ_i or Γ_j) as well as two interaction form factors (each of these is evaluated at the momentum of a connected internal quark line).

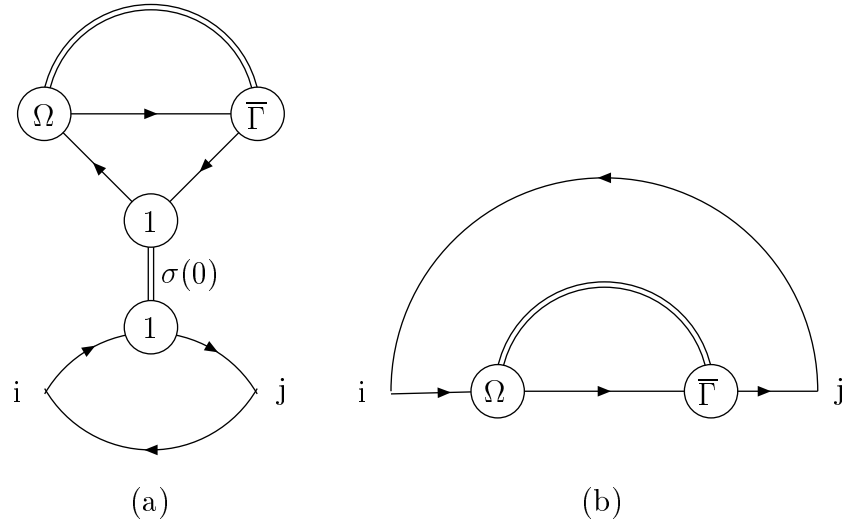


Figure 7.7: Diagrams appearing in the BSE at NLO as a consequence of the NLO quark self-energy. There are also similar diagrams, with fermion arrows in the opposite directions.

An obvious correction to a LO J loop is generated by replacing a LO quark propagator with its NLO part. This results in the following contribution to $J_{Nij}(q^2)$, which is illustrated in Fig. 7.7:

$$\begin{aligned}
 & -i\text{Tr} \int \frac{d^4p}{(2\pi)^4} \Gamma_i S(p_-) \Sigma_N(p_-) S(p_-) \Gamma_j S(p_+) f^2(p_-) f^2(p_+) \\
 & -i\text{Tr} \int \frac{d^4p}{(2\pi)^4} \Gamma_i S(p_-) \Gamma_j S(p_+) \Sigma_N(p_+) S(p_+) f^2(p_-) f^2(p_+). \quad (7.6)
 \end{aligned}$$

Another kind of NLO contribution is based on a Fock diagram. The Fock diagram in the BSE is constructed by a rearrangement of the quark lines at one of the interaction vertices in a chain of LO loops. It is shown on the left-hand side of Fig. 7.8 below. Just as in Chp. 7.2, a diagram of the same order in $1/N_c$ can be generated from it by

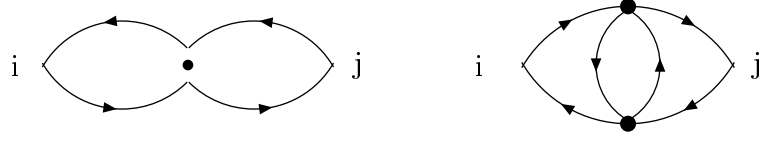


Figure 7.8: The Fock diagram in the Bethe–Salpeter equation is shown on the left-hand side of the figure. Note that it has been distinguished from two successive LO J loops by slightly separating the quark lines associated with each of the $\bar{\psi}\Gamma\psi$ factors in the interaction vertex. Another NLO BSE diagram is shown on the right-hand side of the figure.

inserting a two-quark loop. Doing so gives the diagram shown on the right-hand side of the same figure. One can proceed to create chains of such loops (Fig. 7.3). In fact, just as for the case of the quark propagator, the Fock contribution is only the first term in a set of diagrams which produce a LO scattering matrix when summed. Their total amounts to the exchange of a t-channel virtual meson between the two quark lines of a LO J loop. It is shown in Fig. 7.9c and makes the following contribution to $J_{Nij}(q^2)$:

$$\sum_r \text{Tr} \int \frac{d^4 p}{(2\pi)^4} \int \frac{d^4 k}{(2\pi)^4} \hat{T}(\bar{\Gamma}_r \otimes \Omega_r; p - k) \Gamma_i S(k_-) \Omega_r S(p_-) \Gamma_j S(p_+) \bar{\Gamma}_r S(k_+) \times f^2(k_-) f^2(k_+) f^2(p_-) f^2(p_+). \quad (7.7)$$

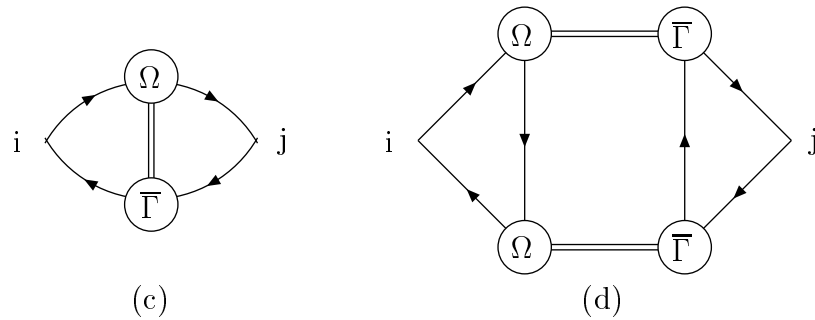


Figure 7.9: Meson exchange diagrams in the BSE at NLO. There are also similar diagrams, with fermion arrows in the opposite directions.

Finally, there is a NLO contribution that involves intermediate two-meson states (it is illustrated in Fig. 7.9d). Diagrams of this form allow the instability of a meson to be reflected in its propagator by introducing an imaginary component above the threshold energy for physical meson decays into two particle final states. They are created by joining together two LO three-meson vertices¹, each of which is of $\mathcal{O}(1/\sqrt{N_c})$. In writing an explicit expression for these BSE diagrams, it is convenient to use functions L and \bar{L} that describe the LO three-meson vertices.

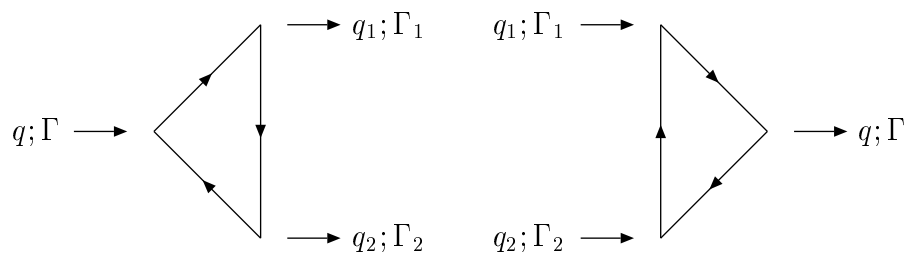


Figure 7.10: The three-point loops L and \bar{L} . They are defined respectively by the diagrams on the left- and right-hand sides of the figure, together with similar diagrams where the fermion arrows point in the opposite directions.

¹Such vertices were considered in the context of meson decays in Chp. 5.3.

L is defined to be:

$$\begin{aligned}
L(q, q_1, q_2; \Gamma, \Gamma_1, \Gamma_2) &= i\text{Tr} \int \frac{d^4 p}{(2\pi)^4} \Gamma S(p_-) \Gamma_2 S(p - \frac{1}{2}(q_1 - q_2)) \Gamma_1 S(p_+) \\
&\quad \times f^2(p_-) f^2(p_+) f^2(p - \frac{1}{2}(q_1 - q_2)) \\
&\quad + i\text{Tr} \int \frac{d^4 p}{(2\pi)^4} \Gamma S(p_-) \Gamma_1 S(p + \frac{1}{2}(q_1 - q_2)) \Gamma_2 S(p_+) \\
&\quad \times f^2(p_-) f^2(p_+) f^2(p + \frac{1}{2}(q_1 - q_2)), \tag{7.8}
\end{aligned}$$

and \bar{L} is a similar function for the $2 \rightarrow 1$ version of the loop,

$$\begin{aligned}
\bar{L}(q, q_1, q_2; \Gamma, \Gamma_1, \Gamma_2) &= i\text{Tr} \int \frac{d^4 p}{(2\pi)^4} \Gamma S(p_+) \Gamma_1 S(p - \frac{1}{2}(q_1 - q_2)) \Gamma_2 S(p_-) \\
&\quad \times f^2(p_-) f^2(p_+) f^2(p - \frac{1}{2}(q_1 - q_2)) \\
&\quad + i\text{Tr} \int \frac{d^4 p}{(2\pi)^4} \Gamma S(p_+) \Gamma_2 S(p + \frac{1}{2}(q_1 - q_2)) \Gamma_1 S(p_-) \\
&\quad \times f^2(p_-) f^2(p_+) f^2(p + \frac{1}{2}(q_1 - q_2)). \tag{7.9}
\end{aligned}$$

Clearly L and \bar{L} are symmetric under $1 \leftrightarrow 2$. Using the cross notation, these functions represent the triangular loops shown in Fig. 7.10. The contribution to $J_{Nij}(q^2)$ from the diagram of Fig. 7.9d can then be written as follows:

$$\begin{aligned}
&-i \sum_{r,s} \int \frac{d^4 p}{(2\pi)^4} \hat{T}(\bar{\Gamma}_r \otimes \Omega_r; p_+) \hat{T}(\bar{\Gamma}_s \otimes \Omega_s; -p_-) L(q, p_+, -p_-; \Gamma_i, \Omega_r, \Omega_s) \\
&\quad \times \bar{L}(q, p_+, -p_-; \Gamma_j, \bar{\Gamma}_r, \bar{\Gamma}_s). \tag{7.10}
\end{aligned}$$

7.4 Diagrams for Coupling to Currents at NLO

A NLO determination of the coupling between a particle and an external current requires the calculation of additional diagrams. Such diagrams are considered in the present section, taking the pion decay constant as an example. (Note that the actual expressions for the various NLO contributions to f_π can be found in Appendix A.1.)

At LO the pion decay constant receives two kinds of contribution, which arise from the local and nonlocal parts of the axial current (see Chp. 4.1). At NLO several of

the extra diagrams can be straightforwardly derived by modifying loops which appear in the LO diagrams. Starting from a one-quark or a two-quark loop at LO, there are NLO corrections which follow by analogy with diagrams from the SDE and BSE respectively. Both the one- and two-quark loops are corrected due to a NLO quark self-energy insertion (which is composed of the two diagrams shown in Fig. 7.5). A two-quark loop should also be corrected due to t-channel virtual meson exchange and due to intermediate two-meson states. Introducing these corrections results in the diagrams of Figs. 7.11 and 7.12.

Other NLO contributions arise from the fact that the vertex function which describes the coupling between a meson and dynamical quarks has a NLO component (Eq. 7.13). Diagrams (*k*) and (*l*) of Fig. 7.13 are the obvious consequences of this point.

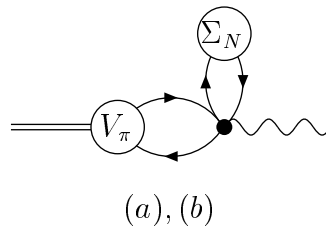


Figure 7.11: The figure shows the sum of the NLO diagrams (*a*) and (*b*) in the coupling of the pion to the axial current. Diagram (*a*) includes only that part of the NLO quark self-energy shown on the left-hand side of Fig. 7.5; diagram (*b*) includes only that part shown on the right-hand side of the same figure.

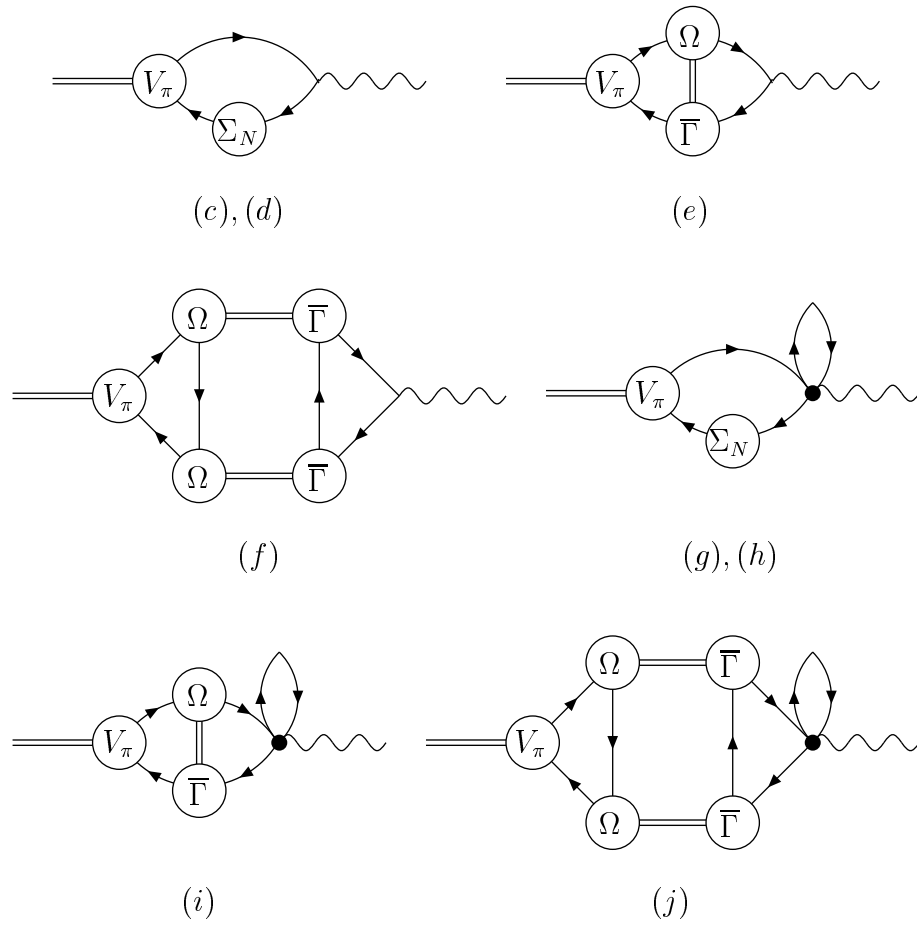


Figure 7.12: The figure shows the sum of the NLO diagrams (c) and (d) in the coupling of the pion to the axial current. Also shown is the sum of diagrams (g) and (h), as well as the diagrams (e), (f), (i) and (j). Diagrams (c) and (g) include only that part of the NLO quark self-energy shown on the left-hand side of Fig. 7.5; diagrams (d) and (h) include only that part shown on the right-hand side of the same figure. Note that there are also similar diagrams, with fermion arrows in the opposite directions.

Since there are four quark fields in the nonlocal part of the axial current one should consider the effects of exchanging the roles played by the fields. As for the interaction vertices, such effects can be described by Fock terms, which are suppressed by one power of N_c in comparison with the original terms of the nonlocal current (see Chp. 2.5). Although there is an ambiguity in defining their transverse components, this is of no concern in the calculation of the pion decay constant. One could of course create further NLO diagrams by appending two-quark loops to the Fock diagram. However, it is demonstrated in Appendix A.1 that such contributions are automatically included in other diagrams and therefore it is more convenient to treat the Fock diagram (Fig. 7.14) separately.

There are two more NLO diagrams to be included in the coupling of a meson to an external current. They are shown in Fig. 7.15. Diagram (*o*) is similar to some other NLO contributions in that it arises from the exchange of a virtual meson between two quarks. It recognizes the possibility that the two quarks need not necessarily belong to the same quark loop. The remaining NLO diagram, (*n*), is somewhat similar to diagram (*j*) of Fig. 7.12 and occurs because the nonlocal current can be coupled through two two-quark loops (cf. the two-body diagrams contributing to several of the electromagnetic processes described in Chp. 6).

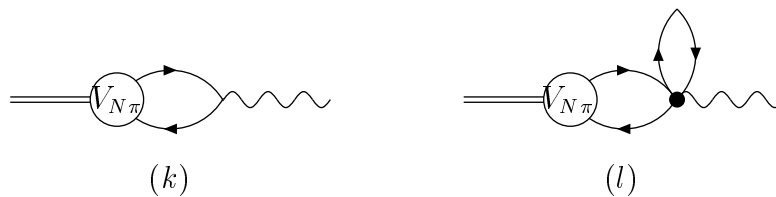


Figure 7.13: The NLO diagrams (*k*) and (*l*) in the coupling of the pion to the axial current. $V_{N\pi}$ is the NLO part of the pion vertex function.

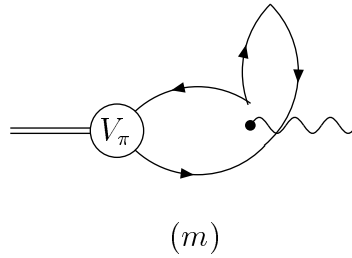


Figure 7.14: The NLO diagram (m) in the coupling of the pion to the axial current. Note that it has been distinguished from a similar LO diagram by slightly separating the quark lines associated with each of the $\bar{\psi}\psi$ factors in the nonlocal current.

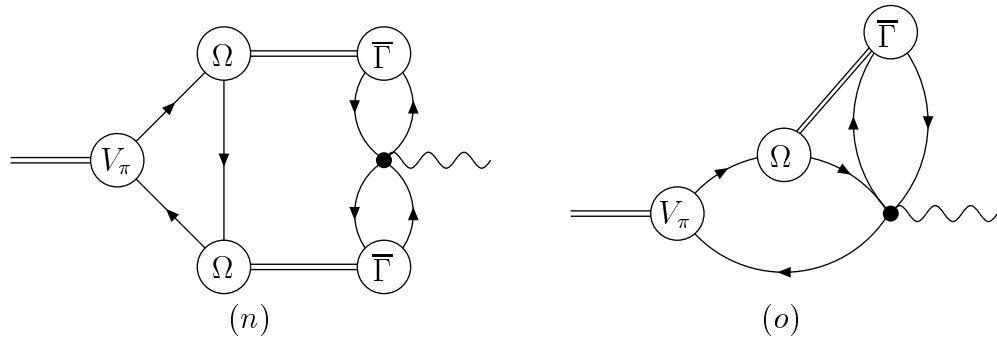


Figure 7.15: The NLO diagrams (n) and (o) in the coupling of the pion to the axial current.

Pion Decay Constant at NLO

As mentioned in Chp. 4.2, the $\not{q}\gamma_5$ identity of Eq. 4.3 is a useful tool for simplifying the various NLO contributions to the pion decay constant. As in the LO proof of GMOR discussed in that section, the identity enables a diagram generated by the local current to be rewritten in such a way as to elicit a cancellation with part of a similar nonlocal contribution. After making such simplifications, some other useful cancellations among the NLO diagrams can be identified. These are discussed in Appendix A.1, which specialises to a version of the model with the G_1 coupling only. In that case, the NLO component of f_π is shown to reduce to the following:

$$\begin{aligned}
f_{N\pi} = & \frac{ig_{\pi qq}G_1}{2m_\pi^2} J_{NPP}(q^2) \int \frac{d^4k}{(2\pi)^4} \text{Tr} [S(k)] f(k) (f(k+q) + f(k-q)) \\
& + \frac{g_{\pi qq}m_c}{m_\pi^2} (J_{NPP}^{(a)} \text{ with } f^2(p_\pm)f^4(p_\mp) \rightarrow f(p_\pm)f^3(p_\mp)) \\
& + \frac{g_{\pi qq}m_c}{m_\pi^2} (J_{NPP}^{(b)} \text{ with } f^2(p_\pm)f^4(p_\mp) \rightarrow f(p_\pm)f^3(p_\mp)) \\
& + \frac{g_{\pi qq}m_c}{m_\pi^2} (J_{NPP}^{(c)} \text{ with } f^2(p_+)f^2(p_-) \rightarrow f(p_+)f(p_-)) \\
& \quad + \frac{g_{\pi qq}m_c}{m_\pi^2} (J_{NPP}^{(d)} \text{ with } \bar{L} \rightarrow \bar{L}') \\
& + i \frac{c g_{\pi qq}}{2m_\pi^2} (1 - G_1 J_{PP}(q^2)) \int \frac{d^4p}{(2\pi)^4} \text{Tr} [S(p)S(p)] f^3(p) (f(p+q) + f(p-q)) \\
& - \frac{g_{\pi qq}}{2m_\pi^2} (1 - G_1 J_{PP}(q^2)) \sum_i \int \frac{d^4p}{(2\pi)^4} \frac{d^4k}{(2\pi)^4} \hat{T}(\bar{\Gamma}_i \otimes \Omega_i; p-k) \text{Tr} [S(p)\bar{\Gamma}_i S(k)\Omega_i S(p)] \\
& \quad \times f^3(p) (f(p+q) + f(p-q)) f^2(k) \\
& \quad + \frac{g_{N\pi qq}}{g_{\pi qq}} f_\pi(\text{LO}), \tag{7.11}
\end{aligned}$$

where $J_{Nij}^{(x)}$ denotes the contribution to J_{Nij} from the BSE diagram labelled (x) (see Figs. 7.7 and 7.9) and \bar{L}' is a variation² on \bar{L} .

7.5 GMOR at NLO

In the previous sections of this chapter, the diagrams required in a NLO treatment of the nonlocal NJL model have been discussed. In all cases the diagrams are deduced by inspection, sometimes using the Fock terms as a guide. Obviously, it is important to have a check that a consistent set of diagrams has been identified. To this end, the Gell-Mann–Oakes–Renner relation is demonstrated to hold at NLO in the model, albeit in the simpler version without vector mesons. As a first step in establishing the relation, consider the chiral expansion of the pion mass.

The pion pole is located at

$$1 - G_1 J_{PP}(q^2) - G_1 J_{NPP}(q^2) = 0, \tag{7.12}$$

²It differs from Eq. 7.9 in having $f(p_+)f(p_-)$ instead of $f^2(p_+)f^2(p_-)$.

and, in the absence of mixing³, the coupling of the particle to dynamical quarks is determined by the relation:

$$(g_{\pi qq} + g_{N\pi qq} + \dots)^{-2} = \left. \frac{d(J_{PP} + J_{NPP} + \dots)}{dq^2} \right|_{q^2=m_\pi^2},$$

$$g_{N\pi qq} = \frac{-g_{\pi qq}}{2} \left. \frac{dJ_{NPP}}{dq^2} \right|_{q^2=m_\pi^2} \left[\left. \frac{dJ_{PP}}{dq^2} \right|_{q^2=m_\pi^2} \right]^{-1}. \quad (7.13)$$

If one substitutes the chiral expansion of $J_{PP}(q^2)$ (Eq. 4.6) into the on-shell condition of Eq. 7.12, it is immediately clear that the chiral expansion of $J_{NPP}(q^2)$ must start at $\mathcal{O}(q^2, m_c)$ in order for the pion to remain a Goldstone boson in the chiral limit. By definition, the coefficient of $\mathcal{O}(q^2)$ in that expansion provides an explicit expression for $g_{N\pi qq0}$, the details of which are not needed here. The calculation of the $\mathcal{O}(m_c)$ term is detailed in Appendix B, where it is also checked that there is indeed no term in J_{NPP} which survives in the chiral limit. It is sufficient here to quote the final result from that appendix, which is obtained by imposing the on-shell condition on Eq. B.15,

$$m_\pi^2 = -(g_{\pi qq0} + g_{N\pi qq0})^2 \frac{m_c [\langle \bar{\psi}\psi \rangle_0 + \langle \bar{\psi}\psi \rangle_{N0}]}{(m_0(0) - c_0)^2} + \mathcal{O}(m_c^2). \quad (7.14)$$

Hence, the chiral expansion of the pion Bethe–Salpeter amplitude retains the same structure as at LO (cf. Eq. 4.11), with NLO changes to the expressions for its on-shell coupling to quarks and for the dynamical quark mass. The shift in the former is just that which might be anticipated from the expanded definition of the pion–quark coupling constant. However, the dynamical mass scale that appears in Eq. 7.14 is not so obvious. The shift in this mass scale is given entirely by the coefficient of the tadpole diagram (see Fig. 7.5). This is despite the fact that the meson cloud of a dressed quark does make a contribution to its scalar self-energy at zero momentum

³Although the G_2 interaction (which causes πa_1 mixing) is not included in the version of the model considered here, it may nevertheless seem plausible that a $\not{q}\gamma_5$ component to the pion Bethe–Salpeter amplitude could appear as a NLO effect. The possibility can be ruled out if the Fierz rearrangement of the $(1 \otimes 1 + i\gamma_5\tau^a \otimes i\gamma_5\tau^a)$ interaction does not contain a NLO exchange interaction of the character $(\gamma_\mu\gamma_5\tau^a \otimes \gamma^\mu\gamma_5\tau^a)$. This is indeed so, as seen in Chp. 2.5.

(see Chp. 8.2)⁴.

The GMOR relation will be satisfied if a modified version of the Goldberger–Treiman relation holds in the chiral limit at NLO,

$$\begin{aligned} f_{\pi 0} &= \frac{m_0(0) - c_0}{g_{\pi qq} + g_{N\pi qq}} \\ &= \frac{m_0(0)}{g_{\pi qq}} - \frac{g_{N\pi qq}}{g_{\pi qq}} \cdot \frac{m_0(0)}{g_{\pi qq}} - \frac{c_0}{g_{\pi qq}} + \mathcal{O}(N_c^{-2}). \end{aligned} \quad (7.15)$$

The term of $\mathcal{O}(N_c^0)$ on the right-hand side of this condition was shown in Chp. 4.2 to be given by the LO part of f_π . Full details of the proof that the chiral limit of Eq. 7.11 produces the $\mathcal{O}(N_c)$ terms can be found in Appendix A.2.

⁴The meson cloud also generates a term of $\mathcal{O}(m_c)$ in the chiral expansion of J_{NPP} (see Eq. B.5).

Chapter 8

Numerical Results — NLO

8.1 Model Parameters

The model at NLO is considered in this chapter mainly in the simple case where only the G_1 interaction is present. Even so, the numerical integrals involved in the evaluation of NLO diagrams are rather complicated and so are difficult to perform to high accuracy within a reasonable time. It is therefore convenient to fit the model parameters at LO and then consider the NLO changes to the observables. Apart from the exclusion of the couplings $G_2 \dots G_5$, the parameters at LO are fitted according to the method described in Chp. 5.1. This means that $m_0(0)$ is left free and used to characterize a possible parameter set. When vector interactions are included in the model an upper bound on $m_0(0)$ is imposed by the behaviour above pseudo-threshold of the LO scattering matrix in the vector channel (see Chp. 5.1). In this simpler version of the model, however, parameter sets over a wider range of $m_0(0)$ can be investigated. Details of the sets used¹ are given in Table 8.1.

¹Note that the parameters given differ slightly from those quoted in Ref. [8] where a very similar fit was made at the same values of $m_0(0)$. This is simply because the calculations of Ref. [8] were performed within the chiral expansion of the model [115].

$m_0(0)$	$G_1(\text{GeV}^{-2})$	m_c	Λ	$m(0)$	Pole
200	14.3	4.8	1459	245	± 261
250	30.5	7.8	1064	298	± 384
300	53.8	11.0	861	351	$\pm 415 \pm 235i$
350	85.9	14.2	734	406	$\pm 338 \pm 292i$
400	128.1	17.5	647	461	$\pm 287 \pm 312i$
450	181.7	20.8	583	516	$\pm 252 \pm 320i$
500	248.0	24.1	535	572	$\pm 225 \pm 322i$

Table 8.1: Values of the model parameters, fitted at LO. Also shown is the dynamical quark mass and the position of the lowest set of poles in the LO quark propagator. Apart from G_1 , all quantities are given in MeV.

Table 8.2 lists the values of various quantities calculated at LO from the parameter sets of Table 8.1. The results are qualitatively quite similar to those obtained in the extended version of the model (as discussed in Chps. 5.2 and 5.3).

$m_0(0)$	Cond.	$g_{\pi qq}$	m_σ	$g_{\sigma qq}$	$g_{\sigma\pi\pi}$	$\Gamma(\sigma \rightarrow \pi\pi)$
200	246	2.56	385	2.56	1092	63.5
250	210	3.13	423	3.24	1336	94.4
300	189	3.70	454	3.91	1562	126.3
350	173	4.28	477	4.54	1732	152.0
400	162	4.87	492	4.98	1783	158.7
450	153	5.46	489	4.56	1489	111.0
500	146	6.04	478	5.25	1515	116.2

Table 8.2: Calculations at LO with the nonlocal NJL model. The couplings to quarks, $g_{\pi qq}$ and $g_{\sigma qq}$ are dimensionless; all other quantities are given in MeV. ‘Cond.’ refers to the quark condensate, evaluated in the chiral limit. Relevant couplings are defined in Eqs. 3.11 and 5.1.

8.2 Corrections to the Quark Propagator

Numerics

The form of the quark self-energy at NLO was described in Chp. 7.2. It contains a piece whose momentum dependence is entirely dictated by the interaction form

factors (the tadpole diagram) and another piece whose evaluation needs a separate integration at each quark momentum. Determining the coefficient of the tadpole requires an integral over five non-trivial dimensions whilst the other piece needs a four-dimensional numerical integration. The NLO quark self-energy is therefore far from easy to evaluate. Furthermore, this must be done many times and over a wide range of quark momenta in order to evaluate NLO diagrams in the BSE (see Eq. 7.6). Thus there are obvious benefits in simplifying the self-energy integrands.

Two of the non-trivial integration variables in Eqs. 7.4 and 7.5 come from the evaluation of J integrals in the LO scattering matrix. Working in Euclidean space, and taking the momentum routings of Eqs. 7.4 and 7.5, these J integrals always have a spacelike momentum argument. With that restriction they are smooth analytic functions, as is illustrated by Fig. 8.1.

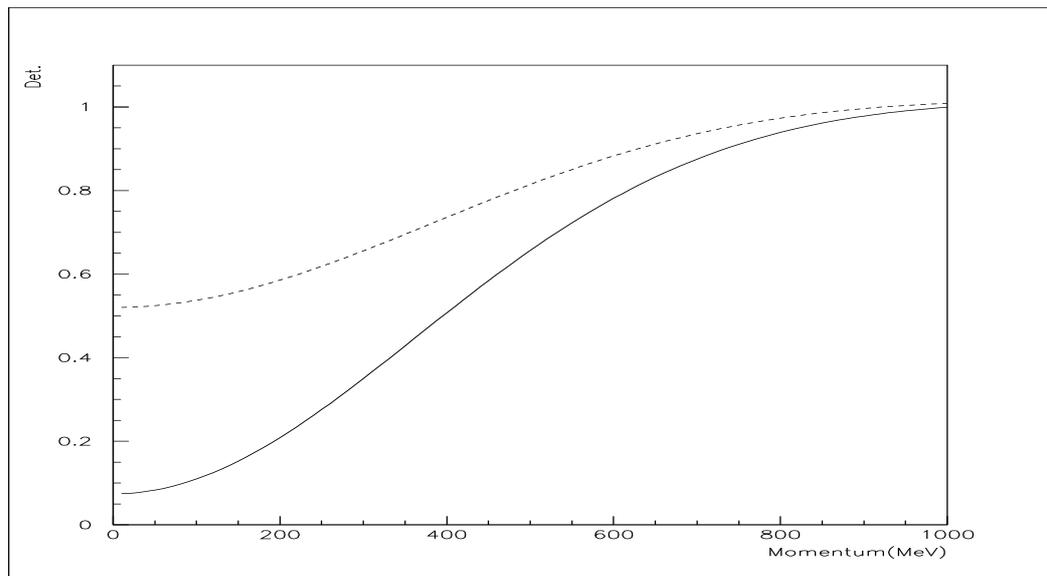


Figure 8.1: The figure shows the denominators of the pion and sigma propagators, $1 - G_1 J_{PP,SS}$, as functions of spacelike meson momentum. The pion channel is plotted with a solid line; the sigma channel with a dashed line. The parameter set used is that with $m_0(0) = 300$ MeV in Table 8.1.

The NLO self-energy integrals may be simplified by approximating J_{SS} and J_{PP} with analytic fits. The remaining two and three dimensional integrations can then

be done both quickly and accurately using Gauss–Laguerre techniques. Rapidly-converging fits are provided by the series expansions

$$J_{ij}(q^2) = \sum_n a_n T_n(x(q^2)), \quad (8.1)$$

where $\{T_n\}$ are Chebyshev polynomials and x is chosen to be

$$x = \exp\left(\frac{q^2}{\Lambda^2}\right). \quad (8.2)$$

In practice ten evaluations in each channel of J are used to calculate the first ten terms in the series. That this procedure gives a good approximation to these functions has been tested from evaluations at other momenta². Moreover, a few of the NLO BSE integrals have been compared to brute force determinations, where J is evaluated numerically at each value of momentum. The results confirm the validity of using the series fits since they are in agreement to within the uncertainties introduced by numerical integration over the other variables.

Results

The results for the NLO quark self-energy are presented below, using the notation of Eq. 1.4. They are in agreement with those found in Ref. [114], where an alternative discussion of Σ_N in the nonlocal NJL model is available. Figs. 8.2 and 8.3 show the functions that describe the vector ($a(p)$) and scalar ($b(p)$) components of the inverse quark propagator respectively. They are plotted for both spacelike and timelike momenta, but only up to an energy given by the real part of the pole in the LO quark propagator. This is because of the form of the contributions where the quark line is dressed by virtual pion and sigma clouds (shown on the right-hand side of Fig. 7.5). The corresponding integral in Eq. 7.4 includes the propagator $S(p-k)$ and so the naive contour of integration along the real k_4 axis becomes pinched above that energy.

²Over the range that dominates the self-energy integrands (up to ~ 500 MeV), the errors in the fits have been found to be less than 0.01% in all cases.

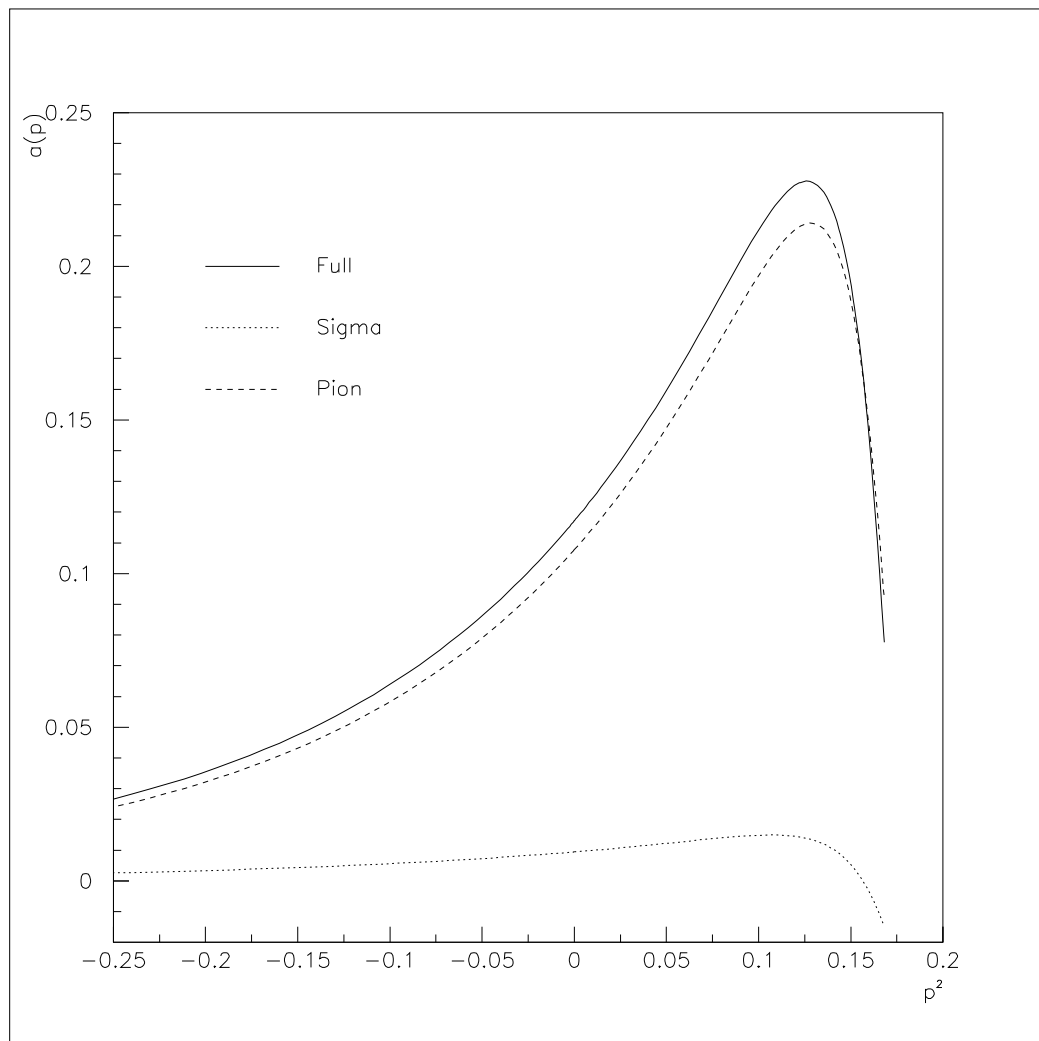


Figure 8.2: The figure shows the dimensionless function $a(p)$ from the inverse quark propagator, plotted against p^2 in GeV^2 . The function is defined by Eq. 1.4 and only becomes non-zero beyond LO. Also shown are the contributions to $a(p)$ obtained by dressing the quark line with pion and sigma clouds. The parameter set used is that with $m_0(0) = 300$ MeV in Table 8.1.

At LO there is no wavefunction renormalization of the quark propagator. There are however NLO contributions to the \not{p} component. Fig. 8.2 shows that these range up to ~ 0.25 , which is consistent with the expected magnitude of $1/N_c$ corrections. An intriguing aspect of the results is the appearance of a sudden dip in $a(p)$ just before the LO pseudo-threshold energy. It would certainly be interesting to examine the behaviour of the function above this energy, although that would require a detailed analysis of the pole structure at NLO, which is beyond the scope of the present work. Also plotted on the figure are the individual contributions to $a(p)$ which arise from dressing the quark line with virtual pions and with virtual sigma mesons. The pion cloud is obviously the main effect. Since its propagator has a pole at small timelike momentum, one expects the T matrix in the pseudoscalar channel to be large at modest values of spacelike momenta (the region which dominates the NLO integrals). This is verified by Fig. 8.1. Note also that an extra factor of three is associated with the pion contributions due to isospin multiplicity.

The scalar component of the NLO quark self-energy receives contributions from both the tadpole and the meson-cloud diagrams of Fig. 7.5. Fig. 8.3 demonstrates that the addition of the tadpole contribution to the LO function, $m(p)$, has very little effect (i.e., the constant c (Eq. 7.5) is much smaller than $m(0)$). The meson-cloud diagrams are rather more significant, increasing $b(0)$ by a typical $1/N_c$ level of $\sim 25\%$. The NLO shift in the quark “mass” function $b(p)/(1+a(p))$ is therefore fairly modest (an increase of $\sim 15\%$ at zero momentum).

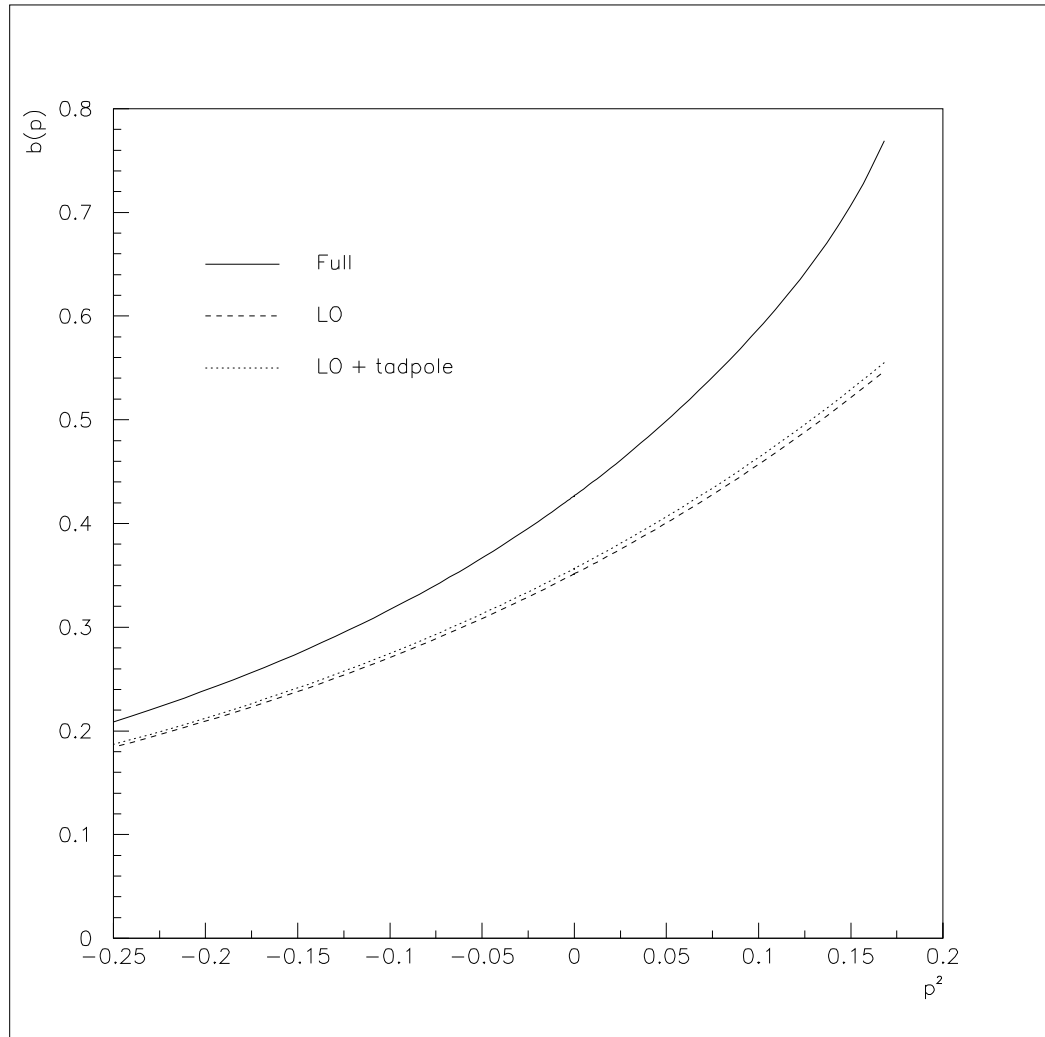


Figure 8.3: The figure shows the function $b(p)$ from the inverse quark propagator, plotted in GeV against p^2 in GeV². The function is defined by Eq. 1.4 and corresponds to $m(p)$ at leading order. It is shown at LO and at NLO, together with the sum of the LO result and the tadpole contribution. The parameter set used is that with $m_0(0) = 300$ MeV in Table 8.1.

The NLO quark self-energy has little impact on the values of the model condensate, which are quoted in Table 8.3. Although there are slight increases for the unconfined parameter sets the results are very close to the LO values given in Table 8.2. The same observation holds true³ in the local NJL model when proper time regularization of the quark loops is used [43], although in the $O(4)$ scheme there are appreciable NLO shifts.

$m_0(0)$	Cond.	c	c_0	$c_0(\pi)$	$c_0(\sigma)$
200	259	-25.0	-25.3	-90.2	64.9
250	215	-12.4	-8.0	-44.2	36.2
300	190	-5.2	1.7	-22.4	24.1
350	174	-0.005	8.8	-8.6	17.4
400	162	4.1	14.6	1.4	13.1
450	153	7.7	19.6	9.5	10.2
500	145	10.8	24.2	16.3	7.9

Table 8.3: Properties of the quark propagator at NLO. All quantities are quoted in MeV. ‘Cond.’ refers to the quark condensate, evaluated in the chiral limit. The constant c from the NLO tadpole diagram is defined in Eq. 7.5, $c(\alpha)$ being the contribution to it from the tadpole in the channel of the α meson.

Fig. 8.4 shows the breakdown of the NLO part of $b(p)$ into contributions coming from intermediate pions and sigma mesons. As for $a(p)$, the diagrams with a pion intermediate are more important than those involving its chiral partner. Quark dressing due to meson clouds in the original NJL model has been investigated by Quack and Klevansky⁴ [112]. They found that the pion cloud tends to increase $b(p)$ but that this is partially cancelled by the sigma cloud. The nonlocal model studied here supports the conclusion and is able to place it on a firmer footing since there are no ambiguities associated with the meson loop regularization⁵.

³At least for values of the quark mass below ~ 600 MeV.

⁴Unfortunately, the tadpole contributions were not identified by those authors.

⁵Moreover, unlike Ref. [112], the present work does not replace the model meson propagators with their canonical forms.

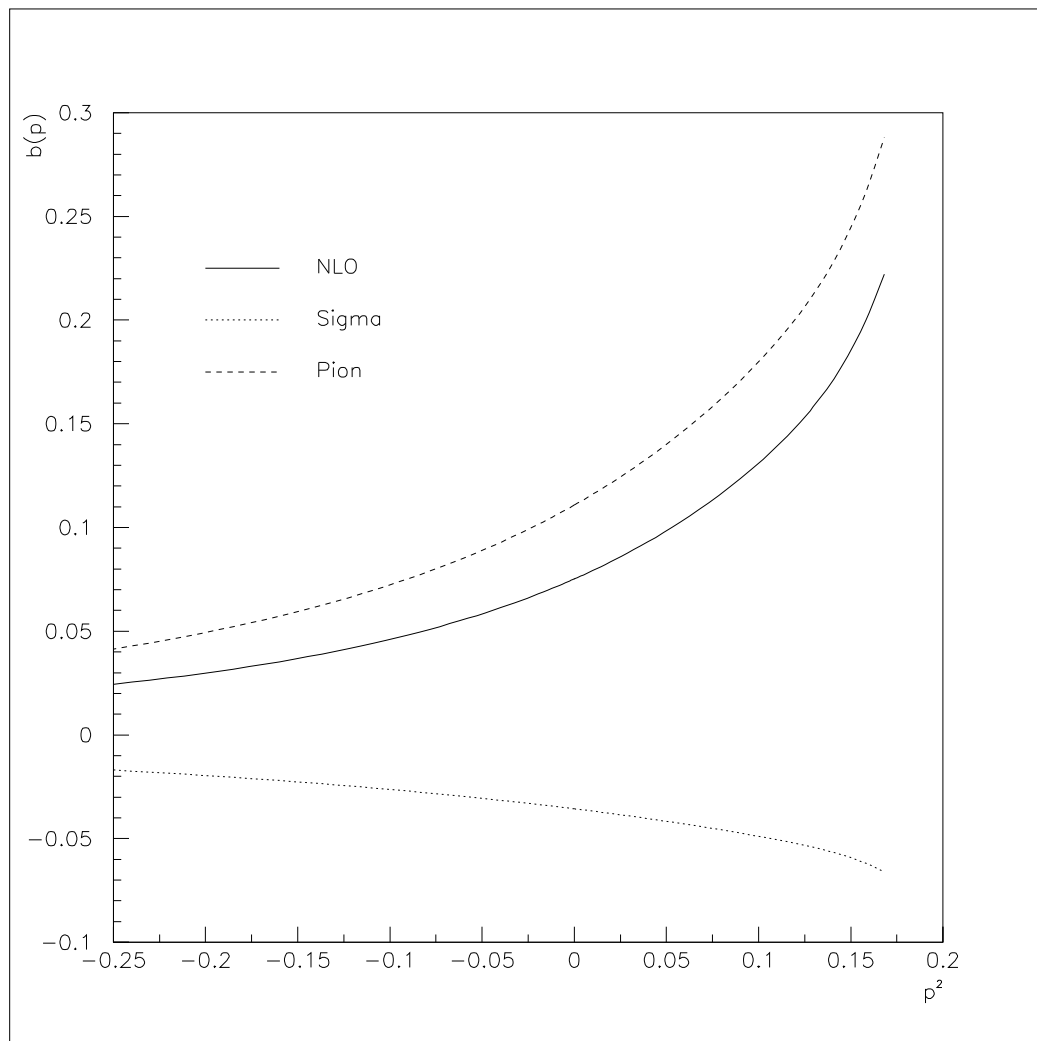


Figure 8.4: The figure shows the NLO contributions to the function $b(p)$. The full NLO component is plotted in GeV against p^2 in GeV^2 , together with its decomposition into the parts that involve intermediate pions and sigma mesons. The parameter set used is that with $m_0(0) = 300$ MeV in Table 8.1.

Although the tadpole diagrams in the NLO quark self-energy are not numerically significant, it is nevertheless interesting to consider them in more detail. As noted in Chp. 7.5, c_0 is an important quantity for NLO changes to the pion mass and decay constant (see Eqs. 7.14 and 7.15). Since c_0 and the NLO shift in the quark condensate are both small, the pion observables will be little altered unless the state is much more strongly coupled to quarks at NLO. One might therefore wonder whether there should be some physical reason for c_0 to be small, perhaps because of chiral symmetry. The entries in Table 8.3 for the pion and sigma tadpoles are quite suggestive at low and intermediate $m_0(0)$. For instance, with the set at $m_0(0) = 200$ MeV, the pion tadpole adds as much as 45% of the LO chiral quark mass, but this is cancelled to a large extent by the sigma tadpole. The process does not persist at larger $m_0(0)$, however, where the pion tadpole changes sign.

NLO Quark Self-Energy in the Extended Model

In the extended version of the model there are additional contributions to the NLO quark self-energy from the tadpoles and meson clouds of other mesonic states. Although calculation of the properties of these mesons at NLO would demand a good deal of further work, it is straightforward to evaluate their contributions to Σ_N . In so doing, the model couplings $G_2 \dots G_5$ are taken to be those set by the LO phenomenology. The parameter sets A, B and C of Chp. 5.1 produce the results of Table 8.4. As in the simple version of the model, there is only a modest change to the condensate and the constant c is small. Comparison with the entries at similar $m_0(0)$ in Table 8.3 indicates that pseudoscalar–axial mixing is an important effect, but one which is cancelled owing to the simultaneous introduction of the model ρ meson. Bearing in mind the freedom to set model couplings independently, the entries of Tables 8.3 and 8.4 argue against any suggestion that c_0 should be *a priori* small due to chiral symmetry.

Quantity	Set A	Set C	Set B
$m_0(0)$	280	300	320
Cond.	187	180	175
c	-9.1	-5.2	-1.2
c_0	-1.2	3.6	8.4
$c_0(\pi)$	17.9	16.8	11.3
$c_0(\sigma)$	31.0	26.5	22.7
$c_0(\rho)$	-63.8	-53.4	-38.4
$c_0(\rho^L)$	25.9	22.3	16.5
$c_0(a_1)$	-5.6	-5.6	-4.8
$c_0(\omega)$	-19.4	-16.2	-11.5
$c_0(\omega^L)$	7.9	6.8	4.9
$c_0(f_1)$	-0.3	-0.7	-1.0
$c_0(\eta^*)$	0.7	3.0	4.5
$c_0(a_0)$	4.5	4.1	4.2

Table 8.4: Properties of the quark propagator of the extended model at NLO. All quantities are quoted in MeV. ‘Cond.’ refers to the quark condensate, evaluated in the chiral limit. The constant c from the NLO tadpole diagram is defined in Eq. 7.5, $c(\alpha)$ being the contribution to it from the tadpole in the channel of the α meson.

The function $b(p)$ for the parameter set C is plotted in Fig. 8.5. Its breakdown is shown in Fig. 8.6. As in the situation with the tadpoles, pseudoscalar–axial mixing makes a definite difference to the contribution from the pion cloud (compare Figs. 8.4 and 8.6). However, the effect is cancelled by vector meson clouds to leave an overall result which is very similar to the one found in the simpler version of the model (compare Figs. 8.3 and 8.5).

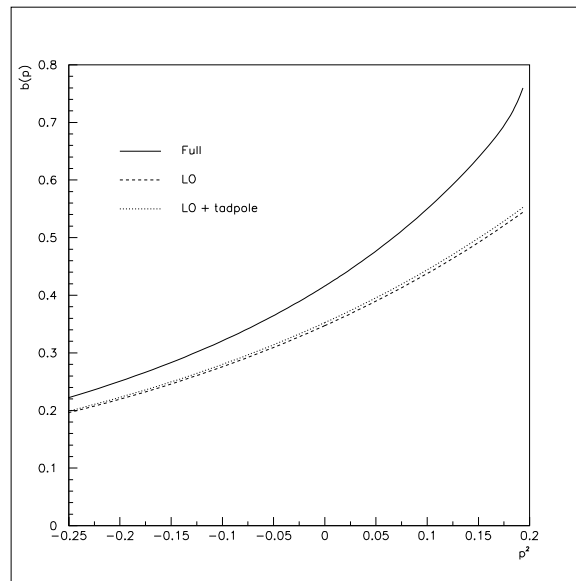


Figure 8.5: The figure shows the function $b(p)$ from the inverse quark propagator of the extended model. It is plotted in GeV against p^2 in GeV². The function is shown at LO and at NLO, together with the sum of the LO result and the tadpole contributions.

In Fig. 8.7 the function $a(p)$ is shown for the parameter set C. It is rather different in character from result obtained in the simpler version of the model (Fig. 8.2). Mixing in the pion channel and the clouds of the spin-1 states are again significant. In $a(p)$ however, these effects reinforce each other. Thus the function is much larger than in the simpler model. This is potentially of concern because it suggests that the NLO diagrams tend to deconfine the quarks in the extended model. A definite statement cannot however be made without a full NLO analysis of meson properties. The set C parameters are fixed from meson masses at LO. Since $1/N_c$ effects could alter these significantly, it is quite possible that set C may not constitute a reasonable choice of model parameters at the NLO level.

An obvious difference between Figs. 8.2 and 8.7 is the absence in the latter of a sharp dip just before the LO pseudo-threshold energy. The contributions from the clouds of the scalar, purely pseudoscalar, transverse vector and transverse axial channels all exhibit such a dip (Figs. 8.2 and 8.7). It is eliminated in the extended model due to the contributions from longitudinal $\bar{q}q$ states. In particular, the removal through mixing of the steep drop that occurs in the pion contribution is crucial in accounting for this behaviour.

8.3 Corrections to the Meson Properties

Numerics

The NLO diagrams in the BSE are of the forms given in Eqs. 7.6, 7.7 and 7.10. Since each of these requires an integration over several non-trivial variables, time constraints suggest that suitable approximation schemes be developed.

In Chp. 8.2, an accurate series fit to the LO J integrals at spacelike momenta was used to assist in the evaluation of the NLO quark self-energy. In performing the Bethe–Salpeter integrals of the structure given in Eq. 7.6, Σ_N can be evaluated just as in Chp. 8.2. It can then be treated as part of a two-dimensional integrand, which

is integrated over the variables \underline{p}^2 and p_4^2 using Gauss–Laguerre methods (p_4 is in the direction of q). For a timelike external momentum the arguments p_\pm^2 of Σ_N in Eq. 7.6 are complex in Euclidean space and hence the NLO part of the quark self-energy can itself be complex. In practice, however, the imaginary part of Σ_N does not contribute to the BSE integral. To see this, note that Σ_N is a real function⁶, satisfying Schwarz’s reflection property: $\Sigma_N(p^{2*}) = \Sigma_N^*(p^2)$. Since this is the case, the imaginary part of Σ_N in the two terms of Eq. 7.6 can be shown to cancel simply by reversing the sign of one of the p_4 integration variables⁷.

Eq. 7.7 represents the exchange of a $\bar{q}q$ state between the two quark lines of a LO bubble loop. With the routing used in that equation, the momentum of the intermediate state is always spacelike and so its propagation can be approximated by a Chebyshev series fit (Eq. 8.1). One is then left with a five–dimensional integrand which may be expressed as a function of p_4 , k_4 , \underline{p}^2 , \underline{k}^2 and ψ , the angle between \underline{p} and \underline{k} . Each of these is summed in the usual way, the first four with Gaussian techniques and the angular variable using the method described in Chp. 5.3 in the context of three-quark loops.

The remaining NLO BSE integral is given in Eq. 7.10. It has a two–dimensional integrand and is summed using Gaussian methods in terms of the variables \underline{p}^2 and p_4 . At each integration point the functions \hat{T} , L and \bar{L} must be determined numerically. The three-quark loops, L and \bar{L} , can be computed in the same way as the $1 \rightarrow 2$ meson decays of Chp. 5.3. The LO scattering matrices in Eq. 7.10 cannot however be represented by using Eq. 8.1 to fit to J_{ij} . The Euclidean momenta of the $\bar{q}q$ intermediates in this diagram is complex for a timelike external momentum. Off the real axis, the LO J integrals are themselves complex and can only be fitted as functions of two variables. In constructing an appropriate fit, the momentum routing of Eq. 7.10 is a judicious choice. Since $k_{-E}^2 = (k_{+E}^2)^*$ and $J(\ell_E^2)$ satisfies the Schwarz reflection

⁶For this statement to be true, one requires that the interaction form factor $f(p)$ is a real function. It then follows that the LO quark self-energy is a real function (see Eq. 3.3), whereupon the property can be seen to hold for Σ_N by inspection of Eq. 7.4.

⁷Assuming that $\Gamma_i = \Gamma_j$.

property⁸, the range of the fit can be restricted to:

$$\Im(\ell_E^2) : 0 \rightarrow \infty. \quad (8.3)$$

A further restriction can be imposed given that the BSE at NLO is only considered up to energies of E_{PT} , the pseudo-threshold energy at twice the real part of the pole in the LO quark propagator⁹. Therefore, a non-zero value for $|\Im(k_{\pm E}^2)|$ indicates a minimum possible $|k_4|$ and hence a lower bound on the required values of $\Re(\ell_E^2)$, specifically:

$$\Re(\ell_E^2) : \left(\frac{\Im(\ell_E^2)}{E_{\text{PT}}} \right)^2 - \frac{E_{\text{PT}}^2}{4} \rightarrow \infty. \quad (8.4)$$

Within the range of arguments probed, the J functions in Eq. 7.10 can be approximated by the Chebyshev expansions

$$J_{ij}(\ell_E^2 = u + iv) = \sum_{mn} a_{mn} T_m(x(u, v)) T_n(y(v)), \quad (8.5)$$

where x and y are taken as:

$$\begin{aligned} y(v) &= \exp\left(\frac{-v}{\Lambda^2}\right), \\ x(u, v) &= \exp\left(\frac{-u}{\Lambda^2}\right) \left[1 + \exp\left(\frac{-u_{\min}(v)}{\Lambda^2}\right) \right]^{-1}, \end{aligned} \quad (8.6)$$

and $u_{\min}(v)$ should be understood as the minimum of $\Re(\ell_e^2)$ in Eq. 8.4. A hundred evaluations in each channel of J have been used to fix the complex coefficients¹⁰ in Eq. 8.5 for $m, n = 0 \dots 9$. Although this is not a very efficient method for evaluating a single NLO BSE integral of the form in Eq. 7.10, the fits need only be done once for a given parameter set. Hence, there is a definite advantage in using them when one wishes to evaluate several such integrals with the same model parameters.

⁸As with the LO and NLO quark self-energies, the property follows directly if the interaction form factor is a real function.

⁹Although the LO J integrals cease to be capable of analytic continuation when $\Re(\ell_E^2)$ is more negative than $-\frac{1}{4}E_{\text{PT}}^2$ (see Chp. 3.3), this is avoided for external energies below E_{PT} .

¹⁰By investigating evaluations at other momenta, the errors for these two-parameter fits are found to be at the $\sim 1\%$ level. Since this is considerably worse than for the fits of Eq. 8.1, it is preferable to use the single-parameter fit in evaluating other NLO diagrams.

8.4 Physical Thresholds

Above the threshold for a physical $1 \rightarrow 2$ meson decay, a NLO diagram of the form in Fig. 7.9d generates an imaginary component to the meson propagator. This can be calculated by applying the Cutkosky cutting rules [104] to the diagram. Consider for example the scattering in the scalar isoscalar channel above the two-pion threshold. At the value of the LO sigma meson mass, the imaginary part reduces to

$$\Im\left(J_{SS}(q^2 = m_\sigma^2)\right) = m_\sigma \cdot \frac{\Gamma(\sigma \rightarrow \pi\pi)}{g_{\sigma qq}^2}, \quad (8.7)$$

where the decay width is identical to that calculated from the relevant three-meson vertex in Chp. 5.3.

Some care must be taken in the evaluation of the real part of such diagrams, owing to the singularities of the scattering matrices in the integrand. The diagram can be defined more formally as the $\epsilon \rightarrow 0$ limit of Eq. 7.7 with the replacements

$$\hat{T} = \frac{G_1}{1 - G_1 J} \longrightarrow \frac{G_1}{1 - G_1 J - i\epsilon}. \quad (8.8)$$

The numerical routines sometimes attempt to evaluate the integrand close to the position of the singularity. Whether or not they do so, the results produced have been found to be stable for $\epsilon \lesssim 0.01$. For the sake of safety therefore, ϵ has been set at this small but non-zero value in the numerical work.

8.5 Corrections to Pion Properties

Figs. 8.8 and 8.9 show the results for the real part of the pion Bethe–Salpeter determinant of Eq. 7.12. At small meson energies, the LO and NLO curves are very close together, indicating that both the pion mass and its coupling to quarks are extremely well represented by the LO approximation. Although the NLO contributions in the pion channel must cancel in the chiral limit (as demonstrated in Appendix B), the results here suggest that such cancellations must persist to a large extent at higher orders. In particular, there is no reason to expect the NLO shift in the pion–quark

coupling to be small. In conjunction with the small value of c_0 , the small change to $g_{\pi qq}$ implies that the pion decay constant is not sensitive to NLO effects (see Eq.7.15). Actual determinations of the NLO shifts to m_π and f_π have not been made in this work. They are sufficiently small¹¹ that the numerical procedures would have to be considerably refined in order to quote values with any meaningful degree of accuracy.

The fact that the NLO corrections to the pion mass and decay constant are small is an encouraging point in support of the usual LO treatment of four-quark models. It also justifies the decision to use the model parameters fitted to the LO pion properties (Chp. 8.1) in these NLO computations with the simple version of the model.

¹¹not more than a few MeV.

As the energy in the pion channel increases, the NLO contributions do start to become significant. Shortly before pseudo–threshold is reached, they are sufficiently important to change the qualitative behaviour of the pion Bethe–Salpeter amplitude. Indeed they are even able to generate an unphysical zero in the real part of the determinant, just before E_{PT} . This is a potentially worrying point and indicates a need for a careful study of the model at NLO around and above E_{PT} . It may also be worthwhile to examine the pion determinant in the extended version of the model. The behaviour in Fig. 8.9 is reminiscent of that exhibited by $a(p)$ in Fig. 8.2. In that instance, the unusual feature was eliminated by the introduction of pseudoscalar–axial mixing. This mixing is certainly important in the LO pion amplitude (compare Fig. 5.1 to Figs. 8.8 and 8.9) and might be so at NLO as well.

In Fig. 8.10, a breakdown of the NLO contributions to the pion amplitude is shown. Each curve corresponds to a different NLO integral: ‘a+b’ represents a NLO quark self-energy insertion (the sum of Figs. 7.7a and 7.7b, given in Eq. 7.6); ‘c’ represents meson exchange between two quark lines (Fig. 7.9c, given in Eq. 7.7); and ‘d’ represents two-meson intermediate states (Fig. 7.9d, given in Eq. 7.10). The results demonstrate that the NLO part of the amplitude is small at low momenta only because of the cancellations amongst the various diagrams that are enforced by chiral symmetry. In both analytical and in numerical work, it is therefore crucial to include all of the diagrams consistently in order to obtain an accurate picture of the pion at NLO.

8.6 Corrections to Sigma Properties

The interpretation of the sigma meson in dynamical quark models is subject to assumptions about its properties which are not probed by such models at LO. Since the state is known to be strongly coupled to the two-pion channel, the diagram of Fig. 7.9d might well be important in model descriptions of the scalar channel. The result of the nonlocal NJL model for the real part of the scattering matrix determinant is plotted

in Fig. 8.11.

In the ladder approximation to four-quark models, the sigma meson tends to be rather light in comparison with many $\pi\pi$ scattering analyses [89]. Fig. 8.11 shows that this statement is also true at NLO. The point is emphasized by Table 8.5 which lists the LO and NLO sigma masses over the full range of parameter sets from Chp. 8.1. The NLO shift is quite modest and (in general) negative.

$m_0(0)$	m_σ at LO	m_σ at NLO
200	385	404
250	423	377
300	454	373
350	477	368
400	492	365
450	489	365
500	478	365

Table 8.5: Sigma meson masses at LO and NLO.

It should be noted that the “masses” quoted in Table 8.5 refer to the energy at which the real part of the scattering matrix vanishes. A common alternative is to consider the complex pole of the scattering matrix. The definition used here has been selected purely for convenience, since it would be more difficult to evaluate the BSE integrals at complex external energies.

Using a derivative expansion of the bosonized NJL model, the $1/N_c$ corrections to the sigma mass were calculated by Pallante [45]. In that framework, the corrections were found to be large and negative¹², prompting the author of Ref. [45] to speculate that the mass of this state is not well described by the $1/N_c$ expansion. The work presented here indicates that higher order terms in momentum are important and that these reduce the magnitude of the mass shift such that perturbation theory seems to be reasonable.

One must therefore take very seriously the view the sigma meson is intrinsically light in four quark models of the NJL form. This view is supported by the observation that the results for the sigma mass at NLO are remarkably insensitive to the parameter set chosen. Even allowing the zero-momentum chiral quark mass to vary by a factor of two, the sigma mass changes by just 12 MeV . Thus, the light sigma is a property of such models which cannot be avoided by including meson loops or by a suitable choice of parameters.

A breakdown of NLO contributions to the scalar channel of the scattering matrix can be found in Fig. 8.12. The same notation is used as in Chp. 8.5 for the pion channel. In Chp. 5.2, it was argued that the contributions from two pion intermediates could be important in the description of the scalar channel and indeed such diagrams dominate the NLO part of the scalar amplitude. They act to reduce the mass of the state, as does the contribution from t-channel meson exchange. Their signs are the same as those of the corresponding contributions to the pion channel. There are also contributions from NLO quark self-energy insertions, which, in both channels, have

¹²One should note, however, that the precise value for the mass shift is highly sensitive to the additional cut-off parameter that is needed to regularize the meson loops.

the opposite effect.

The discussion so far has concerned the real part of J_{NSS} . The imaginary part is shown in Fig. 8.13. Naively, one would expect it to increase with increasing energy since a larger region of phase space becomes available. In practice, there is a very slow increase from the threshold energy up to a peak at ~ 520 MeV, following which the imaginary part falls off quite quickly. Thus, the coupling of the scalar channel to two pions must become significantly weaker as the energy increases. The fact that the model sigma meson is light is therefore inextricably linked with the fact that it is also broad. Interestingly, a similar behaviour of the scalar to two pion coupling was observed in the four-quark model¹³ studied by Efimov et al [58]. In contrast, however, a recent analysis using QCD sum rules [116] suggested that a light scalar state would have to be relatively narrow.

Finally, note that the results of Fig. 8.13 support a suggestion made in Chp. 5.3. The weak coupling of the the scalar channel to two pions above the sigma mass implies that the broad width calculated for $a_1 \rightarrow \sigma\pi$ in the model is by no means inconsistent with the experimental observation of a small contribution to the total a_1 width from $a_1 \rightarrow \pi(\pi\pi)_S$.

¹³A value for the scalar mass in their three-flavoured approach was used as a free parameter and was chosen with the intention of interpreting the model scalar resonances as heavy, narrow states. The authors were however presented with a problem regarding the widths of these states which was ‘resolved’ by the ad hoc introduction of a vector piece to the Bethe Salpeter amplitude.

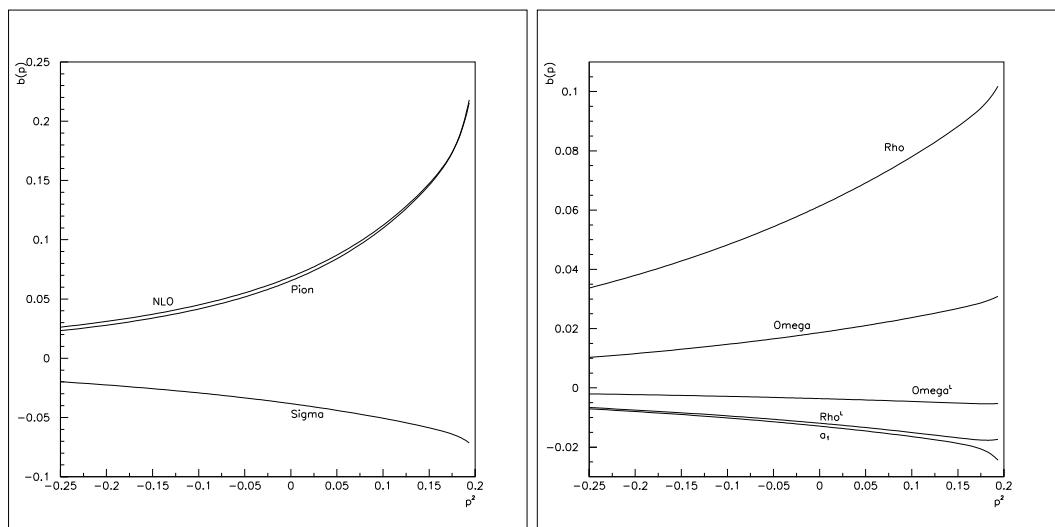


Figure 8.6: The figure shows the NLO contributions to the function $b(p)$ in the extended model. They are plotted in GeV against p^2 in GeV^2 . The full NLO component is shown on the left-hand graph, together with the parts of it that involve intermediate pions and sigma mesons. Contributions involving spin-1 states are shown on the right-hand graph, the superscript L denoting a longitudinal state. Note that the contributions from the f_1 , a_0 and η^* particles are negligible and so are not shown.

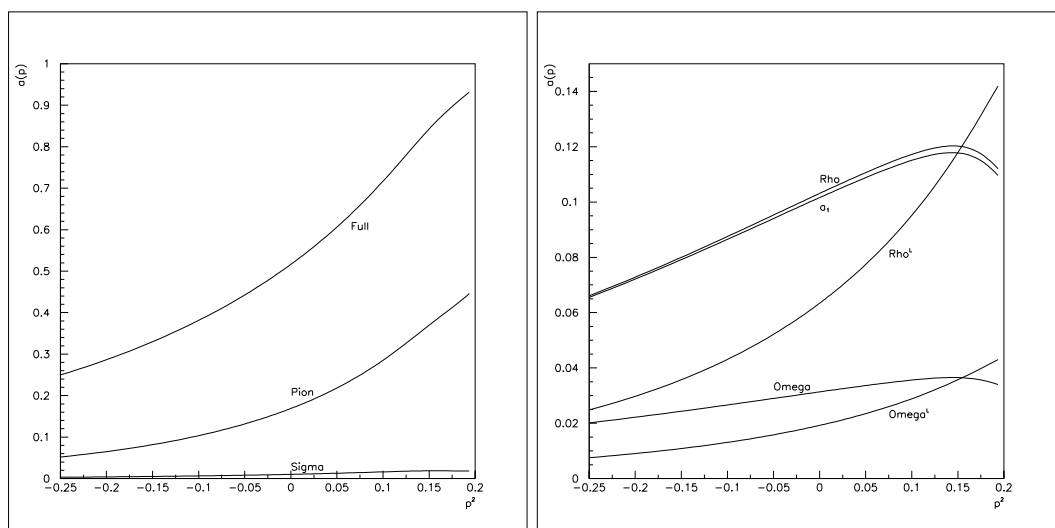


Figure 8.7: The figure shows the dimensionless function $a(p)$ from the inverse quark propagator of the extended model. It is plotted against p^2 in GeV^2 . The full NLO result is shown on the left-hand graph, together with the parts of it that come from dressing the quark line with pion and sigma clouds. Contributions from the clouds of spin-1 states are shown on the right-hand graph, the superscript L denoting a longitudinal state. Note that the contributions from the f_1 , a_0 and η^* particles are negligible and so are not shown.

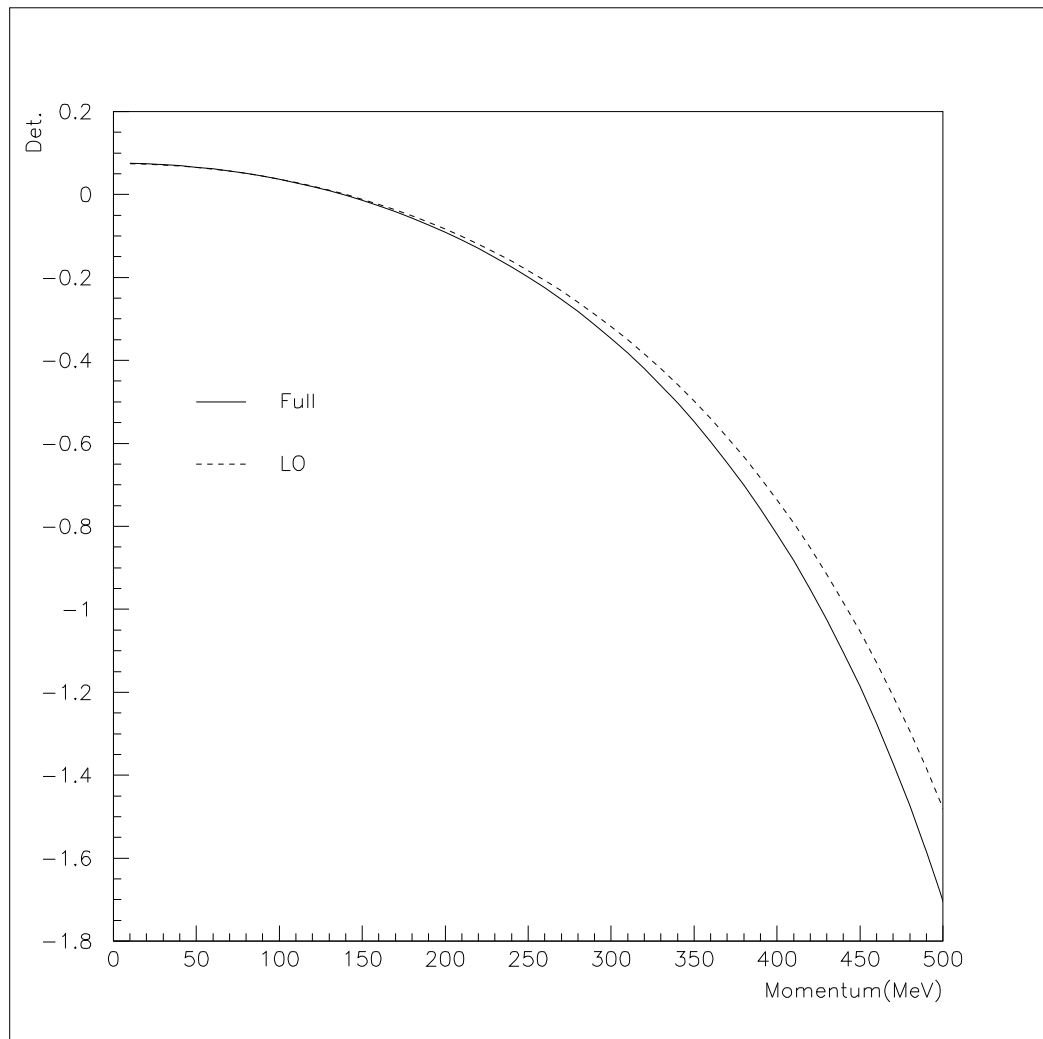


Figure 8.8: The figure shows the determinant of the scattering matrix in the pion channel at LO (dashed curve) and at NLO (solid curve). The parameter set used is that with $m_0(0) = 300$ MeV in Table 8.1.

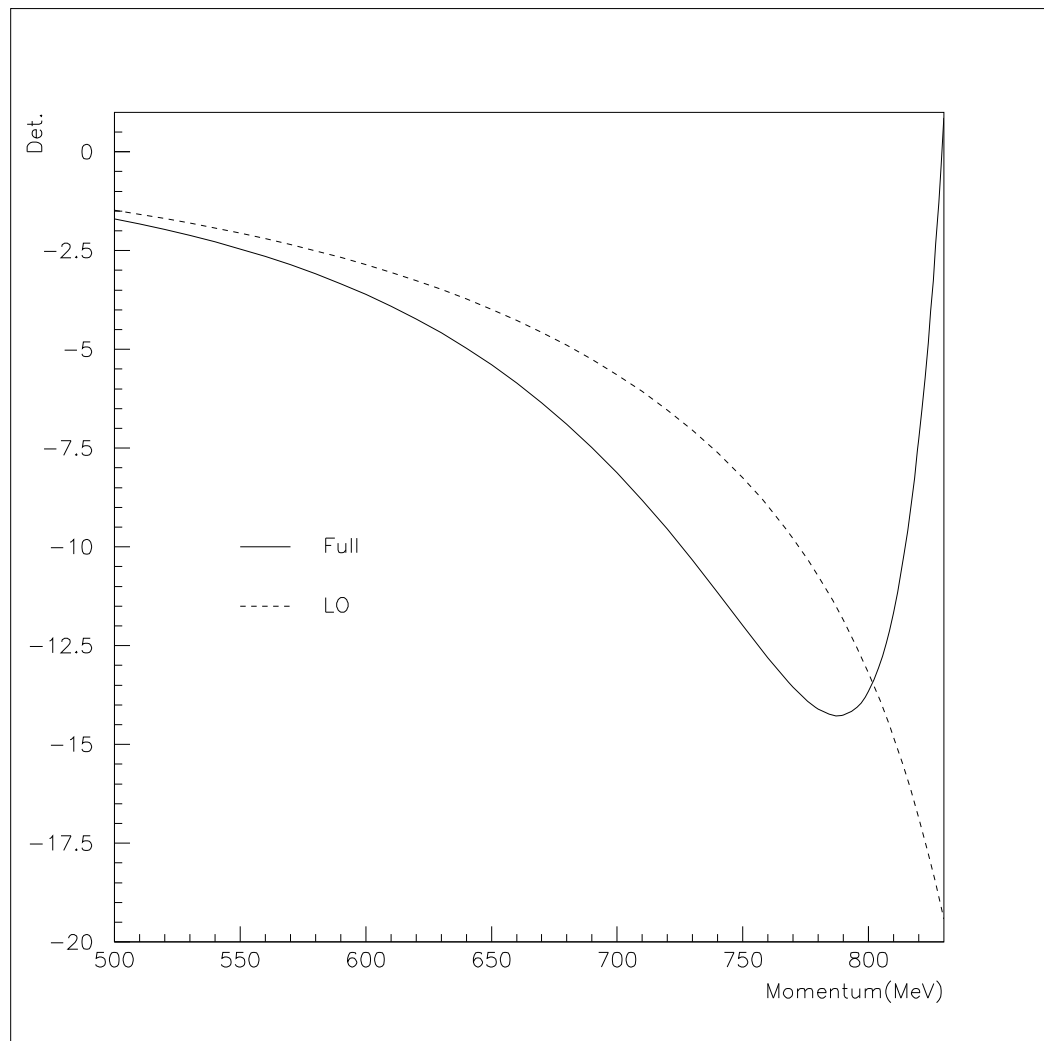


Figure 8.9: The figure shows the determinant of the scattering matrix in the pion channel at LO (dashed curve) and at NLO (solid curve). The curves are plotted for energies up to the pseudo-threshold energy, E_{PT} . The parameter set used is that with $m_0(0) = 300$ MeV in Table 8.1.

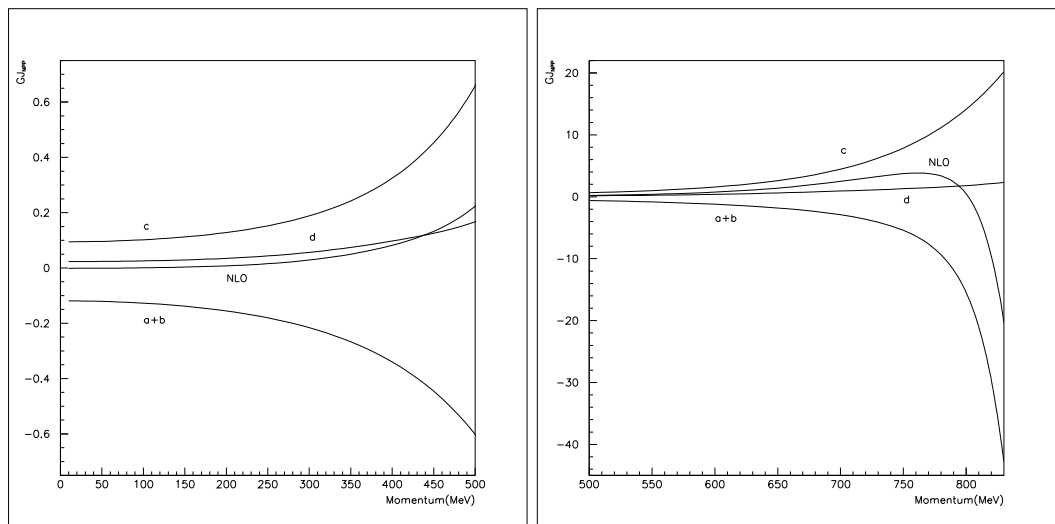


Figure 8.10: The figure shows $G_1 J_{NPP}$ and the various contributions to it, plotted for timelike meson momentum up to the pseudo-threshold energy, E_{PT} . The contributions are defined in the main text. The parameter set used is that with $m_0(0) = 300$ MeV in Table 8.1.

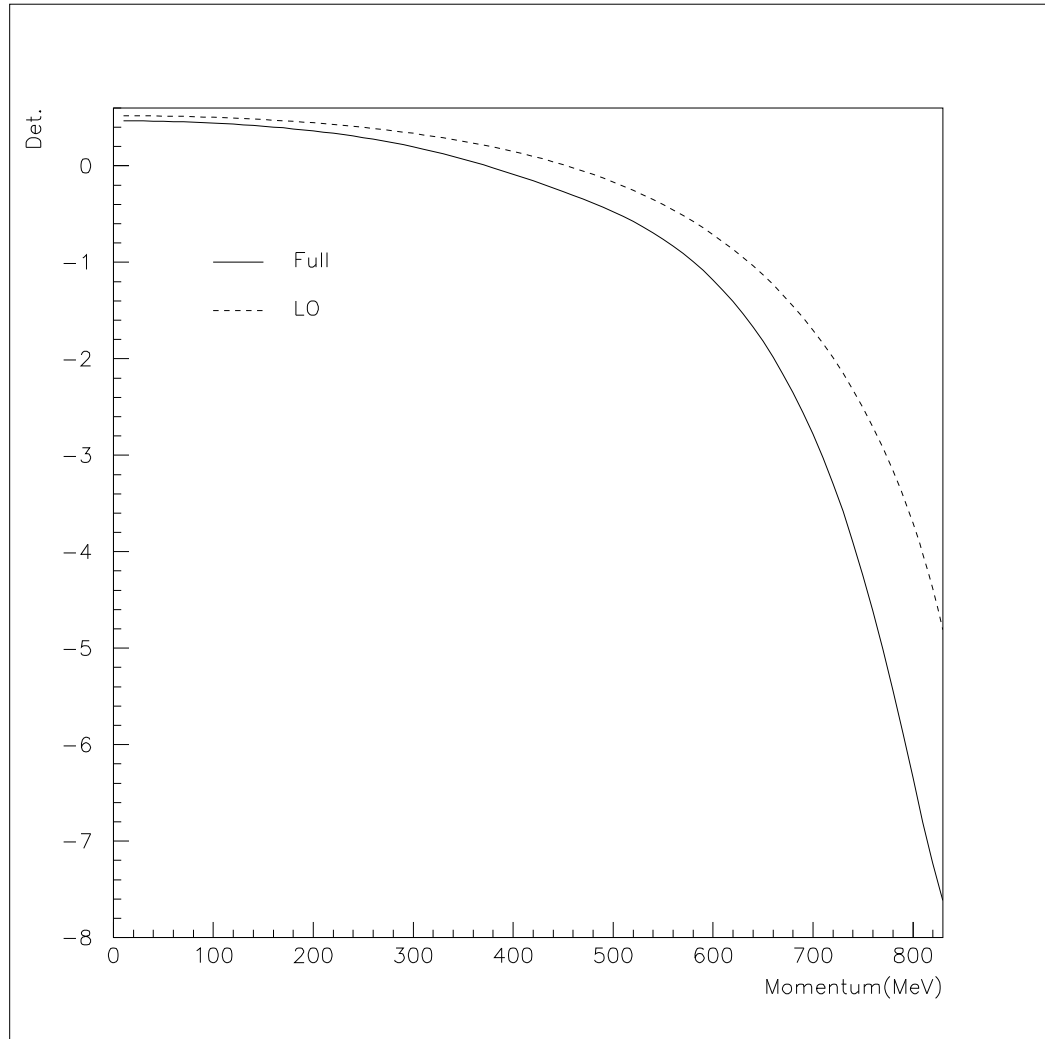


Figure 8.11: The figure shows the real part of the determinant of the scattering matrix in the scalar channel. The dashed curve gives the LO result and the solid curve gives the result at NLO. They are plotted against timelike meson momentum, up to the pseudo-threshold energy, E_{PT} . The parameter set used is that with $m_0(0) = 300$ MeV in Table 8.1.

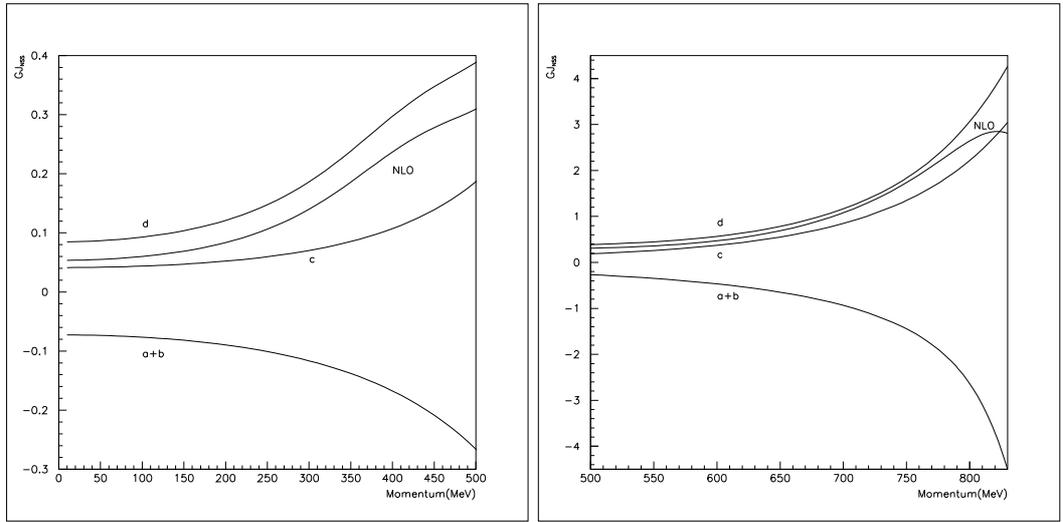


Figure 8.12: The figure shows $G_1 J_{NSS}$ and the various contributions to it, plotted for timelike meson momentum up to the pseudo-threshold energy, E_{PT} . The contributions are defined in the main text. The parameter set used is that with $m_0(0) = 300$ MeV in Table 8.1.

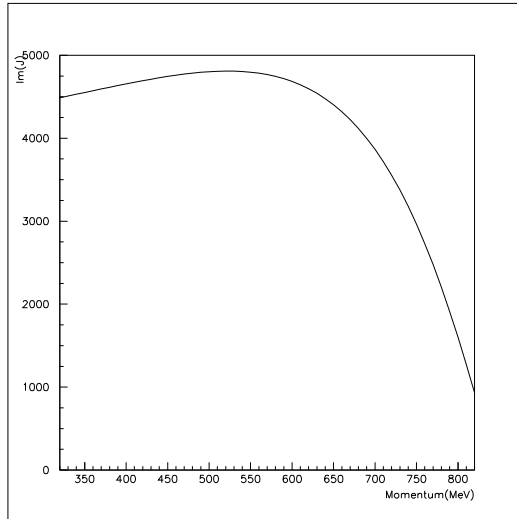


Figure 8.13: The figure shows the imaginary part of J_{SS} . It is plotted from slightly above the two-pion threshold up to the pseudo-threshold energy, E_{PT} . The parameter set used is that with $m_0(0) = 300$ MeV in Table 8.1.

Chapter 9

Conclusions

The structure of light mesons is a much-studied subject but one which is not yet well understood. Treatments based on the QCD Schwinger–Dyson equations provide an attractive approach to the problem, offering a clear link between the particulate and composite levels. However, they are often computationally intensive. Ansätze must be made in order to make the equations tractable, but it is far from simple to test an ansatz through the resulting phenomenology. Such calculations are facilitated by using instead a model field theory, such as the NJL style of model. The work presented has investigated an extended version of the model proposed in Ref. [8], which can be viewed as a nonlocal generalization of the NJL action. It has nonlocal, four-fermion interactions, based on the separable form (Eq. 2.4) suggested by instanton–liquid studies [51]. Symmetry currents consistent with this action have been deduced. The results for the currents have been extensively tested, by means of the constraints imposed by electromagnetic gauge invariance and a variety of Ward identities. The model has also been shown to incorporate the chiral anomaly correctly. Moreover, NLO corrections have been studied. Although a particular model has been used throughout, many of the results from the NLO analysis are likely to be qualitatively true of four-quark models in general.

The interaction form factors which are used in the nonlocal model (Eq. 2.7) ensure the convergence of all loop integrals and (over most of the range of acceptable parameters) also lead to quark confinement. The former point is particularly important in the study of such models at NLO, since it eliminates the need for a cut-off parameter on meson loops. The latter point is relevant to the application of such models to heavier mesons than the pion, since it avoids a threshold for $\bar{q}q$ production occurring at an inconveniently low energy. This feature makes the approach especially well suited as the basis for an extended model, with interactions that bind vector and axial-vector mesons.

The analytic structure of the quark propagator, with poles at complex momenta, means that a scheme has to be specified for continuing amplitudes to Minkowski space. The scheme used at LO (Chp. 3.3) follows the suggestions of Lee and Wick [77] and of Cutkosky *et al.* [78]. It leads to nonanalytic behaviour of the meson propagators above a pseudo-threshold energy. In practice (see Chp. 5.1), this behaviour ensures that no poles appear in the longitudinal vector channels. In addition, it provides restrictions on both the admissible range of model parameters and the region of applicability of the model. No attempt has been made to examine the model beyond the pseudo-threshold energy at NLO. This is because the poles in the quark propagator are shifted by NLO terms in the quark self-energy. Such a shift is not explicit in a perturbative treatment of the BSE, which therefore does not allow a simple extension of the continuation prescription.

In order to calculate the pion decay constant, which sets the basic scale for the model, one needs to use conserved currents which are consistent with the nonlocal interaction. Nonlocal contributions to the currents have been determined (Chp. 2.4) according to the Noether-like method of Ref. [8]. These are analytically and numerically important to the pion decay constant (and to many electromagnetic couplings). Ward identities related to the current conservation follow automatically and several have been checked analytically, including the Gell-Mann–Oakes–Renner relation (Chp. 4.2)

and the low-energy theorem for $\pi^0 \rightarrow \gamma\gamma$ in the chiral limit (Chp. 6.3). The latter involves the axial anomaly, which has long posed a problem to the usual NJL model with its cut-offs on the quark propagators. The nonlocal terms in the vector current of the model yield an ansatz for the photon–quark coupling (Chp. 4.3) which differs from the Ball–Chiu ansatz, relied upon in many similar studies. In particular, one must include two-body diagrams (Chp. 6.2) where the photon is irreducibly coupled to four quarks.

Various electromagnetic quantities have been calculated in the model. The decay rates determined are in fairly good agreement with the observed ones, except for the case of $a_1 \rightarrow \pi\gamma$. The electromagnetic form factor of the pion agrees well with the data, at least below the ρ pole. The form factors for $\gamma\gamma^* \rightarrow \pi$ and $\omega \rightarrow \pi\gamma^*$ are also in agreement with the (admittedly rather limited) data currently available. These results for electromagnetic form factors have been compared with vector–dominance formulae using on-shell couplings as calculated from the model. Although diagrams involving intermediate vector mesons are only significant close to resonance, they combine with diagrams where the photon couples directly to the quarks to produce numerical results that are very close to those of VMD¹. The model is thus able to illustrate how a dynamical system can lead to vector dominance in photon–meson interactions.

The meson masses and various strong decay rates were calculated in Chp. 5, working at tree level in terms of mesons (leading order in $1/N_c$) and to all orders in momentum. With the ρ mass used to fix the strength of the relevant four-quark vertex, the ρ meson width is reasonably well described. The nonlocal model therefore provides an improvement on the underestimated width obtained in the extended NJL model [92]. As in the local NJL model, a light, broad sigma meson is found. The calculated mass of the a_1 meson is somewhat lighter than the observed value. By cutting down the available phase–space, this means that the model gives too small a width for the decay $a_1 \rightarrow \rho\pi$.

¹except at large momenta.

The calculations have been developed to include meson-loop effects ($1/N_c$ corrections) since these could be qualitatively important. Unlike all previous analyses of these effects in four-quark models, the present work has explicitly evaluated the relevant integrals as functions of momentum. These functions are unambiguous, since no regulator is required for the meson loops. It has been checked that the meson-loop diagrams are consistent with the Gell-Mann–Oakes–Renner relation (Chp. 7.5). In so doing, it was established that (in the chiral limit) the changes to the pion mass and decay constant at this improved level of approximation are controlled by the quantity c_0 , the coefficient of the tadpole diagram from the quark self-energy.

The numerical results obtained at next-to-leading order confirm the validity of an expansion in $1/N_c$. Both the scalar and vector components of the quark self-energy are increased by $\sim 25\%$ by the inclusion of meson-loop diagrams, with the pion cloud being the dominant effect. When vector mesons are included in the model, it has been observed that the vector component is further increased, and that πa_1 mixing is qualitatively important. The value of c_0 is found to be small, so that pion properties are accurately represented by the leading order approximation. The sigma meson is very strongly coupled to two-pion states and the associated meson-loop diagram acts to reduce the mass of this state. This is partially cancelled by the changes to the quark self-energy, but the net effect is a reduction of the σ mass to ~ 370 MeV. One should note that this value (along with the results calculated for almost all observables in the model) has been found to be qualitatively similar for all admissible values of the model parameters.

The empirical properties of the sigma meson are a subject of continuing debate. The issue was addressed on several occasions at the HADRON 97 conference [117] and is also discussed in recent preprints (see for example Refs. [116, 118, 119]). In such discussions models of the four-quark type are often cited as theoretical studies in support of the interpretations that favour a light sigma meson. The support offered, however, could hitherto only be regarded as tentative in view of the fact that the

usual leading order approximation to such models does not take account of meson loops involving two pion states. In this work, it has been demonstrated that a full calculation at meson-loop level actually produces a lighter scalar resonance. It therefore appears that the NJL type of model does indeed favour a light and broad sigma. Of course, any resolution of ‘the sigma problem’ will only be established by further analyses of existing and of new experimental data. It may be that future work causes the notion of a light, broad sigma to be rejected. In that case, the results presented here would indicate that there must be some important physics missing from the NJL type of model. In this context, it is interesting to find in Ref. [119] that a group whose analyses find a light sigma has stated that an assumption made in their treatment [120] (the form of the $\pi\pi$ scattering amplitude) is similar to one that is made in NJL models.

In this thesis, a four-quark model suggested in Ref. [8] has been explored in some detail. With only a minimal increase in complexity, the model is theoretically more attractive than the local NJL model. It generates quark confinement, does not require a regulator and (through the inclusion of nonlocal terms in the symmetry currents) satisfies the chiral anomaly in very natural way. Phenomenologically, the level of agreement with observed meson properties is satisfactory, given the simplicity of the model. The results obtained when meson loops are included imply that the usual leading order approximation to this type of model is qualitatively a good one for both the pion and its chiral partner.

Appendix A

Pion Decay Constant at NLO

A.1 Cancellations

It was noted in Chp. 7.4 that there are a number of useful cancellations which can be made amongst the various diagrams contributing to the NLO part of the pion decay constant. The purpose of the present section is to give a description of those cancellations, which lead to Eq. 7.11. Although the NLO diagrams in the coupling to the axial current were discussed quite generally in Chp. 7.4, this section considers a version of the model with the G_1 coupling only.

It is easiest to begin with the diagrams (k) and (l) (see Fig. 7.13) which are generated by the NLO part of the pion vertex function. Their sum is clearly:

$$f_{\pi}^{(k)} + f_{\pi}^{(l)} = \frac{g_{N\pi qq}}{g_{\pi qq}} f_{\pi}. \quad (\text{A.1})$$

One may recall the convention by which the unscripted f_{π} in Eq. A.1 refers to the pion decay constant at LO. The notation $f_{\pi}^{(x)}$ also appears in the above equation and is used to denote the contribution to the pion decay constant from the NLO diagram $(x) = (a) \dots (o)$ (see Figs. 7.11 to 7.15).

Consider next the contributions which arise due to the tadpole diagram in the NLO quark self-energy. This is responsible for the diagrams (a) , (c) and (g) (see

Figs. 7.11 and 7.12), which make the following contributions:

$$\begin{aligned}
f_\pi^{(a)}\delta^{ab} &= \frac{cg_{\pi qq}G_1}{2m_\pi^2} \int \frac{d^4k}{(2\pi)^4} \text{Tr}[S(k)S(k)] f^2(k) \\
&\times \int \frac{d^4p}{(2\pi)^4} \text{Tr}[\gamma_5\tau^b S(p_-)\gamma_5\tau^a S(p_+)] f(p_+)f(p_-) \\
&\times [f^2(k)(f^2(p_+) + f^2(p_-)) - f(k)(f(k+q) + f(k-q))f(p_+)f(p_-)], \quad (\text{A.2})
\end{aligned}$$

$$\begin{aligned}
f_\pi^{(c)}\delta^{ab} &= -i\frac{cg_{\pi qq}}{2m_\pi^2} \int \frac{d^4p}{(2\pi)^4} \text{Tr}[\gamma_5\tau^b S(p_-)\not{q}\gamma_5\tau^a S(p_+)S(p_+)] f^3(p_+)f(p_-) \\
&-i\frac{cg_{\pi qq}}{2m_\pi^2} \int \frac{d^4p}{(2\pi)^4} \text{Tr}[\gamma_5\tau^b S(p_-)S(p_-)\not{q}\gamma_5\tau^a S(p_+)] f(p_+)f^3(p_-), \quad (\text{A.3})
\end{aligned}$$

$$\begin{aligned}
f_\pi^{(g)}\delta^{ab} &= \frac{cg_{\pi qq}G_1}{2m_\pi^2} \int \frac{d^4k}{(2\pi)^4} \text{Tr}[S(k)] \int \frac{d^4p}{(2\pi)^4} f(p_+)f(p_-) \\
&\times \text{Tr}[\gamma_5\tau^b S(p_-)\gamma_5\tau^a S(p_+)S(p_+)f^2(p_+) + \gamma_5\tau^b S(p_-)S(p_-)\gamma_5\tau^a S(p_+)f^2(p_-)] \\
&\times [f^2(k)(f^2(p_+) + f^2(p_-)) - f(k)(f(k+q) + f(k-q))f(p_+)f(p_-)]. \quad (\text{A.4})
\end{aligned}$$

The form factor structure in square brackets appearing in the expressions for diagrams (c) and (g) is characteristic of the type-III nonlocal current structure (Eq. 2.16). It is the type-III term $G_1(i\gamma_5\tau^a \otimes 1)$ which produces these diagrams (and many of the other nonlocal diagrams at NLO), just as it produced the LO nonlocal diagram of Eq. 4.1.

By applying the $\not{q}\gamma_5$ identity of Eq. 4.3 to the local current diagram (c), the contribution coming from the $(m_+ + m_-)$ term on the right-hand side of Eq. 4.3 can be partially cancelled with part of the corresponding nonlocal diagram, (g). As in the corresponding cancellation between LO diagrams (see Chp. 4.2), only $2m_c$ from the $(m_+ + m_-)$ factor is retained in the sum. The other pieces of Eq. 4.3 result in contributions with integrals somewhat similar to those of $J_{SS}(0)$ and $J_{PP}(q)$, but having slightly more complicated form factor structures.

Defining the symbol $J_{Nij}^{(x)}$ to represent the contribution to J_{Nij} from the BSE diagram of type $(x) = (a) \dots (d)$ (see Figs. 7.7 and 7.9), one can write the sum of the

diagrams that involve the tadpole as

$$\begin{aligned}
f_\pi^{(a)} + f_\pi^{(c)} + f_\pi^{(g)} &= \frac{ig_{\pi qq}G_1}{2m_\pi^2} J_{NPP}^{(a)} \int \frac{d^4k}{(2\pi)^4} \text{Tr} [S(k)] f(k) (f(k+q) + f(k-q)) \\
&+ i \frac{cg_{\pi qq}}{2m_\pi^2} (1 - G_1 J_{PP}(q^2)) \int \frac{d^4p}{(2\pi)^4} \text{Tr} [S(p)S(p)] f^3(p) (f(p+q) + f(p-q)) \\
&+ i \frac{cg_{\pi qq}}{2m_\pi^2} (1 - G_1 J_{SS}(0)) \int \frac{d^4p}{(2\pi)^4} \text{Tr} [\gamma_5 S(p_-) \gamma_5 S(p_+)] \\
&\quad \times f(p_+) f(p_-) (f^2(p_+) + f^2(p_-)) \\
&+ \frac{g_{\pi qq} m_c}{m_\pi^2} \left(J_{NPP}^{(a)} \text{ with } f^2(p_\pm) f^4(p_\mp) \rightarrow f(p_\pm) f^3(p_\mp) \right). \tag{A.5}
\end{aligned}$$

The other part of the NLO quark self-energy comes from the meson cloud diagram on the right-hand side of Fig. 7.5. It induces the diagrams (b), (d) and (h) (see Figs. 7.11 and 7.12) in the pion coupling to the axial current.

$$\begin{aligned}
f_\pi^{(b)} \delta^{ab} &= \frac{ig_{\pi qq}G_1}{2m_\pi^2} \int \frac{d^4p}{(2\pi)^4} \text{Tr} [\gamma_5 \tau^b S(p_-) \gamma_5 \tau^a S(p_+)] f(p_+) f(p_-) \\
&\times \sum_i \int \frac{d^4k}{(2\pi)^4} \frac{d^4\ell}{(2\pi)^4} \hat{T}(\bar{\Gamma}_i \otimes \Omega_i; k - \ell) \text{Tr} [S(k) \bar{\Gamma}_i S(\ell) \Omega_i S(k)] f^2(k) f^2(\ell) \\
&\times [f^2(k) (f^2(p_+) + f^2(p_-)) - f(k) (f(k+q) + f(k-q)) f(p_+) f(p_-)] \tag{A.6}
\end{aligned}$$

$$\begin{aligned}
f_\pi^{(d)} \delta^{ab} &= \frac{g_{\pi qq}}{2m_\pi^2} \sum_i \int \frac{d^4p}{(2\pi)^4} \frac{d^4k}{(2\pi)^4} \hat{T}(\bar{\Gamma}_i \otimes \Omega_i; p - k) f(p_+) f(p_-) \\
&\quad \times \text{Tr} [\gamma_5 \tau^b S(p_-) \not{q} \gamma_5 \tau^a S(p_+) \bar{\Gamma}_i S(k_+) \Omega_i S(p_+) f^2(p_+) f^2(k_+) \\
&\quad + \gamma_5 \tau^b S(p_-) \bar{\Gamma}_i S(k_-) \Omega_i S(p_-) \not{q} \gamma_5 \tau^a S(p_+) f^2(p_-) f^2(k_-)] \tag{A.7}
\end{aligned}$$

$$\begin{aligned}
f_\pi^{(h)} \delta^{ab} &= \frac{ig_{\pi qq}G_1}{2m_\pi^2} \int \frac{d^4k}{(2\pi)^4} \text{Tr} [S(k)] \sum_i \int \frac{d^4p}{(2\pi)^4} \frac{d^4\ell}{(2\pi)^4} \hat{T}(\bar{\Gamma}_i \otimes \Omega_i; p - \ell) \\
&\quad \times \text{Tr} [\gamma_5 \tau^b S(p_-) \gamma_5 \tau^a S(p_+) \bar{\Gamma}_i S(\ell_+) \Omega_i S(p_+) f^2(p_+) f^2(\ell_+) \\
&\quad + \gamma_5 \tau^b S(p_-) \bar{\Gamma}_i S(\ell_-) \Omega_i S(p_-) \gamma_5 \tau^a S(p_+) f^2(p_-) f^2(\ell_-)] f(p_+) f(p_-) \\
&\times [f^2(k) (f^2(p_+) + f^2(p_-)) - f(k) (f(k+q) + f(k-q)) f(p_+) f(p_-)] \tag{A.8}
\end{aligned}$$

In $f_\pi^{(d)}$, the $\not{q}\gamma_5$ identity of Eq. 4.3 can again be used to decompose the insertion that comes from the local current. As before, the $(m_+ + m_-)$ term of the decomposition allows cancellation with the part of $f_\pi^{(h)}$ that contains a factor of the ladder SDE integral (Eq. 3.2).

In Eq. A.6, the two pieces of the nonlocal form factor structure enable one to simplify different aspects of the expression. The first piece yields a factor of the same integral as appears in the definition of the constant c (Eq. 7.5); the second piece reduces the p integral to $J_{PP}(q^2)$. The simplified sum of Eqs. A.6, A.7 and A.8 is given below.

$$\begin{aligned}
& f_\pi^{(b)} + f_\pi^{(d)} + f_\pi^{(h)} = r_\pi^{(d)} \\
& + \frac{ig_{\pi qq}G_1}{2m_\pi^2} J_{NPP}^{(b)} \int \frac{d^4k}{(2\pi)^4} \text{Tr}[S(k)] f(k) (f(k+q) + f(k-q)) \\
& - \frac{g_{\pi qq}}{2m_\pi^2} (1 - G_1 J_{PP}(q^2)) \sum_i \int \frac{d^4p}{(2\pi)^4} \frac{d^4k}{(2\pi)^4} \hat{T}(\bar{\Gamma}_i \otimes \Omega_i; p-k) \text{Tr}[S(p)\bar{\Gamma}_i S(k)\Omega_i S(p)] \\
& \quad \times f^3(p) (f(p+q) + f(p-q)) f^2(k) \\
& - i \frac{cg_{\pi qq}}{2m_\pi^2} (1 - G_1 J_{SS}(0)) \int \frac{d^4p}{(2\pi)^4} \text{Tr}[\gamma_5 S(p_-)\gamma_5 S(p_+)] \\
& \quad \times f(p_+) f(p_-) (f^2(p_+) + f^2(p_-)) \\
& + \frac{g_{\pi qq}m_c}{m_\pi^2} (J_{NPP}^{(b)} \text{ with } f^2(p_\pm) f^4(p_\mp) \rightarrow f(p_\pm) f^3(p_\mp)), \tag{A.9}
\end{aligned}$$

where part of the local current contribution, Eq. A.7, has been isolated as

$$\begin{aligned}
r_\pi^{(d)} \delta^{ab} &= \frac{-g_{\pi qq}}{2m_\pi^2} \sum_i \int \frac{d^4p}{(2\pi)^4} \frac{d^4k}{(2\pi)^4} \hat{T}(\bar{\Gamma}_i \otimes \Omega_i; p-k) f(p_+) f(p_-) \\
& \quad \times \text{Tr} \left[\gamma_5 \tau^b S(p_-) \gamma_5 \tau^a \bar{\Gamma}_i S(k_+) \Omega_i S(p_+) f^2(p_+) f^2(k_+) \right. \\
& \quad \left. + \gamma_5 \tau^b S(p_-) \bar{\Gamma}_i S(k_-) \Omega_i \gamma_5 \tau^a S(p_+) f^2(p_-) f^2(k_-) \right]. \tag{A.10}
\end{aligned}$$

It is encouraging to note that the term proportional to c in Eq. A.9 cancels with a term in Eq. A.5.

The other corrections to the two-quark loops of the LO diagrams are due either to virtual meson exchanges between the two quarks,

$$\begin{aligned}
f_\pi^{(e)} \delta^{ab} &= \frac{g_{\pi qq}}{2m_\pi^2} \sum_i \int \frac{d^4 p}{(2\pi)^4} \frac{d^4 k}{(2\pi)^4} \hat{T}(\bar{\Gamma}_i \otimes \Omega_i; p - k) f^2(k_+) f^2(k_-) f(p_+) f(p_-) \\
&\quad \times \text{Tr} \left[\gamma_5 \tau^b S(k_-) \Omega_i S(p_-) \not{q} \gamma_5 \tau^a S(p_+) \bar{\Gamma}_i S(k_+) \right], \tag{A.11}
\end{aligned}$$

$$\begin{aligned}
f_\pi^{(i)} \delta^{ab} &= \frac{i g_{\pi qq} G_1}{2m_\pi^2} \int \frac{d^4 k}{(2\pi)^4} \text{Tr} [S(k)] \sum_i \int \frac{d^4 p}{(2\pi)^4} \frac{d^4 \ell}{(2\pi)^4} \hat{T}(\bar{\Gamma}_i \otimes \Omega_i; p - \ell) \\
&\quad \times \text{Tr} \left[\gamma_5 \tau^b S(\ell_-) \Omega_i S(p_-) \not{q} \gamma_5 \tau^a S(p_+) \bar{\Gamma}_i S(\ell_+) \right] f^2(\ell_+) f^2(\ell_-) f(p_+) f(p_-) \\
&\quad \times \left[f^2(k) \left(f^2(p_+) + f^2(p_-) \right) - f(k) \left(f(k+q) + f(k-q) \right) f(p_+) f(p_-) \right], \tag{A.12}
\end{aligned}$$

or else to two-meson intermediate states,

$$\begin{aligned}
f_\pi^{(f)} \delta^{ab} &= \frac{-g_{\pi qq}}{2m_\pi^2} \sum_{i,j} \int \frac{d^4 p}{(2\pi)^4} \hat{T}(\bar{\Gamma}_i \otimes \Omega_i; p_+) \hat{T}(\bar{\Gamma}_j \otimes \Omega_j; -p_-) \\
&\quad \times L(q, p_+, -p_-; i\gamma_5 \tau^b, \Omega_i, \Omega_j) \bar{L}'(q, p_+, -p_-; \not{q} \gamma_5 \tau^a, \bar{\Gamma}_i, \bar{\Gamma}_j), \tag{A.13}
\end{aligned}$$

$$\begin{aligned}
f_\pi^{(j)} \delta^{ab} &= \frac{-i g_{\pi qq} G_1}{2m_\pi^2} \int \frac{d^4 k}{(2\pi)^4} \text{Tr} [S(k)] \sum_{i,j} \int \frac{d^4 p}{(2\pi)^4} \hat{T}(\bar{\Gamma}_i \otimes \Omega_i; p_+) \hat{T}(\bar{\Gamma}_j \otimes \Omega_j; -p_-) \\
&\quad \times L(q, p_+, -p_-; i\gamma_5 \tau^b, \Omega_i, \Omega_j) \left[f^2(k) \bar{L}_\pm(q, p_+, -p_-; \not{q} \gamma_5 \tau^a, \bar{\Gamma}_i, \bar{\Gamma}_j) \right. \\
&\quad \left. - f(k) \left(f(k+q) + f(k-q) \right) \bar{L}(q, p_+, -p_-; \not{q} \gamma_5 \tau^a, \bar{\Gamma}_i, \bar{\Gamma}_j) \right]. \tag{A.14}
\end{aligned}$$

To assist in writing the above expressions the L, \bar{L} notation defined in Chp. 7.3 has been slightly extended. In diagram (f) there are no form factors associated with the insertion at the local axial current vertex, and hence the appropriate three-quark loop, denoted by \bar{L}' , differs from the integrals in the definition of \bar{L} (Eq. 7.9) by having $f(p_+)f(p_-)$ instead of $f^2(p_+)f^2(p_-)$. Similarly, the symbol \bar{L}_\pm is used to stand for a loop where $f^2(p_+)f^2(p_-)$ in \bar{L} is replaced by $f^2(p_+) + f^2(p_-)$. The $\not{q} \gamma_5$ identity of Eq. 4.3 leads to familiar cancellations between the local and nonlocal diagrams above, yielding:

$$\begin{aligned}
& f_\pi^{(e)} + f_\pi^{(i)} = r_\pi^{(e)} \\
& + \frac{ig_{\pi qq}G_1}{2m_\pi^2} J_{NPP}^{(c)} \int \frac{d^4k}{(2\pi)^4} \text{Tr}[S(k)] f(k) (f(k+q) + f(k-q)) \\
& + \frac{g_{\pi qq}m_c}{m_\pi^2} (J_{NPP}^{(c)} \text{ with } f^2(p_+)f^2(p_-) \rightarrow f(p_+)f(p_-)), \tag{A.15}
\end{aligned}$$

and:

$$\begin{aligned}
& f_\pi^{(f)} + f_\pi^{(j)} = r_\pi^{(f)} \\
& + \frac{ig_{\pi qq}G_1}{2m_\pi^2} J_{NPP}^{(d)} \int \frac{d^4k}{(2\pi)^4} \text{Tr}[S(k)] f(k) (f(k+q) + f(k-q)) \\
& + \frac{g_{\pi qq}m_c}{m_\pi^2} (J_{NPP}^{(d)} \text{ with } \bar{L} \rightarrow \bar{L}'). \tag{A.16}
\end{aligned}$$

The contributions given in Eqs. A.15 and A.16 still contain some fairly complicated pieces, which originated in the $S^{-1}(p_+)\gamma_5 + \gamma_5 S^{-1}(p_-)$ part of the $\not{q}\gamma_5$ identity. These are to be considered separately and are given by:

$$\begin{aligned}
r_\pi^{(e)}\delta^{ab} &= \frac{-g_{\pi qq}}{2m_\pi^2} \sum_i \int \frac{d^4p}{(2\pi)^4} \frac{d^4k}{(2\pi)^4} \hat{T}(\bar{\Gamma}_i \otimes \Omega_i; p-k) f^2(k_+) f^2(k_-) f(p_+) f(p_-) \\
&\times \text{Tr} [\gamma_5 \tau^b S(k_-) \Omega_i (S(p_-) \gamma_5 \tau^a + \gamma_5 \tau^a S(p_+)) \bar{\Gamma}_i S(k_+)], \tag{A.17}
\end{aligned}$$

$$\begin{aligned}
r_\pi^{(f)}\delta^{ab} &= -\frac{g_{\pi qq}}{2m_\pi^2} \int \frac{d^4p}{(2\pi)^4} \frac{G_1}{1 - G_1 J_{PP}(p_+)} \frac{G_1}{1 - G_1 J_{SS}(p_-)} \\
&\times L(q, p_+, -p_-; i\gamma_5 \tau^b, i\gamma_5 \tau^c, 1) \\
&\times \left\{ \int \frac{d^4k}{(2\pi)^4} \text{Tr} [S(k - \frac{1}{2}p_-) \tau^c S(k + \frac{1}{2}p_-) \tau^a] f(k - \frac{1}{2}p_-) f(k + \frac{1}{2}p_-) \right. \\
&\times (f(k - \frac{1}{2}p_-) f(k + \frac{1}{2}p_- + q) + f(k - \frac{1}{2}p_- - q) f(k + \frac{1}{2}p_-)) \\
&+ \int \frac{d^4k}{(2\pi)^4} \text{Tr} [S(k + \frac{1}{2}p_+) \gamma_5 \tau^c S(k - \frac{1}{2}p_+) \gamma_5 \tau^a] f(k + \frac{1}{2}p_+) f(k - \frac{1}{2}p_+) \\
&\left. \times (f(k + \frac{1}{2}p_+) f(k - \frac{1}{2}p_+ + q) + f(k + \frac{1}{2}p_+ - q) f(k - \frac{1}{2}p_+)) \right\}. \tag{A.18}
\end{aligned}$$

Fortunately, the overall result for the NLO part of the pion decay constant is greatly simplified once the remaining NLO diagrams, (*m*), (*n*) and (*o*) are included. The isolated contributions, $r_\pi^{(d)}$, $r_\pi^{(e)}$ and $r_\pi^{(f)}$, can then be eliminated. Consider first diagram (*n*) of Fig. 7.15. This contribution can be written as a sum of terms, in each

of which one of the two-quark loops is given by a LO J integral whereas the other is similar but has a different combination of form factors:

$$\begin{aligned}
f_\pi^{(n)}\delta^{ab} &= \frac{g_{\pi qq}G_1}{2m_\pi^2} \int \frac{d^4p}{(2\pi)^4} \frac{G_1}{1 - G_1 J_{PP}(p_+)} \frac{G_1}{1 - G_1 J_{SS}(p_-)} \\
&\quad \times L(q, p_+, -p_-; i\gamma_5\tau^b, i\gamma_5\tau^c, 1) \\
&\times \left\{ J_{PP}(p_+)\delta^{ac} \int \frac{d^4k}{(2\pi)^4} \text{Tr} \left[S(k - \frac{1}{2}p_-)S(k + \frac{1}{2}p_-) \right] f(k - \frac{1}{2}p_-)f(k + \frac{1}{2}p_-) \right. \\
&\quad \times \left(f(k - \frac{1}{2}p_-)f(k + \frac{1}{2}p_- + q) + f(k - \frac{1}{2}p_- - q)f(k + \frac{1}{2}p_-) \right) \\
&+ J_{SS}(p_-) \int \frac{d^4k}{(2\pi)^4} \text{Tr} \left[S(k + \frac{1}{2}p_+)\gamma_5\tau^c S(k - \frac{1}{2}p_+)\gamma_5\tau^a \right] f(k + \frac{1}{2}p_+)f(k - \frac{1}{2}p_+) \\
&\quad \left. \times \left(f(k + \frac{1}{2}p_+)f(k - \frac{1}{2}p_+ + q) + f(k + \frac{1}{2}p_+ - q)f(k - \frac{1}{2}p_+) \right) \right\}. \tag{A.19}
\end{aligned}$$

Eq. A.19 is clearly very similar to Eq. A.18 for $r_\pi^{(f)}$, which arose as part of the NLO diagram for the local current with two-meson intermediates. In fact, the terms in Eq. A.19 differ from those in Eq. A.18 only by a factor of $-G_1J$. Hence, their sum can be written as a set of contributions which have only a single intermediate meson propagator:

$$\begin{aligned}
(r_\pi^{(f)} + f_\pi^{(n)})\delta^{ab} &= \\
&- \frac{g_{\pi qq}}{2m_\pi^2} \int \frac{d^4p}{(2\pi)^4} \frac{G_1^2}{1 - G_1 J_{SS}(p_-)} L(q, p_+, -p_-; i\gamma_5\tau^b, i\gamma_5\tau^a, 1) \\
&\times \int \frac{d^4k}{(2\pi)^4} \text{Tr} \left[S(k - \frac{1}{2}p_-)S(k + \frac{1}{2}p_-) \right] f(k - \frac{1}{2}p_-)f(k + \frac{1}{2}p_-) \\
&\times \left(f(k - \frac{1}{2}p_-)f(k + \frac{1}{2}p_- + q) + f(k - \frac{1}{2}p_- - q)f(k + \frac{1}{2}p_-) \right) \\
&- \frac{g_{\pi qq}}{2m_\pi^2} \int \frac{d^4p}{(2\pi)^4} \frac{G_1^2}{1 - G_1 J_{PP}(p_+)} L(q, p_+, -p_-; i\gamma_5\tau^b, i\gamma_5\tau^c, 1) \\
&\times \int \frac{d^4k}{(2\pi)^4} \text{Tr} \left[S(k + \frac{1}{2}p_+)\gamma_5\tau^c S(k - \frac{1}{2}p_+)\gamma_5\tau^a \right] f(k + \frac{1}{2}p_+)f(k - \frac{1}{2}p_+) \\
&\times \left(f(k + \frac{1}{2}p_+)f(k - \frac{1}{2}p_+ + q) + f(k + \frac{1}{2}p_+ - q)f(k - \frac{1}{2}p_+) \right). \tag{A.20}
\end{aligned}$$

There are two diagrams of the form (o) which appear in the calculations. Since each contains a two-quark and a three-quark loop as well as an intermediate meson propagator, it is plausible that they may be able to effect a cancellation with contributions like those in Eq. A.20. The type-III nonlocal current term $G_1(i\gamma_5\tau^a \otimes 1)$

has been responsible for all of the NLO nonlocal diagrams presented thus far. It also makes a contribution in this case, as does the type-I term $G_1 \epsilon^{acd} (\tau^d \otimes i\gamma_5 \tau^c)$. In an obvious notation the relevant diagrams are referred to as (oIII) and (oI).

Dealing first with (oIII), one notes that there are always two form factors in a type-III current that are not path-linked, enabling one of the quark loops to be recognized as either a J or an L loop. Making suitable choices of the integration variables, the pieces that involve an L loop can be shown to cancel with Eq. A.20. The other pieces of the diagram (oIII) are

$$\begin{aligned}
(r_\pi^{(f)} + f_\pi^{(n)} + f_\pi^{(oIII)}) \delta^{ab} &= \frac{-g_{\pi qq} G_1}{2m_\pi^2} \int \frac{d^4 k}{(2\pi)^4} \int \frac{d^4 p}{(2\pi)^4} \frac{G_1 J_{PP}(p-k)}{1 - G_1 J_{PP}(p-k)} \\
&\times \left\{ \text{Tr} \left[\gamma_5 \tau^b S(p_-) S(k_+) \gamma_5 \tau^a S(p_+) \right] f(p_+) f(k_+) \right. \\
&\quad \left. + \text{Tr} \left[\gamma_5 \tau^b S(p_-) \gamma_5 \tau^a S(k_-) S(p_+) \right] f(p_-) f(k_-) \right\} \\
&\quad \times f(p_+) f(p_-) \left(f(p_+) f(k_+) + f(p_-) f(k_-) \right) \\
&+ \frac{g_{\pi qq} G_1}{2m_\pi^2} \int \frac{d^4 k}{(2\pi)^4} \int \frac{d^4 p}{(2\pi)^4} \frac{G_1 J_{SS}(p-k)}{1 - G_1 J_{SS}(p-k)} f(p_+) f(p_-) \\
&\times \left\{ \text{Tr} \left[\gamma_5 \tau^b S(p_-) \gamma_5 \tau^a S(k_+) S(p_+) \right] f(p_+) f(k_+) \right. \\
&\quad \left. + \text{Tr} \left[\gamma_5 \tau^b S(p_-) S(k_-) \gamma_5 \tau^a S(p_+) \right] f(p_-) f(k_-) \right\} \\
&\quad \times f(p_+) f(p_-) \left(f(p_+) f(k_+) + f(p_-) f(k_-) \right). \tag{A.21}
\end{aligned}$$

Comparing the above equation with Eq. A.10 for $r_\pi^{(d)}$ one can see the same general structures appearing. Taking due account of isospin factors, $r_\pi^{(d)}$ can be combined with Eq. A.21 to produce:

$$\begin{aligned}
r_\pi^{(d)} + r_\pi^{(f)} + f_\pi^{(n)} + f_\pi^{(o\text{III})} &= \frac{g_{\pi qq} G_1}{2m_\pi^2} \int \frac{d^4 k}{(2\pi)^4} \int \frac{d^4 p}{(2\pi)^4} f(p_+) f(p_-) \\
&\times \left\{ \text{Tr} \left[\gamma_5 S(p_-) \left(S(k_+) \gamma_5 - \gamma_5 S(k_+) \right) S(p_+) \right] f^2(p_+) f^2(k_+) \right. \\
&\quad \left. + \text{Tr} \left[\gamma_5 S(p_-) \left(\gamma_5 S(k_-) - S(k_-) \gamma_5 \right) S(p_+) \right] f^2(p_-) f^2(k_-) \right\} \\
&- \frac{g_{\pi qq} G_1}{2m_\pi^2} \int \frac{d^4 k}{(2\pi)^4} \int \frac{d^4 p}{(2\pi)^4} \frac{G_1 J_{PP}(p-k)}{1 - G_1 J_{PP}(p-k)} f^2(p_+) f^2(p_-) f(k_+) f(k_-) \\
&\quad \times \text{Tr} \left[\gamma_5 S(p_-) S(k_+) \gamma_5 S(p_+) + \gamma_5 S(p_-) \gamma_5 S(k_-) S(p_+) \right] \\
&+ \frac{g_{\pi qq} G_1}{2m_\pi^2} \int \frac{d^4 k}{(2\pi)^4} \int \frac{d^4 p}{(2\pi)^4} \frac{G_1 J_{SS}(p-k)}{1 - G_1 J_{SS}(p-k)} f^2(p_+) f^2(p_-) f(k_+) f(k_-) \\
&\quad \times \text{Tr} \left[\gamma_5 S(p_-) \gamma_5 S(k_+) S(p_+) + \gamma_5 S(p_-) S(k_-) \gamma_5 S(p_+) \right] \\
&+ \frac{g_{\pi qq}}{m_\pi^2} \int \frac{d^4 k}{(2\pi)^4} \int \frac{d^4 p}{(2\pi)^4} \frac{G_1}{1 - G_1 J_{PP}(p-k)} f(p_+) f(p_-) \\
&\quad \times \left\{ \text{Tr} \left[\gamma_5 S(p_-) S(k_+) \gamma_5 S(p_+) \right] f^2(p_+) f^2(k_+) \right. \\
&\quad \left. + \text{Tr} \left[\gamma_5 S(p_-) \gamma_5 S(k_-) S(p_+) \right] f^2(p_-) f^2(k_-) \right\}. \tag{A.22}
\end{aligned}$$

In Eq. A.22, the first term contains pieces from both Eqs. A.10 and A.21, a relative factor of $-G_1 J$ in the latter combining to cancel the LO meson propagator in the sum. The second and third terms are just the remainder of Eq. A.21 and the final term is the rest of Eq. A.10. Now, apart from a factor of $\sim G_1 J$, the second and third terms of Eq. A.22 are very much reminiscent in structure of $r_\pi^{(e)}$ (see Eq. A.17). It is profitable at this point to reintroduce that contribution. This enables the intermediate sigma propagator in the second term of Eq. A.22 to be cancelled and alters a factor in the third term. If one also lets $k \rightarrow -k$ in the k_- arguments of the first term, one has that:

$$\begin{aligned}
 r_\pi^{(d)} + r_\pi^{(e)} + r_\pi^{(f)} + f_\pi^{(n)} + f_\pi^{(o\text{III})} &= \frac{g_{\pi qq} G_1}{2m_\pi^2} \int \frac{d^4 k}{(2\pi)^4} \int \frac{d^4 p}{(2\pi)^4} f(p_+) f(p_-) \\
 &\times \text{Tr} \left[\gamma_5 S(p_-) \left[(S(k_+) f^2(p_+) - S(-k_+) f^2(p_-)), \gamma_5 \right] S(p_+) \right] f^2(k_+) \\
 &- \frac{g_{\pi qq} G_1}{2m_\pi^2} \int \frac{d^4 k}{(2\pi)^4} \int \frac{d^4 p}{(2\pi)^4} \frac{1 + G_1 J_{PP}(p-k)}{1 - G_1 J_{PP}(p-k)} f^2(p_+) f^2(p_-) f(k_+) f(k_-) \\
 &\times \text{Tr} \left[\gamma_5 S(p_-) S(k_+) \gamma_5 S(p_+) + \gamma_5 S(p_-) \gamma_5 S(k_-) S(p_+) \right] \\
 &- \frac{g_{\pi qq} G_1}{2m_\pi^2} \int \frac{d^4 k}{(2\pi)^4} \int \frac{d^4 p}{(2\pi)^4} f^2(p_+) f^2(p_-) f(k_+) f(k_-) \\
 &\times \text{Tr} \left[\gamma_5 S(p_-) \gamma_5 S(k_+) S(p_+) + \gamma_5 S(p_-) S(k_-) \gamma_5 S(p_+) \right] \\
 &+ \frac{g_{\pi qq}}{m_\pi^2} \int \frac{d^4 k}{(2\pi)^4} \int \frac{d^4 p}{(2\pi)^4} \frac{G_1}{1 - G_1 J_{PP}(p-k)} f(p_+) f(p_-) \\
 &\times \left\{ \text{Tr} \left[\gamma_5 S(p_-) S(k_+) \gamma_5 S(p_+) \right] f^2(p_+) f^2(k_+) \right. \\
 &\quad \left. + \text{Tr} \left[\gamma_5 S(p_-) \gamma_5 S(k_-) S(p_+) \right] f^2(p_-) f^2(k_-) \right\}. \tag{A.23}
 \end{aligned}$$

The above equation remains somewhat cumbersome. Moreover, one may feel a little uneasy that it contains pion intermediates but no scalar exchanges. The situation is clarified dramatically, however, by bringing in the diagram (oI). This features a two-quark loop that connects an intermediate meson with one of the matrix structures from the type-I nonlocal current term $G_1 \epsilon^{acd} (\tau^d \otimes i\gamma_5 \tau^c)$. For the flavour trace over this loop to be non-zero, the meson involved must be a pion. Furthermore, the type-I structure (Eq. 2.11) ensures that the form factors associated with this two-quark loop have no path links, and hence the loop reduces to J_{PP} . One can write the contribution from this diagram as:

$$\begin{aligned}
 f_\pi^{(o\text{I})} &= \frac{g_{\pi qq} G_1}{m_\pi^2} \int \frac{d^4 k}{(2\pi)^4} \int \frac{d^4 p}{(2\pi)^4} \frac{G_1 J_{PP}(p-k)}{1 - G_1 J_{PP}(p-k)} f^2(p_+) f^2(p_-) f(k_+) f(k_-) \\
 &\times \text{Tr} \left[\gamma_5 S(p_-) S(k_+) \gamma_5 S(p_+) + \gamma_5 S(p_-) \gamma_5 S(k_-) S(p_+) \right] \\
 &- \frac{g_{\pi qq} G_1}{m_\pi^2} \int \frac{d^4 k}{(2\pi)^4} \int \frac{d^4 p}{(2\pi)^4} \frac{G_1 J_{PP}(p-k)}{1 - G_1 J_{PP}(p-k)} f(p_+) f(p_-) \\
 &\times \left\{ \text{Tr} \left[\gamma_5 S(p_-) S(k_+) \gamma_5 S(p_+) \right] f^2(p_+) f^2(k_+) \right. \\
 &\quad \left. + \text{Tr} \left[\gamma_5 S(p_-) \gamma_5 S(k_-) S(p_+) \right] f^2(p_-) f^2(k_-) \right\}, \tag{A.24}
 \end{aligned}$$

an isospin summation having been performed. The first term of Eq. A.24 is of precisely the right form to cause the $1 + G_1 J_{PP}(p - k)$ piece occurring in Eq. A.23 to become $1 - G_1 J_{PP}(p - k)$ when the two are added, thereby cancelling the pion propagator. Furthermore, the other part of Eq. A.24 cancels the other pion propagator found in Eq. A.23, so that the sum has no net meson intermediates,

$$\begin{aligned}
r_\pi^{(d)} + r_\pi^{(e)} + r_\pi^{(f)} + f_\pi^{(n)} + f_\pi^{(oI)} + f_\pi^{(oIII)} &= \frac{3g_{\pi qq}G_1}{2m_\pi^2} \int \frac{d^4k}{(2\pi)^4} \int \frac{d^4p}{(2\pi)^4} f(p_+)f(p_-) \\
&\times \text{Tr} \left[\gamma_5 S(p_-) \left(S(k_+) f^2(p_+) \gamma_5 + \gamma_5 S(-k_+) f^2(p_-) \right) S(p_+) \right] f^2(k_+) \\
&\quad - \frac{g_{\pi qq}G_1}{2m_\pi^2} \int \frac{d^4k}{(2\pi)^4} \int \frac{d^4p}{(2\pi)^4} f(p_+)f(p_-) \\
&\times \text{Tr} \left[\gamma_5 S(p_-) \left(\gamma_5 S(k_+) f^2(p_+) + S(-k_+) f^2(p_-) \gamma_5 \right) S(p_+) \right] f^2(k_+) \\
&\quad - \frac{g_{\pi qq}G_1}{2m_\pi^2} \int \frac{d^4k}{(2\pi)^4} \int \frac{d^4p}{(2\pi)^4} f^2(p_+) f^2(p_-) f(k_+) f(k_-) \\
&\times \text{Tr} \left[\gamma_5 S(p_-) \{ \gamma_5, S(k_+) \} S(p_+) + \gamma_5 S(p_-) \{ S(k_-), \gamma_5 \} S(p_+) \right]. \tag{A.25}
\end{aligned}$$

Shifting the k integration variable such that the LO quark propagators are evaluated only at k and p_\pm , and substituting from Eq. 3.1 for the explicit form of $S(k)$, Eq. A.25 becomes

$$\begin{aligned}
r_\pi^{(d)} + r_\pi^{(e)} + r_\pi^{(f)} + f_\pi^{(n)} + f_\pi^{(oI)} + f_\pi^{(oIII)} &= g_{\pi qq}G_1 \int \frac{d^4k}{(2\pi)^4} \frac{m(k)}{k^2 - m^2(k)} f^2(k) \\
&\times \int \frac{d^4k}{(2\pi)^4} \text{Tr} \left[\gamma_5 S(p_-) \gamma_5 S(p_+) \right] f(p_+)f(p_-) \left(f^2(p_+) + f^2(p_-) \right) \\
&- g_{\pi qq}G_1 J_{PP}(q^2) \int \frac{d^4k}{(2\pi)^4} \frac{m(k)}{k^2 - m^2(k)} f(k) \left(f(k+q) + f(k-q) \right) \\
&= \frac{-1}{4N_c} (\text{nonlocal } f_\pi \text{ diagram at LO}), \tag{A.26}
\end{aligned}$$

where Eq. 4.1 for the LO nonlocal diagram has been recalled to arrive at the punchline.

There remains one more contribution to the pion decay constant at NLO which has not yet been included in this appendix. This is the Fock diagram, (m), as shown in Fig. 7.14. It consists of a LO nonlocal current diagram, with an N_c suppressed

coefficient deduced by Fierz rearrangement (see Chp. 2.5). The only Fock contribution to f_π comes from the type-III term exchange term $G_1(4N_c)^{-1}(i\gamma_5\tau^a \otimes 1)$. This observation then completes the cancellations amongst the NLO diagrams for f_π , since

$$r_\pi^{(d)} + r_\pi^{(e)} + r_\pi^{(f)} + f_\pi^{(m)} + f_\pi^{(n)} + f_\pi^{(oI)} + f_\pi^{(oIII)} = 0. \quad (\text{A.27})$$

Combining Eq. A.27 with others from this appendix, the full set of NLO contributions to the pion decay constant can be seen to produce Eq. 7.11.

A.2 Chiral Expansion

This section describes the chiral expansion of the NLO part of the pion decay constant. As in Appendix A.1 it specialises to the case where the G_1 coupling is the only one present in the action. The aim is to demonstrate that the various contributions produce the two $\mathcal{O}(1/N_c)$ terms on the right-hand side of Eq. 7.15, thereby establishing the GMOR relation at NLO in the model.

In Chp. 7.4, the various diagrams contributing to f_π at NLO were presented. There are several useful cancellations which operate among the diagrams, holding to all orders in the chiral expansion. They were explained in Appendix A.1 and culminated in Eq. 7.11, the starting point for this section.

The first point to notice about Eq. 7.11 is that each term is of $\mathcal{O}(1)$ in the chiral expansion. Hence, in all of the integrals the chiral limit may be taken directly, without making an expansion of the integrand. Consider first the term in Eq. 7.11 proportional to c . Using Eq. 4.6 for the expansion of the $1 - G_1 J_{PP}(q^2)$ factor, the chiral limit of this term is

$$\frac{-g_{\pi qq0}}{m_\pi^2} c_0 G_1 J_{SS0}(0) \left(\frac{m_c \langle \bar{\psi} \psi \rangle_0}{m_0^2(0)} + \frac{m_\pi^2}{Z_{\pi 0}} \right). \quad (\text{A.28})$$

The other term in Eq. 7.11 which has an explicit factor of $1 - G_1 J_{PP}(q^2)$ also has an integral very like the one in the definition of c (Eq. 7.5). Indeed, the only difference is the presence of q in the form factor structure $f(p+q) + f(p-q)$ and so in the chiral

limit this term in Eq. 7.11 is also proportional to c , being:

$$\frac{-g_{\pi qq0}}{m_\pi^2} c_0 (1 - G_1 J_{SS0}(0)) \left(\frac{m_c \langle \bar{\psi} \psi \rangle_0}{m_0^2(0)} + \frac{m_\pi^2}{Z_{\pi 0}} \right). \quad (\text{A.29})$$

The sum of Eqs. A.28 and A.29 is just

$$\frac{-g_{\pi qq0}}{m_\pi^2} c_0 \left(\frac{m_c \langle \bar{\psi} \psi \rangle_0}{m_0^2(0)} + \frac{m_\pi^2}{Z_{\pi 0}} \right), \quad (\text{A.30})$$

the second term in brackets being clearly identifiable as one of the $\mathcal{O}(1/N_c)$ pieces sought in the condition of Eq. 7.15. Note also that the final term of Eq. 7.11 gives precisely the structure of the other part of the condition but has the wrong sign,

$$\frac{g_{N\pi qq0}}{g_{\pi qq0}} \frac{m_0(0)}{g_{\pi qq0}}. \quad (\text{A.31})$$

Consider now the first term of Eq. 7.11. It can be dealt with straightforwardly, using the ladder SDE to perform the k integral and the results of Appendix B for the chiral expansion of J_{NPP} . This yields:

$$-2m_0(0) \frac{g_{N\pi qq0}}{Z_{\pi 0}} + m_c \frac{g_{\pi qq0}}{m_\pi^2} \cdot \frac{\langle \bar{\psi} \psi \rangle_{N0}}{m_0(0)} + m_c \frac{g_{\pi qq0}}{m_\pi^2} \cdot \frac{\langle \bar{\psi} \psi \rangle_0}{m_0(0)} \cdot \frac{2c_0}{m_0(0)}. \quad (\text{A.32})$$

The first term of the above equation is exactly that needed to reverse the sign of Eq. A.31 in the sum. The contributions discussed so far are therefore:

$$\frac{-c_0}{g_{\pi qq0}} - \frac{g_{N\pi qq0}}{g_{\pi qq0}} \frac{m_0(0)}{g_{\pi qq0}} + \frac{g_{\pi qq0}}{m_0(0)} \frac{m_c}{m_\pi^2} \left(\langle \bar{\psi} \psi \rangle_{N0} + \frac{c_0}{m_0(0)} \langle \bar{\psi} \psi \rangle_0 \right). \quad (\text{A.33})$$

It remains only to cancel the last term in Eq. A.33 with the other terms of Eq. 7.11. These terms are explicitly proportional to m_c and contain integrals very similar to those in J_{NPP} , but with different combinations of form factors. The integrals similar to $J_{NPP}^{(b)}$, $J_{NPP}^{(c)}$ and $J_{NPP}^{(d)}$ are not described here. Procedures for manipulating such integrals so as to simplify their sum were detailed in Appendix B and are not affected by the different form factors appearing in the present case. It therefore suffices to state the end result for the sum of these contributions to f_π , which is:

$$\begin{aligned}
 & \frac{m_c g_{\pi qq0}}{m_\pi^2 m_0(0)} N_c N_f \int \frac{d^4 k}{(2\pi)^4} \frac{d^4 p}{(2\pi)^4} \frac{G_1 f^2(p) f^2(k)}{1 - G_1 J_{SS0}(p-k)} \\
 & \quad \times \frac{[4m_0(k)(p^2 + m_0^2(p)) + 8p \cdot km_0(p)]}{[p^2 - m_0^2(p)]^2 [k^2 - m_0^2(k)]} \\
 & + \frac{m_c g_{\pi qq0}}{m_\pi^2 m_0(0)} N_c N_f \int \frac{d^4 k}{(2\pi)^4} \frac{d^4 p}{(2\pi)^4} \frac{3G_1 f^2(p) f^2(k)}{1 - G_1 J_{PP0}(p-k)} \\
 & \quad \times \frac{[-4m_0(k)(p^2 + m_0^2(p)) + 8p \cdot km_0(p)]}{[p^2 - m_0^2(p)]^2 [k^2 - m_0^2(k)]}. \tag{A.34}
 \end{aligned}$$

If one compares Eq. A.34 to Eq. B.13 and takes account of the subsequent discussion, it is clear that replacing m_c by $m_c + \Delta m(p)$ in Eq. A.34 would make it proportional to $\langle \bar{\psi}\psi \rangle_{N0}$. Such a replacement can in fact be made when the final contribution from Eq. 7.11 is included. This is the term which is similar to $J_{NPP}^{(a)}$. By analogy with the discussion of $J_{NPP}^{(a)}$ in Appendix B, the loop which has a modified form factor structure reduces in the chiral limit to a factor¹ $\sim I_6$ (which was defined in Eq. 4.10). Thus this contribution from Eq. 7.11 can be shown to produce:

$$2 \frac{g_{\pi qq0}}{m_\pi^2} m_c c_0 I_6. \tag{A.35}$$

Adding the above expression to the final term in brackets of Eq. A.33 gives:

$$\begin{aligned}
 g_{\pi qq0} \frac{m_c}{m_\pi^2} \cdot \frac{c_0}{m_0(0)} \cdot \frac{\langle \bar{\psi}\psi \rangle_0}{m_0(0)} & \longrightarrow g_{\pi qq0} \frac{m_c}{m_\pi^2} \cdot \frac{c_0}{m_0(0)} \left(\frac{\langle \bar{\psi}\psi \rangle_0}{m_0(0)} + 2m_0(0) I_6 \right) \\
 & = - \frac{g_{\pi qq0}}{m_\pi^2} \cdot \frac{c_0}{m_0(0)} 2I_8 \Delta m(0), \tag{A.36}
 \end{aligned}$$

where Eq. B.3 has been called upon to introduce Δm . The situation can now be clarified by noticing that the combination $I_8 c_0$ is given by the same integrals as those in Eq. A.34, apart from an additional factor of $f^2(p)$. This is exactly what is needed for the sum of Eqs. A.36 and A.34 to give Eq. A.34 with $m_c \rightarrow m_c + \Delta m(p)$. One has therefore produced a piece proportional to $\langle \bar{\psi}\psi \rangle_{N0}$. As required, this piece cancels with the unwanted term in Eq. A.33. In summary, the chiral limit of the NLO component

¹cf. a factor of $\sim I_8$, which came from the corresponding loop in $J_{NPP}^{(a)}$.

of the pion decay constant (given by the sum of Eqs. A.33, A.34 and A.35) is shown to be precisely that which satisfies the GMOR relation,

$$f_{N\pi^0} = \frac{-c_0}{g_{\pi qq^0}} - \frac{g_{N\pi qq^0}}{g_{\pi qq^0}} \cdot \frac{m_0(0)}{g_{\pi qq^0}}. \quad (\text{A.37})$$

Appendix B

Chiral Expansion of NLO Pion Amplitude

This appendix discusses the chiral expansion of $J_{NPP}(q^2)$, concentrating on the case where G_1 is the only coupling constant in the action. As described in Chp. 7.5, the expansion has two important aspects. That there is no term of $\mathcal{O}(1)$ is required in order to preserve the Goldstone nature of the pion in the chiral limit. Also of interest is the coefficient of the term of $\mathcal{O}(m_c)$ since this is a necessary ingredient in proving the GMOR relation at NLO.

Consider first the contribution $J_{NPP}^{(a)}(q^2)$ coming from the NLO BSE diagram of type (a) (it is drawn in Fig. 7.7 and given by Eq. 7.6 with $cf^2(p)$ replacing $\Sigma_N(p)$). The constant c is given by a three-quark loop with an intermediate pion or sigma meson (see Eq. 7.5). In the former case, as in some other NLO diagrams involving pion states, there is an associated factor of three due to isospin multiplicity. In the rest of $J_{NPP}^{(a)}$, it is useful to note that the Dirac trace in the chiral limit yields a factor that cancels with the denominator of one of the three LO quark propagators. The resulting integral is then proportional to I_8 (defined in Eq. 4.10) and can therefore be cancelled with a factor from the $\sigma(0)$ propagator, since

$$1 - G_1 J_{SS}(0) = G_1 (J_{PP0}(0) - J_{SS}(0)) = 2G_1 I_8 + \mathcal{O}(m_c). \quad (\text{B.1})$$

Eq. B.2 gives the chiral expansion of this diagram.

$$\begin{aligned}
J_{NPP}^{(a)}(q^2) = & -\frac{N_c N_f}{m_0(0)} \int \frac{d^4 k}{(2\pi)^4} \frac{G_1}{1 - G_1 J_{SS_0}(k)} f^2(p-k) f^4(p) \\
& \times \int \frac{d^4 p}{(2\pi)^4} \frac{[8m_0(p)(p^2 - p \cdot k) + 4(p^2 + m_0^2(p))m_0(p-k)]}{[p^2 - m_0^2(p)]^2 [(p-k)^2 - m_0^2(p-k)]} \\
& + 3N_c N_f \int \frac{d^4 k}{(2\pi)^4} \frac{G_1}{1 - G_1 J_{PP_0}(k)} f^2(p-k) f^4(p) \\
& \times \int \frac{d^4 p}{(2\pi)^4} \frac{[8m_0(p)(p^2 - p \cdot k) - 4(p^2 + m_0^2(p))m_0(p-k)]}{[p^2 - m_0^2(p)]^2 [(p-k)^2 - m_0^2(p-k)]} \\
& - \frac{N_c N_f}{m_0(0)} \int \frac{d^4 k}{(2\pi)^4} \frac{d^4 p}{(2\pi)^4} \frac{G_1 f^4(p) f^2(k)}{1 - G_1 J_{SS_0}(p-k)} \\
& \times \left\{ \frac{4[4m_0(k)(p^2 + m_0^2(p)) + 8p \cdot k m_0(p)]}{[p^2 - m_0^2(p)]^3 [k^2 - m_0^2(k)]} m_0(p)(m_c + \Delta m(p)) \right. \\
& + \frac{2[4m_0(k)(p^2 + m_0^2(p)) + 8p \cdot k m_0(p)]}{[p^2 - m_0^2(p)]^2 [k^2 - m_0^2(k)]^2} m_0(k)(m_c + \Delta m(k)) \\
& \left. + \frac{[8(m_c + \Delta m(p))(m_0(p)m_0(k) + p \cdot k) + 4(m_c + \Delta m(k))(p^2 + m_0^2(p))]}{[p^2 - m_0^2(p)]^2 [k^2 - m_0^2(k)]} \right\} \\
& - \frac{N_c N_f}{m_0(0)} \int \frac{d^4 k}{(2\pi)^4} \frac{d^4 p}{(2\pi)^4} \frac{3G_1 f^4(p) f^2(k)}{1 - G_1 J_{PP_0}(p-k)} \\
& \times \left\{ \frac{4[-4m_0(k)(p^2 + m_0^2(p)) + 8p \cdot k m_0(p)]}{[p^2 - m_0^2(p)]^3 [k^2 - m_0^2(k)]} m_0(p)(m_c + \Delta m(p)) \right. \\
& + \frac{2[-4m_0(k)(p^2 + m_0^2(p)) + 8p \cdot k m_0(p)]}{[p^2 - m_0^2(p)]^2 [k^2 - m_0^2(k)]^2} m_0(k)(m_c + \Delta m(k)) \\
& \left. + \frac{[8(m_c + \Delta m(p))(-m_0(p)m_0(k) + p \cdot k) - 4(m_c + \Delta m(k))(p^2 + m_0^2(p))]}{[p^2 - m_0^2(p)]^2 [k^2 - m_0^2(k)]} \right\} \\
& - m_c \frac{N_c N_f}{m_0(0)} \int \frac{d^4 k}{(2\pi)^4} \frac{d^4 p}{(2\pi)^4} \frac{G_1^2 R_{SS}(p-k)}{[1 - G_1 J_{SS_0}(p-k)]^2} \\
& \quad \times \frac{[4m_0(k)(p^2 + m_0^2(p)) + 8p \cdot k m_0(p)]}{[p^2 - m_0^2(p)]^2 [k^2 - m_0^2(k)]} f^4(p) f^2(k) \\
& - m_c \frac{N_c N_f}{m_0(0)} \int \frac{d^4 k}{(2\pi)^4} \frac{d^4 p}{(2\pi)^4} \frac{3G_1^2 R_{PP}(p-k)}{[1 - G_1 J_{PP_0}(p-k)]^2} \\
& \quad \times \frac{[-4m_0(k)(p^2 + m_0^2(p)) + 8p \cdot k m_0(p)]}{[p^2 - m_0^2(p)]^2 [k^2 - m_0^2(k)]} f^4(p) f^2(k) \\
& + 2 \frac{c_0 m_c}{m_0(0)^3} \langle \bar{\psi} \psi \rangle_0 + \mathcal{O}(q^2) + \mathcal{O}(m_c^2, q^4). \tag{B.2}
\end{aligned}$$

In the above equation the combination $m_c + \Delta m(p)$ has been used to denote the $\mathcal{O}(m_c)$ term in the chiral expansion of $m(p)$. From the ladder SDE (Eq. 3.2), one has that

$$\Delta m(p) = -m_c \frac{f^2(p)}{2I_8} \left(\frac{\langle \bar{\psi}\psi \rangle_0}{m_0(0)} + 2m_0(0)I_6 \right). \quad (\text{B.3})$$

The other undefined quantities in Eq. B.2 are R_{SS} and R_{PP} . These are obtained from the chiral expansion of J ,

$$J_{ij}(q^2) = J_{ij0}(q^2) + m_c R_{ij}(q^2) + \mathcal{O}(m_c^2). \quad (\text{B.4})$$

The BSE diagram of type (b) (see Fig. 7.7) contains part of the NLO quark self-energy. It is given by substituting the appropriate part of Σ_N (the second term of Eq. 7.4) into Eq. 7.6. As with diagram (a), there is a useful factor from the Dirac trace of $J_{NPP}^{(b)}$ which cancels (in the chiral limit) one of the denominators of the LO quark propagators:

$$\begin{aligned}
J_{NPP}^{(b)} = & N_c N_f \int \frac{d^4 k}{(2\pi)^4} \frac{G_1}{1 - G_1 J_{SS0}(k)} f^2(p - k) f^6(p) \\
& \times \int \frac{d^4 p}{(2\pi)^4} \frac{8[p^2 - p \cdot k + m_0(p) m_0(p - k)]}{[p^2 - m_0^2(p)]^2 [(p - k)^2 - m_0^2(p - k)]} \\
& + 3N_c N_f \int \frac{d^4 k}{(2\pi)^4} \frac{G_1}{1 - G_1 J_{PP0}(k)} f^2(p - k) f^6(p) \\
& \times \int \frac{d^4 p}{(2\pi)^4} \frac{8[p^2 - p \cdot k - m_0(p) m_0(p - k)]}{[p^2 - m_0^2(p)]^2 [(p - k)^2 - m_0^2(p - k)]} \\
& + 2N_c N_f \int \frac{d^4 k}{(2\pi)^4} \frac{d^4 p}{(2\pi)^4} \frac{G_1 f^6(p) f^2(k)}{1 - G_1 J_{SS0}(p - k)} \\
& \times \left\{ \frac{8[p \cdot k + m_0(p) m_0(k)]}{[p^2 - m_0^2(p)]^2 [k^2 - m_0^2(k)]^2} m_0(k) (m_c + \Delta m(k)) \right. \\
& + \frac{4m_0(p) (m_c + \Delta m(k))}{[p^2 - m_0^2(p)]^2 [k^2 - m_0^2(k)]} + \frac{24m_0(p) [p \cdot k + m_0(p) m_0(k)]}{[p^2 - m_0^2(p)]^3 [k^2 - m_0^2(k)]} (m_c + \Delta m(p)) \\
& \left. + \frac{4[m_0(k) (p^2 - 3m_0^2(p)) - 2p \cdot k m_0(p)]}{[p^2 - m_0^2(p)]^3 [k^2 - m_0^2(k)]} (m_c + \Delta m(p)) \right\} \\
& + 6N_c N_f \int \frac{d^4 k}{(2\pi)^4} \frac{d^4 p}{(2\pi)^4} \frac{G_1 f^6(p) f^2(k)}{1 - G_1 J_{PP0}(p - k)} \\
& \times \left\{ \frac{8[p \cdot k - m_0(p) m_0(k)]}{[p^2 - m_0^2(p)]^2 [k^2 - m_0^2(k)]^2} m_0(k) (m_c + \Delta m(k)) \right. \\
& - \frac{4m_0(p) (m_c + \Delta m(k))}{[p^2 - m_0^2(p)]^2 [k^2 - m_0^2(k)]} + \frac{24m_0(p) [p \cdot k - m_0(p) m_0(k)]}{[p^2 - m_0^2(p)]^3 [k^2 - m_0^2(k)]} (m_c + \Delta m(p)) \\
& \left. - \frac{4[m_0(k) (p^2 - 3m_0^2(p)) + 2p \cdot k m_0(p)]}{[p^2 - m_0^2(p)]^3 [k^2 - m_0^2(k)]} (m_c + \Delta m(p)) \right\} \\
& + 2m_c N_c N_f \int \frac{d^4 k}{(2\pi)^4} \frac{d^4 p}{(2\pi)^4} \frac{G_1^2 R_{SS}(p - k)}{[1 - G_1 J_{SS0}(p - k)]^2} \\
& \times \frac{4[p \cdot k + m_0(p) m_0(k)]}{[p^2 - m_0^2(p)]^2 [k^2 - m_0^2(k)]} f^6(p) f^2(k) \\
& + 6m_c N_c N_f \int \frac{d^4 k}{(2\pi)^4} \frac{d^4 p}{(2\pi)^4} \frac{G_1^2 R_{PP}(p - k)}{[1 - G_1 J_{PP0}(p - k)]^2} \\
& \times \frac{4[p \cdot k - m_0(p) m_0(k)]}{[p^2 - m_0^2(p)]^2 [k^2 - m_0^2(k)]} f^6(p) f^2(k) \\
& + \mathcal{O}(q^2) + \mathcal{O}(m_c^2, q^4). \tag{B.5}
\end{aligned}$$

Neither Eq. B.2 nor Eq. B.5 looks very promising. These contributions can however be combined to advantage if one rewrites the Dirac traces involved in various of the diagram (a) terms as follows:

$$\begin{aligned} \pm 4m_0(k)(p^2 + m_0^2(p)) + 8m_0(p)p \cdot k &= \pm 4m_0(k)(p^2 - m_0^2(p)) \\ &+ 8m_0(p)(p \cdot k \pm m_0(p)m_0(k)). \end{aligned} \quad (\text{B.6})$$

The second term occurring in the representation on the right-hand side has the same structure as pieces appearing in contributions from diagram (b). Meanwhile, the first term simplifies the remaining integrals by cancelling the denominator of a quark propagator. With the assistance of Eq. B.6, one finds that

$$\begin{aligned} J_{NPP}^{(a)} + J_{NPP}^{(b)} &= N_c N_f \int \frac{d^4 k}{(2\pi)^4} \left[\frac{-G_1}{1 - G_1 J_{SS0}(k)} + \frac{3G_1}{1 - G_1 J_{PP0}(k)} \right] \\ &\times \int \frac{d^4 p}{(2\pi)^4} \frac{4f^4(p)f^4(p-k)}{[p^2 - m_0^2(p)][(p-k)^2 - m_0^2(p-k)]} + \mathcal{O}(q^2, m_c). \end{aligned} \quad (\text{B.7})$$

Moving on to diagram (c) (Fig. 7.9 and Eq. 7.7), the Dirac trace in the chiral limit takes a particularly convenient form for both the sigma and pion exchanges. It factorizes into pieces which cancel the denominators from two LO quark propagators, leaving

$$\begin{aligned} J_{NPP}^{(c)} &= -N_c N_f \int \frac{d^4 k}{(2\pi)^4} \left[\frac{G_1}{1 - G_1 J_{SS0}(k)} + \frac{G_1}{1 - G_1 J_{PP0}(k)} \right] \\ &\times \int \frac{d^4 p}{(2\pi)^4} \frac{4f^4(p)f^4(p-k)}{[p^2 - m_0^2(p)][(p-k)^2 - m_0^2(p-k)]} \\ &+ 16N_c N_f \int \frac{d^4 k}{(2\pi)^4} \frac{d^4 p}{(2\pi)^4} \left[\frac{-G_1}{1 - G_1 J_{SS0}(p-k)} + \frac{G_1}{1 - G_1 J_{PP0}(p-k)} \right] \\ &\times \frac{m_0(k)(m_c + \Delta m(k))}{[p^2 - m_0^2(p)][k^2 - m_0^2(k)]^2} f^4(p)f^4(k) \\ &- m_c N_c N_f \int \frac{d^4 k}{(2\pi)^4} \frac{d^4 p}{(2\pi)^4} \left[\frac{G_1^2 R_{SS}(p-k)}{[1 - G_1 J_{SS0}(p-k)]^2} + \frac{G_1^2 R_{PP}(p-k)}{[1 - G_1 J_{PP0}(p-k)]^2} \right] \\ &\times \frac{4f^4(p)f^4(k)}{[p^2 - m_0^2(p)][k^2 - m_0^2(k)]} + \mathcal{O}(q^2) + \mathcal{O}(q^4, m_c^2). \end{aligned} \quad (\text{B.8})$$

Finally, there is a diagram of type (d) to be considered (Fig. 7.9 and Eq. 7.10). It has an intermediate pion and sigma meson. A two sigma intermediate is forbidden

by isospin symmetry whilst a two pion state gives a vanishing Dirac trace over the triangular loops. In the chiral limit of the $\sigma\pi\pi$ loops, the denominator of a quark propagator is cancelled through a factor from the trace, producing:

$$\begin{aligned}
J_{NPP}^{(d)} &= i \int \frac{d^4k}{(2\pi)^4} \frac{G_1}{1 - G_1 J_{SS_0}(k)} \frac{G_1}{1 - G_1 J_{PP_0}(k)} \\
&\times \left\{ 8N_c N_f m_0(0) \int \frac{d^4p}{(2\pi)^4} \frac{4f^4(p)f^4(p-k)}{[p^2 - m_0^2(p)][(p-k)^2 - m_0^2(p-k)]} \right\}^2 \\
&\times \left\{ 1 + m_c \frac{G_1 R_{SS}(k)}{1 - G_1 J_{SS_0}(k)} + m_c \frac{G_1 R_{PP}(k)}{1 - G_1 J_{PP_0}(k)} \right\} \\
&+ 16i(N_c N_f)^2 \int \frac{d^4k}{(2\pi)^4} \frac{G_1}{1 - G_1 J_{SS_0}(k)} \frac{G_1}{1 - G_1 J_{PP_0}(k)} \\
&\times \int \frac{d^4p}{(2\pi)^4} \frac{4f^4(p)f^4(p-k)}{[p^2 - m_0^2(p)][(p-k)^2 - m_0^2(p-k)]} \\
&\times \left\{ \int \frac{d^4\ell}{(2\pi)^4} \frac{8m_0^2(\ell)m_0(\ell-k)(m_c + \Delta m(\ell))f^2(\ell)f^2(\ell-k)}{[\ell^2 - m_0^2(\ell)]^2[(\ell-k)^2 - m_0^2(\ell-k)]} \right. \\
&\left. + \int \frac{d^4\ell}{(2\pi)^4} \frac{2m_0(\ell)(m_c + \Delta m(\ell-k))f^2(\ell)f^2(\ell-k)}{[\ell^2 - m_0^2(\ell)][(\ell-k)^2 - m_0^2(\ell-k)]} \right\} \\
&+ \mathcal{O}(q^2) + \mathcal{O}(q^4, m_c^2). \tag{B.9}
\end{aligned}$$

Since the diagram (d) contribution involves two intermediate meson propagators it is not immediately obvious how it may be combined with the other contributions, each of which has only one such propagator. The crucial point to notice is that the integrals from the triangular loops in $J_{NPP}^{(d)}$ are proportional in the chiral limit to the difference between LO J loops,

$$J_{SS}(q^2) - J_{PP}(q^2) = iN_c N_f \int \frac{d^4p}{(2\pi)^4} \frac{8m_0^2(0)f^4(p)f^4(p-q)}{[p^2 - m_0^2(p)][(p-q)^2 - m_0^2(p-q)]} + \mathcal{O}(m_c). \tag{B.10}$$

The above equation allows one to replace the product of scalar and pseudoscalar meson propagators in Eq. B.9 with their difference:

$$\begin{aligned}
J_{NPP}^{(d)} &= \frac{i}{m_0^2(0)} \int \frac{d^4k}{(2\pi)^4} \left[\frac{-G_1}{1 - G_1 J_{SS_0}(k)} + \frac{G_1}{1 - G_1 J_{PP_0}(k)} \right] (J_{SS_0}(k) - J_{PP_0}(k)) \\
&+ \mathcal{O}(q^2, m_c). \tag{B.11}
\end{aligned}$$

It is now possible to check that the Goldstone nature of the pion has been maintained in the NLO treatment of Chp. 7. From Eqs. B.7, B.8 and B.11 it can be seen that, as required, $J_{NPP}(0)$ vanishes in the chiral limit.

The same statement can also be shown to hold in the extended version of the model¹. The details of the proof are not given here since the general features of the cancellation are similar to those in the above discussion:

- the sum from the diagrams of types (a) and (b) may still be simplified by rewriting the Dirac traces in $J_{NPP}^{(a)}$;
- the cancellation of the denominators of two quark propagators in the diagrams of type (c) also works for other intermediate mesons;
- the products of two meson propagators occurring in the type (d) diagrams can be dealt with² using relations analogous to Eq. B.10, since

$$J_{SS}(q^2) - J_{PP}(q^2) = J_{VV}^T(q^2) - J_{AA}^T(q^2) = J_{VV}^L(q^2) - J_{AA}^L(q^2). \quad (\text{B.12})$$

Returning to the simpler version of the model with the G_1 coupling only, many of the simplifying properties described above can be exploited in the sum of contributions to the $\mathcal{O}(m_c)$ term of J_{NPP} :

¹In the extended model, the pion pole is determined by the zero of the full determinant of Eq. 3.13. Therefore, to complete the proof that the pion is a Goldstone boson at NLO, it would be necessary to establish further that $J_{NAP0}(0) = 0$.

²An additional point of significance is that such diagrams involving the $\not{q}\gamma_5$ component of the pion vertex give triangular loops which are proportional to J_{AP} in the chiral limit.

$$\begin{aligned}
 J_{NPP} = & -\frac{N_c N_f}{m_0^2(0)} \int \frac{d^4 k}{(2\pi)^4} \frac{d^4 p}{(2\pi)^4} \frac{G_1 f^2(p) f^2(k)}{1 - G_1 J_{SS0}(p-k)} (m_c + \Delta m(p)) \\
 & \times \frac{[4m_0(k)(p^2 + m_0^2(p)) + 8p \cdot km_0(p)]}{[p^2 - m_0^2(p)]^2 [k^2 - m_0^2(k)]} \\
 & -\frac{3N_c N_f}{m_0^2(0)} \int \frac{d^4 k}{(2\pi)^4} \frac{d^4 p}{(2\pi)^4} \frac{G_1 f^2(p) f^2(k)}{1 - G_1 J_{PP0}(p-k)} (m_c + \Delta m(p)) \\
 & \times \frac{[-4m_0(k)(p^2 + m_0^2(p)) + 8p \cdot km_0(p)]}{[p^2 - m_0^2(p)]^2 [k^2 - m_0^2(k)]} \\
 & + 2 \frac{c_0 m_c}{m_0(0)^3} \langle \bar{\psi} \psi \rangle_0 + \mathcal{O}(q^2) + \mathcal{O}(q^4, m_c^2) \tag{B.13}
 \end{aligned}$$

Recalling the form of the corresponding $\mathcal{O}(m_c)$ term at LO (see Eq. 4.6) and bearing in mind that the GMOR relation includes the quark condensate, it becomes tempting to compare the integrals in Eq. B.13 with those in the NLO contribution to the condensate,

$$\langle \bar{\psi} \psi \rangle_N = -i \text{Tr} \int \frac{d^4 p}{(2\pi)^4} S_N(p) = i \text{Tr} \int \frac{d^4 p}{(2\pi)^4} S(p) \Sigma_N(p) S(p). \tag{B.14}$$

If one substitutes for $\Sigma_N(p)$ from Eq. 7.4 and takes the chiral limit then some straightforward algebra is sufficient to show that the combination of integrals in Eq. B.13 is indeed reflected in the condensate at NLO. In total, the pion determinant at NLO is given by:

$$\begin{aligned}
 1 - G_1 J_{PP} - G_1 J_{NPP} = & -G_1 m_c \frac{\langle \bar{\psi} \psi \rangle_0}{m_0^2(0)} - G_1 m_c \frac{\langle \bar{\psi} \psi \rangle_{N0}}{m_0^2(0)} - G_1 m_c \frac{\langle \bar{\psi} \psi \rangle_0}{m_0^2(0)} \cdot \frac{2c_0}{m_0(0)} \\
 & - G_1 \frac{q^2}{Z_{\pi 0}} + G_1 \frac{q^2}{Z_{\pi 0}} \cdot \frac{2g_{N\pi qq 0}}{g_{\pi qq 0}} + \mathcal{O}(q^4, m_c^2) \\
 = & -G_1 m_c \frac{\langle \bar{\psi} \psi \rangle_0 + \langle \bar{\psi} \psi \rangle_{N0}}{(m_0(0) - c_0)^2} - G_1 \frac{q^2}{(g_{\pi qq 0} + g_{N\pi qq 0})^2} + \mathcal{O}(q^4, m_c^2). \tag{B.15}
 \end{aligned}$$

Appendix C

$\rho \rightarrow 4\pi$ in Effective Lagrangians

C.1 Effective Chiral Lagrangians

A serious practical difficulty with QCD is that, because of confinement, the degrees of freedom used in writing the QCD Lagrangian do not directly correspond to the observed asymptotic states. The problem is particularly severe at low energies where the fundamental degrees of freedom are far from being straightforwardly manifest in the data. The available data in this regime provides information on the properties of and the interactions amongst the light mesons and baryons. It is therefore liable to be much easier to perform meaningful calculations if equipped with a theory formulated in terms of fields which treat the particles detected as the basic degrees of freedom. In principle at least, effective theories of that type should be completely derivable from QCD. Although any procedure for so doing seems a most impractical prospect at present, there remain useful restrictions which can be imposed on the candidates for such theories. These follow by requiring the symmetries inherent in QCD to be reflected at the hadronic level. Many such restrictions are consequences of the approximate chiral symmetry, discussed in Chp. 1.

The linear sigma model [14] was mentioned in Chp. 1 as a simple theory consistent with chiral symmetry. It includes an explicit scalar field, the dynamics of which are

an essential feature if one wishes to consider chiral symmetry restoration [121] with a simple model of that form. When working at zero temperature and density, however, the absence of an unambiguous suitable scalar meson to identify directly with the field means that one would prefer to deal with the pseudoscalars only. To that end, various field redefinitions can be made [13, 122] to produce a chirally-invariant scalar field, the mass of which can then be sent to infinity. In the resultant theory, the Goldstone modes should only have derivative interactions, since any other terms would have a local chiral invariance and so could be transformed away. At lowest order in the number of derivatives, the theory one arrives at is called the non-linear sigma model, and has the Lagrangian:

$$\mathcal{L}_{\text{NL}\sigma\text{M}} = \frac{1}{4} f_\pi^2 \langle \partial_\mu U \partial^\mu U^\dagger \rangle, \quad (\text{C.1})$$

where the notation $\langle \dots \rangle$ has been used to denote a trace in flavour space of the matrix enclosed in angled brackets. The matrix U specifies an allowed configuration of the pion fields [123] and as such must be an element of the vacuum symmetry, $\text{SU}(2)_V$, transforming under chiral symmetry as

$$U \rightarrow G_l U G_r^\dagger. \quad (\text{C.2})$$

It can be parameterized with the exponential representation,

$$U = \exp(i\mathcal{I}\cdot\boldsymbol{\pi}/f_\pi). \quad (\text{C.3})$$

When the above Lagrangian (Eq. C.1) is used at tree-level, it yields the same results [122] as could be obtained with the more laborious techniques of current algebra and PCAC (see Chp. 1.5). Indeed, it was on that very basis that effective chiral Lagrangians originally became popular (as advocated in Ref. [124] for example).

To proceed further in a systematic construction of an effective theory of pions, one appeals to the power-counting scheme demonstrated by Weinberg [125]. Although the most general effective theory which can be postulated contains an infinite number of terms, each term may be characterised by the number of derivatives involved. A

tractable theory may therefore be obtained by truncating at some finite order in momentum. Hence, the effective theory can be regarded as an expansion in powers of p/Λ , where Λ is a quantity of the order of the mass of the lightest particle neglected in the effective treatment. Obviously it dictates the energy scale below which the low-energy theory may sensibly be applied. The description of the would-be Goldstone bosons in Weinberg's scheme is called chiral perturbation theory (ChPT)[126, 127]. At $\mathcal{O}(p^4)$ in the expansion there exists sufficient experimental information to fix the coefficients of the terms needed. This is not the case, however, at $\mathcal{O}(p^6)$ [128] and higher where the number of undetermined coefficients proliferates¹. When calculations are attempted at $\mathcal{O}(p^6)$, a common prescription for estimating the relevant coefficients [129] is to assume each of them to be generated solely through the exchange of the lightest resonant state with the appropriate discrete quantum numbers. The feasibility of this method rests on its successful application to the $\mathcal{O}(p^4)$ coefficients [126, 130, 131], the empirical values of which are found to be dominated by the contributions from resonance exchange.

Instead of working to progressively higher orders in momentum, an alternative way in which to improve low-energy effective theories of pions is to introduce explicit fields which describe the heavier mesons. The first of these particles to be encountered are the vector mesons ρ and ω . Since the coefficients of terms appearing in any low-energy effective theory are dependent upon the properties of the more massive particles omitted, the development of models which incorporate the vector mesons may prove helpful in improving both the specification and understanding of ChPT. Unfortunately, however, the construction of effective theories that include resonant states is hampered by the loss of power counting, the organizing principle so crucial to ChPT. In essence the breakdown of power counting occurs because the pions are liable to be of high momenta in processes where there is an on-shell resonant particle. Hence, large orders in momentum may be required for the accurate representation of such pions.

¹there are over a hundred terms of $\mathcal{O}(p^6)$.

The loss of power counting is reflected in the considerable freedom allowed in choosing a possible interpolating field to describe the vector mesons. If one were to redefine such a field then the predictions of a given Lagrangian would of course remain unaltered. However, interactions which were ostensibly of some particular order in momentum may be transformed into terms of different orders in the new representation.

The foregoing comments do not mean that a useful effective theory of pions and resonant particles cannot be formulated: they simply note the loss of the scheme which determined the relative importance of each of the infinite number of possible interactions. What is undoubtedly clear, however, is that there is a strong desire to find some other approach which avoids the necessity of considering all possible terms. A practical attitude is to exploit the freedom in the choice of interpolating field. It seems reasonable to suppose that there should exist some choice of field in the framework of which an accurate effective theory² is embodied in a fairly simple form. In searching for a useful theory, a natural starting point is therefore to define some representations for the fields of the resonant particles and then to examine the phenomenology of the simplest Lagrangians in each basis. There are four distinct formulations which are common in the literature:

1. The hidden-gauge form of Bando *et al* [132] ;
2. The massive Yang-Mills form, as suggested in Refs. [124, 133] ;
3. The formalism developed by Coleman, Callan, Wess and Zumino (CCWZ) [134] based on a suggestion by Weinberg [135] ;
4. The use of anti-symmetric tensor fields, as pioneered by Ecker *et al* [131, 136].

Reviews of these approaches are available in Refs. [137, 138]. As emphasized by Birse [138], the approaches are believed to be equivalent [136, 138, 139], differing only in the representation taken for the spin-1 fields.

²whatever that might prove to be.

From both practical and phenomenological perspectives, the simplest Lagrangians of the massive Yang-Mills and hidden-gauge approaches are of particular interest. Within these approaches, one can propose an effective Lagrangian which has only two undetermined parameters: the ρ mass and a gauge coupling. The latter can be set to reproduce the empirical $\rho \rightarrow 2\pi$ decay width, completely specifying a possible effective theory. Furthermore, these representations are motivated on the grounds that they can easily encapsulate phenomenological notions such as VMD and universality (see Chp. 1.6).

In Appendix C.6, the rare decays $\rho \rightarrow 4\pi$ are calculated with various chiral effective models. Before doing so, the models used are briefly described below. Since thorough discussion of these models can be found in the cited literature, it suffices to outline some general points about the approaches and to highlight some of their phenomenological aspects.

C.2 Hidden-Gauge Lagrangians

The hidden-gauge and massive Yang-Mills schemes adopt a gauge style of approach, which is clearly well-suited to the notion of universality. In the hidden-gauge method of Bando *et al.* [132], the Lagrangian of the non-linear sigma model (Eq. C.1) is rewritten with the introduction of an unphysical local symmetry, which may be transformed away. However, if a kinetic term for the gauge field is also included, then the local symmetry becomes physical, generating a non-trivial extension of the model. Although the local symmetry group may contain $SU(2)_A$ [97], it is usual to work with a vector gauge field only. The simplest Lagrangian of π , ρ and ω mesons in the scheme therefore involves these particles only, there being no need to include the a_1 meson.

External gauge fields can be unambiguously introduced into the formalism by separately gauging the global chiral group [140]. The model can also be extended to include an anomalous sector [141]. With the anomalous Ward identity being satisfied by the Wess-Zumino action [142], low-energy theorems, such as those for $\pi^0 \rightarrow \gamma\gamma$

and $\gamma \rightarrow 3\pi$, are automatically satisfied. There are a further four possible terms³ of odd intrinsic parity, with undetermined coefficients. These have no effect on the low-energy theorems⁴ and their strengths should therefore be chosen to reproduce a satisfactory phenomenology of various other anomalous processes.

The couplings in the minimal hidden-gauge model satisfy the relations

$$m_\rho^2 = m_\omega^2 = a\tilde{g}^2 f_\pi^2, \quad g_{\rho\pi\pi} = \frac{a}{2}\tilde{g}, \quad g_{\gamma\pi\pi} = e \left(1 - \frac{a}{2}\right), \quad g_{\rho\gamma} = 2f_\pi^2 g_{\rho\pi\pi}, \quad (\text{C.4})$$

where a is a free parameter, \tilde{g} is the gauge coupling constant and $g_{\gamma\pi\pi}$ has been defined through the vertex

$$\langle \pi^a(q_1)\pi^b(q_2)|\gamma^*(q_1+q_2)\rangle = ig_{\gamma\pi\pi}\epsilon^{ab3}(q_2 \cdot \epsilon - q_1 \cdot \epsilon). \quad (\text{C.5})$$

$g_{\rho\pi\pi}$ is defined similarly in Eq. 5.1. The final relation of Eq. C.4 holds independently of the model parameters and is known as the KSRF relation [144] in its first form. It can be derived straightforwardly as a soft pion theorem for the $\rho \rightarrow 2\pi$ decay [17]. With the parameter choice $a = 2$ the Lagrangian is brought into agreement with several other phenomenological ideas. Combining the first and second relations of Eq. C.4 (with $a = 2$) gives

$$m_\rho^2 = 2g_{\rho\pi\pi}^2 f_\pi^2, \quad (\text{C.6})$$

which is referred to as the second form of the KSRF relation. This version follows from the first under the assumption of the universality relation $g_{\rho\gamma} = m_\rho^2/g_{\rho\pi\pi}$. Universality in the model is therefore imposed at $a = 2$, the value which also produces complete vector dominance of the $\gamma\pi\pi$ coupling.

³Six such terms were originally listed in Ref. [141] but it was soon noticed [143] that two of them (\mathcal{L}_3 and \mathcal{L}_5) are CP odd.

⁴although they do control the relative sizes of different contributions to such amplitudes.

C.3 Massive Yang-Mills Lagrangians

In the massive Yang-Mills approach [124, 133], the spin-1 mesons are represented as though they were external gauge bosons of chiral symmetry⁵. The simplest Lagrangian which can be postulated in the scheme is just the gauged non-linear sigma model along with kinetic and mass terms for the gauge fields. Local chiral symmetry is broken by the mass terms. A significant difference from the hidden-gauge formalism is that global chiral symmetry demands that the a_1 must be included as the chiral partner of the ρ meson.

Expanding the matrix U (Eq. C.3) in the minimal Lagrangian of the scheme, one finds a mixing term between the axial field and the gradient of the pseudoscalar field. To remove this and diagonalize the free-field part of the Lagrangian, a term proportional to the pseudoscalar gradient could be subtracted from the axial field. It is then necessary to rescale the pseudoscalar field⁶ in order to obtain the canonical normalization of the pion kinetic term. Such a procedure constitutes a minimal diagonalization and leads to physical pion and a_1 fields which have complicated chiral transformation properties. Other procedures might also be chosen. For example, if the Lagrangian is first converted into its equivalent CCWZ representation, then a very similar procedure is followed to remove a mixing term. In that case, however, it is convenient to subtract a piece from the axial field proportional to the multi-pion object u_μ (see Appendix C.4), which means that the transformation properties of the mixed and physical fields are the same. Whatever the diagonalization performed, the process induces a mass splitting between the axial and vector fields so that $m_{a_1} = Z^{-1}m_\rho$, where Z is the scaling factor,

$$Z = \left(1 - \frac{g^2 f_\pi^2}{m_\rho^2}\right)^{\frac{1}{2}}. \quad (\text{C.7})$$

In the above equation, g is the gauge coupling of this scheme.

⁵To include a photon field in such a model it is then usual to assume VMD, adding the appropriate terms by hand.

⁶with a corresponding factor being applied to identify the pion decay constant.

The diagonalization is commonly referred to as a partial Higgs mechanism. In the standard Higgs mechanism the degrees of freedom of the would-be Goldstone boson are transmuted into those required to give a mass to the gauge field. In the massive Yang-Mills formalism, however, the Goldstone boson is preserved because of the gauge-symmetry-breaking mass term.

The minimal field redefinition described above has a side effect of producing more complicated interaction vertices, since additional interaction terms are generated in rewriting the gauge-invariant kinetic energies of the spin-1 fields. Where such additional terms contribute to vertices present in the remainder of the Lagrangian the extra terms always contain more powers of momentum. Nevertheless, they can have important effects. For instance, the $\rho\pi\pi$ coupling at the rho mass is reduced by a factor of $\frac{1}{2}(1 + Z^2)$ as compared to its value at zero-momentum; i.e., by $\approx \frac{3}{4}$ for a normal choice of parameters. This means that the minimal model is unable simultaneously to account for the empirical ρ meson mass and width. To overcome the problem, it would be necessary to add new interactions to the Lagrangian, such as those proposed in Refs. [137, 145, 146]. One possibility is the term

$$-i\frac{\xi}{2g}\langle D_\mu U D_\nu U^\dagger F_L^{\mu\nu} + D_\mu U^\dagger D_\nu U F_R^{\mu\nu} \rangle, \quad (\text{C.8})$$

which would cancel the diagonalization-induced part of the $\rho\pi\pi$ vertex if $\xi = 1$.

Extending the definition of the vector field to include an isoscalar component, representing the ω meson, there are then interactions in the anomalous sector [145, 147]. Since the spin-1 fields are identified with external gauge fields of the chiral group, the anomalous vertices are given by Bardeen's form [148] of the anomaly⁷.

Comment and $\rho\pi$ Scattering

In comparison with the simplest hidden-gauge Lagrangian, calculations with the minimal massive Yang-Mills model are rather more involved. Not only does one have

⁷to obtain an anomaly-free vector current entails breaking global chiral symmetry in this sector.

to deal with the more complex interaction vertices produced by diagonalization but there may be additional contributions to processes from diagrams with intermediate a_1 states. Note also that the higher-order contributions to vertices violate universality above the lowest energies. This is certainly no problem of principle, but since the universality hypothesis is an important aspect of the motivation for a gauge-style of approach, one might nevertheless be concerned about such violations. It is therefore easy to see why several authors [9, 10, 149, 150] have found it attractive to work with Lagrangians of the massive Yang-Mills form which do not have an axial field, the source of the unwanted complications. In such models great care should be taken to maintain global chiral symmetry, the guiding principle in the construction of any plausible effective Lagrangian. It is not valid simply to discard the a_1 , as in one of the Lagrangians considered by Ref. [9], since the resulting model would not then respect (for example) the low-energy theorem for $\pi\pi$ scattering [149]. If the a_1 is to be omitted then counterterms [138, 149] are required to restore such theorems.

The authors of Refs. [149, 150] found suitable counterterms such that the VMD extension of the resulting $\pi\rho\omega$ Lagrangian, when integrated over the vector-meson degrees of freedom, reproduces the vertices of the $U(1)_V$ -gauged non-linear sigma model. Although their Lagrangian is therefore consistent with low-energy theorems involving pions and photons only, it is not chirally symmetric. This statement can be illustrated with $\rho\pi$ scattering. Fig. C.1 shows the contributing diagrams in effective Lagrangians of π , ρ , ω and a_1 mesons.

The amplitude for scattering a soft pion from an arbitrary hadron target should vanish in the chiral limit [17]. Considering only that part of each of the vertices in Fig. C.1 which is of lowest order in the pion momentum, then the $\rho\pi\pi$ vertex to be used in diagrams C.1a and C.1b is $g\rho_\mu \cdot \underline{\pi} \times \partial^\mu \underline{\pi}$. As the external pion momentum tends to zero the momentum of the intermediate pion state will tend towards that of the external ρ meson, whose transversality means that there is no contribution from these diagrams in the soft pion limit. In both the hidden gauge (Appendix C.2) and

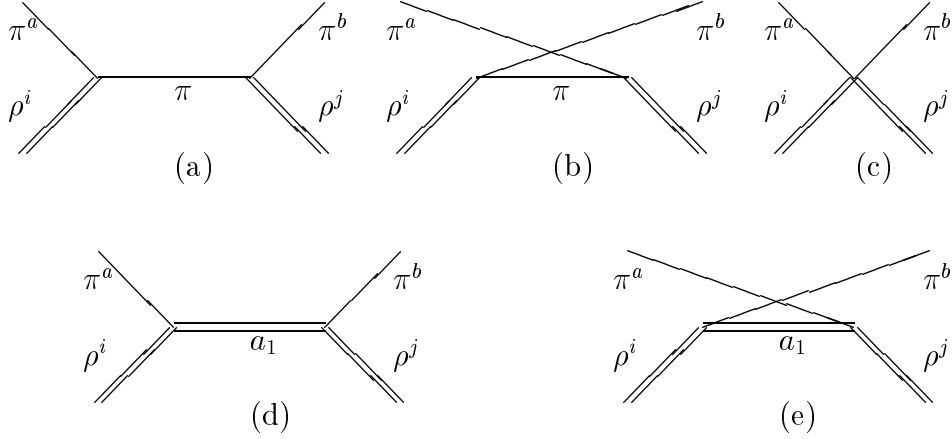


Figure C.1: Diagrams contributing to $\rho\pi$ scattering in chiral effective Lagrangians of π , ρ and a_1 mesons. Single lines denote pions, double lines spin-1 mesons. The suffixes label isospin states. Anomalous terms in the effective Lagrangian introduce diagrams (f) and (g) similar to those of (d) and (e) respectively, but with an ω meson replacing the a_1 .

CCWZ formalisms (Appendix C.4) any interactions which might produce a contribution from diagrams C.1c to C.1e contain powers of the external pion momentum. For the same reason, diagrams C.1f and C.1g vanish in the soft pion limit with all three formalisms. Non-zero diagrams at threshold only appear in the massive Yang-Mills scheme, which has momentum-independent $\rho\rho\pi\pi$ and $\rho\pi a_1$ vertices of $\frac{1}{2}g^2 Z^{-2}(\underline{\pi} \times \underline{\rho}_\mu)^2$ and $g^2 f_\pi Z^{-2} \underline{a}_\mu \cdot \underline{\pi} \times \underline{\rho}^\mu$ respectively. These result in an amplitude from the $\rho\rho\pi\pi$ contact diagram of

$$i \frac{g^2}{Z^2} (2\delta^{ab}\delta^{ij} - \delta^{ai}\delta^{bj} - \delta^{aj}\delta^{bi}) \epsilon \cdot \epsilon^*, \quad (\text{C.9})$$

and a piece coming from diagrams with an intermediate a_1 of

$$i \frac{g^4 f_\pi^2}{Z^4 (m_\rho^2 - m_{a_1}^2)} (2\delta^{ab}\delta^{ij} - \delta^{ai}\delta^{bj} - \delta^{aj}\delta^{bi}) \epsilon \cdot \epsilon^*. \quad (\text{C.10})$$

Using the prediction for the $\rho - a_1$ mass splitting from the massive Yang-Mills Lagrangian, these two contributions cancel, as they should. The Lagrangians proposed in Refs. [149, 150], however, retain a momentum-independent $\rho\rho\pi\pi$ vertex (which is $\frac{1}{2}g^2(\underline{\pi} \times \underline{\rho}_\mu)^2$) without there being an a_1 field present. This gives rise to a non-zero

amplitude in the soft pion limit, violating the chiral low-energy theorem. The model of Refs. [149, 150] is therefore inconsistent with chiral symmetry.

C.4 CCWZ Lagrangians

In the CCWZ formalism the spin-1 fields transform homogeneously under a non-linear realization of chiral symmetry. The following Lagrangian is written in that formalism, using the notation⁸ of Ref. [138]. It gives all of the interaction terms relevant for $\rho \rightarrow 4\pi$ in the models considered.

$$\begin{aligned}
 \mathcal{L}_{\text{CCWZ}} = & \frac{f_\pi^2}{4} \langle u_\mu u^\mu \rangle + m_\rho^2 \langle V_\mu V^\mu \rangle + m_{a_1}^2 \langle A_\mu A^\mu \rangle - \frac{1}{2} \langle V_{\mu\nu} V^{\mu\nu} \rangle - \frac{1}{2} \langle A_{\mu\nu} A^{\mu\nu} \rangle \\
 & - \frac{i}{2} g_1 \langle V_{\mu\nu} [u^\mu, u^\nu] \rangle + \frac{i}{2} g_2 \langle V_{\mu\nu} [V^\mu, V^\nu] \rangle + \frac{i}{2} g_3 \langle V_{\mu\nu} ([u^\mu, A^\nu] - [u^\nu, A^\mu]) \rangle \\
 & + \frac{i}{2} g_4 \langle A_{\mu\nu} ([u^\mu, V^\nu] - [u^\nu, V^\mu]) \rangle + \frac{1}{8} c_1 \langle [u_\mu, u_\nu]^2 \rangle - \frac{1}{4} c_2 \langle [u_\mu, u_\nu] [V^\mu, V^\nu] \rangle \\
 & + \frac{1}{8} c_3 \langle ([u_\mu, V_\nu] - [u_\nu, V_\mu])^2 \rangle - \frac{1}{4} c_4 \langle [u_\mu, u_\nu] ([u^\mu, A^\nu] - [u^\nu, A^\mu]) \rangle. \tag{C.11}
 \end{aligned}$$

Unlike the hidden-gauge and massive Yang-Mills formalisms, there is no natural concept of a minimal Lagrangian in this framework. Each of the above interactions is chirally symmetric and hence the coefficients of Eq. C.11 can be set individually according to the assumptions made about the dynamics. It should be pointed out, however, that there are some restrictions on the coefficients which can be deduced by demanding that the corresponding Hamiltonian has a lower bound [151]. Such constraints can be strengthened into equalities if assumptions about resonance saturation are imposed.

The simplest Lagrangian of the hidden-gauge approach corresponds to the following choices of the coefficients⁹:

$$g_1 = \frac{1}{2\tilde{g}}, \quad g_2 = 2\tilde{g}, \quad c_1 = g_1^2, \quad c_2 = 1, \tag{C.12}$$

⁸apart from the labelling of the coefficients.

⁹Note that the coefficients in Eqs. C.12, C.13 and C.14 do not provide a complete specification of the respective models. To do so would require other terms in the CCWZ Lagrangian.

all other coefficients in Eq. C.11 being zero. The choices appropriate to the simplest massive Yang-Mills model are¹⁰:

$$\begin{aligned} g_1 &= \frac{1}{2g}(1 - Z^4), & g_2 &= 2g, & g_3 &= g_4 = Z^2, \\ c_1 &= g_1^2, & c_2 &= 1 - Z^4, & c_3 &= Z^4, & c_4 &= g_1 g_3. \end{aligned} \quad (\text{C.13})$$

If one includes the non-minimal term of Eq. C.8 then the above coefficients become:

$$\begin{aligned} g_1 &= \frac{1}{2g}(1 + (\xi - 1)Z^4), & g_2 &= 2g, & g_3 &= Z^2(1 - \xi), & g_4 &= Z^2, \\ c_1 &= \frac{1}{4g^2}(1 - Z^4)(1 + (2\xi - 1)Z^4), & c_2 &= 1 + (\xi - 1)Z^4, & c_3 &= Z^4, \\ c_4 &= \frac{1}{2g}Z^2(1 - Z^4)(1 - \xi). \end{aligned} \quad (\text{C.14})$$

The strength at the $\rho\pi\pi$ vertex in the CCWZ Lagrangian of Eq. C.11 is controlled by the value of g_1 . Taking $\xi = 1$ cancels the piece of this vertex which involves the diagonalization parameter, Z , and (at the KSRF value of $Z^2 = \frac{1}{2}$) enforces the identity between the gauge coupling parameter and the *on-shell* coupling $g_{\rho\pi\pi}$.

C.5 $\rho \rightarrow 4\pi$, Motivation and Background

The testing of chiral effective theories of pions and ρ mesons requires that a variety of observables be calculated with the candidate Lagrangians. Two such quantities are the partial widths for the rare ρ^0 decay modes to $2\pi^+2\pi^-$ and to $2\pi^0\pi^+\pi^-$. These decays provide a potentially useful probe of aspects of the effective Lagrangians. For example, the amplitude for the $2\pi^0\pi^+\pi^-$ mode has a contribution involving the $\rho\rho\rho$ vertex that appears in models with gauge-type couplings of the ρ . The partial width calculation might therefore enable the strength at that vertex to be tested.

¹⁰Note that letting $Z \rightarrow 0$ in Eq. C.13 would give the same coefficients as in Eq. C.12. Although $Z \rightarrow 0$ corresponds to the unrealistic situation of $m_\rho \rightarrow gf_\pi$ and $m_{a_1} \rightarrow \infty$ this limit does provide a basis for useful cross checks (both analytic and numeric) between the hidden-gauge and minimal massive Yang-Mills calculations.

Some recent attention has been given to these rare decays [9, 10], stimulated by the prospect that they might soon be detected in experiments at high luminosity e^+e^- machines, such as VEPP-2M [152] or DAΦNE [153]. The present experimental limits on the partial widths are 30 keV for the $2\pi^+2\pi^-$ mode [154] and 6 keV for the $2\pi^0\pi^+\pi^-$ mode [155]. These are already stringent enough to rule out some early estimates, such as that by Prashar [11]¹¹ which was dominated by πa_1 and πa_2 intermediate states. In the more recent attempts of Refs. [9, 10] rather smaller predictions were made, all but one of the models being consistent with the existing limits but quite close to them. Those results offered grounds for optimism since even a modest reduction in the present limits could have significant implications. Note, however, that all of these calculations of the decays did not correctly incorporate chiral symmetry. As is demonstrated in Appendix C.6, the symmetry constraints have a very important effect, the partial widths obtained in chiral models being substantially narrower.

In the work of Bramon, Grau and Pancheri [9], the $2\pi^+2\pi^-$ decay mode was treated within two of the common formalisms for including the ρ meson in chiral effective Lagrangians. Using the simplest hidden-gauge Lagrangian (Appendix C.2) the authors calculated a partial width¹² of 7.5 ± 0.8 keV. In contrast, with a simplified Lagrangian of the massive Yang-Mills type they found 60 ± 7 keV, indicating that the process could distinguish between the models and indeed that the massive Yang-Mills one was inconsistent with experiment. The Yang-Mills Lagrangian used in Ref. [9] coupled the ρ meson to the sigma model as a gauge boson of $SU(2)_V$, being identical to that in Ref. [147] but without an axial field. As was first pointed out in Ref. [10] (see also Appendix C.3) by Eidelman, Silagadze and Kuraev such a simplified model does not respect chiral symmetry. Although the hidden-gauge Lagrangian used by Bramon *et al.* is a perfectly legitimate chiral model, there was unfortunately an error made in the evaluation of the corresponding decay amplitude. As explained in Appendix C.6, the impact of this mistake is dramatic, the partial width being

¹¹where a partial width of 172 keV was quoted for the $2\pi^+2\pi^-$ mode.

¹²the error comes from the range of values considered for the gauge coupling parameter.

significantly overestimated.

Having noted that the massive Yang-Mills Lagrangian of Ref. [9] is not chirally symmetric, Eidelman *et al.* [10] were motivated to revisit the calculation. They did not attempt to work with the full minimal massive Yang-Mills Lagrangian involving the a_1 meson (Appendix C.3), but rather they followed the proposal of Brihaye, Pak and Rossi [149] to introduce counterterms to the naive π, ρ Lagrangian of Ref. [9]. With correction terms that modified the 4π , $\rho 4\pi$ and $\omega 3\pi$ vertices, the authors of Ref. [10] obtained a partial width of 16 ± 1 keV for the $2\pi^+ 2\pi^-$ mode and of 0.6 ± 0.2 keV for the $2\pi^0 \pi^+ \pi^-$ mode. However, their Lagrangian is still not chirally symmetric (see Appendix C.3). As is described in Ref. [138], one could construct a chiral Lagrangian by adding further counterterms to the model. It is, however, practicable to calculate the rare ρ^0 decays while adopting a manifestly chiral approach from the start.

C.6 Decay Amplitude

Working at tree level, the relevant diagrams for $\rho \rightarrow 4\pi$ are shown in Fig. C.2. The amount of available phase space in the decays is greatly reduced by the masses of the decay products. A realistic calculation therefore requires a term in the effective Lagrangians which accounts for the non-zero pion mass. In ChPT, explicit symmetry-breaking terms can be introduced as though there were an external scalar field proportional to the mass matrix, $\text{diag}(m_u, m_d)$. Conserving isospin, the term required is

$$\frac{f_\pi^2}{4} m_\pi^2 \langle U + U^\dagger \rangle. \quad (\text{C.15})$$

The above term is clearly independent of the formalism used to describe the spin-1 fields. It has the additional effect of modifying the 4π vertex which appears in diagram C.2b. The effect is quantitatively significant in the results, since they are much smaller than those found previously [9, 10, 11], but it does not change their qualitative features.

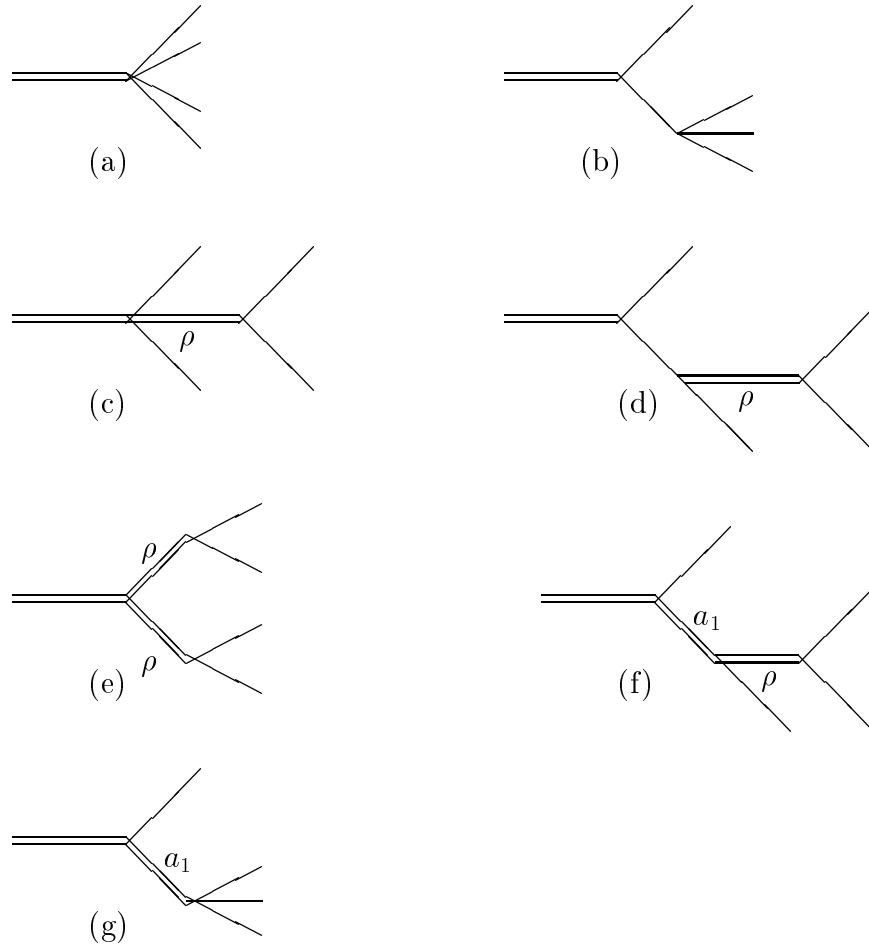


Figure C.2: Diagrams contributing to the $\rho^0 \rightarrow 4\pi$ decays in chiral effective Lagrangians of π , ρ and a_1 mesons. Single lines denote pions, double lines spin-1 mesons. Anomalous terms in the effective Lagrangians introduce diagrams (h) and (i) similar to those of (f) and (g) respectively, but with an ω meson replacing the a_1 .

Consider first the simplest Lagrangian in the hidden-gauge formalism. It includes four gauge-covariant terms in the anomalous sector with undetermined coefficients. Three of these are relevant to the off-shell ω decay occurring in diagrams C.2h and C.2i. The suggestion of Ref. [141] regarding those coefficients is adopted here, so that one includes an $\omega\rho\pi$ vertex but no $\omega 3\pi$ contact term. Consistency with various phenomenological notions (see Appendix C.2) requires that the parameter a of the model be set to 2. In the numerical work this choice is indeed made, whilst the gauge

coupling is fixed so as to reproduce the empirical ρ meson mass¹³ through Eq. C.4. The parameters used are then:

$$f_\pi = 92.4\text{MeV}, \quad m_\pi = 139.6\text{MeV}, \quad m_\rho = m_\omega = 770\text{MeV},$$

$$a = 2, \quad \tilde{g} = 5.89. \quad (\text{C.16})$$

The amplitudes derived for the $\rho^0 \rightarrow 4\pi$ decays by the authors of Ref. [10] were stated in that paper. Although the model used in that case did not include the a_1 meson, all of the other graphs shown in Fig. C.2 were calculated. With the simplest hidden-gauge Lagrangian the a_1 is also absent, as indeed is the $\rho\rho\pi\pi$ vertex which can enter through diagram C.2c. However, for those vertices relevant to $\rho^0 \rightarrow 4\pi$ which are present in the simplest hidden-gauge model, the differences from the corresponding vertices in the Lagrangian of Ref. [10] lie not in their structures but only in their overall strengths. Making appropriate changes to coefficients, the present calculation of the decay amplitudes agrees with that of Ref. [10]. For the decay mode $\rho^0 \rightarrow 2\pi^+2\pi^-$, explicit expressions for the amplitude were also given by Bramon *et al.* [9]. A careful comparison of these two references indicates a discrepancy in the momentum structure of the graph C.2b contribution. Although the present calculation supports the version of Eidelman *et al.*, numerically one finds that the error in Ref. [9] has only a small effect in practice. Certainly, it is not sufficient to invalidate the numerical results quoted by Bramon *et al.*.

Having calculated the amplitudes, a five-dimensional integral over phase space must be performed to obtain the corresponding partial widths. The integrals are expressed in terms of the Mandelstam-like variables of Kumar [156] and evaluated numerically using the NAG routine D01FDF, which maps the region of integration onto the n -dimensional sphere and uses the method of Sag and Szekeres [81] to perform the integration. The accuracy of the integration routine can be estimated by varying the two parameters which specify the mapping onto the n -sphere. In all cases it is

¹³This procedure results in a 2π decay width of 143.4 MeV, a fraction narrower than the observed 151.1 MeV.

found that 50,000 integration points are sufficient to give the integrals to within one part in a thousand.

The results obtained with simplest hidden-gauge model are shown in the first line of Table C.1, labelled HG. They are around an order of magnitude smaller than any of the results of the other recent calculations [9, 10] of the decays.

Model	$\rho^0 \rightarrow 2\pi^+2\pi^-$	$\rho^0 \rightarrow 2\pi^0\pi^+\pi^-$
HG	0.89	0.44
HGNA	0.89	0.24
HGCS	0.59	0.37
MMYM	0.68	0.37
MYM+1	0.63	0.34
MYM+2	1.03	0.39

Table C.1: Decay widths for $\rho^0 \rightarrow 4\pi$ using various chiral effective Lagrangians. The widths are quoted in keV with the specific models being defined in the text.

It was stated in Appendix C.5 that when Bramon *et al.* calculated the $\rho^0 \rightarrow 2\pi^+2\pi^-$ width using the same hidden-gauge model as above they arrived at 7.5 ± 0.8 keV, in sharp contrast with the result given in Table C.1. The crucial difference between the calculations lies in the strength of the direct $\rho 4\pi$ coupling. Bramon *et al.* assumed that the expression for this vertex is identical to that in a massive Yang-Mills model, being generated by the following term in the Lagrangian:

$$-ig \frac{f_\pi^2}{2} \langle \rho^\mu (U^\dagger \partial_\mu U + U \partial_\mu U^\dagger) \rangle = g \left(1 - \frac{1}{3f_\pi^2} \underline{\pi}^2 + \dots \right) \underline{\rho}_\mu \cdot \underline{\pi} \times \partial^\mu \underline{\pi}. \quad (\text{C.17})$$

In fact, the appropriate term in the hidden-gauge model should be written, in the unitary gauge, as

$$-2ia\tilde{g}f_\pi^2 \langle \rho^\mu (u^\dagger \partial_\mu u + u \partial_\mu u^\dagger) \rangle = \frac{a}{2} \tilde{g} \left(1 - \frac{1}{12f_\pi^2} \underline{\pi}^2 + \dots \right) \underline{\rho}_\mu \cdot \underline{\pi} \times \partial^\mu \underline{\pi}, \quad (\text{C.18})$$

where u is the square root of U . Although these terms both yield the same $\rho\pi\pi$ coupling, the $\rho 4\pi$ terms differ by a factor of four. Hence one cannot take the latter coupling to be the same as in a massive Yang-Mills model. Reducing the contribution

of diagram C.2a by a factor of four has a large effect on the total amplitude, explaining the difference between the present result and that of Ref. [9].

In order to examine the relative importance of the anomalous and non-anomalous processes in the amplitude, the partial widths can be evaluated with only the non-anomalous contributions. Doing so leads to the result for $\rho^0 \rightarrow 2\pi^0\pi^+\pi^-$ which is labelled HGNA in Table C.1. It can be compared with a value of 0.24 keV which is obtained for the partial width of this decay mode if one integrates over just the anomalous part of the amplitude. The two types of contribution are therefore of similar importance with the interference between them being small and destructive in character. It is also of interest to look at the effect of omitting the symmetry-breaking 4π interaction of Eq. C.15 (but retaining the physical pion mass in the propagator etc.). The results in this case, labelled HGCS, indicate that this interaction does indeed provide a significant contribution.

As a simple estimate of contributions beyond tree level, one can allow for the finite width of the ρ meson in its propagator (as in Ref. [10]). The method is a rather crude probe of the possible size of such effects, being sensitive to the representation chosen for the model. For instance, whilst the amplitudes calculated for any process should be the same using either the minimal hidden-gauge Lagrangian or its CCWZ equivalent, the two representations may attribute different weights to the contributions involving an intermediate ρ meson. Notwithstanding this disclaimer, it is nevertheless somewhat reassuring to note that the modification to the ρ propagator produces only a modest shift in the results.

For the above calculations to be seen as reliable, an important point to check is that the results are fairly robust under changes to the model parameters. Instead of the choices in Eq. C.16, one might reasonably decide to take $a = 2.108$ and $\tilde{g} = 5.74$ so as to simultaneously reproduce the empirical ρ meson mass and width¹⁴. With these parameters the partial widths remain close to those in Table C.1, being 0.93 keV for

¹⁴The observed width implies that $g_{\rho\pi\pi} = 6.05$.

the $2\pi^+2\pi^-$ mode and 0.42 keV for the $2\pi^0\pi^+\pi^-$ mode.

Consider now the decay amplitude in the massive Yang-Mills type of theory, beginning with the simplest Lagrangian of that formalism (see Appendix C.3). As is illustrated by $\rho\pi$ scattering, in this approach chiral symmetry may require strong cancellations among the various contributions to an amplitude. In deriving the amplitudes the Lagrangian is first rewritten in terms of the fields defined by the minimal diagonalization procedure. The additional three- and four-point interactions which are thereby generated produce contributions to the $\rho \rightarrow 4\pi$ amplitudes which are different in structure from any of the expressions quoted in Refs. [9, 10]. Graphs C.2f and C.2g, featuring intermediate a_1 states, also make contributions of a form not considered in the earlier references. Note, however, that powerful checks can be made by repeating the present calculations in the equivalent CCWZ representation of the model, as will be discussed shortly.

The parameters of the minimal Yang-Mills model are set analogously to those in the simplest hidden-gauge model: that is, they are chosen to satisfy the KSRF relation ($Z^2 = \frac{1}{2}$) and to reproduce the empirical ρ meson mass (implying that $g = 5.89$). As described in Appendix C.3, there is a diagonalization-induced $\rho\pi\pi$ interaction in the minimal Yang-Mills model which reduces the ρ meson width to 107.6 MeV. Persevering with the model despite this drawback, then the resulting partial widths for $\rho^0 \rightarrow 4\pi$ are as shown in Table C.1, labelled MMYM. They are similar in magnitude to those of the hidden-gauge model. As already emphasized, the calculations of Refs. [9, 10] used Yang-Mills models that do not respect chiral symmetry. Without the ensuing cancellations, they lead to partial widths that are too large by an order of magnitude.

Just as with the hidden-gauge model discussed earlier, the partial widths obtained with the minimal massive Yang-Mills Lagrangian are found to depend only mildly on the value taken for the gauge coupling. The non-anomalous and anomalous parts of the decay amplitude to $2\pi^0\pi^+\pi^-$ are again of almost equal importance¹⁵ and interfere

¹⁵Taking just the non-anomalous part gives a partial width of 0.18 keV whereas the anomalous piece alone gives 0.21 keV.

destructively, albeit to a very small extent.

The simple hidden-gauge and massive Yang-Mills models used above can be converted by a change of variables into equivalent CCWZ Lagrangians [136, 138], which should yield the same predictions for any observable as the original representations. Repeating the $\rho^0 \rightarrow 4\pi$ calculations with these models in their CCWZ forms therefore provides a stringent and useful check on the previous results. Furthermore, the CCWZ formalism is a convenient framework in which to examine the sensitivity of these results to assumptions about the a_1 meson. In contrast to the massive Yang-Mills approach, the parameters describing the a_1 mass and couplings may be changed independently, without the need to introduce compensating terms into the Lagrangian.

The relevant non-anomalous interactions in the CCWZ versions of the hidden-gauge and massive Yang-Mills models used above were given in Appendix C.4. The anomalous sectors can be similarly converted into CCWZ form. Having done so, the sum of amplitudes for the anomalous diagrams (C.2h and C.2i) must remain unaltered by the change of variables. For example, this is easily checked for the $\omega\rho\pi$ vertex of the hidden-gauge Lagrangian which yields $\omega\rho\pi$ and $\omega 3\pi$ terms in the CCWZ language. The conversion of the anomalous sector is rather involved in the massive Yang-Mills case, however, and so for simplicity the anomalous piece of the decay amplitude is taken directly from the original version of the minimal Yang-Mills model. Working with the same parameter sets as above, the results presented earlier have been successfully verified.

Starting from the CCWZ Lagrangians which are the equivalents of the models used above, it is then straightforward to investigate the effects of relaxing some of the assumptions imposed in those models. For instance, one could consider whether there might be any significance in adjusting the masses of the ω and a_1 mesons to their empirical values [12], $m_\omega = 783$ MeV and $m_{a_1} = 1230$ MeV. Doing so, and using the couplings of the minimal massive Yang-Mills model (Eq. C.13), gives the results

labelled as MYM+1 in Table C.1. This Lagrangian corresponds to a massive Yang-Mills Lagrangian with non-minimal terms, such as those suggested in Refs. [137, 145, 146]. The results are quite similar to those labelled MYM. This is in stark contrast to the effect of setting these meson masses to their empirical values in the massive Yang-Mills representation of the Lagrangian. In that case the partial widths would be 12.1 keV and 3.18 keV for the $2\pi^+2\pi^-$ and $2\pi^0\pi^+\pi^-$ final states respectively. These are much larger than any of the widths calculated with Lagrangians that respect chiral symmetry and provide a clear demonstration of the need to work consistently when using the massive Yang-Mills formalism.

The parameter choice of simplest massive Yang-Mills Lagrangian suffers from the fact that it gives too small a width for $\rho \rightarrow 2\pi$. It is a simple matter to change the CCWZ coefficients to remove this deficiency. One method is equivalent to adding the non-minimal term of Eq. C.8 to the massive Yang-Mills Lagrangian [137, 145]. In order to cancel the diagonalization-induced $\mathcal{O}(p^3)$ $\rho\pi\pi$ coupling in the original framework, one takes $\xi = 1$. Inclusion of this term gives the CCWZ coefficients listed in Eq. C.14. Using those couplings and the empirical meson masses produces the results for $\rho \rightarrow 4\pi$ which are labelled as MYM+2 in Table C.1. The partial widths are a little larger than those from other Lagrangians considered, but are of the same order of magnitude.

In the hidden-gauge and Yang-Mills Lagrangians described above the 3ρ coupling is equal to the $\mathcal{O}(p)$ $\rho\pi\pi$ one because of the assumed universal coupling of the ρ . Using the CCWZ equivalents of these models, this assumption can be tested by varying the 3ρ coupling strength, g_2 . The results are not fortunate. In all cases, shifts of $\pm 30\%$ in the coupling only alter the decay rate for $\rho^0 \rightarrow 2\pi^0\pi^+\pi^-$ by about $\pm 1\%$. Since such shifts can easily be accommodated through moderate changes in the other parameters, a measurement of this decay cannot therefore be used as an experimental probe of the 3ρ vertex.

Since the partial widths in all of the chirally symmetric cases have been found to be small, it is interesting to consider whether small symmetry-breaking contributions

to the ρ meson mass could prove to be significant. If isospin symmetry is assumed to hold then there are two suitable symmetry-breaking terms in the CCWZ Lagrangian,

$$\epsilon \langle V_\mu V^\mu (U + U^\dagger) \rangle, \quad -\frac{1}{4} \eta \langle V_{\mu\nu} V^{\mu\nu} (U + U^\dagger) \rangle. \quad (\text{C.19})$$

The second term, involving the field strength, alters the ρ mass because one would need to rescale the field to recover the canonical normalization of the kinetic term. Allowing such terms to contribute up to 10 MeV of the empirical mass, one finds that the ϵ term changes the partial widths by just $\pm 1\%$ whereas the η term can have effects at the $\sim 10\%$ level.

The results of this appendix have shown that the partial widths for $\rho^0 \rightarrow 4\pi$ are sensitive to the choice of Lagrangian, receiving significant contributions from anomalous processes and symmetry-breaking interactions. However, for all of the chirally symmetric models considered, the widths are of the order of 1 keV, corresponding to cross sections of the order of 5 pb. Although the processes may be hard to observe in future experiments, they should not be beyond the reach of DAΦNE, which is designed to have a luminosity of $5 \times 10^8 \text{ b}^{-1}\text{s}^{-1}$ [153].

References

- [1] W. Marciano and H. Pagels, Phys. Rep. **36** (1978) 137.
- [2] G. 't Hooft, Nucl. Phys. **B72** (1974) 461.
- [3] M. A. Shifman, A. I. Vainshtein and V. I. Zakharov, Nucl. Phys. **B147** (1979) 385, 448, 519; J. Gasser and H. Leutwyler, Phys. Rep. **87** (1982) 77; L. J. Reinders, H. Rubenstein and S. Yazaki, Phys. Rep. **127** (1986) 1.
- [4] M. Creutz, *Quarks, gluons and lattices*, (Cambridge University Press, Cambridge, 1983).
- [5] C. D. Roberts and A. G. Williams, Prog. Part. Nucl. Phys. **33** (1994) 477.
- [6] R. Delbourgo and M. D. Scadron, J. Phys. **G5** (1979) 1621; P. Maris, C. D. Roberts and P. C. Tandy, nucl-th/9707003 (1997).
- [7] Y. Nambu and G. Jona-Lasinio, Phys. Rev. **122** (1961) 345; **124** (1961) 246.
- [8] R. D. Bowler and M. C. Birse, Nucl. Phys. **A582** (1995) 655.
- [9] A. Bramon, A. Grau and G. Pancheri, Phys. Lett. **B317** (1993) 190.
- [10] S. I. Eidelman, Z. K. Silagadze and E. A. Kuraev, Phys. Lett. **B346** (1995) 186.
- [11] D. Prashar, Phys. Rev. **D26** (1982) 1183.
- [12] Particle Data Group, Phys. Rev. **D54** (1996) 1.

-
- [13] J. F. Donoghue, E. Golowich and B. R. Holstein, *Dynamics of the standard model*, (Cambridge University Press, Cambridge, 1992).
- [14] M. Gell-Mann and M. Lévy, *Nuovo Cim.* **16** (1960) 705.
- [15] H. Georgi, *Weak interactions and modern particle theory*, (Benjamin/Cummings, California, 1984).
- [16] M. Gell-Mann, R. Oakes and B. Renner, *Phys. Rev.* **175** (1968) 2195.
- [17] V. de Alfaro, S. Fubini, G. Furlan and C. Rossetti, *Currents in hadron physics*, (North Holland, Amsterdam, 1973).
- [18] R. Machleidt, K. Holinde and Ch. Elster, *Phys. Rep.* **149** (1987) 1.q
- [19] M. J. Iqbal, X. Jin and D. B. Leinweber, *Phys. Lett.* **B367** (1996) 45; H. B. O'Connell, B. C. Pearce, A. W. Thomas and A. G. Williams, *hep-ph/9501251* (1995); T. Hatsuda, E. M. Henley, Th. Meissner and G. Krein, *Phys. Rev.* **C49** (1994) 452; K. L. Mitchell, P. C. Tandy, C. D. Roberts and R. T. Cahill, *Phys. Lett.* **B335** (1994) 282; J. Piekarewicz and A. G. Williams, *Phys. Rev.* **C47** (1993) R2462; L. C. L. Hollenberg, C. D. Roberts and B. H. J. McKellar, *Phys. Rev.* **C46** (1992) 2057.
- [20] P. G. Blunden and M. J. Iqbal, *Phys. Lett.* **B198** (1987) 14; S. A. Coon and R. C. Barrett, *Phys. Rev.* **C36** (1987) 2189.
- [21] G. A. Miller, B. M. K. Nefkens and I. Šlaus, *Phys. Rep.* **194** (1990) 1.
- [22] R. Enomoto and M. Tanabashi, *hep-ph/9706340* (1997).
- [23] Y. Nambu, *Phys. Rev.* **106** (1957) 1366.
- [24] J. L. Gammel and R. M. Thaler, *Phys. Rev.* **107** (1957) 291.
- [25] G. Breit, *Proc. Nat. Acad. Sci. (U.S.)* **46** (1960) 746.

-
- [26] J. J. Sakurai, *Ann. Phys.* **11** (1960) 1.
- [27] G. Breit, *Phys. Rev.* **120** (1960) 287; J. J. Sakurai, *Phys. Rev.* **119** (1960) 1784.
- [28] W. R. Frazer and J. R. Fulco, *Phys. Rev.* **117** (1960) 1609.
- [29] L. M. Barkov et al., *Nucl. Phys.* **B256** (1985) 365; I. B. Vasserman et al., *Sov. J. Nucl. Phys.* **33** (1981) 709; L. M. Barkov et al., Novosibirsk preprint INP 79–69 (1979); G. Cosme et al., ORSAY preprint LAL–1287 (1976); A. Quenzer et al., *Phys. Lett.* **B76** (1978) 512; S. R. Amendolia et al., *Phys. Lett.* **B138** (1984) 454.
- [30] L. G. Landsberg, *Phys. Rep.* **128** (1985) 301.
- [31] M. Gell-Mann, D. Sharp and W. G. Wagner, *Phys. Rev. Lett.* **8** (1962) 261; J. W. Durso, *Phys. Lett.* **B184** (1987) 348.
- [32] D. W. G. S. Leith, *Electromagnetic interactions of hadrons* Volume 1 (ed. A. Donnachie and G. Shaw, Plenum Press, New York and London, 1978).
- [33] N. M. Kroll, T. D. Lee and B. Zumino, *Phys. Rev.* **157** (1967) 1376.
- [34] M. Gell-Mann and F. Zachariasen, *Phys. Rev.* **124** (1961) 953.
- [35] G. Höhler and E. Pietarinen, *Nucl. Phys.* **B95** (1975) 210; W. Grein, *Nucl. Phys.* **B131** (1977) 255.
- [36] U. Vogl and W. Weise, *Prog. Part. Nucl. Phys.* **27** (1991) 195; S. P. Klevansky, *Rev. Mod. Phys.* **64** (1992) 649; T. Hatsuda and T. Kunihiro, *Phys. Rep.* **247** (1994) 221.
- [37] J. Bijnens, *Phys. Rep.* **265** (1996) 369.
- [38] V. A. Miransky, *Int. J. Mod. Phys.* **A6** (1991) 1641.
- [39] J. Bijnens, E. de Rafael and H. Zheng, *Z. Phys.* **C62** (1994) 437.

-
- [40] J. Bijnens and J. Prades, Phys. Lett. **B320** (1994) 130; Z. Phys. **C64** (1994) 475.
- [41] T. Meissner, E. Ruiz Arriola and K. Goeke, Z. Phys. **A336** (1990) 91.
- [42] R. S. Willey, Phys. Rev. **D48** (1993) 2877; T. Gherghetta, Phys. Rev. **D50** (1994) 5985.
- [43] E. Nikolov, W. Broniowski, C. V. Christov, G. Ripka and K. Goeke, Nucl. Phys. **A608** (1996) 411.
- [44] V. Dmitrašinović, H.-J. Schulze, R. Tegen and R. H. Lemmer, Ann. Phys. **234** (1994) 225.
- [45] E. Pallante, Z. Phys. **C75** (1997) 305.
- [46] C. Schüren, F. Döring, E. Ruiz Arriola and K. Goeke, Nucl. Phys. **A565** (1993) 687.
- [47] R. Alkofer, H. Reinhardt, H. Weigel and U. Zuckert, Phys. Lett. **B298** (1992) 132; U. Zuckert, R. Alkofer, H. Reinhardt and H. Weigel, Nucl. Phys. **A570** (1994) 445.
- [48] E. Ruiz Arriola and L. L. Salcedo, Phys. Lett. **B316** (1993) 148; Nucl. Phys. **A590** (1995) 703.
- [49] I. J. R. Aitchison and G. Ripka, Nucl. Phys. **A606** (1996) 292.
- [50] R. Alkofer and P. A. Amundsen, Nucl. Phys. **B306** (1988) 305; A. A. Bel'kov, D. Ebert and A. V. Emelyaneko, Nucl. Phys. **A552** (1993) 523; K. Langfeld, C. Kettner and H. Reinhardt, Nucl. Phys. **A608** (1996) 331; T. Hamazaki and T. Kugo, Prog. Theor. Phys. **92** (1994) 645.
- [51] D. I. Dyakonov and V. Yu. Petrov, Nucl. Phys. **B245** (1984) 259; Sov. Phys. JETP **62** (1985) 204, 431; Nucl. Phys. **B272** (1986) 457.
- [52] G. 't Hooft, Phys. Rev. Lett. **37** (1976) 8; Phys. Rev. **D14** (1976) 3432.

-
- [53] M. A. Novak, J. J. M. Verbaarschat and I. Zahed, Phys. Lett. **B228** (1989) 251.
- [54] H. Ito, W. W. Buck and F. Gross, Phys. Lett. **B248** (1990) 28.
- [55] H. Ito, W. W. Buck and F. Gross, Phys. Rev. **C43** (1991) 2483.
- [56] H. Ito, W. W. Buck and F. Gross, Phys. Rev. **C45** (1992) 1918.
- [57] S. Schmidt, D. Blaschke and Y. L. Klavinovsky, Phys. Rev. **C50** (1994) 435.
- [58] G. V. Efimov and M. A. Ivanov, *The Quark Confinement Model of Hadrons* (IOP, Bristol and Philadelphia, 1993).
- [59] G. V. Efimov and S. N. Nedelko, Phys. Rev. **D51** (1995) 176; Ja. V. Burdanov, G. V. Efimov, S. N. Nedelko and S. A. Solunin, Phys. Rev. **D54** (1996) 4483.
- [60] K. Langfeld and M. Rho, Nucl. Phys. **A596** (1996) 451.
- [61] H. Reinhardt, Phys. Lett. **B257** (1991) 375; K. Langfeld and M. Schaden, Phys. Lett. **B272** (1991) 100; K. Langfeld, R. Alkofer and H. Reinhardt, Phys. Lett. **B277** (1992) 163.
- [62] P. T. Cahill and C. D. Roberts Phys. Rev. **D32** (1985) 2419; J. Praschifka, C. D. Roberts and R. T. Cahill, Phys. Rev. **D36** (1987) 209.
- [63] M. R. Frank and C. D. Roberts, Phys. Rev. **C53** (1996) 390.
- [64] M. Buballa and S. Krewald, Phys. Lett. **B294** (1992) 19.
- [65] V. Bernard and U.-G. Meissner, Nucl. Phys. **A489** (1988) 647.
- [66] M. Wakamatsu and W. Weise, Z. Phys. **A331** (1988) 173; D. Ebert and H. Reinhardt, Nucl. Phys. **B271** (1986) 188; J. Bijnens, C. Bruno and E. de Rafael, Nucl. Phys. **B390** (1993) 501; E. Ruiz Arriola, Phys. Lett. **B253** (1991) 430.
- [67] J. Prades, Z. Phys. **C63** (1994) 491.

-
- [68] S. Klimt, M. Lutz, U. Vogl and W. Weise, Nucl. Phys. **A516** (1990) 429, 469.
- [69] V. Bernard, R. L. Jaffe and U.-G. Meissner, Nucl. Phys. **B308** (1988) 753.
- [70] M. Kobayashi and T. Maskawa, Prog. Theor. Phys. **44** (1970) 1422; M. Kobayashi, H. Kondo and T. Maskawa, Prog. Theor. Phys. **45** (1971) 1955.
- [71] J. W. Negele, hep/lat 9709129 (1997).
- [72] G. C. Wick, Phys. Rev. **96** (1954) 1124.
- [73] E. Witten, Nucl. Phys. **B160** (1979) 57.
- [74] C. J. Burden, C. D. Roberts and A. G. Williams, Phys. Lett. **B285** (1992) 347.
- [75] M. Stingl, Phys. Rev. **D34** (1986) 3863; **D36** (1987) 651 (E); U. Häbel, R. Könning, H.-G. Reusch, M. Stingl and S. Wigard, Z. Phys. **A336** (1990) 435.
- [76] C. Savkli and F. Tabakin, hep-ph/9702251 (1997).
- [77] T. D. Lee and G. C. Wick, Nucl. Phys. **B9** (1969) 209.
- [78] R. E. Cutkosky, P. V. Landshoff, D. I. Olive and J. C. Polkinghorne, Nucl. Phys. **B12** (1969) 281.
- [79] M. Bando, M. Harada and T. Kugo, Prog. Theor. Phys. **91** (1994) 927.
- [80] J. A. Nelder and R. Mead, J. Comput. **7** (1965) 308.
- [81] T. W. Sag and G. Szekeres, Math. Comput. **18** (1964) 245.
- [82] W. Broniowski, G. Ripka, E. Nikolov and K. Goeke, Z. Phys. **A354** (1996) 421.
- [83] M. Goldberger and S. Treiman, Phys. Rev. **110** (1958) 1178, 1478.
- [84] M. R. Frank, Phys. Rev. **C51** (1995) 987.

-
- [85] C. D. Roberts, Nucl. Phys. **A605** (1996) 475; C. J. Burden, C. D. Roberts and M. J. Thompson, Phys. Lett. **B371** (1996) 163; P. C. Tandy, Prog. Part. Nucl. Phys. **36** (1996) 97; R. Alkofer, A. Bender and C. D. Roberts, Int. J. Mod. Phys. **A10** (1995) 3319; C. D. Roberts, R. T. Cahill, M. E. Sevier and N. Iannella, Phys. Rev. **D49** (1994) 125.
- [86] D. Kekez and D. Klabučar, Phys. Lett. **B387** (1996) 14.
- [87] M. R. Frank, K. L. Mitchell, C. D. Roberts and P. C. Tandy, Phys. Lett. **B359** (1995) 17.
- [88] J. Ball and T. Chiu, Phys. Rev. **D22** (1980) 2542.
- [89] K. L. Au, D. Morgan and M. Pennington, Phys. Rev. **D35** (1987) 1633; D. Morgan and M. R. Pennington, Phys. Rev. **D48** (1993) 1185.
- [90] S. Ishida, M. Y. Ishida, H. Takahashi, T. Ishida, K. Takamatsu and T. Tsuru, Prog. Theor. Phys. **95** (1996) 745; B. S. Zou and D. V. Bugg, Phys. Rev. **D50** (1994) 591; N. A. Tornqvist and M. Roos, Phys. Rev. Lett. **76** (1996) 1575; M. Harada, F. Sannino and J. Schechter, Phys. Rev. **D54** (1996) 1991.
- [91] C. J. Burden, L. Qian, C. D. Roberts, P. C. Tandy and M. J. Thomson, Austr. J. Phys. **50** (1997) 95.
- [92] V. Bernard, A. H. Blin, B. Hiller, U.-G. Meissner and M. C. Ruivo, Phys. Lett. **B305** (1993) 163.
- [93] A. Polleri, R. A. Broglia, P. M. Pizzochero and N. N. Scoccola, hep/ph 9611300 (1996).
- [94] A. N. Ivanov, M. Nagy and M. K. Volkov, Phys. Lett. **B200** (1988) 171.
- [95] S. Weinberg, Phys. Rev. Lett. **65** (1990) 1177.
- [96] V. Bernard, A. A. Osipov and U.-G. Meissner, Phys. Lett. **B292** (1992) 205.

-
- [97] M. Bando, T. Kugo and K. Yamawaki, Nucl. Phys. **B259** (1985) 493; M. Bando, T. Fujiwara and K. Yamawaki, Prog. Theor. Phys. **79** (1988) 1140.
- [98] H. Albrecht et al., Z. Phys. **C58** (1993) 61.
- [99] S. Weinberg, Phys. Rev. Lett. **18** (1967) 507.
- [100] M. Goldberger, D. Soper and A. Guth, Phys. Rev. **D14** (1976) 1117.
- [101] S. R. Amendolia et al., Nucl. Phys. **B277** (1986) 168.
- [102] C. N. Brown et al., Phys. Rev. **D8** (1973) 92; C. J. Bebek et al., Phys. Rev. **D9** (1974) 1229.
- [103] V. Bernard and U.-G. Meissner, Phys. Rev. Lett. **61** (1988) 2296.
- [104] C. Itzykson and J.-B. Zuber, *Quantum field theory* (McGraw-Hill 1980).
- [105] H.-J. Behrend et al., Z. Phys. **C49** (1991) 401.
- [106] J. Gronberg et al., CLEO collaboration, preprint CLNS 97/1477 / CLEO 97-7 (1997).
- [107] S. I. Eidelman, *The DAΦNE Physics Handbook*, eds. L. Maiani, G. Pancheri and N. Paver (INFN, Frascati, 1995), p. 499.
- [108] R. I. Dzhelyadin et al., Phys. Lett. **B102** (1981) 296.
- [109] M. Bando and M. Harada, Phys. Rev. **D49** (1994) 6096; G. Köpp, Phys. Rev. **D10** (1974) 932.
- [110] F. Klingl, N. Kaiser and W. Weise, hep/ph 9607431 (1996).
- [111] M. Zielinski et al., Phys. Rev. Lett. **52** (1984) 1195.
- [112] E. Quack and S. P. Klevansky, Phys. Rev. **C49** (1994) 3283.

- [113] N.-W. Cao, C. M. Shakin and W.-D. Sun, Phys. Rev. **C46** (1992) 2535; P. P. Domitrovich, D. Bückers and H. Mütter, Phys. Rev. **C48** (1993) 413; P. Zhuang, J. Hüfner and S. P. Klevansky, Nucl. Phys. **A576** (1994) 525; P. Zhuang, J. Hüfner, S. P. Klevansky and H. Voss, Ann. Phys. **234** (1994) 225; Y. B. He, J. Hüfner, S. P. Klevansky and P. Rehberg, nucl-th 9712051 (1997).
- [114] R. D. Bowler, PhD thesis, University of Manchester (1995).
- [115] M. C. Birse, private communication.
- [116] V. Elias, A. H. Fariborz, Fang Shi and T. G. Steele, hep-ph 9708466 (1997).
- [117] M. Svec, hep-ph 9711376 (1997); J. A. Oller and E. Oset, hep-ph 9710554 (1997); R. Kamiński, L. Leśniak and B. Loiseau, hep-ph 9712337 (1997).
- [118] M. R. Pennington, hep-ph 9710456 (1997).
- [119] M. Ishida, S. Ishida and T. Ishida, hep-ph 9802272 (1998).
- [120] S. Ishida, hep-ph 9712229 (1997); K. Takamatsu, M. Ishida, S. Ishida, T. Ishida and T. Tsuru, hep-ph 9712232 (1997).
- [121] M. C. Birse, J. Phys. **G20** (1994) 1537.
- [122] S. Weinberg, Phys. Rev. Lett. **18** (1967) 188.
- [123] L. S. Brown, Phys. Rev. **163** (1967) 1802.
- [124] B. W. Lee and H. T. Nieh, Phys. Rev. **166** (1968) 1507.
- [125] S. Weinberg, Physica **A96** (1979) 327.
- [126] J. Gasser and H. Leutwyler, Ann. Phys. **B158** (1984) 142.
- [127] J. Gasser and H. Leutwyler, Nucl. Phys. **B250** (1985) 465.
- [128] H. W. Fearing and S. Scherer, Phys. Rev. **D53** (1996) 315.

- [129] S. Bellucci, J. Gasser and M. Sainio, Nucl. Phys. **B423** (1994) 80; Nucl. Phys. **B431** (1994) 413 (E); M. Jetter, Nucl. Phys. **B459** (1996) 283; J. Bijnens, G. Colangelo, G. Ecker, J. Gasser and M. E. Sainio, hep-ph/9707291 (1997).
- [130] J. Donoghue, C. Ramirez and G. Valencia, Phys. Rev. **D39** (1989) 1947.
- [131] G. Ecker, J. Gasser, A. Pich and E. de Rafael, Nucl. Phys. **B321** (1989) 311.
- [132] M. Bando, T. Kugo, S. Uehara, K. Yamawaki and T. Yangida, Phys. Rev. Lett. **54** (1985) 1215; M. Bando, T. Kugo and K. Yamawaki, Phys. Rep. **164** (1988) 217.
- [133] S. Gasiorowicz and D. A. Geffen, Rev. Mod. Phys. **41** (1969) 531.
- [134] S. Coleman, J. Wess and B. Zumino, Phys. Rev. **177** (1969) 2239; C. G. Callan, S. Coleman, J. Wess and B. Zumino, *ibid* 2247.
- [135] S. Weinberg, Phys. Rev. **166** (1968) 1568.
- [136] G. Ecker, H. Leutwyler, J. Gasser, A. Pich and E. de Rafael, Phys. Lett. **B223** (1989) 425.
- [137] U.-G. Meissner, Phys. Rep. **161** (1988) 213.
- [138] M. C. Birse, Z. Phys. **A355** (1996) 231.
- [139] K. Yamawaki, Phys. Rev. **D35** (1987) 412; J. Bijnens and E. Pallante, Mod. Phys. Lett. **A11** (1996) 1069.
- [140] M. Bando, T. Kugo and K. Yamawaki, Prog. Theor. Phys. **73** (1985) 1541.
- [141] T. Fujiwara, T. Kugo, H. Terao, S. Uehara and K. Yamawaki, Prog. Theor. Phys. **73** (1985) 1541.
- [142] J. Wess and B. Zumino, Phys. Lett. **B37** (1971) 95.
- [143] S. Furui, R. Kobayashi and K. Ujiie, Prog. Theor. Phys. **76** (1986) 963.

-
- [144] K. Kawarabayashi and M. Suzuki, Phys. Rev. Lett. **16** (1966) 255; Riazuddin and Fayyazuddin, Phys. Rev. **147** (1966) 1071.
- [145] H. Gomm, Ö. Kaymakçalan and J. Schechter, Phys. Rev. **D30** (1984) 2345.
- [146] M. F. L. Gotterman and N. D. Hari Dass, Nucl. Phys. **B272** (1986) 739.
- [147] Ö. Kaymakçalan, S. Rajeev and J. Schechter, Phys. Rev. **D30** (1984) 594.
- [148] W. A. Bardeen, Phys. Rev. **184** (1969) 1848.
- [149] Y. Brihaye, N. K. Pak and P. Rossi, Nucl. Phys. **B254** (1985) 71; Phys. Lett. **B164** (1985) 111.
- [150] E. A. Kuraev and Z. K. Silagadze, Phys. Lett. **B292** (1992) 377.
- [151] D. Kalafatis, Phys. Lett. **B313** 115; D. Kalafatis and M. C. Birse, Nucl. Phys. **A584** 589.
- [152] S. I. Dolinsky *et al.*, Phys. Rep. **202** (1991) 99.
- [153] G. Pancheri, Nuovo Cim. **A107** (1994) 2149.
- [154] L. M. Kurdadze *et al.*, JETP Lett. **47** (1988) 512.
- [155] V. M. Aulchenko *et al.*, Novosibirsk preprint YAF 87-90 (1987).
- [156] R. Kumar, Phys. Rev. **185** (1969) 1865.